

University of Warwick institutional repository: <http://go.warwick.ac.uk/wrap>

A Thesis Submitted for the Degree of PhD at the University of Warwick

<http://go.warwick.ac.uk/wrap/34686>

This thesis is made available online and is protected by original copyright.

Please scroll down to view the document itself.

Please refer to the repository record for this item for information to help you to cite it. Our policy information is available from the repository home page.

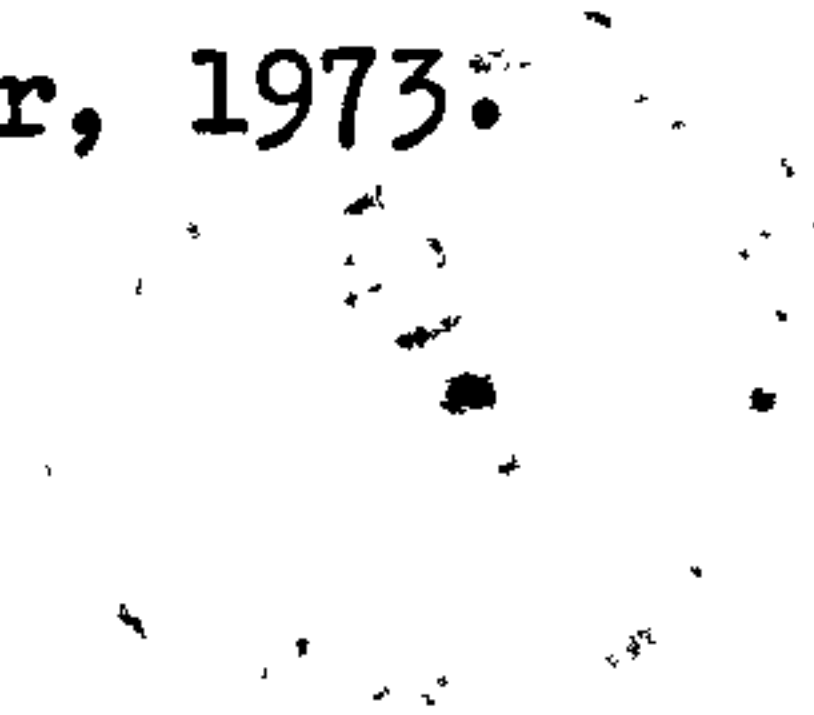
THE THEORY AND PERFORMANCE OF
A.C. AXIAL FLUX MACHINES

by

Bernard Capaldi

A thesis submitted to the
University of Warwick
for the degree of Doctor of Philosophy

October, 1973.



" Enough is Enough "

Anon.

Acknowledgements

I would like to express my thanks to the following:-

To my wife for her continual support and encouragement and my children for their ability to bring me down from the 'dizzy' heights of research to the more mundane matters of playing football and swimming.

To my parents and father-in-law who magically changed, on occasion, my red bank account into a beautiful black.

To Mr. A.E Corbett for his assistance, for giving me a free hand and for reading the manuscript.

To Mr. P campbell for the quiet discussions.

To Mr.F Holloway for his great cups of tea and Mr. H Fowkes for helping in the manufacture, building and testing of the machine, for breaking my watch and his fictitious friend "for King and Country".

To all members of theEngineering Department Workshop, particularly Ron, Jim 1, Jim 2, Mike, Jan, Bert, Sid, Tom and Les for their advice on "what to do" and to all the underworked and overpaid members of the D.O.

Finally the Science Research Council for Financial assistance.

PAGE

NUMBERING

AS ORIGINAL

Abstract

The work reported in this thesis is concerned with the design, testing and manufacture of a disc machine in order to compare its power to weight ratio with conventional (radial) machines. In the former machine the active current carrying conductors are radially positioned while the useful airgap flux is parallel to the rotor shaft. Both the squirrel cage induction motor and reluctance motor are covered.

The airgap flux is obtained directly from the product of the airgap permeance and the airgap m.m.f. The errors involved in using the permeance wave concept is assessed for the reluctance motor by comparing fundamental and harmonic components in the airgap flux waveform obtained using permeance waves with that obtained from conformal transformation techniques. An equation is determined that can be used for calculating the magnitude of the maximum inertia that can be synchronised by the reluctance motor for the practical range of pole, arc/pole pitch ratios.

It is shown that both machines have a potential power/weight ratio of twice that of the radial machine. For the induction motor and reluctance motor maximum outputs of 1260 watts and 1100 watts were obtained respectively in a frame size of 220 mm O/D and 110 mm long. The limitations of the prototype machines are discussed and the relationship between the reluctance motor performance and the principal machine parameters is obtained.

List of Symbols

B = flux density (B_{ave} , B_{peak} etc)

C' = induction motor constant

D_2 = outer principal diameter

D_1 = inner principal diameter

E, e = induced e.m.f

g = mechanical airgap

g' = effective airgap

h = half the axial thickness of the rotor

I = peak fundamental current

i = current in phase 1

i_b = bar current

\hat{J} = maximum inertia

$K_{6k\pm1}$ = product of pitch and distribution factors for $6k\pm1$ harmonic

K_1 = fundamental winding factor

n, k = harmonic number

m = thickness of stator yoke

N = turns/pole per phase

n_b = rotor bars

n = turns ratio of induction motor

p = pole pairs

R_e = effective resistance

R_1 = phase resistance of stator winding

r = resistance of bar load impedance

r_2 = r referred to primary of the equivalent circuit

s = slip

v = component of supply voltage opposing e

X_e = effective reactance

x_1 = stator leakage reactance per phase

X_d, X_q = direct- and quadrature axis reactance

x = reactance of bar load impedance
 x_2 = x referred to the primary of the equivalent circuit
 Z_b = bar load impedance
 Z_e = effective impedance
 Z = phase impedance
 α = angular distance around airgap
 β = pole arc/pole pitch ratio
 γ = constant
 δ = load angle
 ϕ = power factor angle
 Φ_r = total airgap flux/pole
 ϕ_a = airgap flux
 η = efficiency
 μ_0 = permeability of free space
 θ = instantaneous rotor position
 θ_b = bar load impedance phase angle
 w = frequency

Additional symbols used in the text
 are defined where necessary

Acknowledgements	i
Abstract	ii
List of symbols	iii
Contents	v
<u>CONTENTS</u>	
Chapter I Axial Flux Machine	
1.1 Introduction	1
1.2 Historical Background	3
1.3 Axial Flux Machine	5
1.3.1 Active Length	7
1.3.2 Operational Modes	11
1.3.3 Optimisation	13
1.4 Conclusion	14
Chapter II Theory of Axial Machine	
2.1 Introduction	16
2.2 Assessment of Analytical Errors	16
2.3 Airgap Flux	26
2.4 Induction Motor Performance	30
2.4.1 Airgap Flux	30
2.4.2 Torque/Speed Relationship	31
2.4.3 Magnetising Reactance	32
2.4.4 Turns Ratio of Squirrel Cage Motor	34
2.5 Synchronous Performance of Reluctance Motor	35
2.5.1 Phase Impedance	35
2.5.2 Performance Equations	36
2.5.2.1 Pull-out	38
2.6 Asynchronous Performance	39
2.6.1 Equivalent Circuit $s \rightarrow 1$	40
2.6.2 Pull-in Criteria	42
2.7 Conclusion	49

Chapter III Experimental Machine

3.1	Introduction	51	e
3.2	Choice of Lamination Material	52	
3.3	Axial Machine Stator	54	
3.4	Axial Machine Rotor	56	ed
3.5	Stator Winding	59	l
3.6	Skewed Slots	62	
3.7	Torque Measurement	67	
3.8	Coupled Inertia for Reluctance Motor	67	
3.9	Effective Airgap Length	67	
3.10	Conclusion	71	

Chapter IV Experimental Results

4.1	Introduction	74	re
4.2	Preliminary Tests	74	t
4.2.1	Classification of Losses	74	
4.2.2	Comparison of Rotor and Stator Iron Losses	76	
4.2.3	Calibration of Torque Unit	78	y
4.2.4	Measurement of Load Angle	78	
4.2.5	Inertia	80	
4.2.6	D.C Resistance of Stator Winding	80	nes
4.2.7	Temperature Rise	82	
4.3	Performance of the Induction Motor	82	
4.3.1	Iron Loss as a Function of Speed	82	
4.3.2	Friction and Windage of the d.c machine	83	
4.3.3	Equivalent Circuit Parameters	86	
4.3.4	Torque/Speed curves	89	
4.3.5	Efficiency, Power Factor, and Input Current	90	L
4.3.6	Starting Torque	90	
4.3.7	Discussion of Results	90	

4.4	Performance of the Reluctance Motor	97
4.4.1	Maximum Inertia	103
4.5	Conclusion	108
Chapter V Optimisation		
5.1	Introduction	110
5.2	Assumptions	111
5.3	Performance Equations	112
5.3.1	Synchronous Operation	112
5.3.1.1	Phase Current	115
5.3.1.2	Power Factor	118
5.3.1.3	Output Power	120
5.3.1.4	Efficiency	123
5.3.1.5	Copper Loss	125
5.3.1.6	Summary	126
5.3.2	Maximum Inertia	126
5.4	Conclusion	130
Chapter VI General Discussion		
6.1	Introduction	132
6.2	Aspects of the Machine Performance	132
6.3	Improvements to the Experimental Machine	134
6.4	Comparison of Machine Performance	135
6.5	Suggestions for Further Work	136
6.5.1	Unbalanced Magnetic Pull	136
6.5.2	Variation in Rotor Configuration	137
6.5.2.1	Induction Motor (Ironless rotor)	137
6.5.2.2	Induction Motor (Iron rotor)	137
6.5.2.3	Reluctance Motor	139
6.6	Type of Market	139
6.7	Conclusion	140

Appendix I	
Airgap Permeance	142
Appendix II	
Bar Load Impedance	144
Appendix III	
Calculation of Squirrel Bar Impedance	150
Appendix IV	
Impedance of Squirrel Cage Endring	155
Appendix V	
Rotor Inertia	163
References	164

Chapter I

Axial Flux Machines

1.1. Introduction

It is a necessary condition for electromagnetic energy conversion that the magnetic field and active current carrying conductors should not lie along the same axis and that optimum energy conversion is obtained if the field and conductors are mutually perpendicular. There are a limited number of ways in which this optimum can be achieved, the three major ways being,

- 1) The use of a radial magnetic field and axial conductors which combine together to produce rotary movement. This is referred to as a "radial machine".
- 2) The use of an axial magnetic field and radial conductors which again combine to produce rotary movement. This is referred to as an "axial machine".
- 3) Mutually perpendicular field and conductors arranged in parallel to produce linear motion

The majority of electrical machines fall into category 1) though well known examples of categories 2) and 3) are the Printed Circuit Motor⁽¹⁾ and the Linear Induction Motor⁽²⁾.

Because of the geometry, modern radial machines have certain inherent limitations which have been accepted by successive generations of machine engineers and designers as inevitable. Firstly, and probably the most well known is the flux bottleneck associated with the root of the rotor tooth. As a result, this part of the magnetic circuit in the machine generally works at a much higher flux density than anywhere else. Next to the tips of the teeth, or the pole tips in salient pole machines, this particular region is the first to become saturated. It is not

normal engineering practice to design the machine so that saturation does not occur in these regions, as this would necessitate the inefficient loading of the remainder of the circuit. Secondly, though not immediately apparent, is the poor utilisation of the space within the framework of the machine. This latter point is developed more fully in the following sections.

The removal of these limitations, particularly the second, leads to a machine with a higher power to weight ratio. This is successfully achieved by changing the geometry of the machine, that is by changing from a radial flux configuration to its axial flux counterpart. This also leads to a machine which has a high diameter to length ratio, as opposed to the normal length to diameter ratio (which is typically greater than unity) of the radial machine.

Two types of axial machines are studied:- the reluctance motor and the induction motor. Primarily this is to allow a broader knowledge of a.c. machines in this configuration to be obtained. Inevitably, of course, comparison between these two machines can be made. Indeed it is a fairly common practice to compare the performance of two such machines having the same frame size and it is generally accepted that the former machine is inferior in many respects to the latter. Where in radial machines the reluctance motor is basically a modified induction motor, i.e. where the rotor has been machined to provide saliency, then the output can be as low as one third ($\frac{1}{3}$) that of the induction motor. More modern designs, e.g. the segmental rotor machines⁽³⁾ are supposedly capable of matching the equivalent frame size induction motor.

The reluctance motor design chosen is basically a modified induction motor. The arrangement is such, however, that a segmental motor in its most basic form can be obtained. By employing two stators with mutually assisting m.m.f.'s the modified induction motor is obtained, while with

mutually opposed m.m.f's. the segmental rotor machine is obtained. This is elaborated more fully in section 1.3.2.

It is not the intention of the writer to draw comparisons between the two machines nor to comment on why one type is used in preference to the other. The method of analysis is based on the theories employed in performance predictions of radial machines. Modifications are incorporated to account for the special shape of the axial machine. Finally, any radial machine can be transposed into the axial form, hence the modern techniques used to improve the performance of the former can also be applied to this new machine.

1.2 Historical Background

The development of electric machines has been well chronicled^(4, 5) and only a brief outline is given here. Many of the earliest machines were basically axial flux but the change to radial machines, in terms of the historical life of electrical machines, was achieved in a relatively short period of time. The first recorded instance of an electric motor was Faraday's disc (c.1821) and this about a year after Ampere discovered the nature of the electric current and its relationship to magnetism - Faraday employed an axial field. The first patent to be taken out on an electric motor was by an American Inventor, Thomas Davenport⁽⁴⁾, in 1837, and this was a radial machine. Radial machines developed rapidly with axial machines even more rapidly becoming a topic of historical interest. Although the existence of many patents⁽⁶⁾ would seem to contradict this, it is a fact that since 1837 axial machines have not received any serious attention. Two exceptions to this are the printed circuit motor⁽¹⁾ already mentioned and the superconducting homopolar machine⁽⁷⁾ developed by I.R.D.C. The reason for this lack of attention probably lies in the fact that in the single rotor/stator disc configuration there exists a strong magnetic pull due to the presence of iron in the rotor. This condition however can be overcome by either using a double stator machine or by using an ironless rotor as in the printed circuit motor.

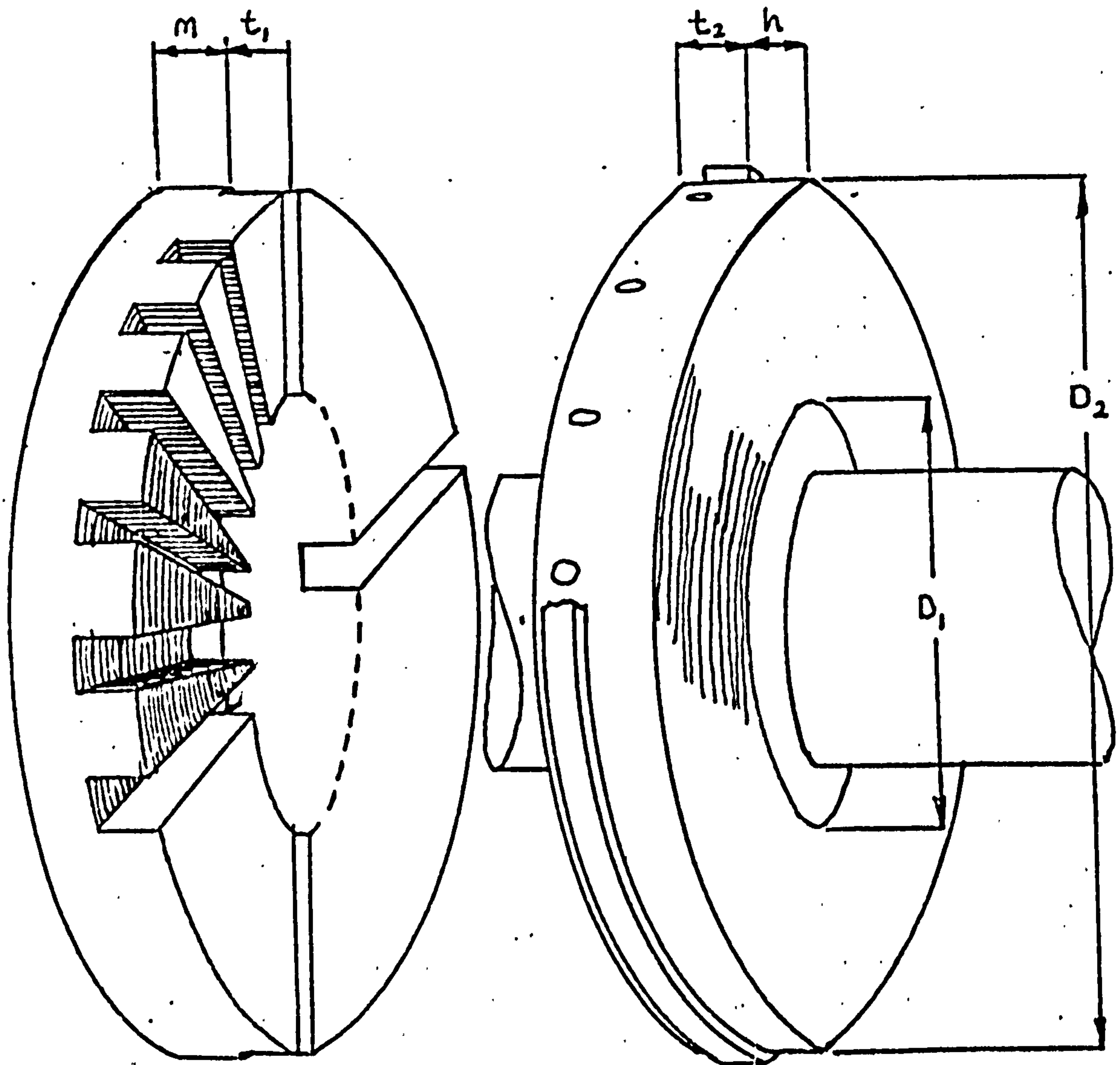


Figure 1.1

Exploded view of single stator Axial Field Machine.

Both stator and rotor are laminated in the form of a coiled spring. (stator windings, part of squirrel cage and casing not included)

1.2. Axial Flux Machines

Work on d.c. axial machines has progressed at the University of Warwick since 1967, and several domestic and industrial applications^(8,9,10) have been pursued using these machines. It is as a result of this interest that work on a.c. versions was initiated. Figure 1.1. shows an exploded view of an induction motor using this configuration. In this machine the following features are of interest.

- 1) The slots on the stator and rotor are radial.
- 2) The slot to tooth ratio varies from a maximum at the inner diameter (D_1).
- 3) The air-gap flux is axial while the flux in the return paths (the yoke of the stator and rotor) is circumferential.
- 4) The slots (and teeth) at any diameter are constant in width over their full depth.
- 5) The effect of skewing is to make the slots lie on the arc of a circle. The relationship that the radius and origin of this circle has with the number of slots, D_1 and D_2 and the amount of skew is given in Chapter III, Section 3.6. p 62.
- 6) The overall diameter of this machine is dependant on the active length of the conductors ($\frac{1}{2}(D_2 - D_1)$), the number of conductors, since this effectively determines D_1 , and the conductor overhang at D_2 . Basically, the overall diameter is to the first order determined by the electric loading of the machine.
- 7) The overall length can be approximated to the rotor and stator axial length. These two are determined by,
 - (a) the electric loading represented by the slot depth on both members (t_1 and t_2).

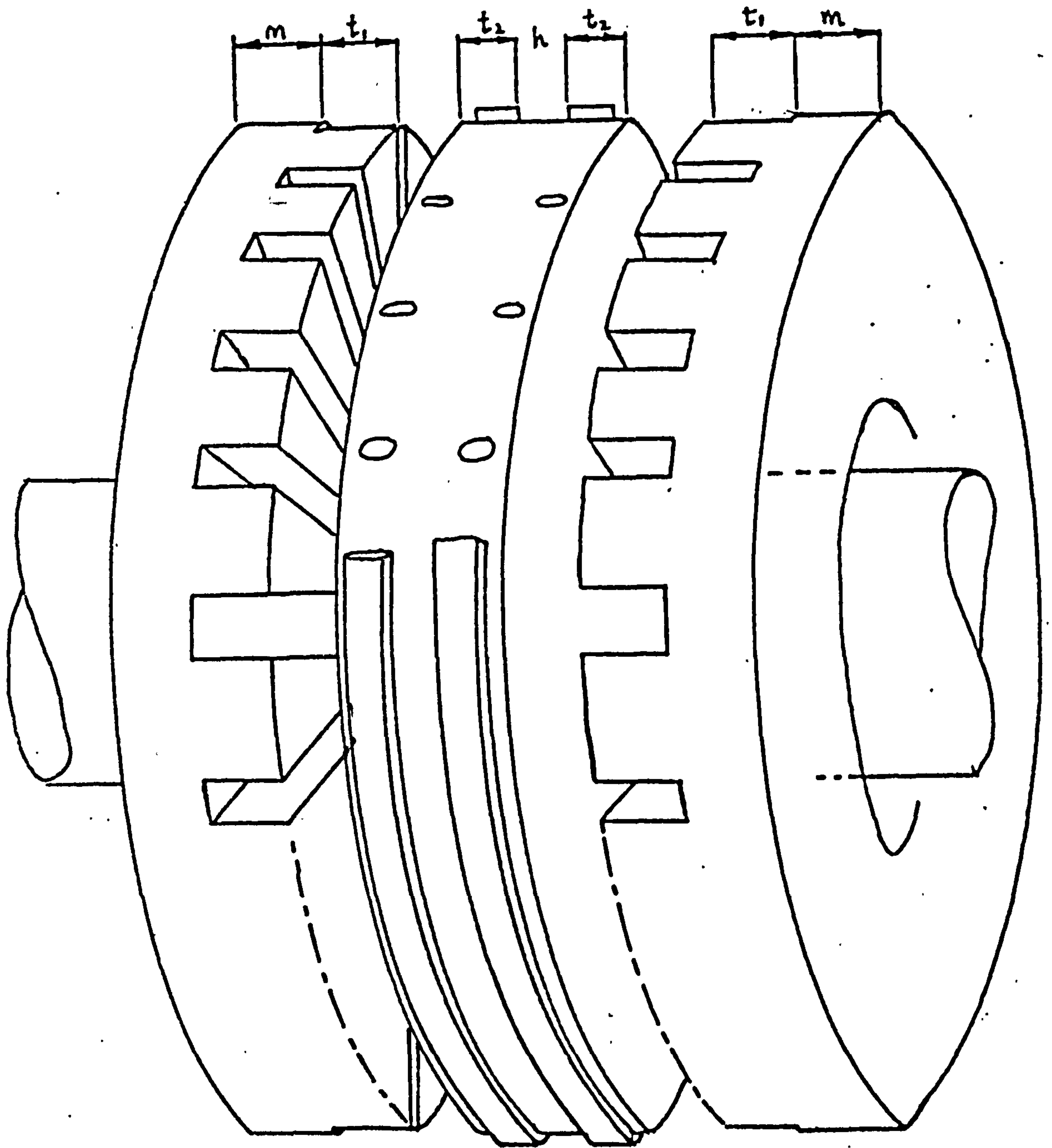


Figure 1.2

Double Stator Axial Field Machine.

The two stators and one rotor are laminated in the form of a coiled spring.

- (b) the magnetic loading represented by the thickness of yokes or flux return paths of the magnetic circuit (m and h).

This machine, as with the majority of radial flux machines, has only one stator, one rotor and one airgap. In this basic form, the performance capabilities of the axial machine in terms of power to weight ratio could not be expected to be any better than that for radial machines. It does, however, relieve the restriction on flux levels imposed in radial machines by the reduced cross-sectional area of the tooth root. If we now consider the machine shown in Figure 1.2., some interesting results are obtained.

1.3.1. Active Length

This arrangement shows an axial machine having two stators, two airgaps and one rotor member. In the single stator machine, the overall length is given approximately by,

$$L_s = m_1 + t_1 + t_2 + g + m_2$$

and by assuming zero leakage

$$m_1 = m_2 = m$$

hence $L = 2m + t_1 + t_2 + g$

For the double stator machine, however,

$$L_d = 2m + 2t_1 + 2t_2 + 2g + h$$

By arranging the two stator m.m.f.'s to assist each other, the flux from either stator will cross both airgaps. This machine then becomes, in effect, two identical machines placed back to back. In such a machine the dimension ' h ' can go to zero and as the flux is in the one direction only, the lamination material used in the rotor can be anisotropic with the grain of the material lying in the axial direction.

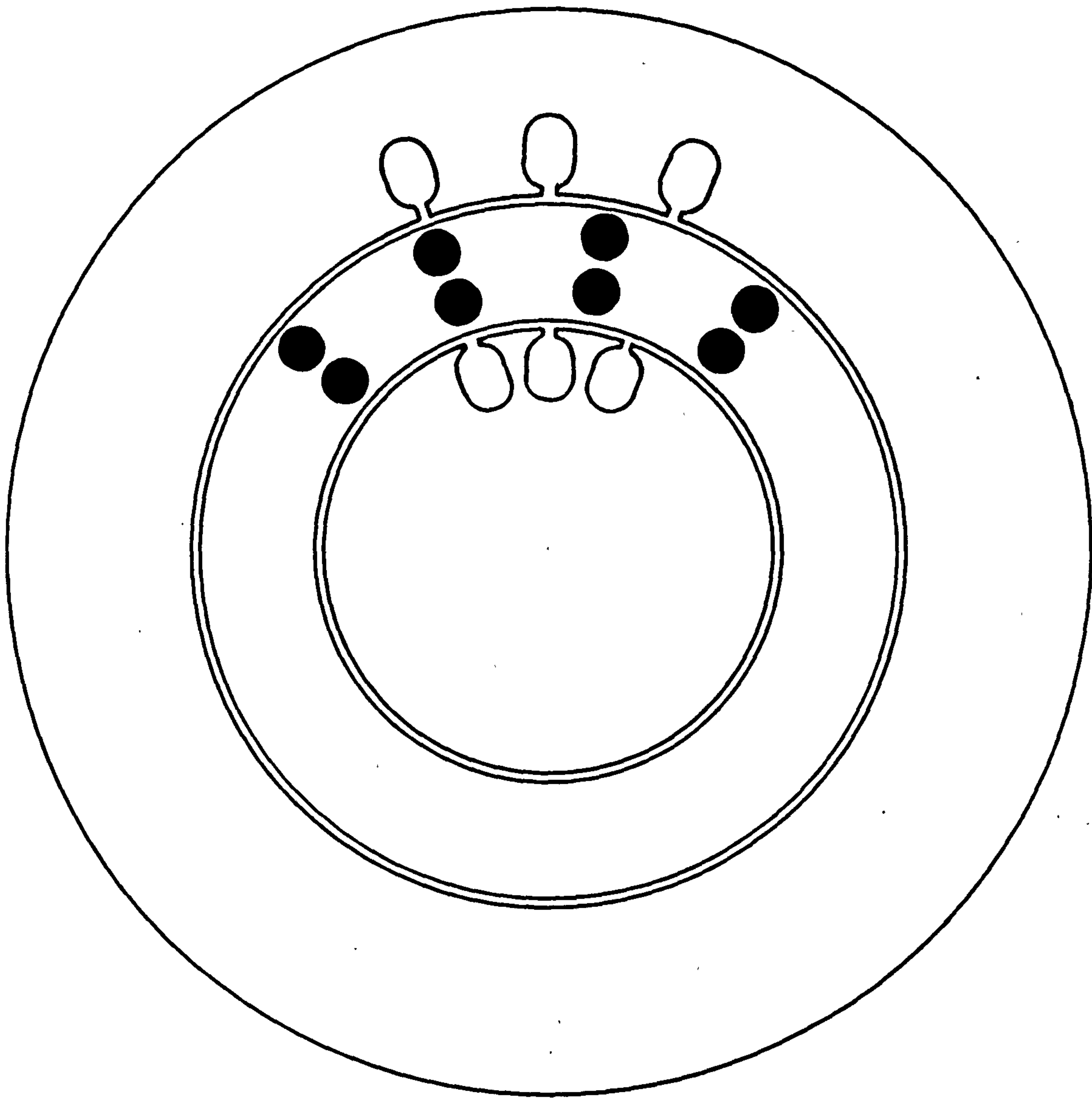


FIG 1.3

POSSIBLE DOUBLE STATOR INDUCTION MACHINE WITH
SQUIRREL CAGE END RINGS REMOVED

The other case exists when the stator m.m.f.'s are mutually opposed, consequently the flux produced by one stator m.m.f. will cross the same airgap twice via the return path 'h'. Either double stator machine is capable of twice the output of the single stator machine. But for the particular case where the m.m.f.'s are mutually additive,

$$L_d = 2m + 2t_1 + 2t_2 + 2g$$

and this represents an increase in overall length of

$$(t_1 + t_2 + g)$$

which is of the order of a 20% increase. By changing the geometry of the machine it is possible to obtain a higher power to weight ratio, a reduction in rotor inertia, a more efficient utilisation of the available space and a more efficient working of the magnetic circuit.

Double stator machines are not generally used in radial flux machines though there are exceptions, as for example in the a.c. drag cup generator⁽¹¹⁾. In this instance, however, the double stator is not used directly to improve the power to weight ratio. Its operation is such that a supply is fed into the outer stator. The rotor, which is a thin aluminium cup, is driven externally and an output is taken from the inner stator. This generator is used to obtain an output which is proportional to the speed of the rotor in an overall system in which the rotor inertia must be kept to a minimum. There are, however, a number of disadvantages in incorporating a double stator into a radial machine in order to obtain some of the good features evident in axial machines. The first is the dis-similarity of the two identifiable motors. Figure 1.3. shows in cross section the possible layout of a double stator induction motor. The flux bottleneck is still evident and the inner machine would inevitably have different input characteristics because:-

- 1) The active to inactive ratio of the winding is greater for the inner stator than for the outer.
- 2) It would be impractical to use the same number of slots of

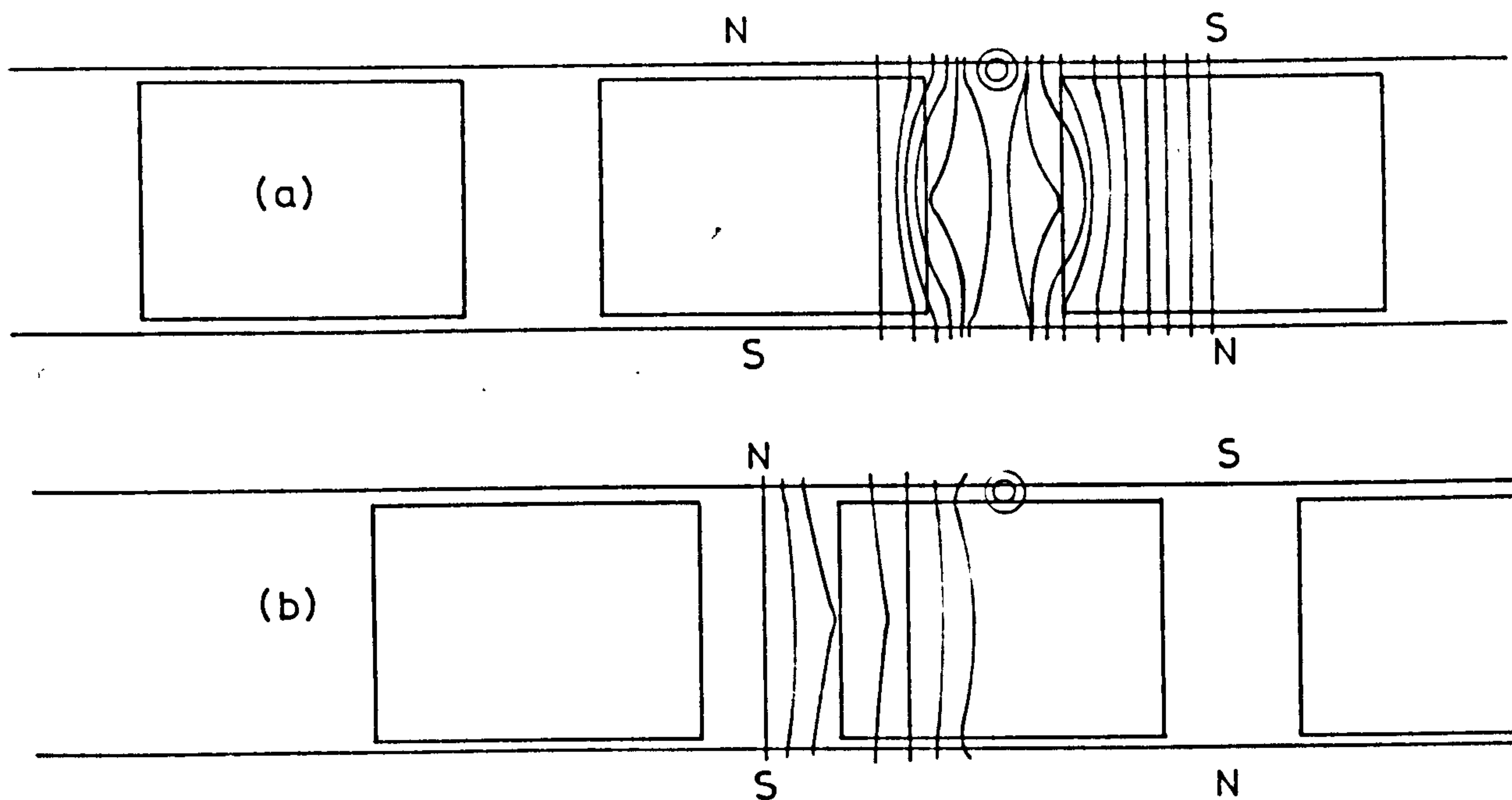


FIG 1.4 DEVELOPED DIAGRAM MAGNETIC CIRCUIT

(a) Direct Axis Position } Additive Stator
(b) Quadrature Axis } m.m.f's.

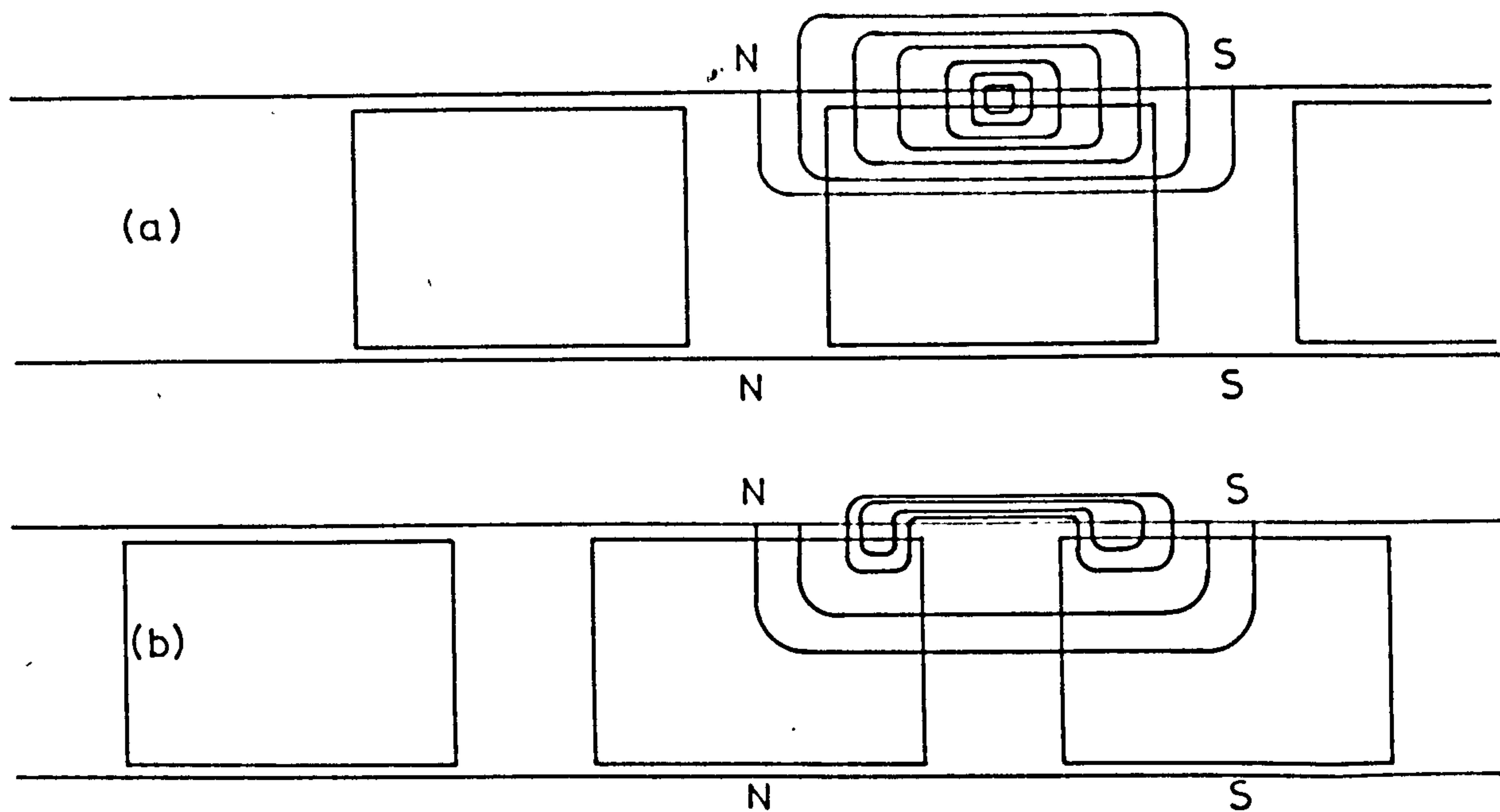


FIG 1.5. DEVELOPED DIAGRAM MAGNETIC CIRCUIT

(a) Direct Axis Position } Opposed Stator
(b) Quadrature Axis Position } m.m.f's.

identical size on each slot. This is demonstrated visually in Figure 1.3. where an extreme example of slot size and number of slots is used.

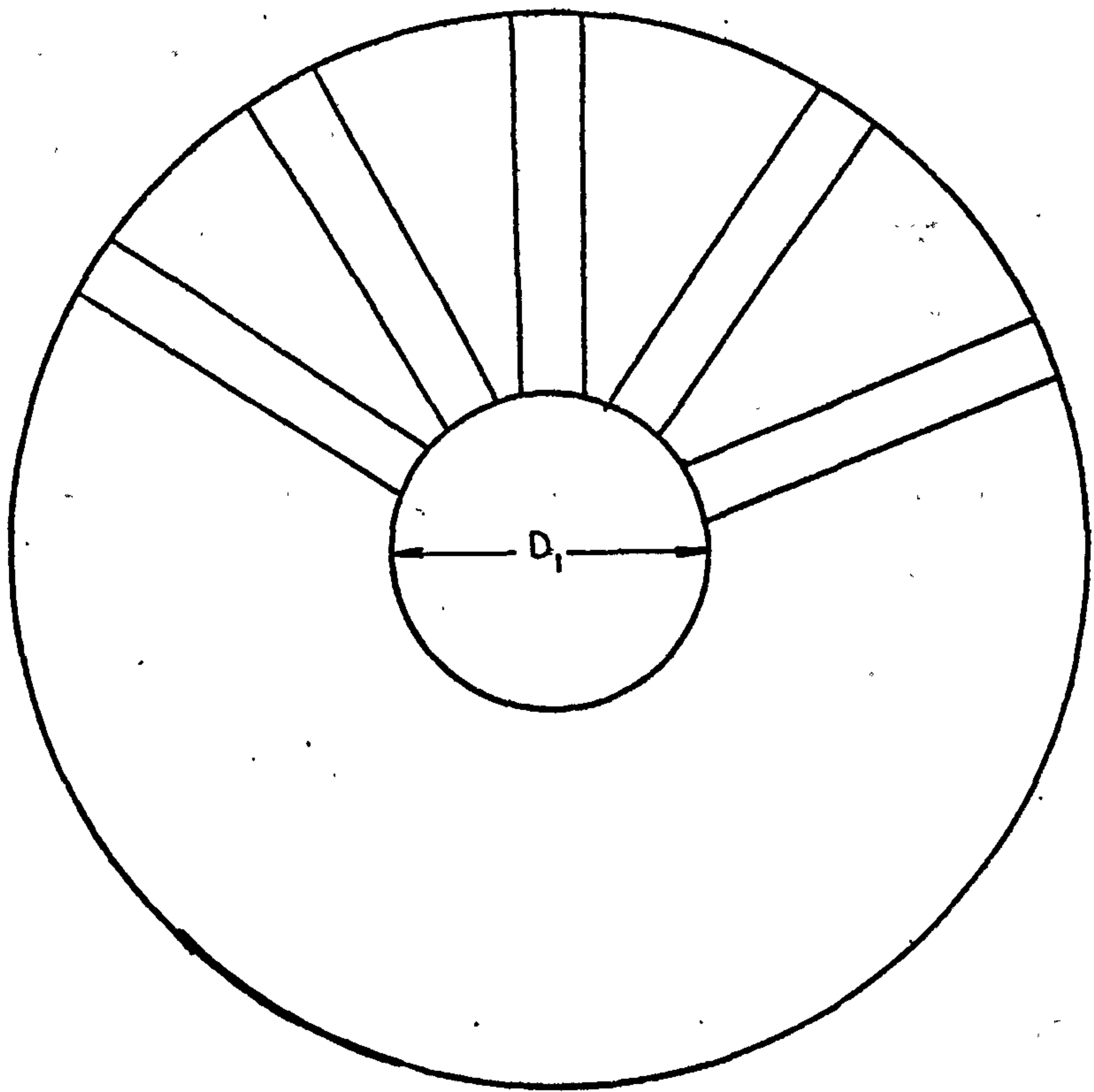
- 3) In order to maintain the same number of turns per slot on both stators, the inner stator would require a smaller diameter conductor.

Finally, the bearing arrangement tends to be cumbersome even for small frame motors.

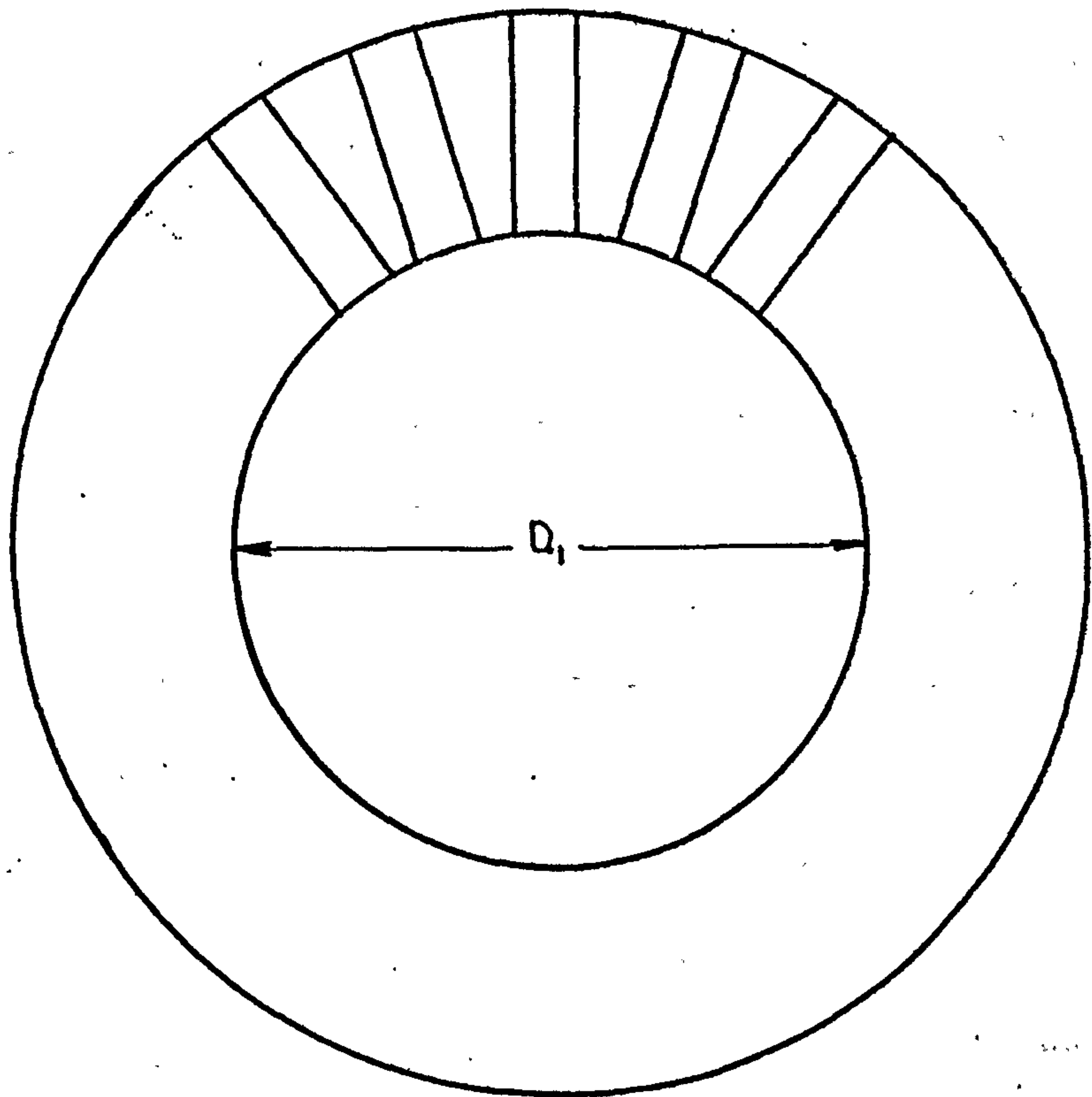
1.3.2. Operational Modes of the Double Stator Machines

It has been previously stated that the length of the machine will depend on whether or not the stator m.m.f.'s are in opposition. A further effect is in the change in performance. This is best demonstrated with the reluctance machine and in fact is more pertinent to this motor than to the induction motor.

Firstly, the situation arises in which the direct and quadrature axes of the rotor alters. By definition the direct axis is that in which the rotor must lie to make the reactance of the machine a maximum (X_d) while the quadrature axis is that in which the rotor must lie to give minimum reactance (X_q). Figure 1.4. shows the two axis positions for the condition when the stator m.m.f.'s are additive. The N, S, etc. pole system shown represents part of a p pole pair rotating m.n.f. wave set up by the stator windings. In this case, the main airgap flux crosses both airgaps and the rotor will be at zero potential relative to the stators at all times. In changing the stator potentials relative to each other, and this is effectively achieved by moving one stator through one half of a pole pitch, the situation of Figure 1.5 is obtained. It is clear that the direct and quadrature axis have now interchanged. Secondly, the rotor potential assumes some value other than zero as suggested by the field lines shown. This feature has been noted



(a)



(b)

Figure 1.6

Stator with two extreme values of D_1

by Lawrenson⁽³⁾ in the segmental machine, Cruickshank⁽¹²⁾ in the axial laminated anisotropic motor and several other authors. In this form the resemblance to the segmental rotor machine is apparent. Thirdly, the machine dimensions, notably the pole arc to pole pitch ratio and the axial length of the rotor will be different in order to obtain the best operating conditions. Finally, the inertia of the rotor and the weight of the machine will be increased. This is to enable the rotor, which now acts as a return path in the magnetic circuit, to carry the flux at a suitable working level.

1.3.3. Optimisation

The aim of the engineer is to optimise his design within certain terms of reference. Two radically different machines are obtained if for one the cost, volume and temperature rise and weight are unimportant while for the other machine these four parameters were to be kept below or within certain well defined limits. Both machines could well be optimised designs, though it would generally be accepted that the term would have more meaning in relation to the latter machine. It is evident, however, that the design is initially based on the required performance, that is the required efficiency, power, phase angle, etc. The design method for radial machines whether a.c. or d.c. has now become a well laid down procedure based on theoretical and/or empirical equations combined with experience on the engineer's part. In Chapter V similar equations are developed for the axial machine. In the type of work reported in this thesis, it is not necessary or indeed always possible to produce a machine which is in any sense of the word 'optimised'. If for the chosen machine size the output and input characteristics can be predicted, then it naturally follows that the optimum design can be produced using not only the theoretical equations but also the additional knowledge obtained from the experimental machine. It is important to note that in this experimental machine in which one of the variables is the pole arc to pole pitch ratio, it is not possible to optimise all

aspects of the design. It is well known that, for example, in reluctance machines, the maximum pull-in torque and maximum pull-out torque do not occur for the same value of pole arc to pole pitch ratio, yet in order to enhance either feature, different stator windings or squirrel cages could be necessary.

One of the most important parameters in the axial machine is the D_2/D_1 ratio where D_2 and D_1 are the outer and inner diameters of the stator (or rotor) respectively. In Figure 1.6 two stators are shown. In the first instance D_1 is small, giving a small number of slots, a large airgap cross sectional area and a high active to overhang length for the copper. For the second case D_1 is large and approaching D_2 . Consequently the number of slots can be increased to a much higher number, there is a smaller airgap cross sectional area, a small ratio of active to inactive copper and for the same physical airgap length the magnetic airgap is larger. It is apparent that the best value of D_1 lies somewhere between these two extremes.

Variation of D_1 is comparable to altering the airgap diameter D of radial machines. For both types the number of slots, size of slot, number of conductors and the amount of copper are directly affected. These in turn will determine the power of the machine, the efficiency, indeed all aspects of the performance. It is worthwhile noting that for axial machines the total weight and the inertia of the rotor is relatively independent of the value of D_1 whereas with radial machines the rotor mass and inertia are intimately related to the airgap diameter. The value of D_1 is not a variable in the experimental machine but the relationship between this diameter and all aspects of the machine performance is developed in Chapter V.

1.4. Conclusion

The experimental machine design has been influenced by several factors. A comparison between axial machines and radial machines was desired and since there are an abundance of the latter under 5 h.p. for

which performance figures are available, this seemed a sensible limitation to place on the output. Secondly, one of the best of modern reluctance machines is the segmental rotor version. Since one of the claims made for the axial machine is its better power to weight ratio, in order to make suitable comparisons on performance the physical size of the experimental machine should be similar to the segmental machine for which the performance is known. In order to conform to this requirement the overall diameters were made the same. This limits the major principal diameter D_2 which in turn influenced the number of stator slots and the type of winding.

Although the machine has two operational modes, only the mutually assisting m.m.f. condition was considered. The cost of producing the two basic rotor types, the production time and the testing required meant that only the one mode could be investigated fully. The final limitation on the machine design was the necessity to use suitable test procedures and the availability of equipment. There already existed in the department an excellent method of measuring shaft torques up to about 50 Nm. To complement this it was necessary to obtain a d.c. machine for loading the experimental machine. Again, in order to keep down the costs, a relatively small d.c. machine was purchased.

Chapter II

Theory Of "Axial Machines"

2.1 Introduction

The analysis is based on the fact that the airgap flux can be equated to the product of the m.m.f acting across the airgap and its permeance. The use of permeance waves is a fairly common procedure in the analysis of electrical machines and an attempt is made to assess the errors involved in using this concept. The analysis follows closely that of Gupta⁽¹³⁾ and Lawrenson⁽³⁾ who use the permeance wave concept to predict the performance of the segmental rotor machine. Modifications have necessarily been included to take account of the different shape of the axial machine. The remarks made concerning the accuracy of this method are only relevant to the analysis of the reluctance motor. For the induction motor the permeance of the airgap is represented by the average magnetic airgap. This is clarified in chapter III where the effects of the slotted airgap boundaries are simulated using Carters coefficient.

In all parts of the analysis only laminated stators and rotors are considered and the permeability of the iron is considered to be infinite. No attempt is made to determine the iron losses theoretically; these are obtained experimentally.

2.2 Assessment of analytical errors

The flux density wave is obtained by taking the product of the m.m.f acting across and the permeance of the airgap. This latter concept implies that the flux crosses the airgap in parallel straight lines as suggested by figure 2.1a. The airgap flux and hence density then becomes a square wave for a constant and uniform distribution of airgap m.m.f. (figure 2.1b). In practice such a situation is never encountered. Some of the flux in the interpolar region near the edges will bend into the airgap under the

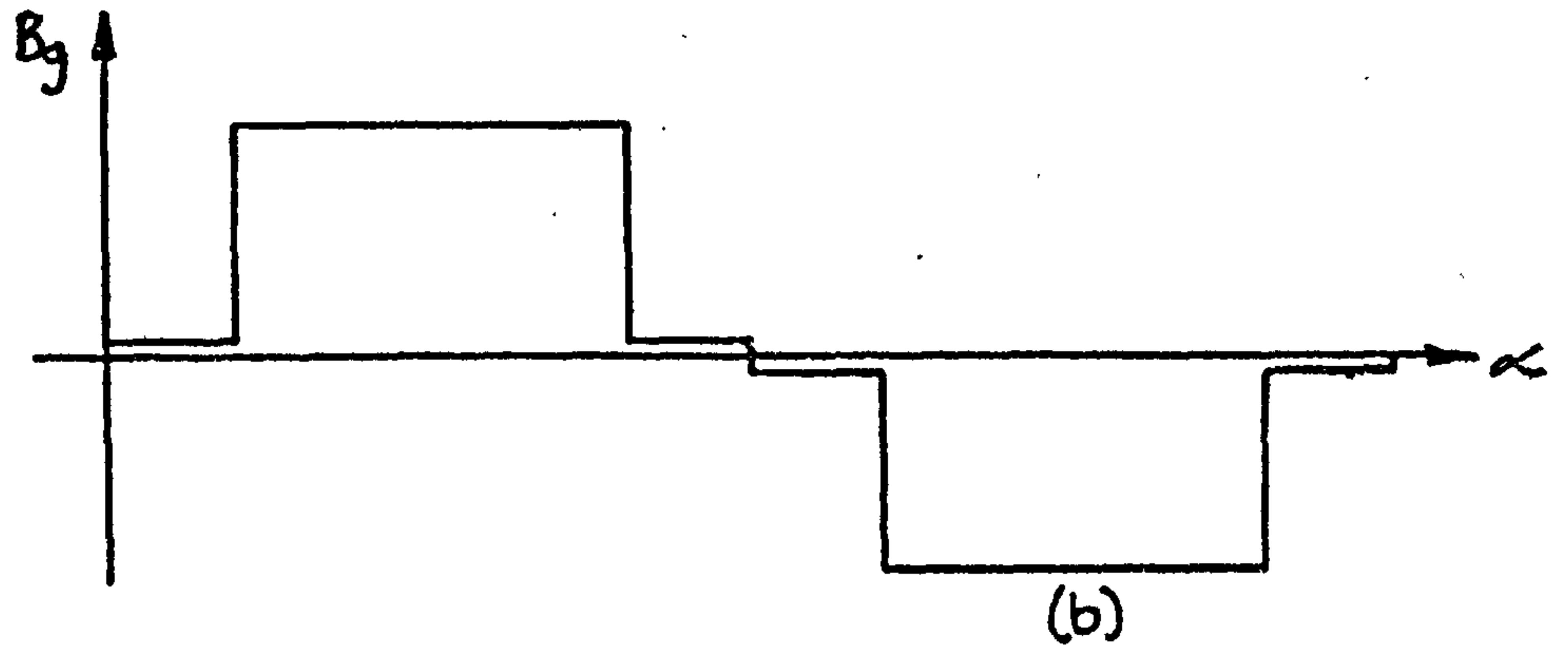
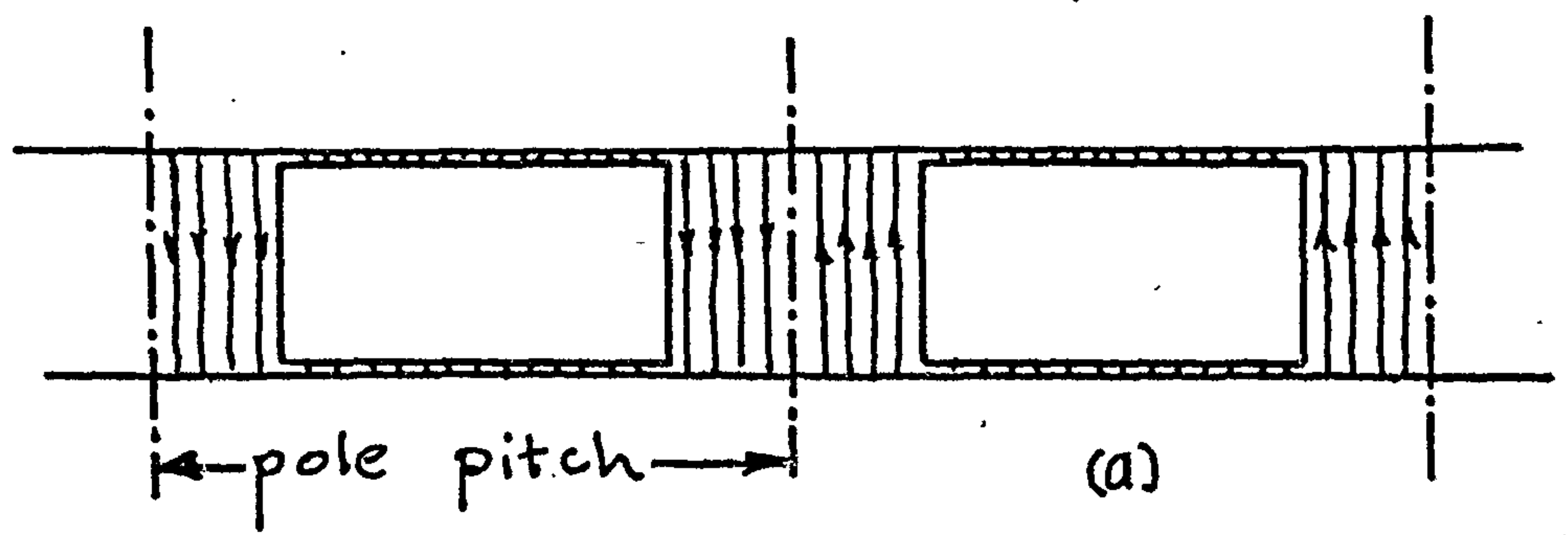


Figure 2.1 (a) Airgap field pattern
(b) Variation of B_g with angular position

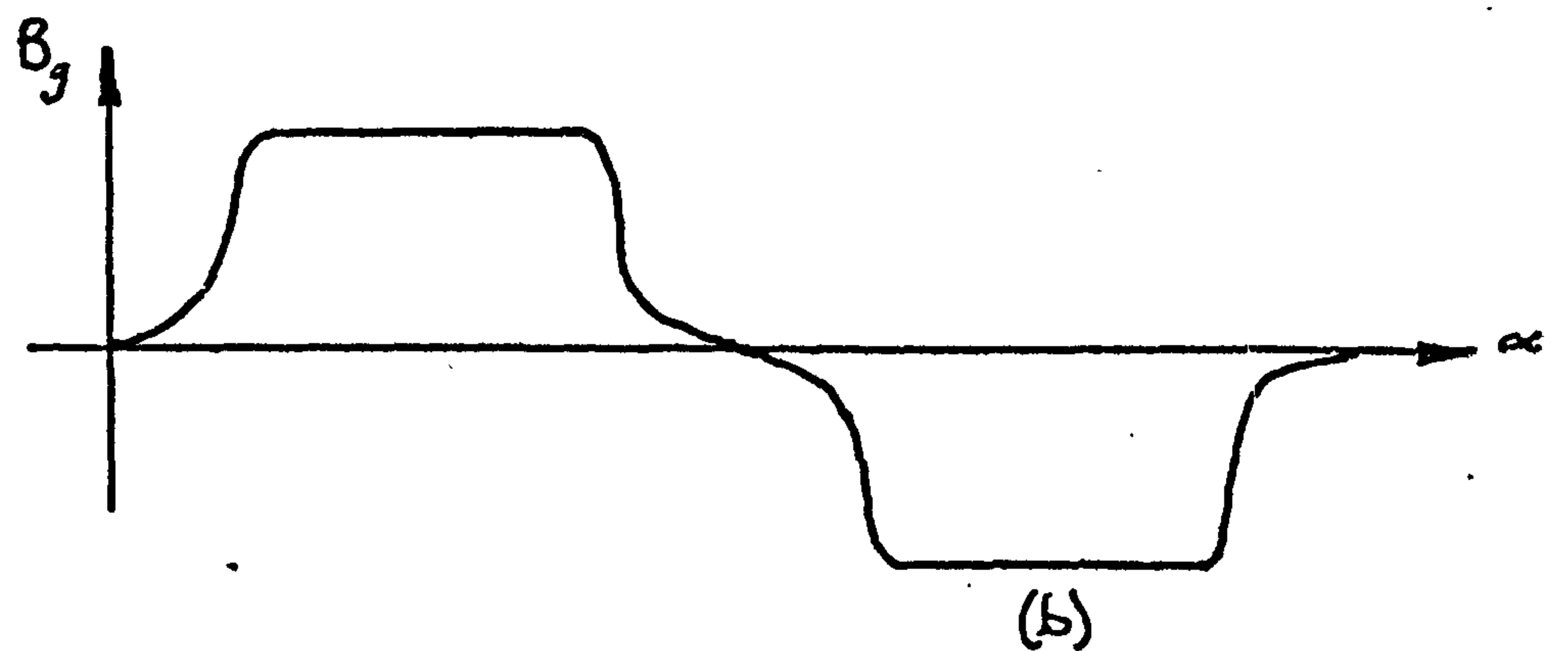
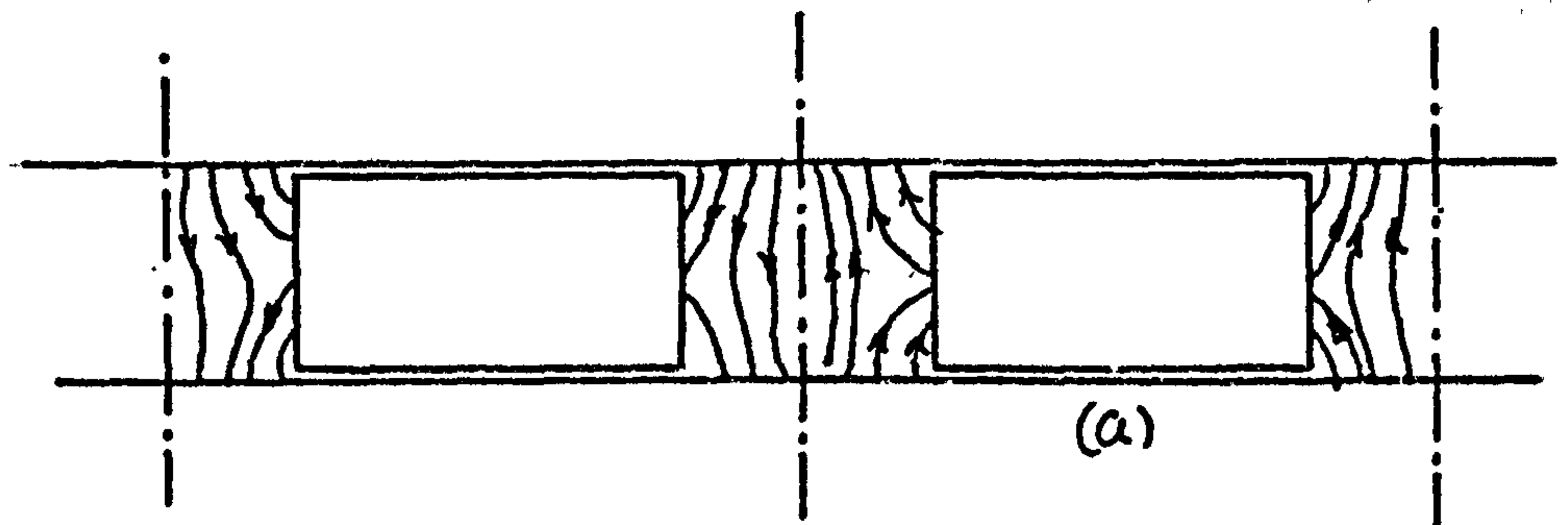
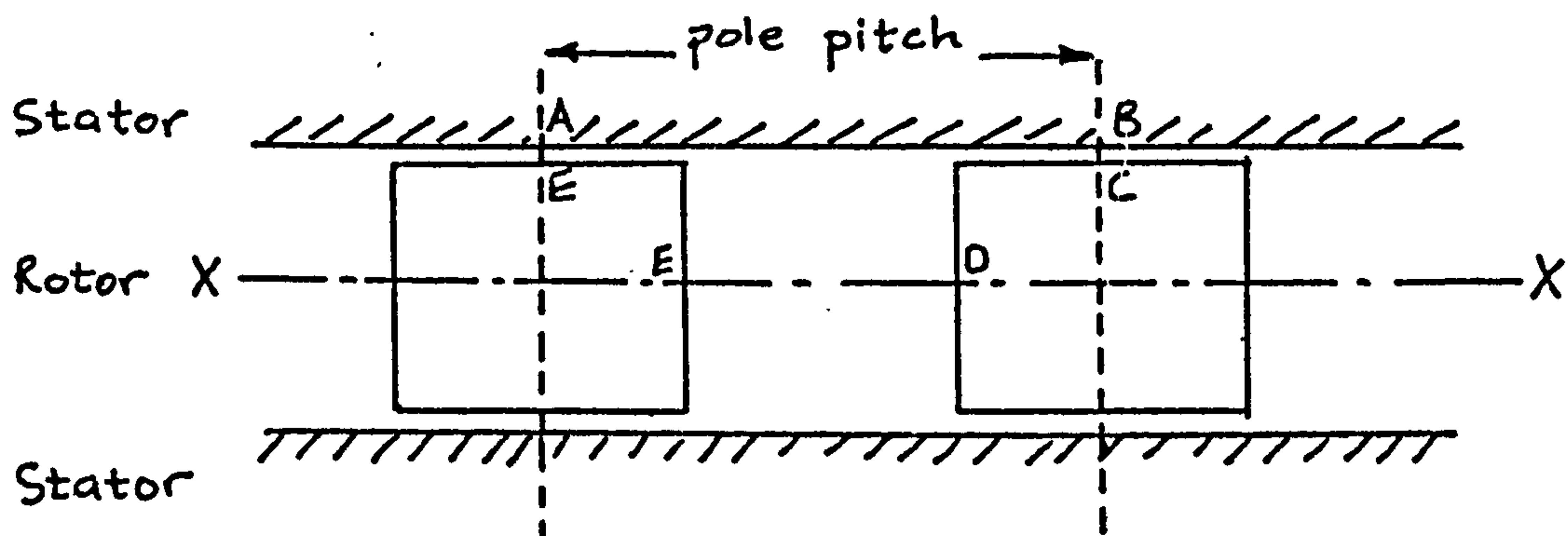


Figure 2.2 (a) Airgap field pattern
(b) Variation of B_g with angular position

poles and some will go to the sides of the poles as these paths represent regions of lower reluctance. This effect on the shape of the airgap flux distribution and waveform is shown in figures 2.2a and 2.2b. The accuracy of the analysis which uses the permeance wave will depend therefore on the differences suggested by the situations depicted by figures 2.1 and 2.2.

A completely accurate method of obtaining the airgap flux density is to use conformal transformation techniques. A large variety of airgap shapes and boundaries have been analysed using this method and these have been well documented^(14,15,16,17,). This method entails mapping the actual airgap which exists in say the Z-plane and in which the lines of flux and equipotentials are not regular, straight and parallel into a complex χ -plane in which the field is everywhere regular. This invariably requires two transformations and with increasing complexity of the airgap boundary the transformation equation will contain trigonometric, hyperbolic and/or elliptic functions.

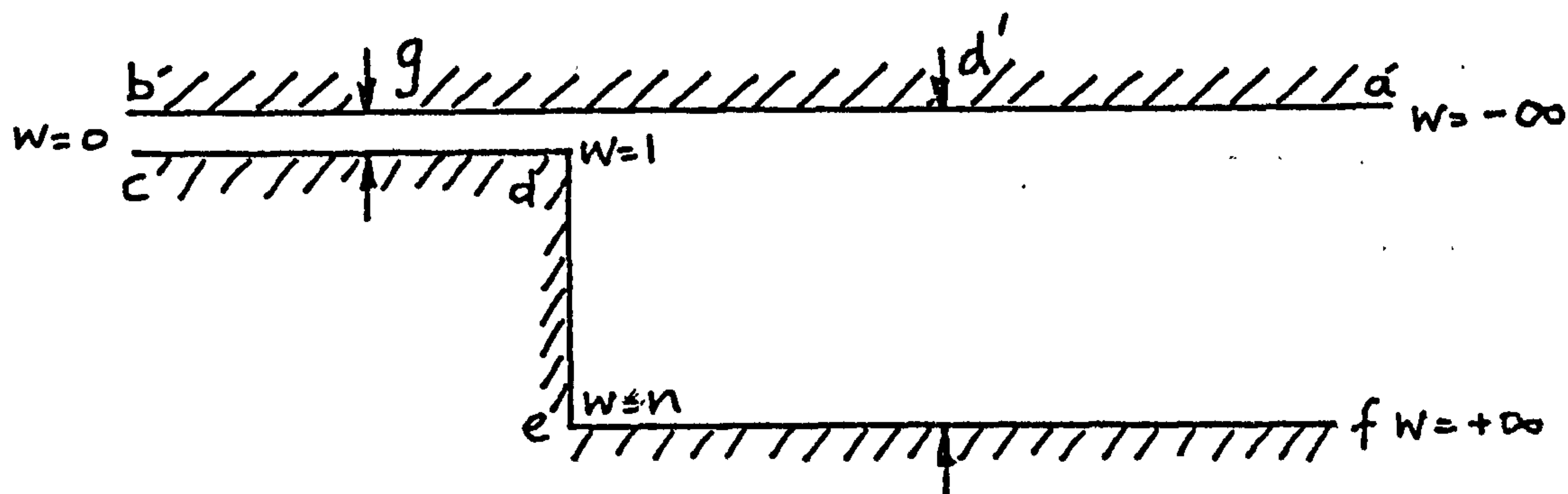


Developed Magnetic Diagram

Figure 2.3

The developed magnetic diagram (figure 2.3 above) of the axial machine is analytically complex. By making two valid assumptions, however, about the airgap the analysis is greatly simplified. Firstly, because of the

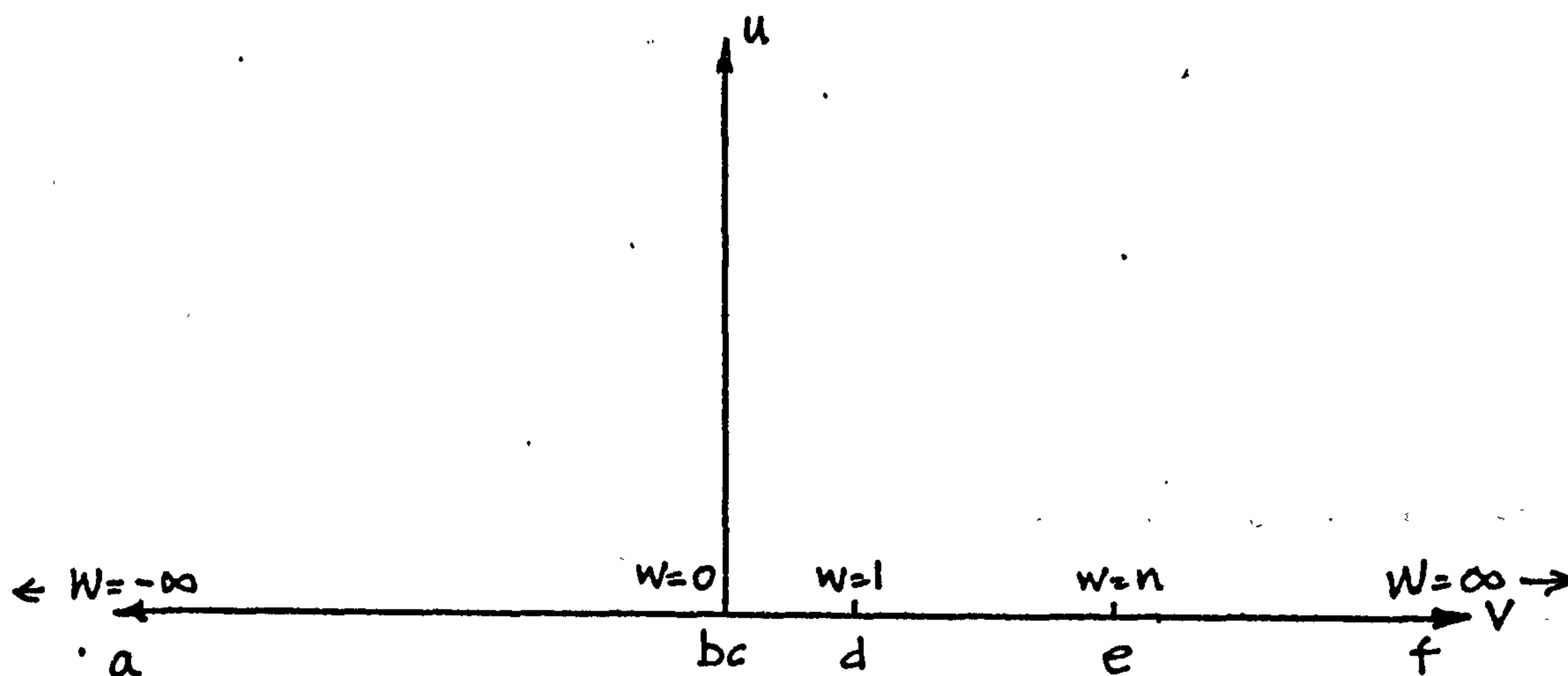
symmetry of the machine about XX (this represents a plane through the centre of the rotor) only a region such as ABCDEF needs to be mapped. Secondly, because the poles are generally remote from each other only one pole need be considered. The effect that these two assumptions have is shown in figure 2.4.



Section of airgap to be mapped

Figure 2.4

By using the Schwartz-Christoffel transformation the region abcdef can be mapped into the complex W-plane (figure 2.5).



Complex W-plane

Figure 2.5

The relationship between these two planes is given by,⁽¹⁷⁾

$$\frac{dZ}{dW} = \frac{k(W-1)}{W(W-n)} \quad (2.1)$$

hence,

$$\int dZ = k \int \frac{(W-1)dW}{W(W-n)} \quad (2.2)$$

where 'k' is a constant of proportionality.

Because of the common use of this transformation technique it is felt unnecessary to develop or expand upon equation (2.1). References (13) to (17) deal more fully with the mathematics involved.

Evaluation of 'k'

Crossing the airgap as x approaches infinity in the Z -plane is accompanied by movement around a large semicircle in the W -plane the equation of which is given by,

$$W = Re^{j\theta}$$

giving, $dW = jRe^{j\theta} d\theta$

and substitution of W and dW in equation (2.2) gives,

$$jd' = k \int_0^\pi \frac{(Re^{j\theta} - 1)^{1/2} jRe^{j\theta} d\theta}{(Re^{j\theta} - n)^{1/2} Re^{j\theta}}$$

hence, $jd' = k \int_0^\pi j d\theta$

and $k = d'/\pi$

Evaluation of 'n'

The value of 'n' is found by crossing the airgap as x approaches minus infinity. This is accompanied by movement in the W -plane as W approaches zero around a small semicircle given by,

$$W = re^{j\theta}$$

therefore, $jd' = \frac{d'}{\pi} \int_0^\pi \frac{(re^{j\theta} - 1)^{1/2} jre^{j\theta} d\theta}{(re^{j\theta} - n)^{1/2} re^{j\theta}}$

giving, $ig = \frac{d'}{\pi\sqrt{n}} \int_0^\pi j d\theta$

hence, $g = d'/(n)^{\frac{1}{2}}$

and, $n = (d'/g)^2$

Returning to equation (2.2) and using the substitution

$$p^2 = \frac{(W-n)}{(W-1)}$$

the new relationship for Z becomes,

$$Z = \frac{2d'(n-1)}{\pi} \int \frac{dp}{(p^2-n)(p^2-1)}$$

and performing the integration gives,

$$Z = \frac{d'}{\pi} \left[\log \frac{p+1}{p-1} + \frac{1}{\sqrt{n}} \log \frac{\sqrt{n}-p}{\sqrt{n}+p} \right] \quad (2.3)$$

It will be noticed that the field lines in the W-plane are not represented by parallel straight lines but rather by semicircles of increasing radii. To obtain a regular field a further transformation is required from the W-plane to the χ -plane shown in figure 2.6. In this plane the field lines are regular and parallel everywhere.

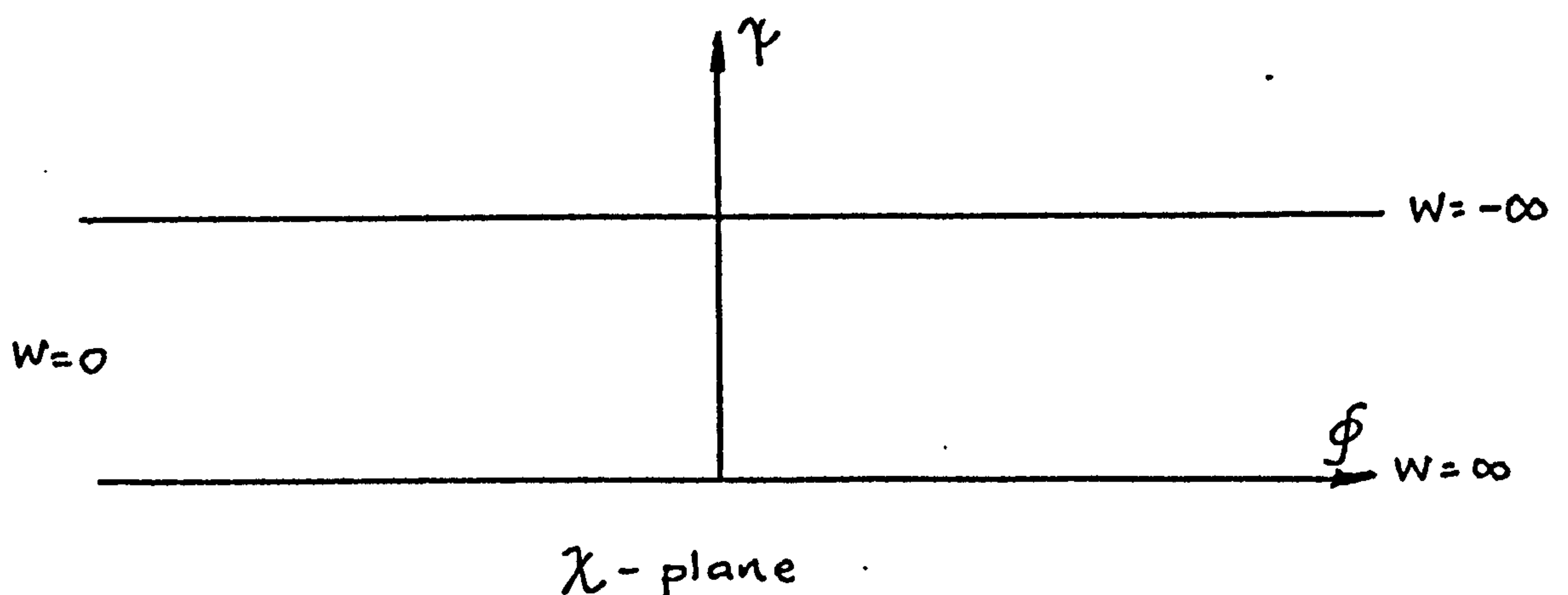


Figure 2.6

The transformation from the W-plane into the λ -plane is given by,

$$\frac{d\lambda}{dW} = \frac{M}{W} \quad (2.4)$$

and 'M' is evaluated with the same procedure used for 'n' in the first transformation. Hence,

$$M = 1/\pi$$

$$\text{and } \lambda = \frac{\log(W)}{\pi}$$

The flux density is given by the product of (2.4) and the reciprocal of (2.1), thus,

$$B = \mu \left| \frac{d\lambda}{dW} \cdot \frac{dW}{dZ} \right|$$

$$\text{giving, } B = \frac{1}{k\pi} \sqrt{\frac{(W-n)}{(W-1)}} \quad (2.5)$$

Equations (2.3) and (2.5) with the substitution for ' p^2 ' gives the variation of the flux density wave in the airgap in a region surrounding a pole edge. This is shown in figure 2.7 for a physical gap, $g=0.5\text{mm}$ and $d'=14\text{mm}$. It can be seen that a movement of 0.5mm under the pole of the machine gives a flux density that is within 0.1% of its maximum value and that 5mm movement away from the edge of the pole gives a flux density that is within 5% of the minimum of the permeance wave. The value of the flux density using the permeance wave is simply proportional to the reciprocal of the distance between the equipotentials 'ab' and 'cdef' shown in figure 2.4. The maximum (100%) is proportional to $(1/g)$ and the minimum to $(1/d')$.

In fact the second assumption that the poles are generally remote from each other for this machine is now seen to be valid provided the minimum circumferential distance is greater than 10mm between the poles. For this machine this minimum distance will occur at the inner diameter (D_1) when

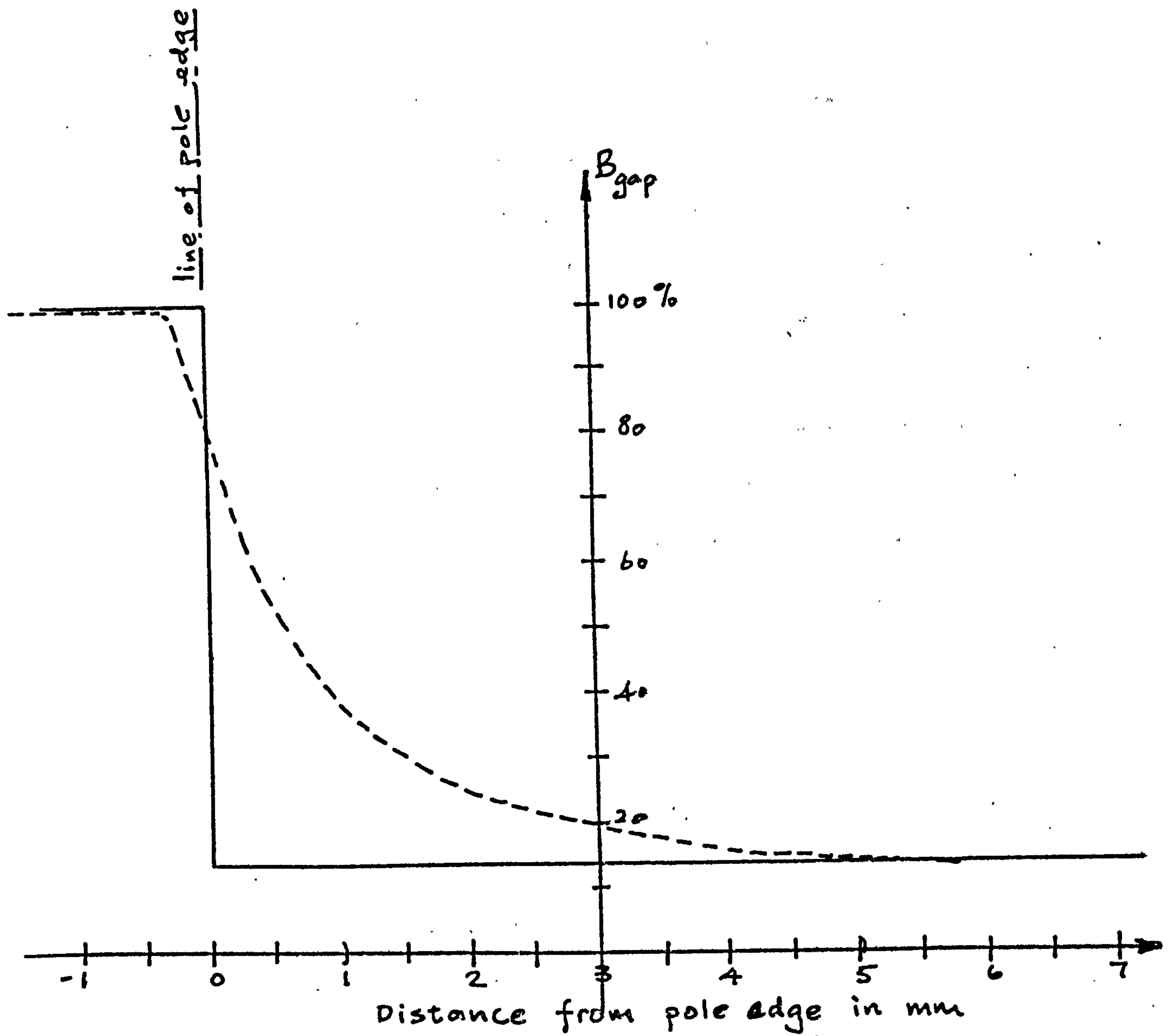


Figure 2.7

Comparison of B_g along the stator surface in the vicinity of a pole edge using Permeance wave (full line) and conformal transformation (dashed line)

the pole arc/pole pitch ratio is equal to 0.85.

A method of determining the errors involved by using the permeance wave is to compare the magnitudes of the harmonics in both waveforms. A wide range of pole arc/pole pitch ratios (β) is considered and for any given value of this parameter, different regions of the airgap corresponding to different radii (lying between the principal diameters) are analysed. Low values of β are seen to have the highest harmonic content for both the permeance wave and the waveform obtained using the conformal transformation. This is to be expected since for these conditions the angle over which the maximum occurs is small in proportion to the pole pitch. The greatest differences between the harmonic contents of the two waves occurs at higher values of β . However for such values the magnitudes are themselves generally much smaller than the fundamental.

The following table (table 2.1) shows the comparison between the harmonics and in every case the fundamentals have been set to unity. In fact there is a difference between the fundamentals of the two waveforms but this is never more than 5% for any of the given machine parameters. The % column is the ratio of the permeance wave harmonic (pwh) divided by the conformal harmonic (cth). The majority of the harmonics obtained from the permeance wave are within 15% of the corresponding transformation harmonic. In view of their relative magnitudes it is felt that where the effects of high frequency are not being investigated the permeance wave method is justified. In the analysis of the axial machine it is only the fundamental component that is used and the effects of the harmonics in the form of iron losses is obtained experimentally. In the experimental machine the pole arc to pole pitch ratio is confined to the range $0.8 \geq \beta \geq 0.45$.

n	pwh	cth	%	cth	%	cth	%
1	1.000	1.000	1.000	1.000	1.000	1.000	1.000
3	0.757	0.751	1.009	0.755	1.004	0.756	1.002
5	0.712	0.660	1.079	0.678	1.05	0.687	1.036
7	0.509	0.421	1.207	0.450	1.130	0.466	1.093
9	0.366	0.249	1.465	0.285	1.283	0.305	1.201
11	0.164	0.049	3.372	0.080	2.042	0.099	1.659
13	0.033	0.060	0.546	0.039	0.833	0.025	1.289
$\beta = 0.15$		R = 50mm		R = 70mm		R = 90mm	
1	1.000	1.000	1.000	1.000	1.000	1.000	1.000
3	0.397	0.358	1.109	0.370	1.073	0.376	1.055
5	0.101	0.132	0.766	0.124	0.813	0.120	0.844
7	0.210	0.181	1.158	0.192	1.096	0.197	1.068
9	0.019	0.056	0.334	0.046	0.400	0.041	0.456
11	0.127	0.108	1.183	0.116	1.096	0.120	1.059
13	0.030	0.011	2.816	0.004	69.94	0.006	5.000
$\beta = 0.45$		R = 50mm		R = 70mm		R = 90mm	
1	1.000	1.000	1.000	1.000	1.000	1.000	1.000
3	0.263	0.277	0.949	0.274	0.961	0.272	0.968
5	0.083	0.106	0.781	0.100	0.827	0.097	0.858
7	0.006	0.023	0.264	0.015	0.405	0.010	0.584
9	0.054	0.024	2.221	0.033	1.625	0.038	1.415
11	0.074	0.048	1.526	0.057	1.298	0.061	1.202
13	0.073	0.056	1.299	0.063	1.161	0.066	1.102
$\beta = 0.85$		R = 50mm		R = 70mm		R = 90mm	

Table 2.1

2.3 Airgap Flux

The following assumptions, general in machine analysis, are made.

- (1) The current in every slot is concentrated at the intersection of the slot centre line and the boundary of the iron surface.
- (2) The effect of the slot opening on the winding factor can be ignored. This is discussed more fully in chapter III.
- (3) The airgap is represented by the "average magnetic airgap".
- (4) The stator and rotor surfaces are parallel.
- (5) The iron has infinite permeability, hence the magnetic circuit is considered linear.
- (6) The flux crosses the airgap in parallel straight lines in an axial direction.

The permeance, as a function of α , of an elemental strip dR wide at a radius R is obtained fully in Appendix I and is given by,

$$P_r = \frac{\mu_0 R dR}{g'(h+g')} \left[\frac{\beta h + g'}{2} + \frac{h}{\pi} \sum_{n=1}^{\infty} \frac{\sin n\beta\pi \cos 2np(\alpha - \theta)}{n} \right] \quad (2.6)$$

and therefore the total airgap permeance becomes,

$$P_t = \int_{D_1/2}^{D_2/2} P_r dR$$

giving,

$$P_t = \frac{\mu_0 (D_2^2 - D_1^2)}{8g'(h+g')} \left[\frac{\beta h + g'}{2} + \frac{h}{\pi} \sum_{n=1}^{\infty} \frac{\sin n\beta\pi \cos 2np(\alpha - \theta)}{n} \right] \quad (2.7)$$

Both stators accomodate standard double layer three phase windings. The m.m.f of the winding is found by Fourier analysing the product of the current and the turns distribution⁽¹⁸⁾. This is a standard procedure and since the m.m.f of both stator windings are mutually additive the m.m.f acting across the total airgap is given by,

$$\begin{aligned} \text{m.m.f} = \frac{6NI}{\pi} & \left[K_1 \cos(p\alpha - wt) + \sum_{k=1}^{\infty} (-1)^k \frac{K_{6k+1}}{6k+1} \cos(p\alpha(6k+1) - wt) \right. \\ & \left. - \sum_{k=1}^{\infty} (-1)^k \frac{K_{6k-1}}{6k-1} \cos(p\alpha(6k-1) - wt) \right] \quad (2.8) \end{aligned}$$

In this expression for the m.m.f,

$$i_1 = I \cos(\omega t)$$

is the magnetising component of current in phase 1. In the expression for P_t , g' is the average magnetic airgap length between one stator and one rotor. The developed model of the airgap (figure 2.8) shows that the instantaneous displacement between the axis of phase 1 and the nearest pole centre line is equal to θ

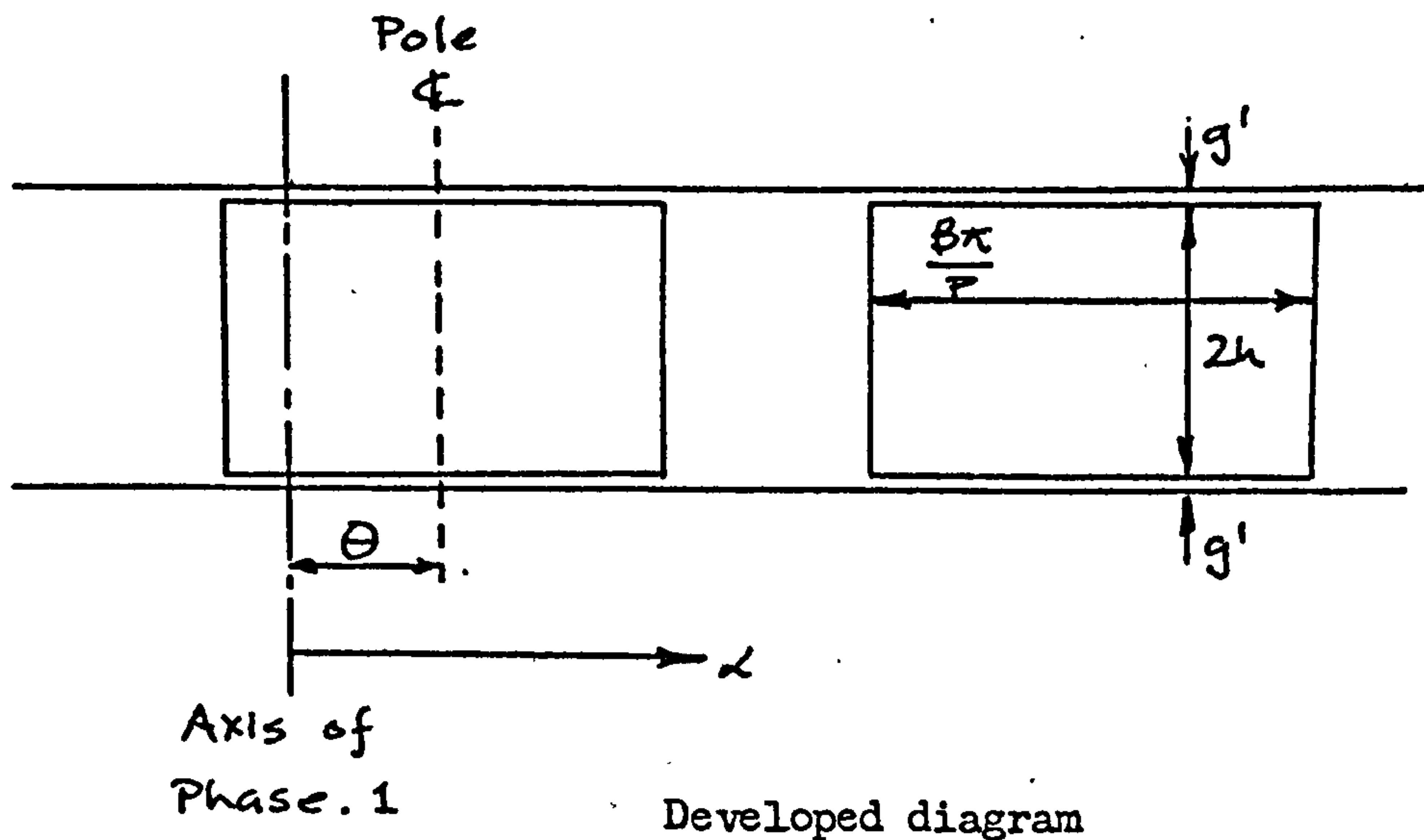


Figure 2.8

Consequently for a rotor moving at ω_r mech rads/sec

$$\theta = \omega_r t + \delta$$

where δ is the angular displacement between the pole centre line and the axis of phase 1 at $t = 0$.

But since $\omega_r = \frac{(1-s)\omega}{p}$

$$\text{then } \theta = \frac{(1-s)\omega t}{p} + \delta$$

Multiplying equation (2.7) by (2.8) and using the substitution for θ , gives the airgap flux as a function of α . The angle α is defined as the position in the airgap of the machine relative to the axis of phase 1. The airgap flux is given below in equation (2.9)

$$\begin{aligned}
\phi_\alpha = & \left[\frac{\mu_0(D_2^2 - D_1^2) \cdot 3NI}{4\pi g'(h+g')} \right] x \\
& \left[\frac{Bh+g'}{2} + \frac{h}{\pi} \sum_{n=1}^{\infty} \frac{\sin \beta \pi}{n} \cos 2np \left(\alpha - (1-s) \frac{\omega t}{P} - \delta \right) \right] x \\
& \left[K_1 \cos(p\alpha - \omega t) + \sum_{k=1}^{\infty} (-1)^k \frac{K_{6k+1}}{6k+1} \cos(p\alpha(6k+1) - \omega t) \right. \\
& \quad \left. - \sum_{k=1}^{\infty} (-1)^k \frac{K_{6k-1}}{6k-1} \cos(p\alpha(6k-1) - \omega t) \right]
\end{aligned}$$

(2.9)

$$\text{let } C = \frac{3\mu_0(D_2^2 - D_1^2)N(Bh+g')K_1}{8\pi g'(h+g')}$$

$$\text{and } D = \frac{3\mu_0(D_2^2 - D_1^2)NhK_1}{4\pi^2 g'(h+g')}$$

then,

$$\begin{aligned}
\phi_\alpha = & IC \cos(p\alpha - \omega t) + ID \sum_{n=1}^{\infty} \frac{\sin n\beta\pi}{n} \cos(p\alpha - \omega t) \cos 2np \left(\alpha - \frac{\omega t}{P} (1-s) - \delta \right) \\
& + \frac{IC}{K_1} \sum_{k=1}^{\infty} (-1)^k \left[\frac{K_{6k+1}}{6k+1} \cos(p\alpha(6k+1) - \omega t) - \frac{K_{6k-1}}{6k-1} \cos(p\alpha(6k-1) - \omega t) \right] \\
& + \frac{ID}{K_1} \sum_{n=1}^{\infty} \sum_{k=1}^{\infty} \frac{\sin n\beta\pi \cdot K_{6k+1}}{n(6k+1)} \cos 2np \left(\alpha - \frac{\omega t}{P} (1-s) - \delta \right) \cos(p\alpha(6k+1) - \omega t) \\
& - \frac{ID}{K_1} \sum_{n=1}^{\infty} \sum_{k=1}^{\infty} \frac{\sin n\beta\pi \cdot K_{6k-1}}{n(6k-1)} \cos 2np \left(\alpha - \frac{\omega t}{P} (1-s) - \delta \right) \cos(p\alpha(6k-1) - \omega t)
\end{aligned}$$

Rearranging and combining like terms gives,

$$\begin{aligned}
 \phi_a = & IC \cos(p\alpha - \omega t) + \\
 & \frac{ID}{2} \sum_{n=1}^{\infty} \frac{\sin n\beta\pi}{n} \left[\cos(p\alpha(2n+1) - \omega t(2n-2ns+1) - 2np\delta) + \right. \\
 & \left. \cos(p\alpha(2n-1) - \omega t(2n-2ns-1) - 2np\delta) \right] + \\
 & \frac{IC}{K_1} \sum_{k=1}^{\infty} (-1)^k \left[\frac{K_{6k+1}}{6k+1} \cos(p\alpha(6k+1) - \omega t) - \frac{K_{6k-1}}{6k-1} \cos(p\alpha(6k-1) - \omega t) \right] + \\
 & \sum_{n=1}^{\infty} \frac{ID}{2K_1} \sum_{k=1}^{\infty} \frac{(-1)^k K_{6k+1} \sin n\beta\pi}{n(6k+1)} \left[\cos(p\alpha(2n+6k+1) - \omega t(2n-2ns+1) - 2np\delta) + \right. \\
 & \left. \cos(p\alpha(2n-6k+1) - \omega t(2n-2ns-1) - 2np\delta) \right] - \\
 & \sum_{n=1}^{\infty} \frac{ID}{2K_1} \sum_{k=1}^{\infty} \frac{(-1)^k K_{6k-1} \sin n\beta\pi}{n(6k-1)} \left[\cos(p\alpha(2n+6k-1) - \omega t(2n-2ns+1) - 2np\delta) + \right. \\
 & \left. \cos(p\alpha(2n-6k+1) - \omega t(2n-2ns-1) - 2np\delta) \right] \quad (2.10)
 \end{aligned}$$

This expression for ϕ_a contains a fundamental and an infinite series of harmonics. It can be seen how the harmonic content is influenced by the rotor speed. The total flux per pole is given by the integral of $\phi_a d\alpha$ between the limits $(-\pi/2p)$ and $(\pi/2p)$ hence,

$$\begin{aligned}
 \phi_T = & \frac{2IC}{P} \left[1 + \sum_{k=1}^{\infty} \frac{K_{6k+1}}{K_1(6k+1)^2} + \sum_{k=1}^{\infty} \frac{K_{6k-1}}{K_1(6k-1)^2} \right] \cos \omega t + \\
 & \frac{ID}{P} \sum_{n=1}^{\infty} \frac{(-1)^n \sin n\beta\pi}{n} \left[\frac{\cos(\omega t(2n-2ns+1) + 2np\delta)}{2n+1} - \frac{\cos(\omega t(2n-2ns-1) + 2np\delta)}{2n-1} \right] + \\
 & \frac{ID}{PK_1} \sum_{n=1}^{\infty} \sum_{k=1}^{\infty} \frac{(-1)^n \sin n\beta\pi K_{6k+1}}{n(6k+1)} \left[\frac{\cos(\omega t(2n-2ns+1) + 2np\delta)}{2n+6k+1} - \frac{\cos(\omega t(2n-2ns-1) + 2np\delta)}{2n-6k-1} \right] + \\
 & \frac{ID}{PK_1} \sum_{n=1}^{\infty} \sum_{k=1}^{\infty} \frac{(-1)^n \sin n\beta\pi K_{6k-1}}{n(6k-1)} \left[\frac{\cos(\omega t(2n-2ns+1) + 2np\delta)}{2n+6k+1} - \frac{\cos(\omega t(2n-2ns-1) + 2np\delta)}{2n-6k-1} \right] \quad (2.11)
 \end{aligned}$$

In their present form equations (2.10) and (2.11) are extremely cumbersome. However, they are easily simplified and depending on machine and speed range to be analysed will be reduced to more easily manipulated relationships

2.4 Induction Motor Performance

2.4.1. Airgap Flux

Since the induction motor does not have a salient pole rotor the air-gap flux is obtained by substituting for $\beta = 1$ into equation (2.10), hence,

$$\phi_\alpha = \left[\frac{3\mu_0 (D_2^2 - D_1^2) NI}{8\pi g'} \right] \times \left[K_1 \cos(p\alpha - \omega t) + \sum_{k=1}^{\infty} (-1)^k \frac{K_{6k+1}}{6k+1} \cos(p\alpha(6k+1) - \omega t) - \sum_{k=1}^{\infty} (-1)^k \frac{K_{6k-1}}{6k-1} \cos(p\alpha(6k-1) - \omega t) \right]$$

Now $K_1 \gg \frac{K_{6k+1}}{6k+1}, \frac{K_{6k-1}}{6k-1}$

hence,

$$\phi_\alpha = IC' \cos(p\alpha - \omega t) \quad \text{where } C' = \frac{3\mu_0 (D_2^2 - D_1^2) K_1 N}{8\pi g'}$$

therefore the total flux per pole is,

$$\phi_T = \int_{-\pi/2p}^{\pi/2p} \frac{2IC'}{p} \cos(p\alpha - \omega t) d\alpha$$

Consequently the average flux density per pole becomes,

$$B_{ave} = \frac{2IC'}{pA_p} \quad \text{where } A_p = \text{pole area} = \frac{\pi(D_2^2 - D_1^2)}{4p}$$

therefore the peak of flux density becomes,

$$B_{peak} = \frac{8IC'}{(D_2^2 - D_1^2)}$$

and the flux density variation as a function of α and B_{peak} becomes,

$$B_\alpha = \frac{4IC'}{(D_2^2 - D_1^2)} \cos(p\alpha - \omega t) \quad (2.12)$$

This expression for B_α is used in obtaining the turns ratio of the induction motor and the bar currents in the squirrel cage.

2.4.2 Torque/Speed relationship

Relative to an imaginary stationary B_{α} wave, the rotor moves backwards at a speed equal to $-sw_s$ rads/sec. By considering an elemental length dR at radius R of one of the squirrel cage bars the e.m.f induced in the element due to relative motion between the bar and B_{α} is,

$$\begin{aligned} de &= -sw_s B_{\alpha} R dR \\ &= \frac{-sw B_{\alpha} R dR}{p} \end{aligned}$$

therefore the e.m.f induced across the whole bar is,

$$\begin{aligned} E &= \int de \\ &= \frac{-sw(D_2^2 - D_1^2) B_{\alpha}}{8p} \end{aligned}$$

Substitution for B_{α} from equation (2.12) gives,

$$E = \frac{-IC' sw}{p} \cos(p\alpha)$$

or, $E = \hat{E} \cos(p\alpha)$

The current in this bar is equal to the e.m.f divided by the impedance of the cage associated with the bar. This is determined in Appendix II and is seen to be equal to the sum of the bar impedance and part of the inner and outer end rings. Let $(r + jsx)$ be this bar load impedance, then,

$$i_b = \frac{-IC' sw \cos(p\alpha - \theta_b)}{p(r^2 + (sx)^2)^{\frac{1}{2}}} \quad (2.13)$$

where θ_b = bar load impedance phase angle. Therefore,

$$i_b = \frac{-IC' w \cos(p\alpha - \theta_b)}{p((r/s)^2 + x^2)^{\frac{1}{2}}}$$

The force on the element dR is,

$$dF = B_{\alpha} i_b dR$$

and the torque is,

$$dT = B_{\alpha} i_b R dR$$

consequently the torque on the bar becomes,

$$T = \int_{D_1/2}^{D_2/2} B_{\alpha} i_b R dR$$

giving,

$$T = \frac{(IC')^2 w \cos(p\alpha - \theta_b) \cos(p\alpha)}{pZ_b}$$

where $Z_b = ((r/s)^2 + x^2)^{\frac{1}{2}}$

and r and x are the values at $s = 1$

The average torque on the bar then becomes,

$$T_{ave} = \frac{(IC')^2 w \cos\theta_b}{2pZ_b}$$

$$\text{but } \cos\theta_b = \frac{(r/s)}{((r/s)^2 + x^2)^{\frac{1}{2}}}$$

therefore,

$$T_{ave} = \frac{(IC')^2 w \cdot \frac{r}{s}}{2pZ_b^2}$$

For n_b rotor bars the total torque available at the shaft is,

$$T_t = \left[\frac{IC' w}{pZ_b} \right]^2 \frac{p r n_b}{2 s w} \quad \text{Nm} \quad (2.14)$$

2.4.3 Magnetising Reactance

The voltage induced in phase 1 by the airgap flux is given by,

$$\begin{aligned} e_{\text{phase}} &= -2pNK_1 \frac{d}{dt} \left[\int_{-\pi/2p}^{\pi/2p} \phi_{\alpha} d\alpha \right] \\ &= -2pNK_1 \frac{d\phi_r}{dt} \end{aligned}$$

Equation (2.11) gives ϕ_r and this is simplified by putting $\beta = 1$ and ignoring all harmonics as these are negligible, hence,

$$\begin{aligned} e_{\text{phase}} &= -2pNK_1 \frac{d(2IC' \cos wt)}{dt} \\ &= 4NK_1 C' I_w \sin wt \end{aligned}$$

This component of voltage is the e.m.f induced across the magnetising reactance of the machine and is opposed by a component of the supply, v , hence,

$$v = -4NK_1 C' I_w \sin wt$$

But the magnetising current was previously defined as,

$$i_1 = I \cos wt$$

$$\text{giving, } \frac{di_1}{dt} = -wI \sin wt$$

$$\text{and } v = 4NK_1 C' \frac{di}{dt}$$

in which can be recognised the magnetising reactance of the machine,

$$x_m = 4NwK_1 C' \quad (2.15)$$

Substitution for wC' in equation (2.14) gives,

$$T_t = \left[\frac{Ix_m}{4pNK_1 Z_b} \right]^2 \frac{prn_b}{2sw}$$

In this equation the current I is the peak value of the magnetising current therefore substitution for I_m the r.m.s value gives,

$$T_t = \left[\frac{I_m x_m}{4pZ_b NK_1} \right]^2 \frac{prn_b}{sw} \quad \text{Nm} \quad (2.16)$$

and the total power as,

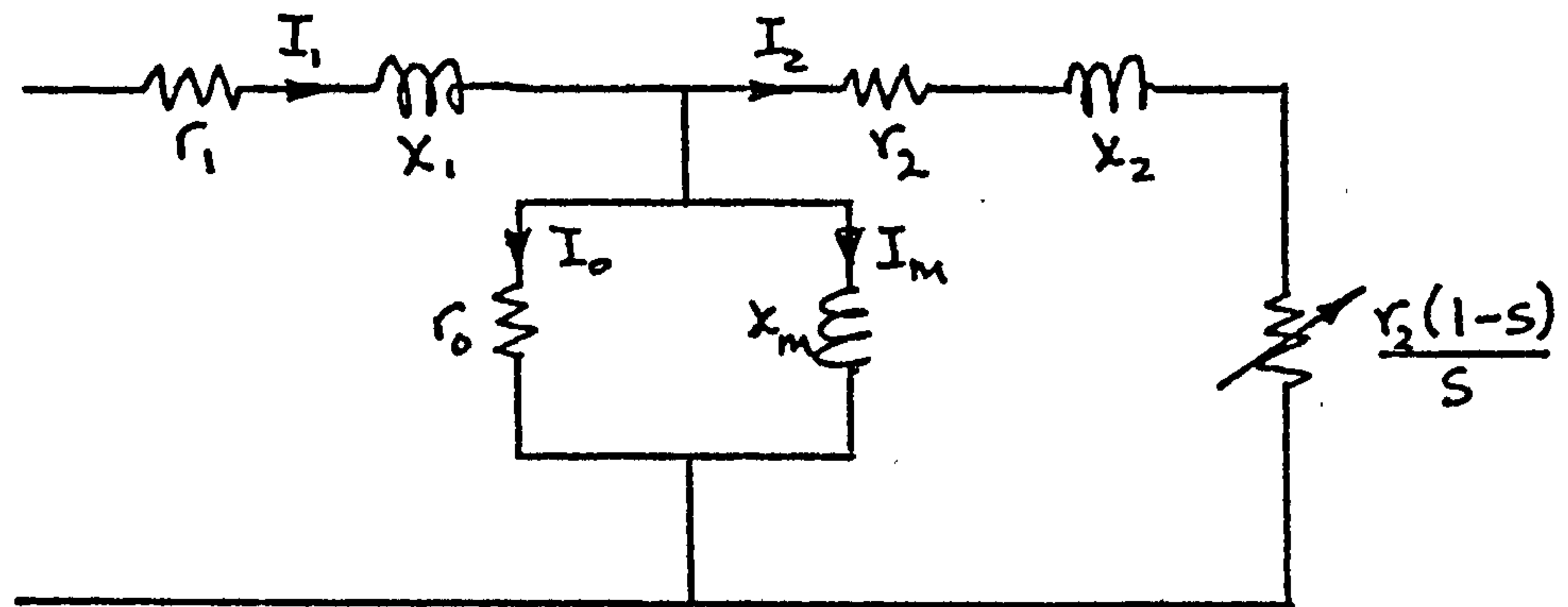
$$P_t = \left[\frac{I_m x_m}{4pZ_b NK_1} \right]^2 \frac{r(1-s)n_b}{s} \quad \text{Watts} \quad (2.17)$$

The turns ratio of the machine can now be obtained from the equivalent circuit by equating the the effective shaft power to equation (2.17)

2.4.4 Turns Ratio of Squirrel Cage Motor

The equivalent circuit on a per phase basis is shown below and using this equivalent circuit the power developed per phase is given by,

$$P_p = \frac{I_2^2 r_2 (1-s)}{s}$$



But, $I_2 \left(\frac{r_2}{s} + jx_2 \right) = jI_m x_m$

therefore substitution for I_2 in the expression for P_p gives,

$$P_p = \left(\frac{I_m x_m}{\frac{r_2}{s} + jx_2} \right)^2 r_2 \frac{(1-s)}{s} \quad (2.18)$$

Dividing equation (2.17) by the number of phases q and equating to (2.18) gives,

$$\frac{r_2}{\left(\frac{r_2}{s} + jx_2 \right)^2} = \frac{r}{\left(\frac{r}{s} + jx \right)^2} \frac{n_b}{(4pNK_1)^2 q} \quad (2.19)$$

The turns ratio n can be defined as,

$$n = 4pNK_1 \sqrt{\frac{q}{n_b}}$$

Substitution of ' n ' into equation (2.19) and equating real and imaginary parts gives,

$$\begin{aligned} r_2 &= n^2 r \\ x_2 &= n^2 x \end{aligned} \quad (2.20)$$

2.5 Synchronous Performance of Reluctance Motor

2.5.1 Phase Impedance

The airgap flux is obtained by putting $s=0$ in equation (2.10). Furthermore, since the m.m.f harmonics are very much smaller than the fundamental these can be ignored giving,

$$\phi_{\alpha} = IC \cos(p\alpha - \omega t) + \frac{ID}{2} \sum_{n=1}^{\infty} \frac{\sin n\beta\pi}{n} \left[\cos(p\alpha(2n+1) - \omega t(2n+1) - 2np\delta) + \cos(p\alpha(2n-1) - \omega t(2n-1) - 2np\delta) \right] \quad (2.21)$$

The voltage induced in phase 1 is then given by,

$$\begin{aligned} e &= -2pNK_1 \frac{d\phi_T}{dt} \\ &= -2pNK_1 \frac{d}{dt} \left[\int_{-\pi/2p}^{\pi/2p} \phi_{\alpha} d\alpha \right] \\ &= 2NK_1 \left[2IC\omega \sin \omega t + ID \sum_{n=1}^{\infty} \frac{(-1)^n \sin n\beta\pi}{n} \left[\sin(\omega t(2n+1) + 2np\delta) - \sin(\omega t(2n-1) + 2np\delta) \right] \right] \end{aligned}$$

Extracting only the fundamental from this expression by putting $n = 1$ into the $(2n - 1)$ factor gives,

$$e_1 = 2NK_1 \left[2IC\omega \sin \omega t + ID\omega \sin \beta\pi \sin(\omega t + 2p\delta) \right]$$

and the component of applied voltage which opposes this is ,

$$v_1 = -2NK_1 \left[2IC\omega \sin \omega t + ID\omega (\sin \omega t \cos 2p\delta + \cos \omega t \sin 2p\delta) \sin \beta\pi \right]$$

The magnetising current ($I \cos \omega t$) and its differential ($-\omega I \sin \omega t$) are present in this voltage equation and it follows that the remaining terms represent an impedance, hence,

$$Z_e = -(2NK_1 D \omega \sin \beta\pi \sin 2p\delta) + j(4NK_1 C \omega + 2NK_1 D \omega \sin \beta\pi \cos 2p\delta)$$

The in phase component is an effective resistance and the power dissipated in this is equal to the mechanical output of the machine. The imaginary

component is an effective reactance representing the magnetising reactance of the machine. The dependance of both these terms on the pole arc/pole pitch ratio is clear. These effective parameters are given below as,

$$R_e = -2NK_1 Dw \sin \beta \pi \sin 2p\delta$$

$$X_e = 2NK_1 w(2C + D \sin \beta \pi \cos 2p\delta)$$

If the iron loss component is ignored the phase impedance becomes,

$$Z = (r - 2NK_1 Dw \sin \beta \pi \sin 2p\delta) + j(x_1 + 2NK_1 w(2C + D \sin \beta \pi \cos 2p\delta)) \quad (2.22)$$

It is possible to express the phase impedance in terms of the direct axis reactance (X_d) and the quadrature axis reactance (X_q). The reactance of the machine (X) is given in (2.22) as,

$$X = x_1 + 2NK_1 w(2C + D \sin \beta \pi \cos 2p\delta)$$

thus when $p\delta = 0$ the direct axis reactance is given as,

$$X_d = x_1 + 2DK_1 w(2C + D \sin \beta \pi) \quad (2.23)$$

and similarly when $p\delta = \pi/2$

$$X_q = x_1 + 2NK_1 w(2C - D \sin \beta \pi) \quad (2.24)$$

Taking both the sum and the difference of (2.23) and (2.24) gives,

$$\frac{X_d - X_q}{2} = 2wNK_1 D \sin \beta \pi$$

$$\frac{X_d + X_q}{2} = x_1 + 4NK_1 wC$$

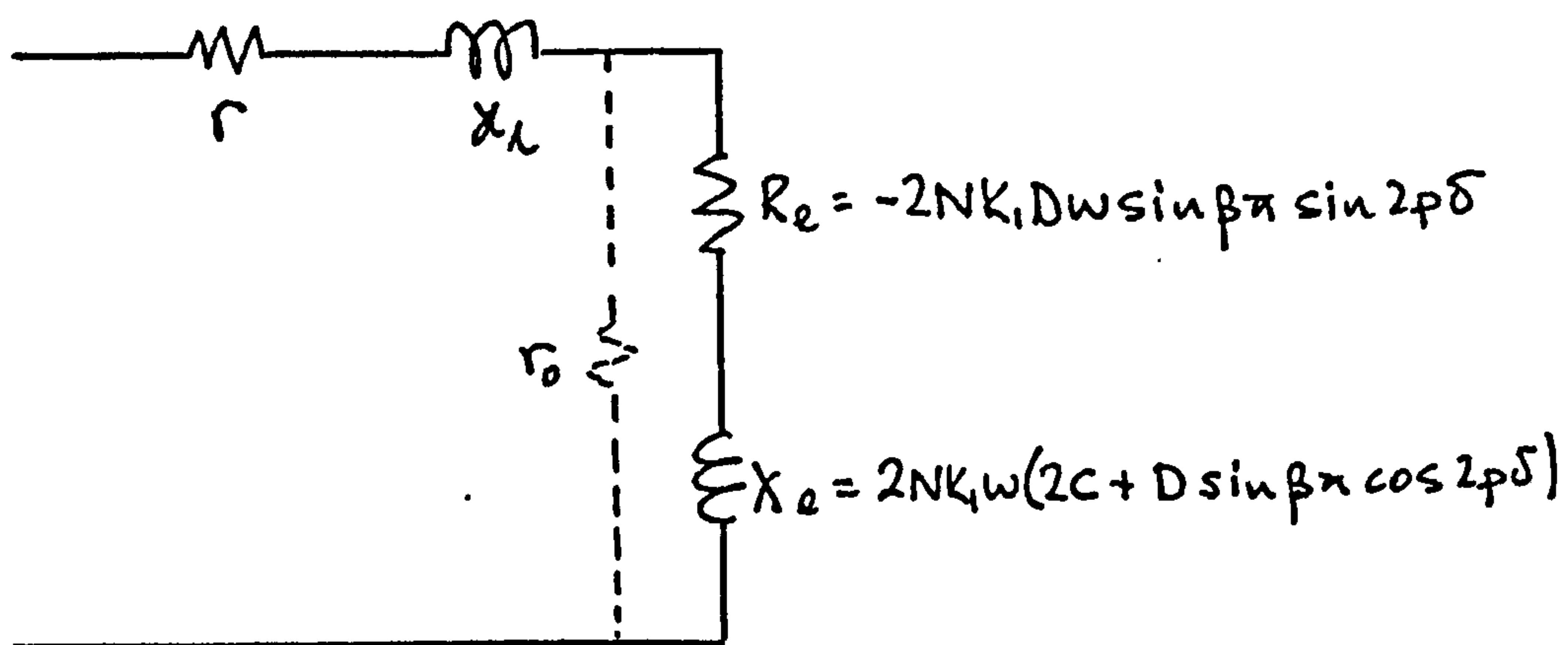
hence,

$$Z = (r - \frac{1}{2}(X_d - X_q) \sin 2p\delta) + j(\frac{1}{2}(X_d + X_q) + \frac{1}{2}(X_d - X_q) \cos 2p\delta) \quad (2.25)$$

2.5.2 Performance Equations

The equivalent circuit as indicated by the phase impedance is simply a series connected resistance and reactance circuit in which the iron

loss component has been ignored.



Approximate Equivalent Circuit

The accuracy of computations based on the approximate circuit depends on the magnitude of the iron losses. For this to be included in the equivalent circuit and in keeping with conventional notation this component would be represented by a resistance (r_o) and would occupy a position similar to the one shown dashed in the above circuit. In the circuit the effective resistance (R_e) has a negative sign associated with it and this indicates that for motoring operation the load angle (δ) is negative. Hence the rotor lags behind the rotating magnetic field produced by the stator. For a star connected winding the power output becomes,

$$P_o = 3I^2 \frac{(X_d - X_q)}{2} \sin 2p\delta$$

$$\text{where, } I = \frac{V/\sqrt{3}}{(RZ^2 + IZ^2)^{\frac{1}{2}}}$$

and (RZ) and (IZ) are the real and imaginary components of Z (2.25).

Therefore,

$$P_o = \frac{V^2 (X_d - X_q) \sin 2p\delta}{2(RZ^2 + IZ^2)} \quad (2.26)$$

and the power factor is,

$$\cos \phi = \frac{RZ}{(RZ^2 + IZ^2)^{\frac{1}{2}}} \quad (2.27)$$

2.5.2.1 Pull-out

The maximum load angle is the angle at which pull-out occurs. The substitution of r , X_d and X_q into RZ and IZ gives,

$$P_o = \frac{2V^2(X_d - X_q)\sin 2p\delta}{(2r - (X_d - X_q)\sin 2p\delta)^2 + (X_d + X_q + (X_d - X_q)\cos 2p\delta)^2}$$

But,

$$\frac{dP_o}{d\delta} = 0 \text{ for maximum and minimum}$$

Performing the differentiation shows that the pull-out angle is given by,

$$\cos 2p\delta = \frac{-(X_d^2 - X_q^2)}{2r^2 + X_d^2 + X_q^2} \quad (2.28)$$

Substitution of the pull-out angle into the expression for power gives the pull-out power as,

$$P_{po} = \frac{V^2(X_d - X_q)}{((2r^2 + X_d^2 + X_q^2)^2 - (X_d^2 - X_q^2)^2)^{\frac{1}{2}} + 4r(X_d - X_q)} \quad (2.29)$$

If the winding resistance is ignored this expression is greatly simplified and the dependence of the pull-out power on the values of X_d and X_q is made clear. Hence,

$$\begin{aligned} \frac{P_{po}}{r=0} &= \frac{V^2(X_d - X_q)}{X_d X_q} \\ &= V^2 \left(\frac{1}{X_q} - \frac{1}{X_d} \right) \end{aligned} \quad (2.30)$$

2.6 Asynchronous Performance

The airgap flux is again obtained from equation (2.10) and, by ignoring the m.m.f harmonics, becomes,

$$\phi_{\alpha} = IC \cos(p\alpha - \omega t) + \frac{ID}{2} \sum_{n=1}^{\infty} \frac{\sin n\beta\pi}{n} \left[\cos(p\alpha(2n+1) - \omega t(2n-2ns+1) - 2np\delta) + \cos(p\alpha(2n-1) - \omega t(2n-2ns-1) - 2np\delta) \right]$$

Furthermore the total flux per pole is equal to the integral of ϕ_{α} between the limits $(-\pi/2p)$ and $(\pi/2p)$ giving,

$$\phi_r = \frac{2IC \cos \omega t}{P} + \frac{ID}{P} \sum_{n=1}^{\infty} \frac{\sin n\beta\pi}{n} \left[\frac{\cos(\omega t(2n-2ns+1) + 2np\delta)}{2n+1} + \frac{\cos(\omega t(2n-2ns-1) + 2np\delta)}{2n-1} \right] \quad (2.31)$$

The voltage induced in phase.1 by ϕ_r is given by,

$$e = -2pNK_1 \frac{d\phi_r}{dt}$$

and the component of applied voltage which opposes this becomes,

$$\begin{aligned} v = & -4NK_1 \omega IC \sin \omega t \\ & -2NK_1 \omega ID \sum_{n=1}^{\infty} \frac{\sin n\beta\pi}{n} \left[\frac{2n-2ns+1}{2n+1} \left[\sin(\omega t(2n-2ns+1) \cos 2np\delta + \cos(\omega t(2n-2ns+1) \sin 2np\delta) \right] \right. \\ & \left. -2NK_1 \omega ID \sum_{n=1}^{\infty} \frac{\sin n\beta\pi}{n} \left[\frac{2n-2ns-1}{2n-1} \left[\sin(\omega t(2n-2ns-1) \cos 2np\delta + \cos(\omega t(2n-2ns-1) \sin 2np\delta) \right] \right] \right] \end{aligned} \quad (2.32)$$

Since only the fundamental component of voltage and current produce any useful mechanical output it is necessary to confine the analysis to this component alone. The remaining sections are concerned with two slip conditions namely $s \rightarrow 1$ and $s \rightarrow 0$ and for either condition the expression for v is greatly simplified. It is assumed that for intermediate slip conditions the reluctance motor performance is overshadowed by the action of the squirrel cage as the prime mover.

2.6.1 Equivalent Circuit s → 1.

At starting and for high values of slip the equation for the voltage drop across the magnetising branch of the equivalent circuit becomes,

$$v = -4NK_1\omega I C \sin\omega t - 2NK_1\omega I D \sum_{n=1}^{\infty} \sin n\beta\pi \left[\frac{\sin\omega t \cos 2np\delta + \cos\omega t \sin 2np\delta}{2n+1} + \frac{\sin\omega t \cos 2np\delta - \cos\omega t \sin 2np\delta}{2n-1} \right] \quad (2.33)$$

The fundamental is obtained when $n = 1$, hence,

$$v_f = -4NK_1\omega I C \sin\omega t - 2NK_1\omega I D \sin\beta\pi \left[\frac{4\sin\omega t \cos 2p\delta}{3} - \frac{2\cos\omega t \sin 2p\delta}{3} \right]$$

Since $i_1 = I \cos\omega t$

and $\frac{di_1}{dt} = -\omega I \sin\omega t$

the effective resistance and reactance are,

$$R_e = \frac{4NK_1\omega D \sin\beta\pi \sin 2p\delta}{3} \quad (2.34)$$

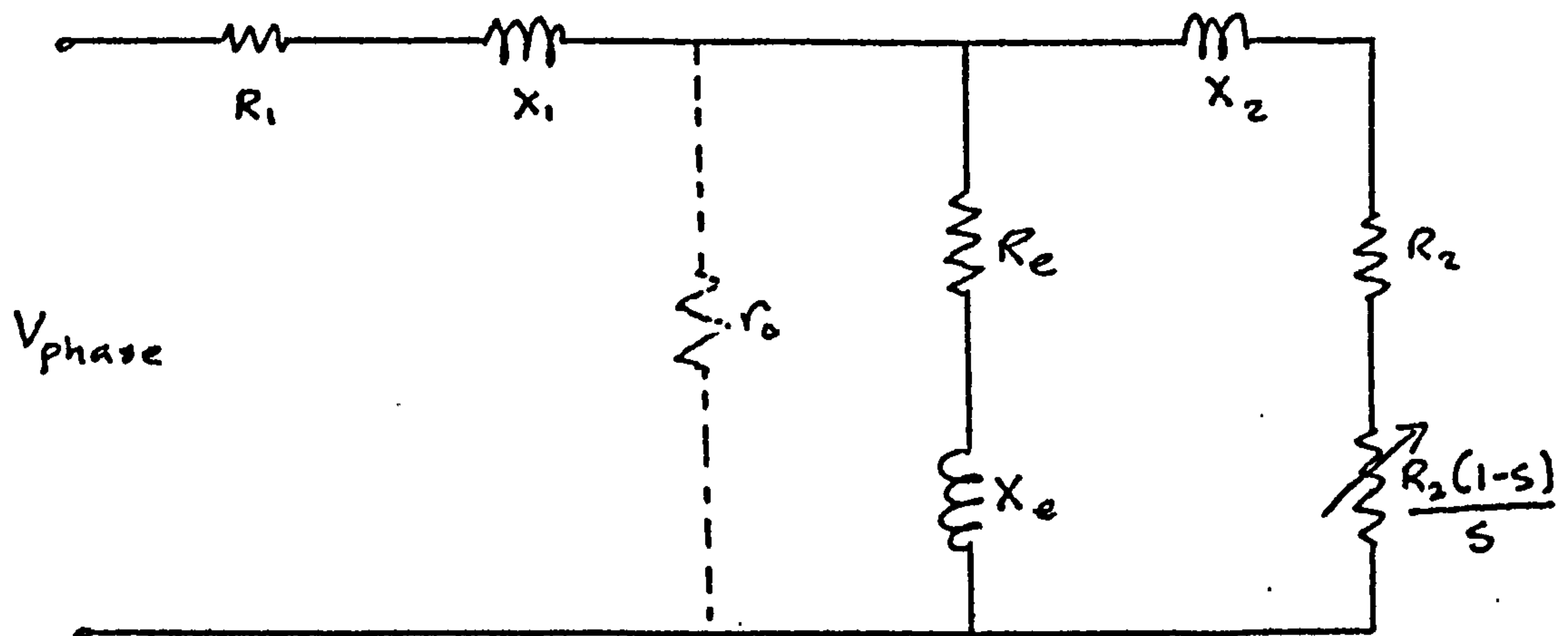
$$X_e = 4NK_1\omega \left(C + \frac{2D}{3} \sin\beta\pi \cos 2p\delta \right)$$

$s = 1$

The equivalent circuit for the reluctance motor is shown in figure 2.9 and although the iron losses are ignored in the analysis the component that represents this is included (dashed) in the same circuit.

In section 2.4.4 the turns ratio between a stator phase and the squirrel cage was obtained on the assumption that all the rotor bars had the same impedance, that the inner and outer end rings had a constant impedance

per unit length and that each bar e.m.f was loaded by the same impedance. In the reluctance motor the same turns ratio is used even though these three assumptions are not true since the bars and endring sections in the interpolar region have different iron boundaries to the copper in the intrapolar region.



Equivalent Circuit of the Reluctance Motor

Figure 2.9

In practice and particularly for the copper cross section used in the experimental machine the resistance per unit length of the bars and of the endrings is relatively independent of its position with respect to the rotor poles. On the other hand the reactance is much smaller for the interpolar copper than for the intrapolar copper. The following table shows the resistance and reactance per metre length for a copper bar 2.5mm in diameter and an endring section 4mm x 8mm. These have been calculated in Appendix III and Appendix IV

	R_{bar}	R_{endring}	X_{bar}	X_{endring}
Interpolar	.73067	.54349	.00785	.00549
Intrapolar	.73568	.54354	.07371	.01099
R_{dc}	.73064	.54348		

Table 2.2

The maximum variation in resistance at 50 Hz from the d.c value (R_{dc}) is seen to be less than 1% while the reactance figures differ by a factor of 2 for the endring and nearly 10 for the bar. Fortunately, because the resistive component is always greater than the reactance even at $s = 1$ it is felt that no serious error is introduced by using the turns ratio and bar load impedance calculated for the induction motor.

The power dissipated in R_e and $r_2(1-s)/s$ is available at the shaft as a mechanical output. In effect this is a continuously variable quantity and depends on the instantaneous load angle since both R_e and X_e are functions of δ . However the average shaft power is given by the average power dissipated in $r_2(1-s)/s$ and the stall or starting torque becomes,

$$T_s = \frac{3I_2^2 r_2}{w_s} \quad \text{Nm} \quad w_s = \text{synchronous rads/sec} \quad (2.35)$$

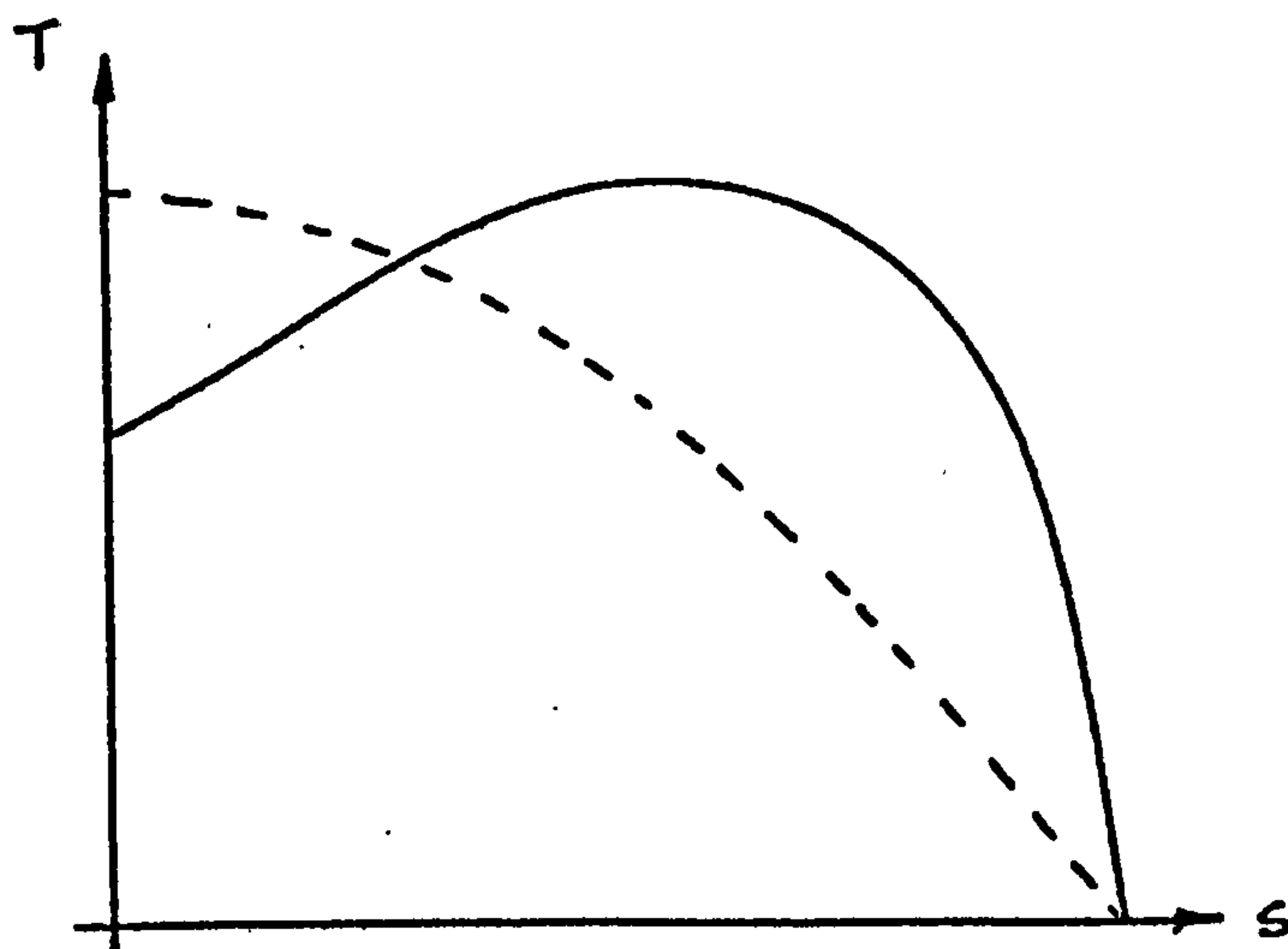
It must be remembered that this represents an average value and in practice the starting torque can be greater than this value.

2.6.2 Pull-in Criteria

The ability of a synchronous motor to achieve synchronous speed is a very important feature of the machine performance. The analysis of this is complex and Talaat⁽¹⁹⁾, Douglas⁽²⁰⁾, Lipo⁽²¹⁾, Krause⁽²²⁾, and Khanijo⁽²³⁾ are among the many researchers to have approached this problem. Each claim some degree of success and while it is not possible or necessary to give a resumé of their work, the duration of the pullin is treated, in general, as a period of instability. This is because speed oscillations generally occur about synchronous speed as synchronous speed is achieved. The stability and stability margin are affected by such machine parameters as direct and quadrature axis reactance, motor voltage and frequency, stator resistance and leakage reactance, the rotor direct and quadrature axis resistances and the total coupled inertia. Cruickshank⁽¹²⁾ classifies,

in general terms, the parameters which have a stabilising or anti-stabilising effect. He groups the stator leakage reactance, the motor voltage, the quadrature axis rotor resistance and the coupled inertia under a stability producing heading. On the other hand increases in the stator winding resistance, direct rotor resistance and the reactance ratio (X_d/X_q) are said to lead to instability. This is not an isolated opinion and has been confirmed by others.

The method used to obtain theoretically the maximum inertia that can be synchronised is the one used by Douglas⁽²⁰⁾. Hence the change in the kinetic energy of the rotor and the coupled inertia must be supplied by the variation of the reluctance torque due to an angular misalignment between the rotor and the stator poles. In operation the squirrel cage of the reluctance motor is assumed to have a low resistance giving a torque/speed curve similar to the one shown in full in the following curve.



Preferred Torque/Speed curve

of Reluctance Motor (during run-up)

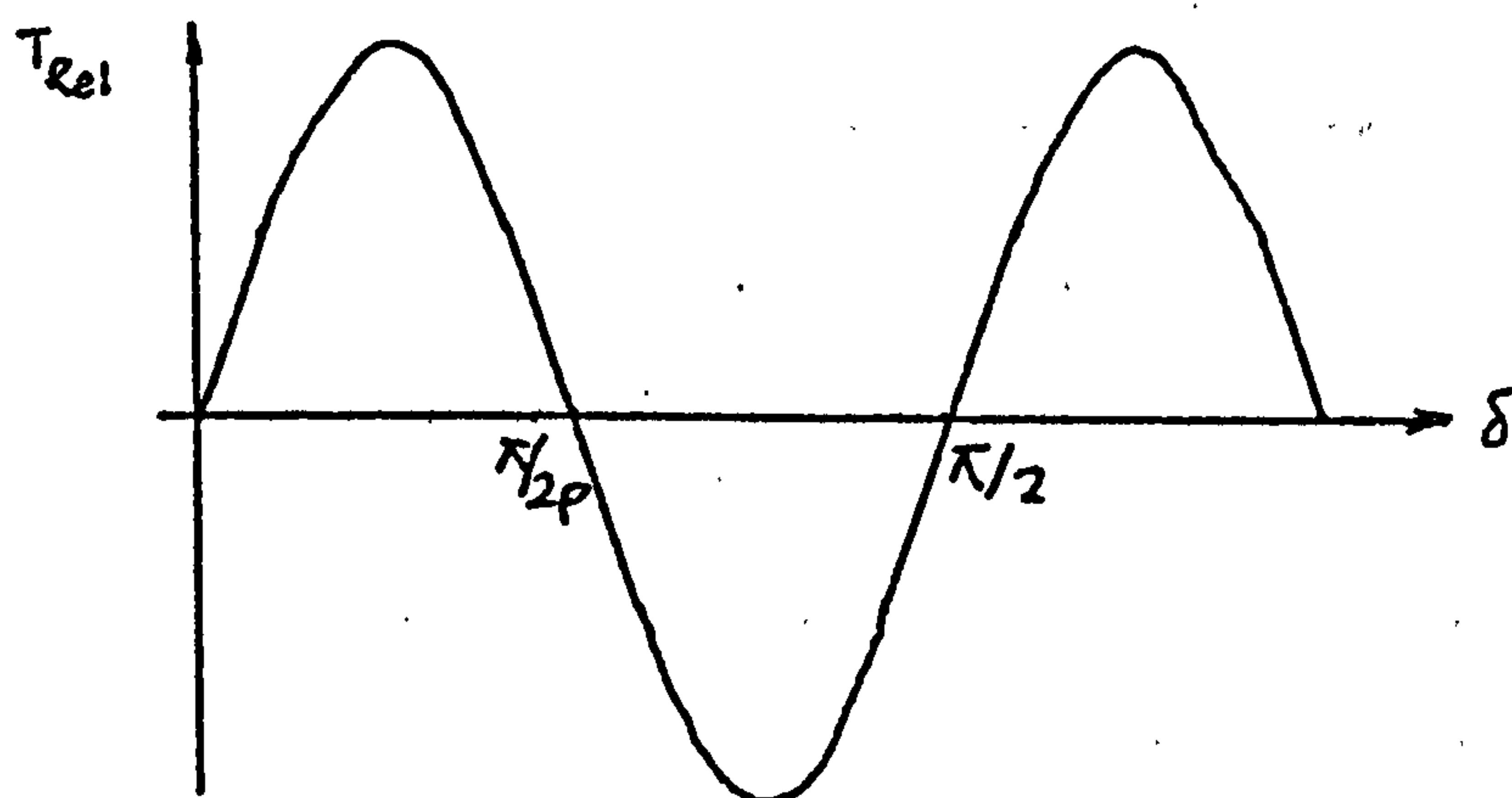
Successful synchronisation relies, among other factors, on the sub-synchronous speed attained by the rotor due to the action of the squirrel cage. In general the lower this slip the greater are the chances of pull-in. The necessary pull-in power is equated to the rate of change of kinetic

energy of the rotor. The power needed to accelerate an inertia linearly is given by,

$$\text{Power} = \frac{J(w_2^2 - w_1^2)}{2t}$$

where w_2 and w_1 are the initial and final speeds respectively and t is the time taken. During the process of pull-in the rotor is not necessarily accelerated linearly, but this simple equation serves to demonstrate the need for a high initial speed. For a given inertia, minimum power is necessary if the terms $(w_2^2 - w_1^2)$ and t are a minimum and maximum respectively. In this instance w_1 would be the minimum rotor speed before pull-in and w_2 would be synchronous speed. The torque, acting upon and assisting the rotor during pull-in consists of two components:- the induction torque and reluctance torque. The former reduces in magnitude as the rotor speeds up but since the rotor is assumed to be close to synchronous speed when pull-in starts this component is assumed to be negligible.

Before obtaining an equation for the maximum inertia, the possible reaction of the rotor and coupled inertia to the torque/load angle variation is considered. Initially therefore this variation is assumed to be sinusoidal and is shown in figure 2.10



Assumed Instantaneous Reluctance Torque

Figure 2.10

The acceleration on the rotor is given by,

$$\alpha = T/J$$

consequently the acceleration curve is of the same form as T . Because the speed is an integral of acceleration the rotor speed can vary in a variety of ways as a function of δ . If for example the coupled rotor inertia is too great to be synchronised then w_r never reaches w_s and curve 'a' of figure 2.11 would be a typical speed variation.

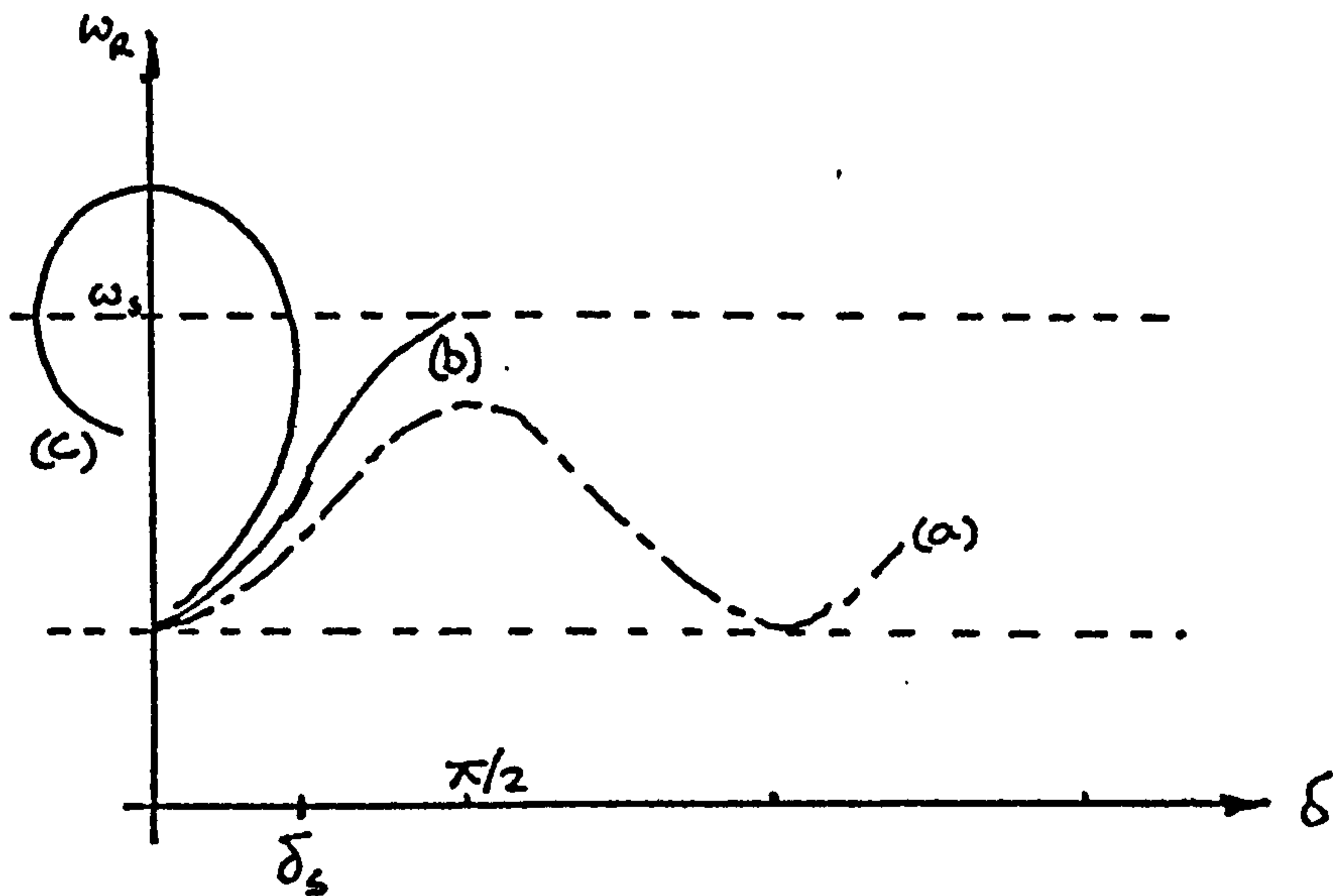
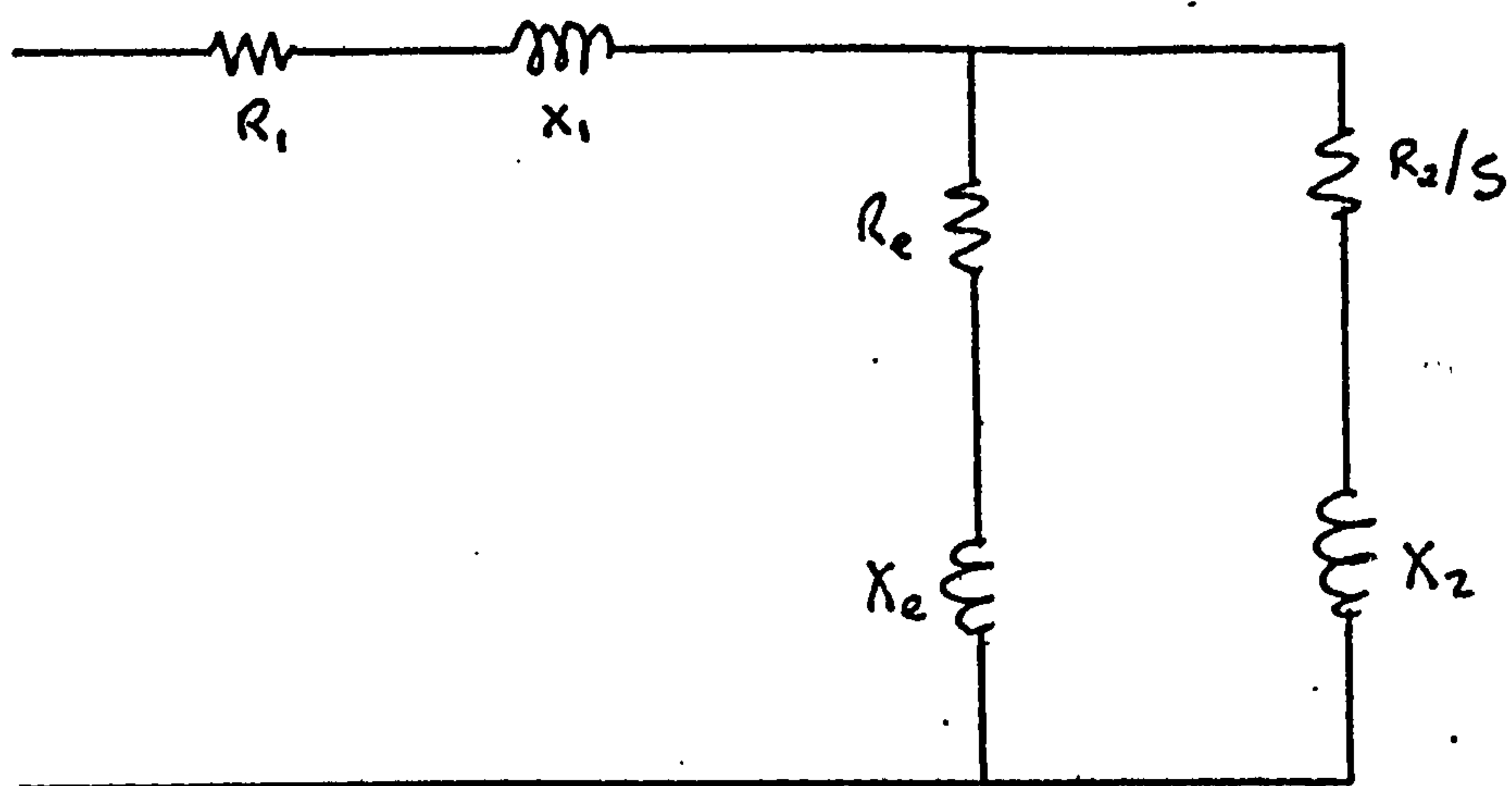


Figure 2.11

As the inertia decreases in magnitude the maximum rotor speed approaches w_s until a critical inertia is reached when synchronous speed is reached at $\delta = \pi/2p$ (curve 'b'). Further decrease in the inertia will allow w_s to be reached before $\delta = \pi/2p$, say $\delta = \delta_s$, and the angular misalignment between the stator and rotor poles decreases rather than increases until the stator and rotor poles are coincident. The angle then becomes positive (δ is negative for motoring), the torque negative and the rotor is decelerated as in curve 'c'. Two separate conditions must be satisfied before synchronisation can be achieved. Firstly, the rotor must reach w_s before $\delta = \pi/2p$ and secondly the machine parameters such as resistance, inertia etc must damp out any oscillations about $\delta = 0$. It is assumed,

therefore, that the critical inertia is the limiting factor for maximum pull-in and although speed oscillations around synchronous speed are likely this is a condition that must be satisfied before pull-in is at all possible.

The equivalent circuit of the reluctance motor as $s \rightarrow 0$ is similar to that used as $s \rightarrow 1$. The difference lies in the values of R_e and X_e . Since the slip is approaching zero the effective resistance and reactance are the same as the values used for the synchronous performance. The power dissipated in R_e of figure 2.12 is the power available at the shaft due to the reluctance torque.



Equivalent Circuit per Phase

Figure 2.12

Now the change in kinetic energy, dKE , of the rotor, shaft and load is due to the torque on the shaft acting through a small angle $d\delta$ which also corresponds to a change ds in the slip, hence,

$$dKE = T_r d\delta$$

The total power developed in R_e is equal to $3I_e^2 R_e$ and the apparent torque at the shaft is,

$$T_a = 3I_e^2 R_e / \omega_r$$

The ratio of rotor speed to slip speed is $(1-s)/s$ and the resultant torque

bears the same ratio to the apparent torque, hence,

$$T_r/T_a = (1-s)/s$$

giving,

$$T_r = \frac{3I_e^2 R_e}{s w_s}$$

The kinetic energy of the rotor and associated load is given by,

$$KE = J w_r^2 / 2$$

therefore, $dKE = J w_r dw_r$

But $w_r = w_s (1-s)$

and $dw_r = -w_s ds$

giving,

$$dKE = -\hat{KE} \cdot 2(1-s) ds \quad \text{where } \hat{KE} = \hat{J} w_s^2 / 2$$

= maximum kinetic energy

and since, $dKE = T_r d\delta$

$$\text{then, } \hat{KE} 2(1-s) ds = -\frac{3I_e^2 R_e}{s w_s} d\delta$$

Now if S_m is the maximum slip then the change in slip from S_m to zero corresponds to a change in rotor load angle from zero to $\pi/2p$, hence,

$$-\int_{S_m}^0 \hat{KE} 2s(1-s) ds = 3 \int_0^{\pi/2p} \frac{I_e^2 R_e}{w_s} d\delta$$

and ignoring powers of S_m higher than S_m^2 gives,

$$\hat{J} = \frac{6}{S_m^2 w_s^3} \int_0^{\pi/2p} I_e^2 R_e d\delta$$

Although the effect of the induction torque for low values of slip is ignored the equivalent circuit of figure 2.12 is used and R_e and X_e are

$$R_e = 2NK_1 D w \sin \beta \pi \sin 2p\delta = K \sin 2p\delta$$

$$X_e = 2NK_1 w (2C + D \sin \beta \pi \cos 2p\delta) = X + K \cos 2p\delta$$

The term $I_e^2 R_e$ represents a power loss. Expressing I_e as a function of the equivalent circuit parameters gives,

$$I_e^2 R_e = \frac{EV^2 \sin 2p\delta}{(AX+Q)^2 + (BX+M)^2 + (AK)^2 + (BK)^2 + 2K(AM-BQ)\sin 2p\delta + 2K(B^2X+BM+A^2X+AQ)\cos 2p\delta}$$

where,

$$A = (R_1 R_2 + R_2^2 + X_1 X_2 + X_2^2)$$

$$B = (R_1 X_2 - R_2 X_1)$$

$$E = K(R_2^2 + X_2^2) ; M = R_1(R_2^2 + X_2^2) ; Q = X_1(R_2^2 + X_2^2) ;$$

then,

$$I_{nt} = \int_0^{\pi/2p} I_e^2 R_e d\delta$$

Let,

$$F = (AX+Q)^2 + (BX+M)^2 + (AK)^2 + (BK)^2$$

$$G = 2K(AM-BQ)$$

$$H = 2K(B^2X+BM+A^2X+AQ)$$

and

$$I_{nt} = \int_0^{\pi/2p} \frac{EV^2 \sin 2p\delta d\delta}{F + G\sin 2p\delta + H\cos 2p\delta}$$

further let

$$b = \sqrt{G^2 + H^2}$$

$$\gamma = \cos^{-1}(G/b) = \sin^{-1}(H/b)$$

then,

$$I_{nt} = \int_0^{\pi/2p} \frac{EV^2 \sin 2p\delta d\delta}{F + b\sin(2p\delta + \gamma)}$$

and using the substitution $2p\delta + \gamma = x$ gives,

$$I_{nt} = \frac{V^2 E}{2p} \int_{\gamma}^{\pi+\gamma} \frac{\sin(x-\gamma) dx}{F+b \sin x}$$

$$= \frac{V^2 E}{2p} \left[\int_{\gamma}^{\pi+\gamma} \frac{\cos \gamma \sin x dx}{F+b \sin x} - \int_{\gamma}^{\pi+\gamma} \frac{\sin \gamma \cos x dx}{F+b \sin x} \right]$$

These are both standard integrals but the form of the solution depends on the relative magnitudes of F and b ⁽²⁴⁾. These two factors are functions of β and S_m ($R_2 = r_2/s_m$) and for the complete range of β and the typical maximum values of S_m that would be encountered it is seen that $F^2 > b^2$, hence,

$$I_{nt} = \frac{V^2 E}{2pb} \left[\cos \gamma \left(\pi - \frac{2F}{\sqrt{F^2 - b^2}} \left(\tan^{-1} \frac{F \tan \frac{1}{2}(\pi + \gamma) + b}{\sqrt{F^2 - b^2}} - \tan^{-1} \frac{F \tan \frac{1}{2} \gamma + b}{\sqrt{F^2 - b^2}} \right) + \sin \gamma \left(\log \frac{(F + b \sin \gamma)}{(F - b \sin \gamma)} \right) \right] \right] \quad (2.38)$$

The maximum inertia that can be synchronised is determined from the expression

$$\hat{J} = \frac{6I_{nt}}{S_m^2 \omega_s^3} \quad (2.39)$$

2.7 Conclusion

In chapter IV the theoretical and measured results are compared for both the machines. In general the performance equations are fairly standard, apart from the expression for pull-in, and do not require any further discussion. It is worthwhile, however, summarising the analysis of the pull-in criteria.

The effect that the maximum slip and phase voltage have on the maximum inertia is clear from equation (2.39). The shape of the torque/angle curve is not necessarily sinusoidal as suggested by figure 2.10 and the peak torque will not occur at $\delta = \pi/4p$. The position of this peak depends largely on the pole arc to pole pitch ratio. Douglas ⁽²⁰⁾ assumes a sinusoidal torque curve but it is seen in chapters IV and V that the pull-out angle and hence maximum torque occur at angles greater than $\pi/4p$.

Since the expression $I_e^2 R_e$ represents power it is apparent that the magnitude of the maximum inertia depends also on the area under the power/load angle curve (for $0 \leq \delta \leq \pi/2p$). For the experimental machine the

theoretical value of β which gives maximum pull-out power (hence maximum torque) is approximately 0.23. This condition does not however coincide with the maximum area under the power/load angle curve. As β is further decreased the peak torque decreases but initially the slope of the power curve (for $0 \leq \delta \leq \pi/4p$) increases. This maintains the increase in the area of this curve until $\beta \approx 0.1$ after which the area of the curve starts to decrease. When $\beta = 0$ there is no reluctance torque and the motor would run sub-synchronously as an induction motor with a very large airgap. The validity of equation (2.38) is not checked for the complete range of β . This parameter is limited in the experimental machine to approximately 0.45 because of the high current densities encountered. It follows that the condition for peak pull-out power cannot be tested.

Chapter III

Experimental Machine

3.1. Introduction

From the outset it was realized and confirmed from talks with practising engineers that the main disadvantage of the axial machine was that industry in general was not geared to produce a machine of this shape. Since it was felt that such machines could become a viable asset, and one firm to the writers' knowledge has proved this, then in order to make the machine more attractive to engineers two courses of action should be pursued. Firstly, some of the normal practices and conventions employed in the production of machines could possibly be discarded. During the manufacturing process of radial machines there exist a number of sub-assembly stages consisting of the production of the laminated stator and rotor, the windings for these components (sometimes the winding is manufactured separately and then loaded or alternatively the whole process is automated) and the final assembly of the separate items with the bearings into the casing. Naturally an axial machine would pass through similar stages and it is in the production of the stators and rotors that a different procedure is suggested. Secondly, and equally important, both domestic and industrial applications should be suggested for which the special shape of the motor is ideally suited. This latter point is discussed more fully in Chapter VI.

The reluctance motor rotor is obtained from the induction motor by machining the rotor to give saliency thus forming the identifiable poles. Successful pull-in relies upon several factors and these have been pointed out and discussed fairly comprehensively in the previous chapter. The radial machine which is used as a comparative standard for the axial machine had the following overall dimensions, not including the shaft

extensions:-

Outside diameter = 7.625" (194 mm)

length = 8.5" (216 mm)

3.2. Choice of Lamination Material

The laminated rotor and stator are ideally suited for production from a continuous strip into a tightly coiled spring form. Because of the direction of the flux in the magnetic circuit it can be seen that a non-oriented steel for the stator and an oriented steel for the rotor with the grain growth in the axial direction would be ideal. However, such a rotor material having suitably modifiable dimensions and with the correct grain growth could not be obtained and consequently both the rotor and stators were made from non-oriented steel.

In radial machines, stampings that have been produced from fully annealed iron, generally using punch and die techniques, need only a stress relief anneal to return the iron to its original good magnetic state. A coating can then be applied to give good inter-laminar resistance to eddy currents. Indeed it is possible to obtain some grades of material whose surface coating will withstand the annealing temperature and still give good inter-laminar resistance. It was found, however, after extensive enquiries that such a coating was applied only to oriented steels. This precipitated the question as to whether or not the steel which has been obtained in a fully annealed condition would need the final stress relieving operation. If this final operation was necessary, then in order to use a continuous strip method for producing the stators and rotor, a high temperature coating would also be necessary. Once the coil has been formed and machined it would not be possible to unwind it after annealing to coat the surfaces. Rather than build two machines, one of which needed this final operation on the stators and rotors, for a

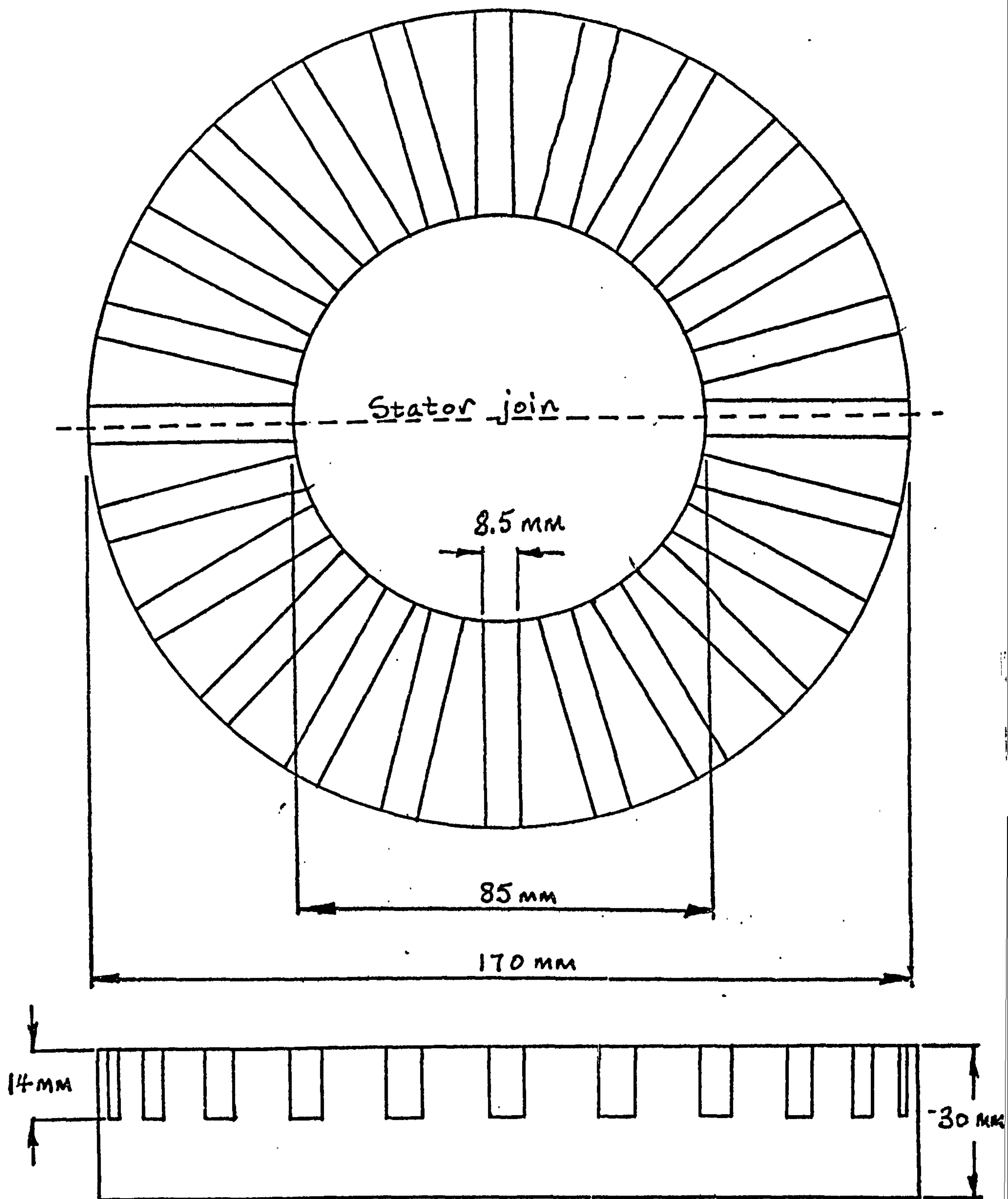


Figure 3.1

Stator

Material:- 0.5mm thick non-oriented iron

(Trade name Unisil)

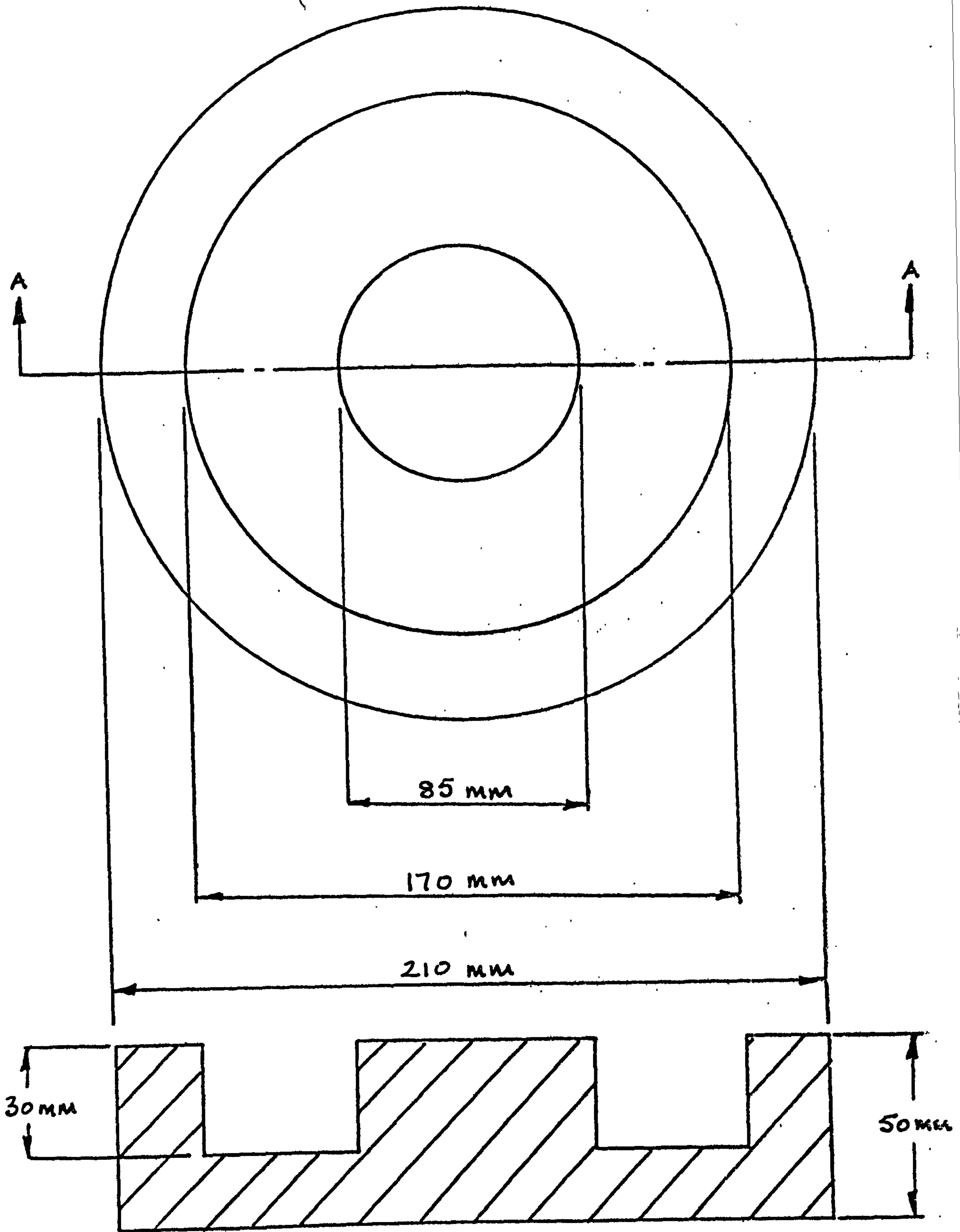
comparison it was decided to give the stress anneal to the two stators only. Furthermore, in view of what has already been said, the continuous strip method could not be employed, at least not on the stators.

In order to be able to anneal and give the material an inter-laminar coating, then the requirement that each layer was separable from its neighbour would be a necessity. Although the rotor could have been produced as a continuous strip, because it would not be annealed, it was manufactured in the same way as the stators. Thus both stators and rotors were initially given very similar treatments enabling a more realistic comparison of their magnetic states to be made when tested as an induction motor.

There are two other fairly common methods of producing electrical machine laminations these being spark erosion and etching and generally are employed for small batch numbers. They were not considered because of the expertise and specialised knowledge that is required.

3.3. Axial Machine Stator

To meet the requirement that the lamination layers should be separable the stator was made in two halves (Fig. 3.1). The material (trade name Unisil) was obtained in strips measuring 30 mm x 0.5 mm x 300 mm and placed in a cup jig (Figure 3.2) whose principal diameters (D_1 and D_2) matched the required diameters of the stators. The radial slots were milled, retaining holes (radial) were drilled in the yoke, the slotted surface of the laminations were machined to remove any irregularities and the whole assembly was slit along a diameter through the bottom of a slot. The laminations were annealed and removed from the jig. It was a relatively easy step then, due to the fact that the laminations maintained their semi-circular form, to re-assemble after coating into the stator housing. The radial retaining holes which had been drilled in the yoke were used



Section "AA"

Figure 3.2

Lamination assembly jig

to assist in the re-alignment of the teeth. Because the stators were made in two halves it was important that the slitting mentioned above was done accurately. This ensured that the contribution that the join made to the stator-rotor airgap was negligible.

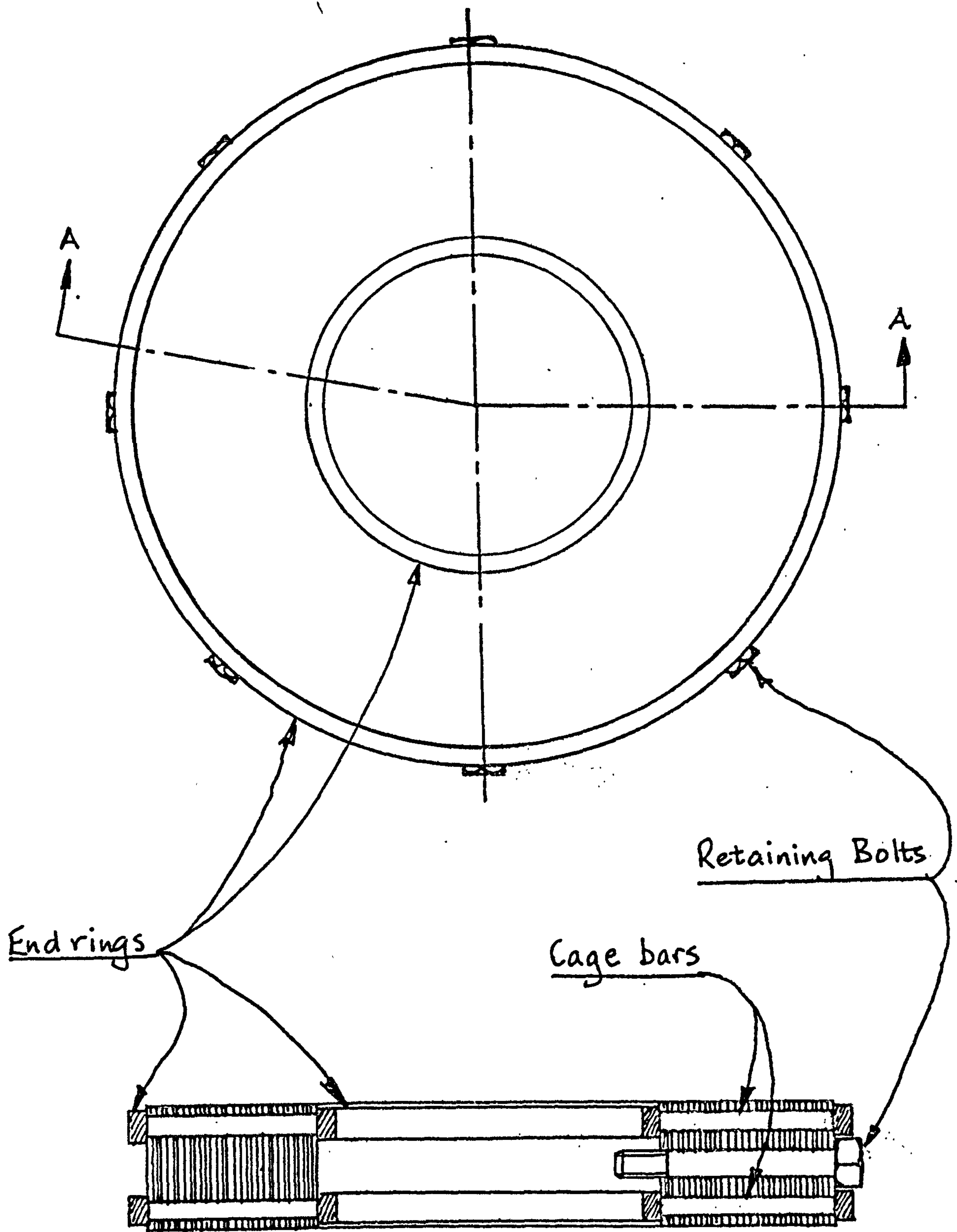
3.4. Axial Machine Rotor

A similar procedure was employed for the manufacture of the rotor laminations as for the stator with a few minor changes in the assembly details. The cup-jig was initially treated with an araldite release agent and the strips of lamination were coated with an araldite/acetone mixture. The strips were then placed in the jig and heated to cure the adhesive. This ensured that the laminations maintained their semi-circular form after ejection from the jig. The squirrel cage bar holes together with eight retaining holes were radially drilled.

The rotor has two squirrel cages (Figure 3.3), one for each stator. A variable in the testing is to be the amount of copper in, or the resistance of, the squirrel cage. In order to ease the problems that would be associated with the changing of the squirrel cage bars and end rings it was felt that the two cages were preferable. The design of a single cage rotor would have been radically different. Figure 3.4 shows a single cage rotor design and it is apparent that the bolts used to fix the poles onto the rotor shaft would necessarily have to lie in the plane of the cage. In order to change the cage resistance, these same bolts would have to be removed. With the double cage this operation is not necessary and it is a relatively easy job to alter the cage resistance. However, the double cage does unfortunately mean that the axial length of the rotor is larger than would be necessary in practice. For the single cage rotor the axial length would be big enough to meet two requirements,

- 1) To accommodate the copper bars.
- 2) To ensure sufficient mechanical strength.

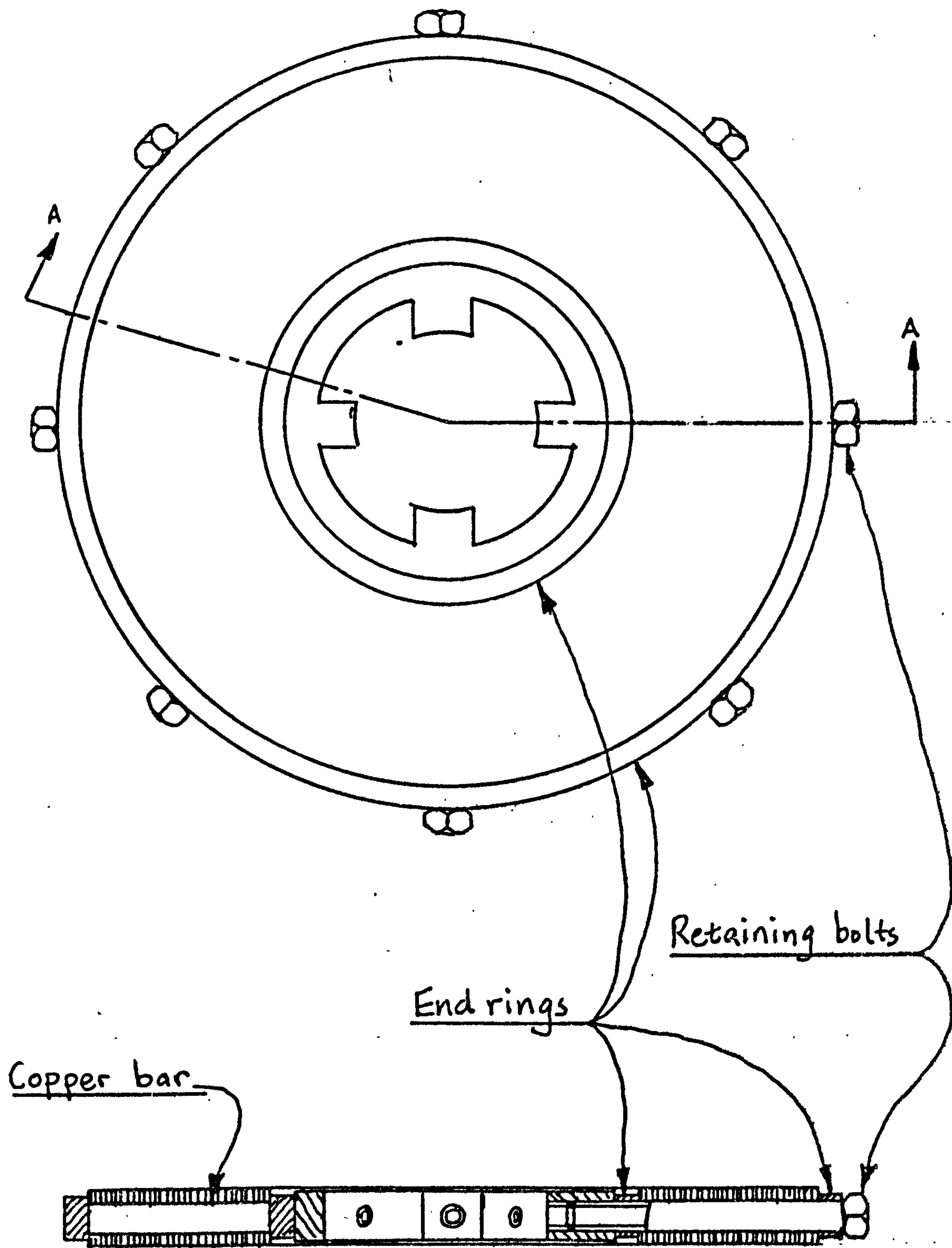
The need for the first requirement is apparent. For the second criterion, provided the stators, airgaps and cages are identical there will be no



Section AA

Figure 3.3

Double cage rotor



Section AA

Figure 3.4

Single cage rotor

resultant magnetic pull on the rotor tending to reduce one of the airgaps. In practice such symmetry is impossible and the resulting unbalanced magnetic pull will be transferred to the bearings (in an axial direction) and onto the fixing bolts. These bolts serve two purposes. Firstly, they must be able to withstand part of the unbalanced magnetic pull. Secondly, they have to transmit the torque produced by the various combinations of the induction motor and/or reluctance motor.

The drive end of the rotor shaft (Figure 3.5) has a female morse taper. This accommodates the hollow connecting shaft between the experimental machine and the load. It is on this shaft that the torque measurements are made.

3.5. Stator Winding

The winding is a standard three-phase double layer winding in 24 slots. Each phase per stator has two coils per pole with 20 turns per coil and a coil pitch of 5/6. The two stators are connected in series giving a total d.c. resistance per machine phase of 2.12 ohms (cold). The m.m.f. distribution for the winding is (Chapter II Section 2.3)

$$\text{m.m.f.} = \frac{6NI}{\pi} \left[K_1 \cos(p\alpha - \omega t) + \sum_{k=1}^{\infty} (-1)^k \frac{K_{6k+1}}{6k+1} \cos(p\alpha(6k+1) - \omega t) - \sum_{k=1}^{\infty} (-1)^k \frac{K_{6k-1}}{6k-1} \cos(p\alpha(6k-1) - \omega t) \right]$$

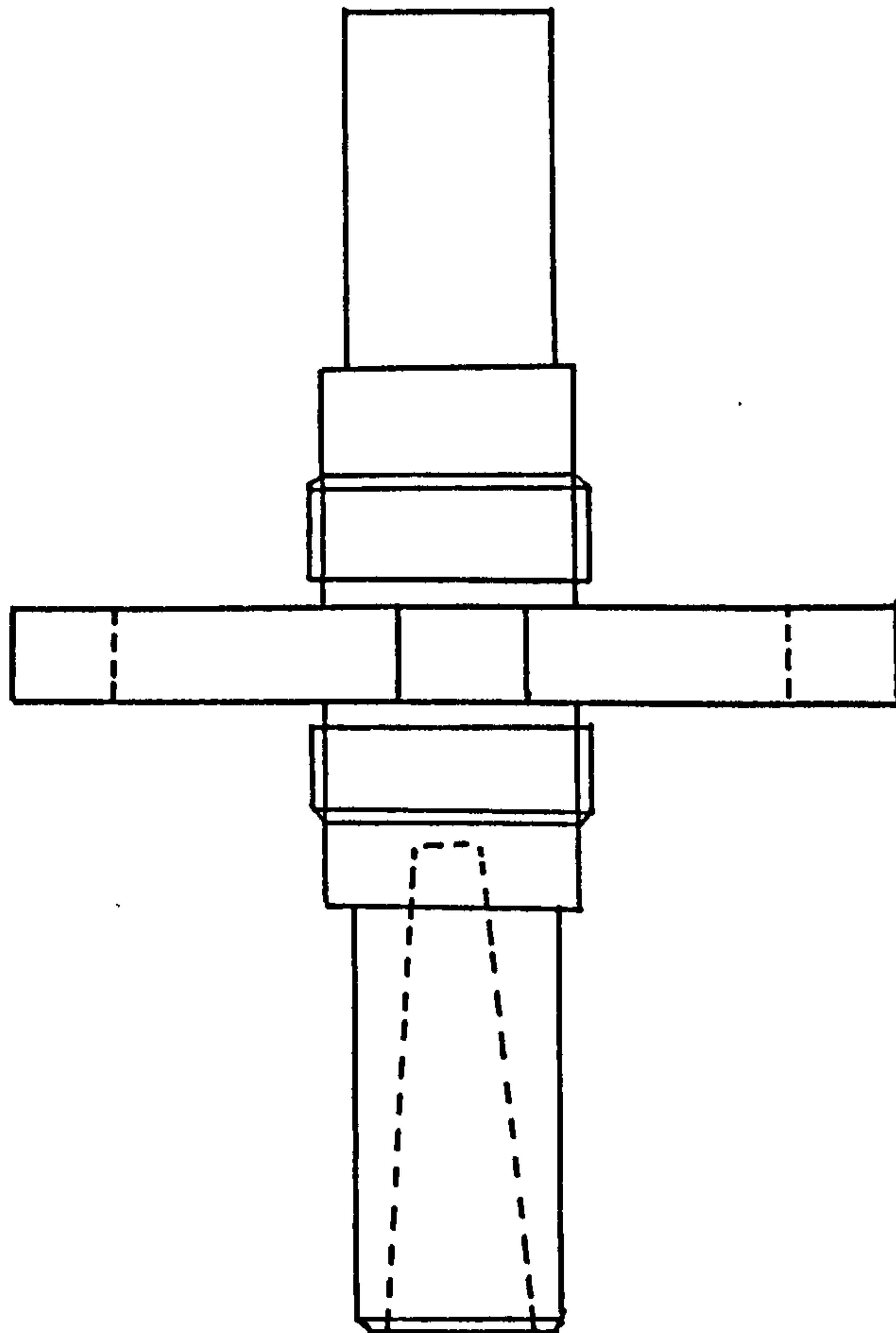
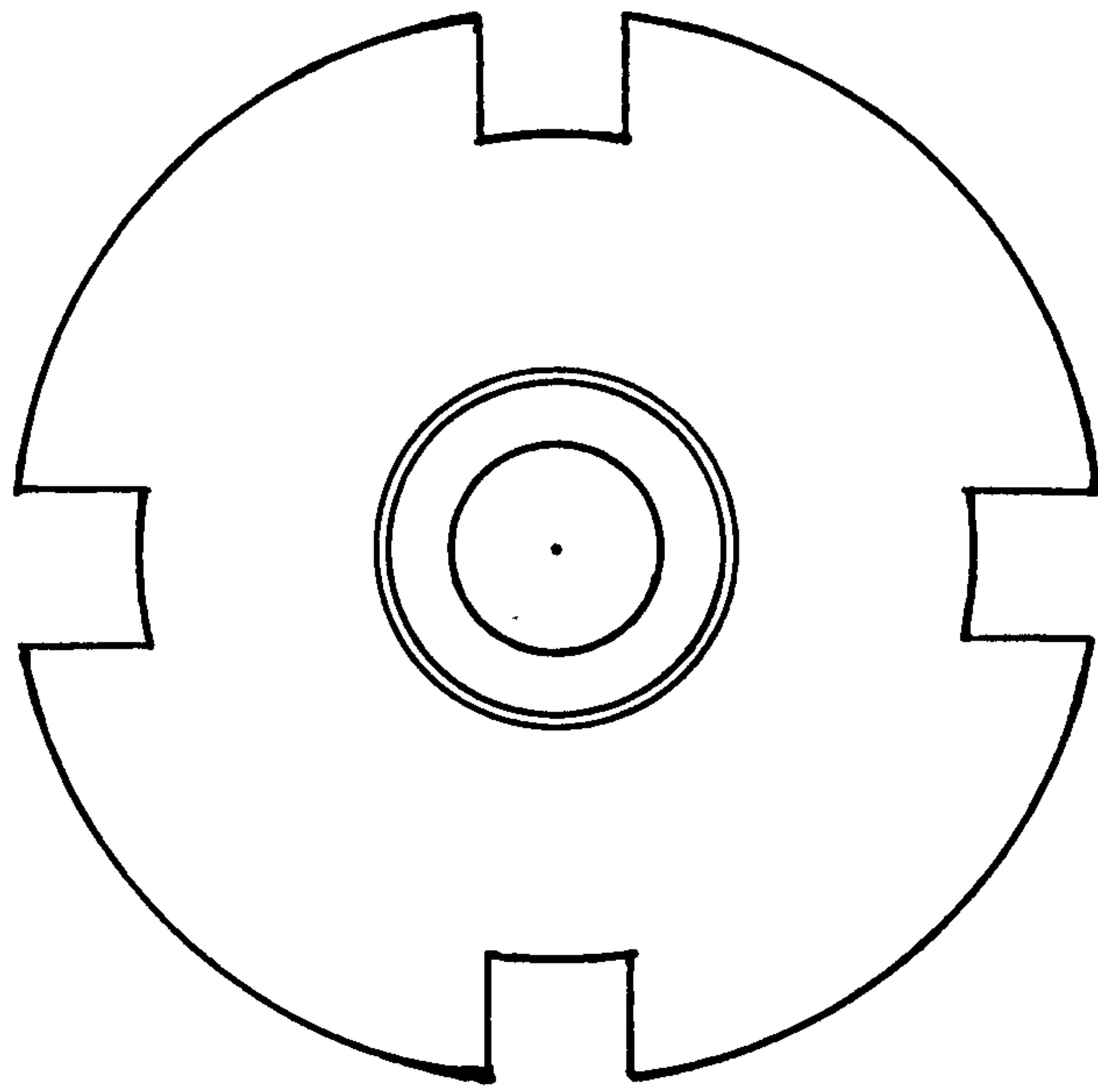
The winding factors denoted by K_1 and $K_{(6k \pm 1)}$ are normally taken as the product of the coil pitch and slot pitch factors giving,

$$K_1 = \frac{\sin p\lambda}{2} \cdot \frac{\sin(p\tau/2)}{c \sin(p\tau/2)}$$

$$K_{6k \pm 1} = \frac{\sin((6k \pm 1)p\lambda)/2}{c \sin((6k \pm 1)p\tau)/2} \cdot \frac{\sin((6k \pm 1)p\tau/2)}{c \sin((6k \pm 1)p\tau/2)}$$

Although it is not normally given much prominence, there is another component which can be introduced which is equal to the slot opening

factor and is given by, $\frac{\sin p\epsilon}{p\epsilon}$ or $\frac{\sin(6k \pm 1)p\epsilon}{p(6k \pm 1)\epsilon}$



N.T.S

Figure 3.5
Rotor shaft and collar

where ϵ is the slot width in radians. This has very little effect on the fundamental since as ϵ approaches zero, as it would do in radial machines

$$\frac{\sin(p\epsilon)}{p\epsilon} \rightarrow 1$$

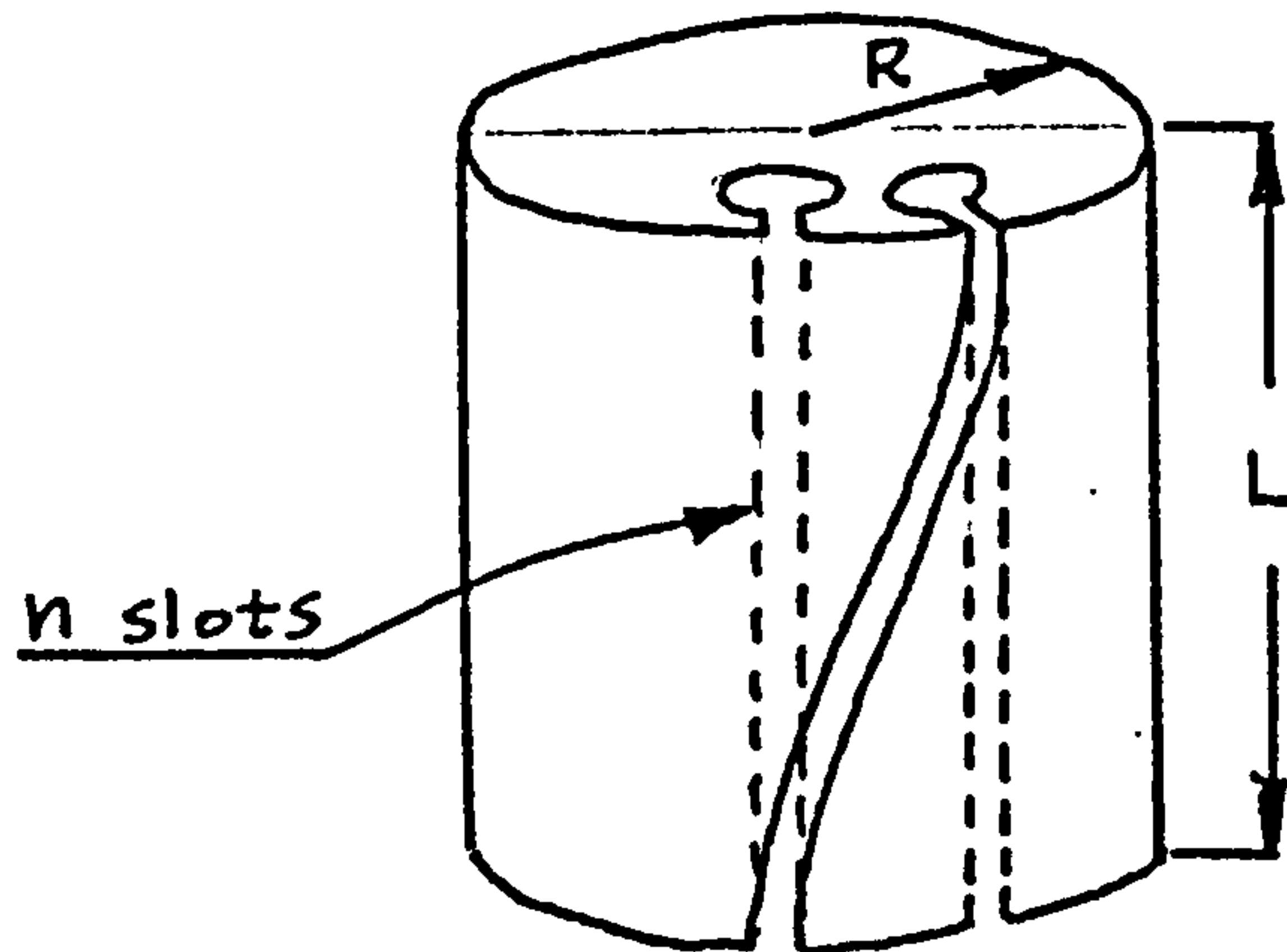
It is nevertheless possible to use this to suppress high order harmonics though generally such harmonics are small in magnitude due to the coil pitch and slot pitch factors. In axial machines the slot to tooth ratio varies between D_1 and D_2 . At the inner diameter the slot (or slot opening) to tooth ratio can be quite high. In the experimental machine this is about three but even under these adverse conditions the slot opening does not greatly affect the magnitude of the fundamental. The following table gives the relative magnitudes of the slot opening factor (S_o), the slot pitch factor (S_p) and the coil pitch factor (C_p) for the chosen winding, up to and including the thirteenth.

	S_o	S_p	C_p
K_1	0.973	0.966	0.966
K_5	0.454	0.258	0.258
K_7	0.118	- 0.258	0.258
K_{11}	-0.216	-0.966	0.966
K_{13}	-0.169	-0.966	0.966

3.6. Skewed Slots

In radial machines the amount of skew is related to the length of slot and the number of slots by a constant helix angle. For a slot skew equal to one slot pitch this angle is given by,

$$\alpha = \tan^{-1}(2\pi R/nL)$$

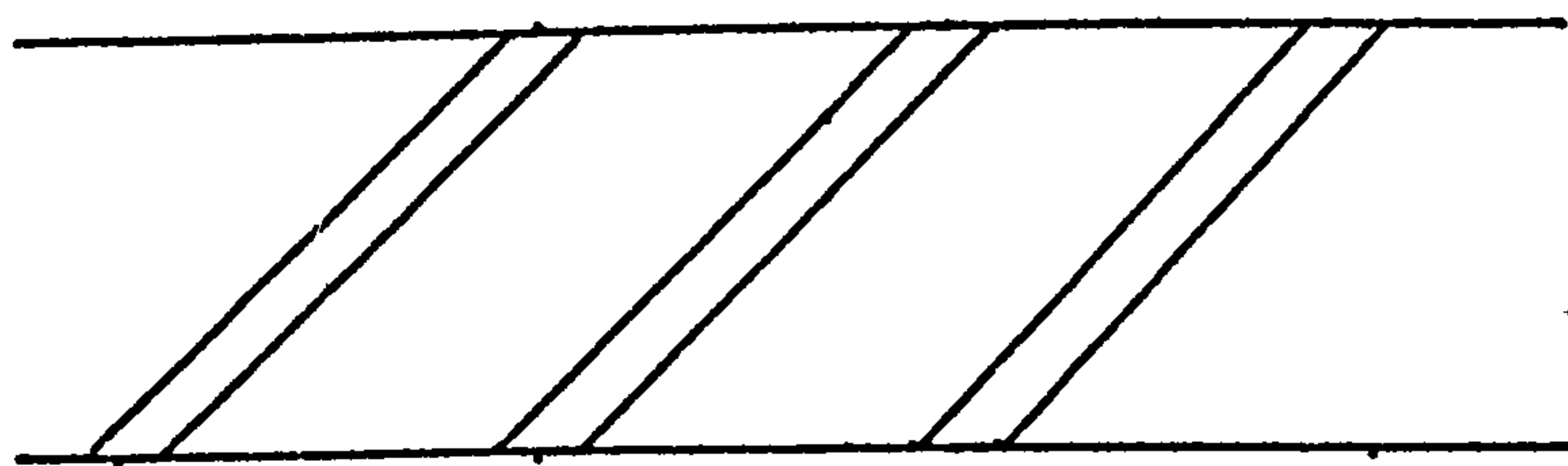


Skewed Radial Machine Rotor

For the more general case of a slot pitch equal to k times a slot pitch

then, $\alpha = \tan^{-1}(2\pi Rk/nL)$

and the developed diagram is accurately obtained by simply "unrolling" the motor about the axis (Figure 3.6)



Developed diagram of skewed radial machine rotor
Skew = 1 slot pitch

Figure 3.6

In the axial machine the shape of a skewed slot is a curve which is related to the amount of skew, the number of slots and the diameters D_1 and D_2 . However, the developed diagram (Figure 3.6b) that is obtained by unrolling the stator or rotor about its axis has an angular relationship between consecutive slots. In order to achieve the required shape of a

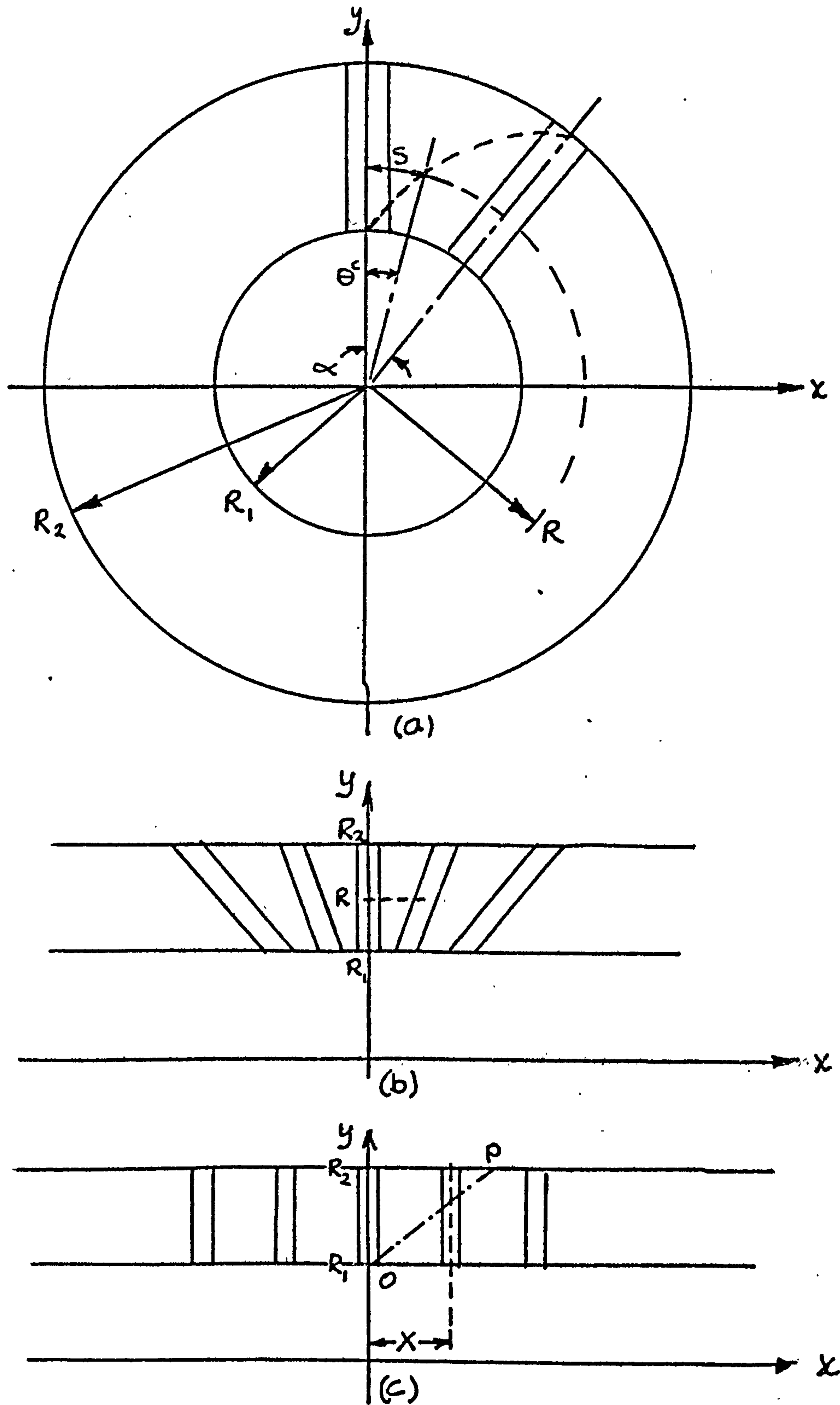


Figure 3.6 (a) Plan view of stator
 (b) Developed diagram
 (c) Weighted developed diagram

skewed slot a "weighted" developed diagram is used (Figure 3.6c) in which the slots are constrained to give an equal pitch for any value of radius. Hence we arrive at a diagram that is identical to the developed view of the radial machine. The value of X (Figure 3.6c) is obtained by taking the slot pitch at $R_1 = D_1/2$ as a base value, hence for n slots,

$$X = 2\pi R_1/n$$

To retain uniform skew for the axial machine, unit linear movement in the radial direction must be accompanied by unit angular movement about the axis. Consequently for a skew of one slot pitch and with reference to Figure 3.6a, at,

$$\begin{aligned} R &= R_1, & \theta &= 0 \\ R &= R_1 + \frac{R_2 - R_1}{10} ; & \theta &= \frac{\alpha}{10} \text{ etc.} \end{aligned}$$

In figure 3.6c the slot at $x = 0$ is skewed by an amount kX and is represented by the straight line OP . The equation of this line is,

$$y = mx + c$$

$$\text{or } y = ((R_2 - R_1)/mX)x + R_1 \quad (3.1)$$

since $y = R$ and $X = 2\pi R_1/n$ then

$$y = ((R_2 - R_1)/2\pi R_1 k)nx + R_1$$

When the transposition from the weighted developed diagram to the stator is made then the relationship is used,

$$S = (xS_x)/X \text{ where } S_x = R\alpha$$

$$\text{or } S/R = \theta^c = x/R_1$$

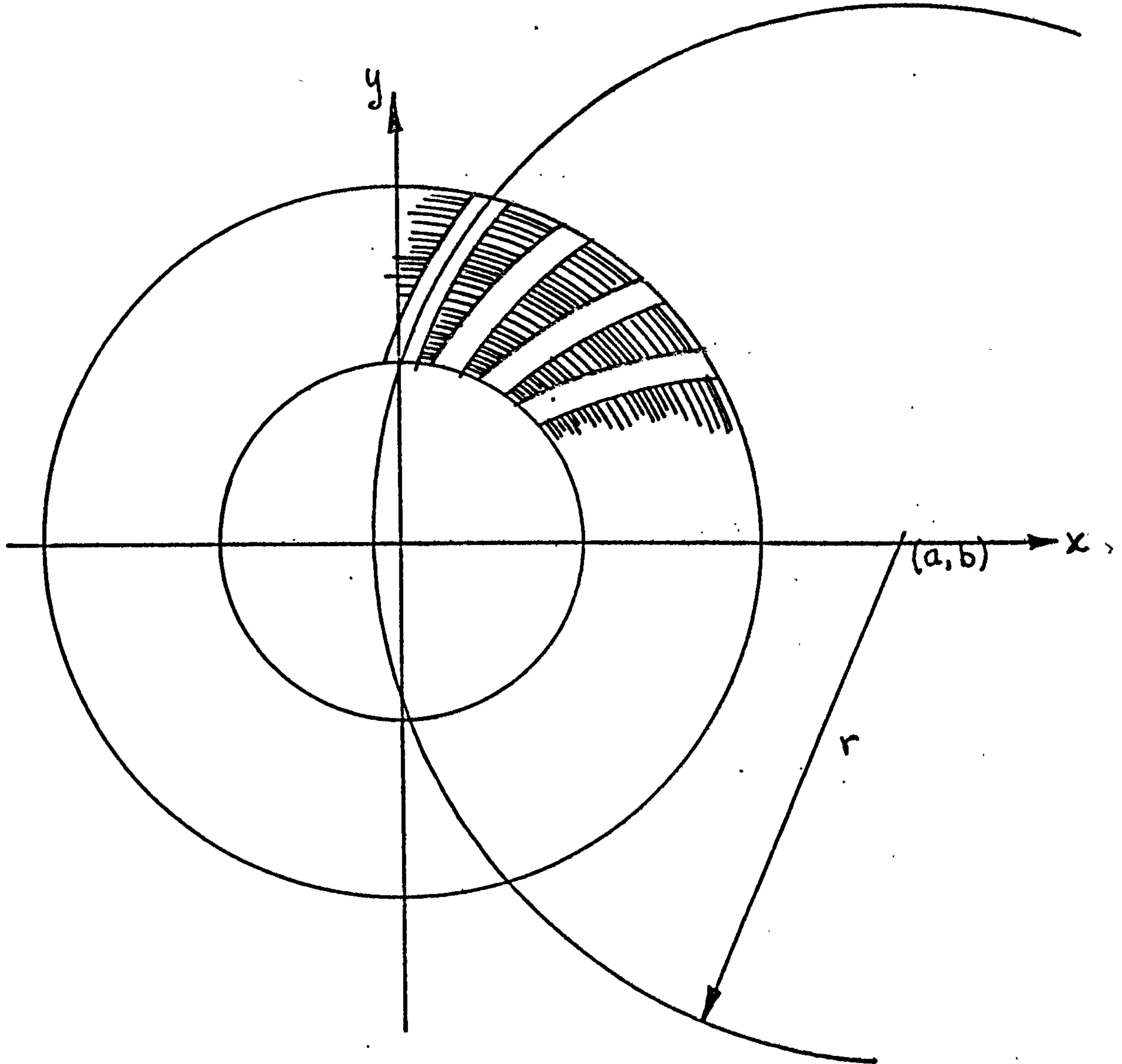


Figure 3.7

Locus of skewed stator slot (skew equal to one slot pitch)

Substitution in equation (3.2) and rearranging gives,

$$\theta^c = \frac{(R - R_1)2k}{(R_2 - R_1)n}$$

This equation gives the locus of the curve with respect to the axis of the machine and satisfies the condition that unit angular movement is accompanied by unit radial movement. The locus of the curve can be accurately fitted to the arc of a circle radius 'r' whose centre is at (a,b) relative to the axis of the machine. Consider, therefore, figure 3.7 on which the circle is shown and for which,

$$r^2 = (x - a)^2 + (y - b)^2$$

The slot has a skew equal to k and to find a, b, and r any three known conditions on the skewed slot are used, as for example,

- 1) $R = \frac{1}{2}(R_2 + R_1)$; $y = \frac{1}{2}(R_2 + R_1)\cos(\frac{1}{2}k\alpha)$; $x = \frac{1}{2}(R_2 + R_1)\sin(\frac{1}{2}k\alpha)$
- 2) $R = R_2$; $y = R_2\cos(k\alpha)$; $x = R_2\sin(k\alpha)$
- 3) $R = R_1$; $y = R_1$; $x = 0$

Substitution of these conditions into the equations of the circle gives three simultaneous equations with three unknowns, hence,

$$\begin{aligned} r^2 &= \left(\frac{1}{2}(R_2 + R_1)\sin(\frac{1}{2}k\alpha) - a\right)^2 + \left(\frac{1}{2}(R_2 + R_1)\cos(\frac{1}{2}k\alpha) - b\right)^2 \\ r^2 &= (R_2\sin(k\alpha) - a)^2 + (R_2\cos(k\alpha) - b)^2 \\ r^2 &= a^2 + (R_1 - b)^2 \end{aligned}$$

which when solved give,

$$\begin{aligned} b &= \frac{(D_1 + D_2)^2 D_2 \cos \alpha - 4 D_1^2 D_2 \cos \alpha - (D_1 + D_2)^2 (D_2 - D_1)}{8 D_2 (D_1 + D_2) \cos^2 \alpha + 4 (D_1 + D_2) (D_1 - D_2 \cos 2\alpha) - 16 D_1 D_2 \cos \alpha} \\ a &= \left[\frac{D_2^2 - D_1^2}{4} + (D_1 - D_2 \cos 2\alpha)(b) \right] \frac{1}{D_2 \sin 2\alpha} \\ r^2 &= \frac{D_1^2}{4} - b D_1 + a^2 + b^2 \end{aligned}$$

where $D_1 = 2R_1$ and $D_2 = 2R_2$

3.7. Torque Measurement

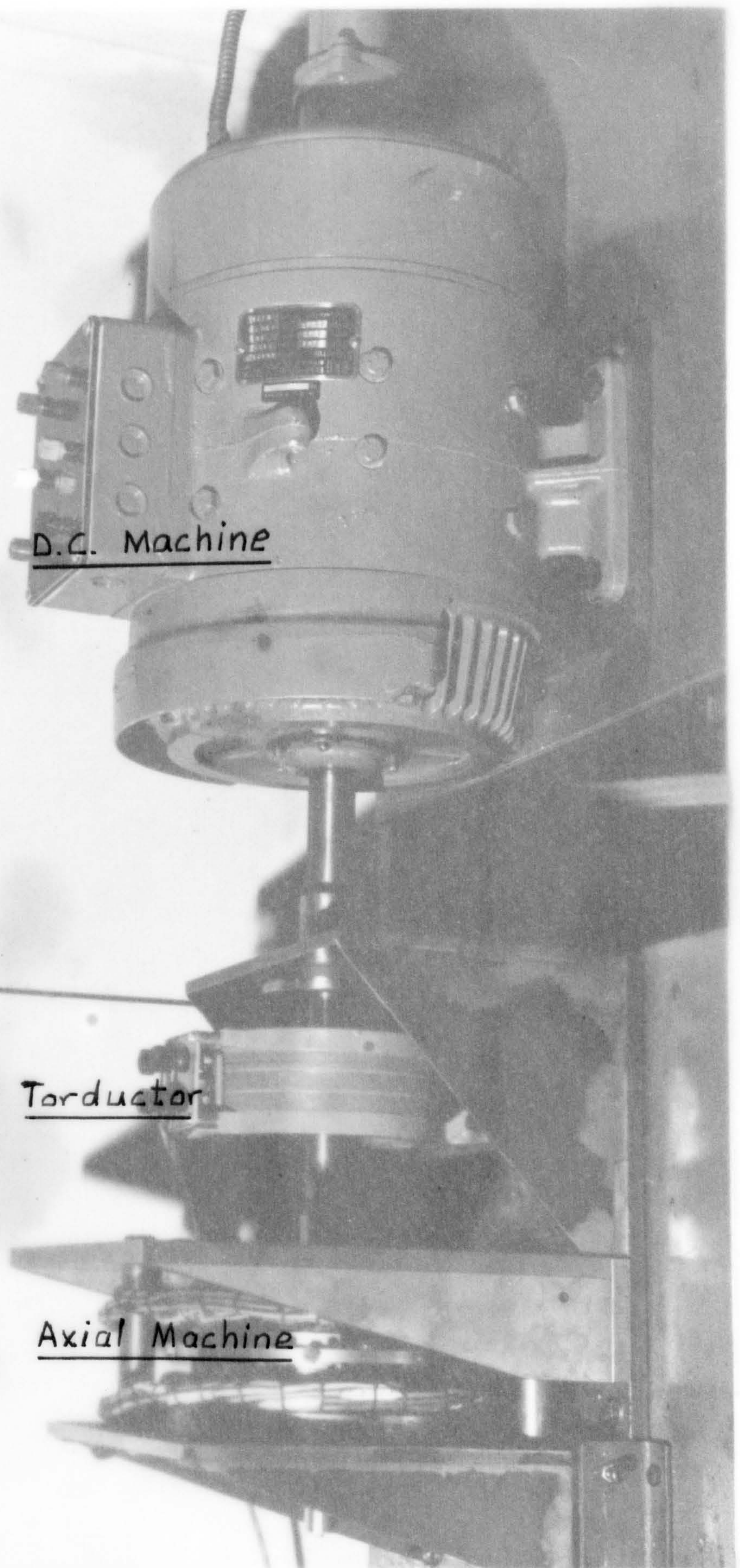
The torque measuring unit enables accurate measurement of both steady state and transient torque to be made. Its operation depends on the fact that in a shaft subjected to torsional stress, changes occur in the permeability of the shaft. This unit does not require slip rings and consists of one set of excited coils wound in a similar fashion to a stator of a radial machine. The shaft which connects the experimental machine (via a morse taper) to the load (via a solid coupling) acts as the rotor and consequently as a magnetic return path. The output is taken from two identical pick-off coils connected in opposition. When there is no torsional stress on the shaft the flux linking both pick-off coils is identical and the voltages induced in these coils cancel. When the shaft is put under stress the field is distorted and the two induced e.m.f.'s are no longer equal, giving a resultant output. The torque unit was calibrated and found to have an accuracy of $\pm 2\%$. Figure 3.8 shows the test bed with the torque unit.

3.8. Coupled Inertia for Reluctance Motor

The pull-in capability of the reluctance motor was determined by using a variable inertia flywheel. The inertia of the flywheel could be increased to approximately ten (10) times the maximum rotor inertia which coincided with the maximum pole arc to pole pitch ratio tested in the machine. The rotor inertia of the d.c. motor was also approximately ten(10) times the rotor of the experimental machine. The synchronous performance of the axial machine was determined using the d.c. machine in the motoring mode.

3.9. Effective Airgap Length

The effective or magnetic airgap length in electrical machines is determined by the physical length and whether or not the airgap is bounded by slotted and/or smooth surfaces. The factor by which the physical airgap must be multiplied to obtain the magnetic airgap is well



D.C. Machine

Torductor

Axial Machine

known as Carter's coefficient. For a given radial machine with a known slot to tooth and slot to gap ratio, this coefficient is ^{assumed} constant over the active length of the machine. In axial machines, however, the former ratio is a function ^{of} radius and varies from a maximum at D_1 to a minimum at D_2 . In order to include a magnetic airgap into the equations of the machine performance on average value, which does not necessarily occur at $\frac{1}{2}(D_2 + D_1)$ in the experimental machine, is used. Gibbs⁽²⁵⁾ defines Carter's coefficient as,

$$C = \frac{t + s}{t + s - s\sigma} \quad \text{and} \quad g' = Cg$$

where $\sigma = \frac{2}{\pi} \left((\tan^{-1} s/2g) - \frac{g}{s} \text{LOG}(1 + (s/2g)^2) \right)$

The average magnetic airgap

is then given by,

$$g' = \frac{2}{D_2 - D_1} \int_{D_1/2}^{D_2/2} Cg \, dR$$

The expression for σ is independent of R , therefore substitution for

$$(t + s) = 2\pi R/n$$

gives

$$g' = \frac{2g}{D_2 - D_1} \int_{D_1/2}^{D_2/2} \frac{2\pi R \, dR}{2\pi R - s\pi n}$$

hence,

$$g' = g \left(1 + \frac{s \cdot n \sigma}{(D_2 - D_1)} \cdot \frac{\text{LOG} \frac{(D_2 - s\pi n)}{(D_1 - s\pi n)}}{1} \right)$$

For the experimental machine,

$$s = 8 \text{ mm}; \quad D_2 = 170 \text{ mm}; \quad D_1 = 85 \text{ mm}; \quad n = 24$$

and the variation of g' as a function of D is shown below in Figure 3.9.

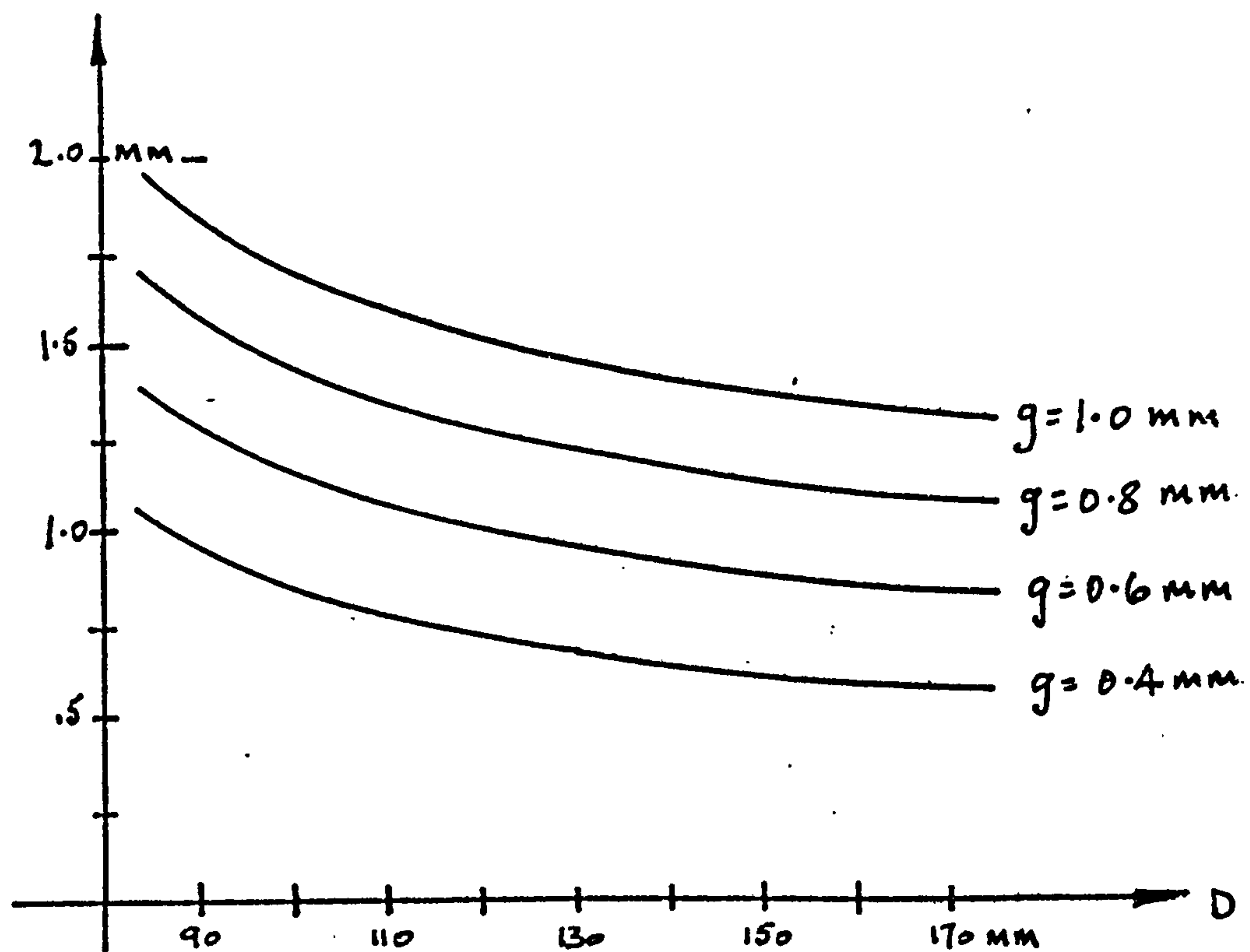


Figure 3.9

Variation of magnetic airgap as a function of diameter D

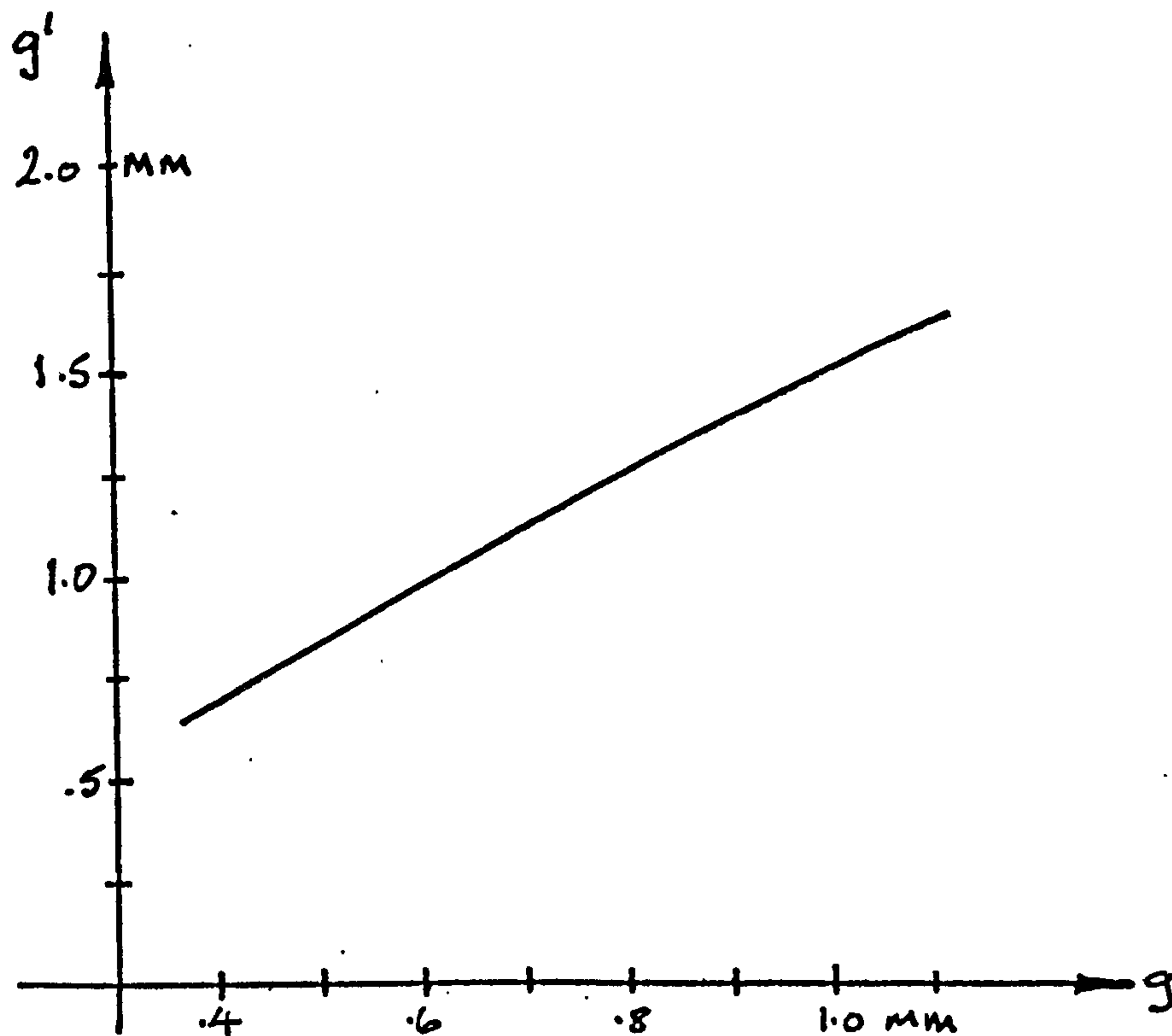


Figure 3.10

Variation of average magnetic airgap (g') as a function of g .

The average magnetic airgap length is also given and it is apparent that

- (1) For the range of physical airgaps used in the experimental machine, typically 0.5 mm to 0.7 mm, the relationship between g' and g is seen to be quite linear.
- (2) The effective value of Carters coefficient used to obtain g' is seen to be much greater than unity. This is a direct result of using fully open slots.

3.10. Conclusion

The stators and rotor have fully open and fully closed slots respectively. These features were preferred because of the simplifications they introduced into the production of the experimental machine. For the stator an open, or at least semi-open, slot is necessary in order to load the winding. But to produce the semi-open version requires two machining operations as opposed to one for the open slot. Coupled with this is the difficulty of maintaining the shape of the semi-open slot, particularly at D_1 , during the milling operation. It follows that a semi-open slot is not to be preferred on the rotor either. Initially, therefore, there is a choice of fully open or fully closed slots for the rotor. The former can be discarded on the grounds that the squirrel cage requires some means of retention. It is an occasional practice in radial machines to have closed slots on the rotor but the bridge across the slot is generally quite thin. A compromise is necessary because,

- 1) If the bridge is of a relatively substantial cross section, the bridge will itself form part of the return path for the main flux (Figure 3.10). This will reduce the amount of flux that links the circuit on the rotor.
- 2) If the bridge is too small it quickly saturates and the slot behaves as a semi-open slot in which the opening is of an

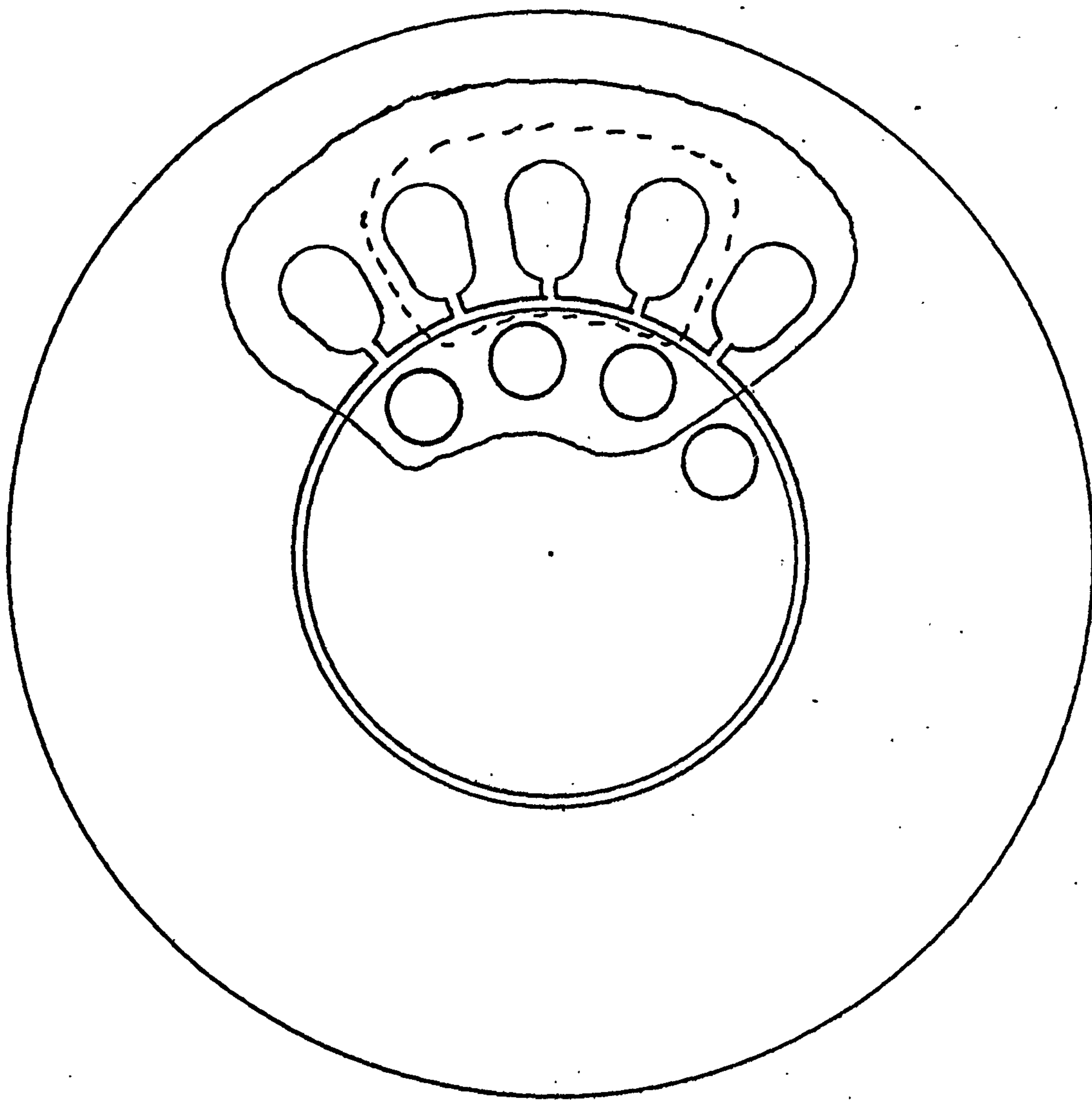


Figure 3.11

Closed rotor slots in radial machine. Rotor slot bridge acts as
return path for field as
indicated by dotted line

indeterminate size.

However, for the axial machine the cross section of the bridge is not limited by either of the conditions given above because the useful flux is constrained to take an axial path due to the mutual effect of the stator m.m.f.'s. The parameter most likely to limit the size of the bridge is the slot leakage reactance of current carrying conductors on the rotor.

The experimental machine has an overall diameter of 230 mm and an overall length of 110 mm. This ratio of diameter to length equal to approximately two has been met consistently with all axial machine designs both a.c. and d.c. produced at the University of Warwick.

Chapter IV

Experimental Results

4.1 Introduction

The three main sections of this chapter deal with:-

(1) Preliminary Tests:-

These are concerned with the calibration of the tor ductor, comparison of the magnetic states of the rotor and stator iron, iron losses etc.

(2) Performance of the induction motor:-

The main variable is the squirrel cage resistance but different airgaps are also considered.

(3) Performance of the reluctance motor:-

The pull-in and synchronous performance are investigated as functions of the pole arc/pole pitch ratio.

Because of the special shape of the axial machine and the presence of the two stators it is possible to obtain reliable figures for the losses in the stator and the rotor. The procedure used to divide the iron losses into stator or rotor components is extremely simple and is discussed more fully in the following sections.

4.2 Preliminary tests

4.2.1 Classification of losses

The losses in all electrical machines can be divided into three main categories:-

(1) Copper losses:-

These are relatively easy to calculate provided the resistance of and the current in the winding are known. However, even this can be considered a fairly intricate subject since although a current in a winding can often be measured the

resistance of the winding depends on the temperature of the winding and the surrounding media. This is seen to be one of the major loss components in the experimental machine.

(2) Iron losses:-

There exists a wide variety of formulae for the computation of iron losses in machines. The dependance of this loss component on the flux density, the resistivity of the iron, the frequency of the flux density and on whether or not the loss is due to a rotational or pulsating flux brings the complexity of the subject into perspective. Because of the presence of the double stator in the axial machine it is comparatively easy to divide the losses into rotor and stator components. In determining these losses the magnetic states of the rotor and stator irons can be compared. Very often the condition of laminated steels is expressed in terms of saturation flux density, permeability or the shape of the B-H loop. In practical terms however it would seem that a meaningful indication of the state of a particular grade of iron is obtained by making a comparison on the basis of power loss.

(3) Friction and Windage:-

These are generally determined after the machine has been built and are assumed to be constant over the speed range. This is seen to be true for the d.c. machine used in the testing of the experimental machine.

4.2.2 Comparison of the rotor and stator iron loss

Figure 4.1 shows the developed model, including the stator teeth, of the induction machine and the reluctance machine. By removing the rotor the two stators can be brought together until separated by any required airgap length. By measuring the total input power the iron loss in the stator can be obtained by subtracting the copper losses. If the rotor is replaced, without the squirrel cage, the new value of the iron loss can again be found and because the stator iron losses are already known a set of rotor iron loss figures can be determined. However it transpires that this is a meaningless exercise as far as the reluctance motor is concerned. For either machine the removal of the rotor introduces an inherent error in the measurement of the losses. But because the rotor of the induction motor is represented by (and in practice is) a smooth continuous surface the harmonic flux in the stator and the magnitude of the flux will not be substantially different for the stator-stator or the stator-rotor-stator configuration. On the other hand, the discontinuous nature of the reluctance motor rotor is the source of harmonic flux in the stator and the iron losses that these produce would not be measured in a stator-stator arrangement. Consequently the comparison of the condition of the stator and rotor iron is made using the induction motor.

The airgap flux was monitored using a single turn search coil and for the range of magnetising current, corresponding to a supply voltage variation from zero to 224volts (maximum) the flux was seen to remain substantially sinusoidal for both stator-stator and stator-rotor-stator configurations. The iron loss is shown plotted as a function of input current in figure 4.2. The total rotor losses are seen to be much greater than the total stator losses by a factor of approximately three times. The variation of the losses

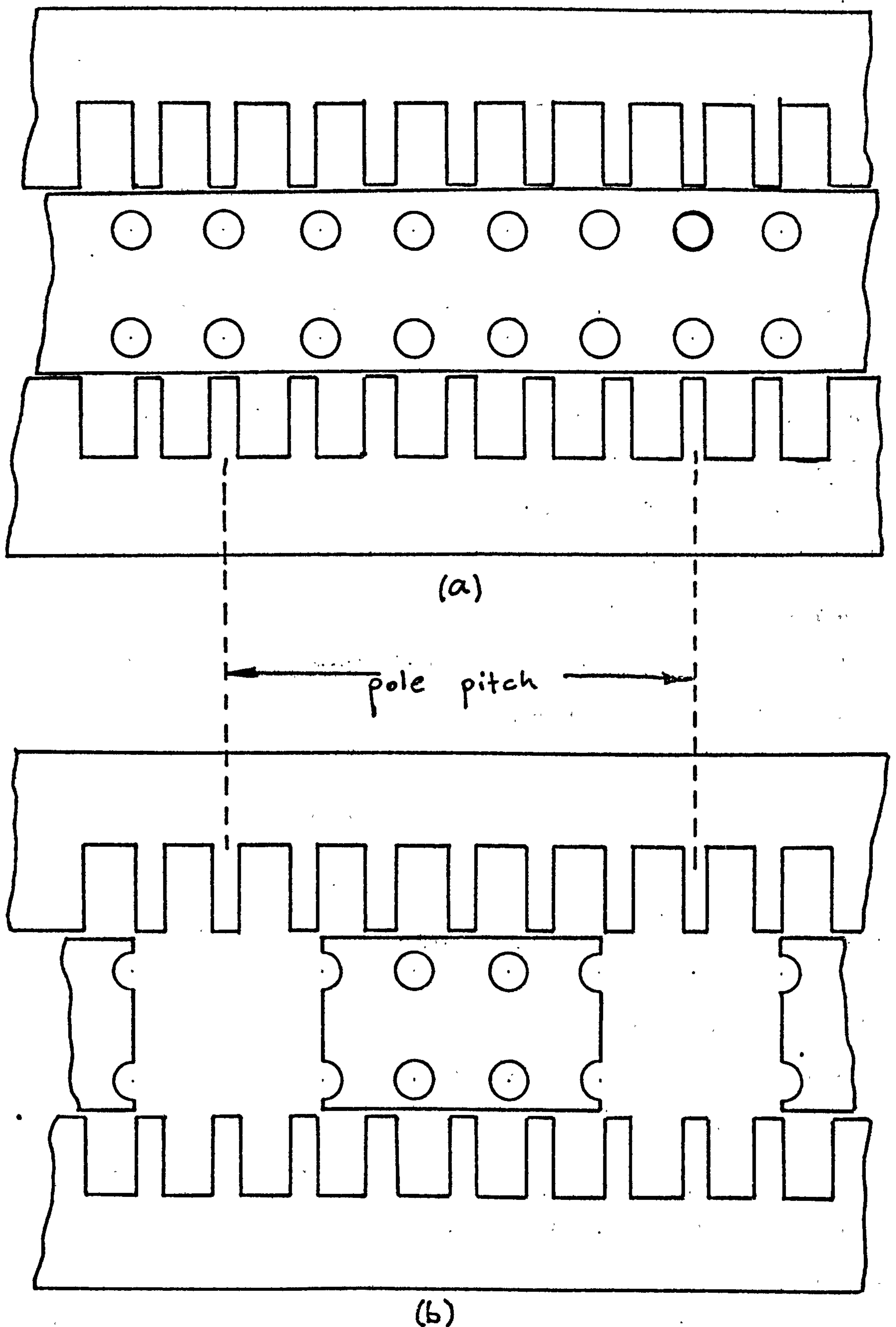


Figure 4.1 (a) Developed diagram of Induction Motor
(b) Developed diagram of Reluctance Motor

for both stator and rotor are seen to be given by,

$$\text{loss} = f(i^x)$$

where x is less than two

and i = magnetising current.

It is not possible with this test to determine how these losses are divided into eddy current and hysteresis components but it becomes apparent, when the induction motor is tested, that these iron losses are due mainly to the latter. It will be recalled that the rotor did not receive a final stress relief anneal (Chapter III). This was done specifically to determine whether or not the manufacture of this type of machine could be simplified as it would undoubtedly be if this annealing was unnecessary. The difference in loss figures for these two members could in themselves be sufficiently conclusive to warrant a stress relief anneal. However, such a decision would inevitably be determined by cost, and the overall requirements or specification of the motor. This in turn would necessarily be affected by the type of market, whether domestic or industrial, for which such machines could be used.

4.2.3 Calibration of torque unit

A static calibration was carried out on the torque unit. The output was loaded with 1000ohm in series with a milliammeter and the torque factor was measured at 0.5 Nm/mA. The linear accuracy was found to be within $\pm 3\%$ over its full range (up to 60 Nm). Over the working range (up to 15 Nm for the experimental machine) the error was reduced to $\pm 2\%$. The accuracy and torque factor hold for clockwise and anti-clockwise loading of the rotor shaft extension.

4.2.4 Measurement of load angle

A dial calibrated in degrees was fitted to the casing at the non-drive end and a pointer was attached to the shaft to run concentrically against the

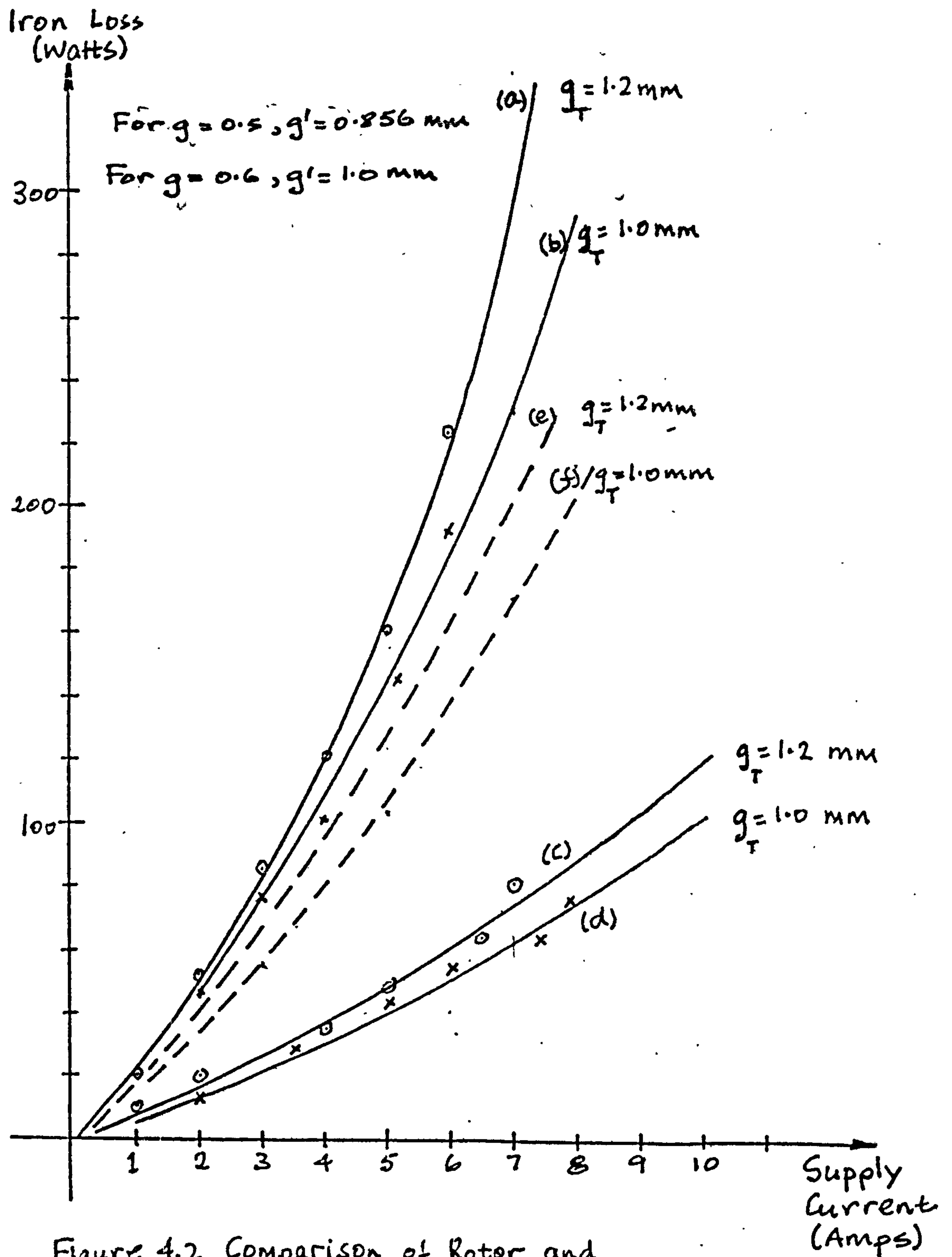


Figure 4.2 Comparison of Rotor and stator iron loss

- (a) Stator plus rotor iron loss
- (b) Stator plus rotor iron loss
- (c) Stator iron loss
- (d) Stator iron loss
- (e) Rotor iron loss
- (f) Rotor iron loss

face of the dial. By using a stroboscope switched to mains calibration the pointer is seen to remain stationary, except for load changes, once the machine has synchronised. This is a common method of measuring load angle.

Under no load conditions the load angle was seen to be approximately constant for all supply voltages down to pull-out. This was taken as the zero load angle reading and was consistently repeatable.

4.2.5 Inertia

The inertia of the d.c. machine rotor was obtained from the manufacturer as,

$$J_{dc} = 176 \text{ lb.in}^2 = 0.052 \text{ Kgm.m}^2$$

The inertia of the rotor of the experimental machine was calculated using the expression,

$$\begin{aligned} J_r &= 8.3(\beta 6.87 + 3.38) \text{ lb.in}^2 & \text{Appendix V} \\ &= 0.00245(\beta 6.87 + 3.38) \text{ Kgm.m}^2 \end{aligned}$$

4.2.6 D.C resistance of stator winding

This was measured using a Wheatstone bridge. To obtain the value of the operating resistance the experimental machine was operated at full load as an induction motor until the temperature became constant. The motor was switched from the supply to the bridge and the resistance was measured as,

$$R_{dc} = 2.6 \text{ ohm at 10 Amps (per phase)}$$

For the computation of the machine performance the winding resistance was taken as 2.4 ohm. The resistance (cold) of the three phases was 2.1, 2.05 and 2.12 ohm. The inherent error in this method of measuring the resistance is negligible. It will depend on how quickly the measurement (hot) can be taken and will be less than 16%. This figure is based on the % difference between the cold readings (minimum 2.05 ohm) and the hot value.

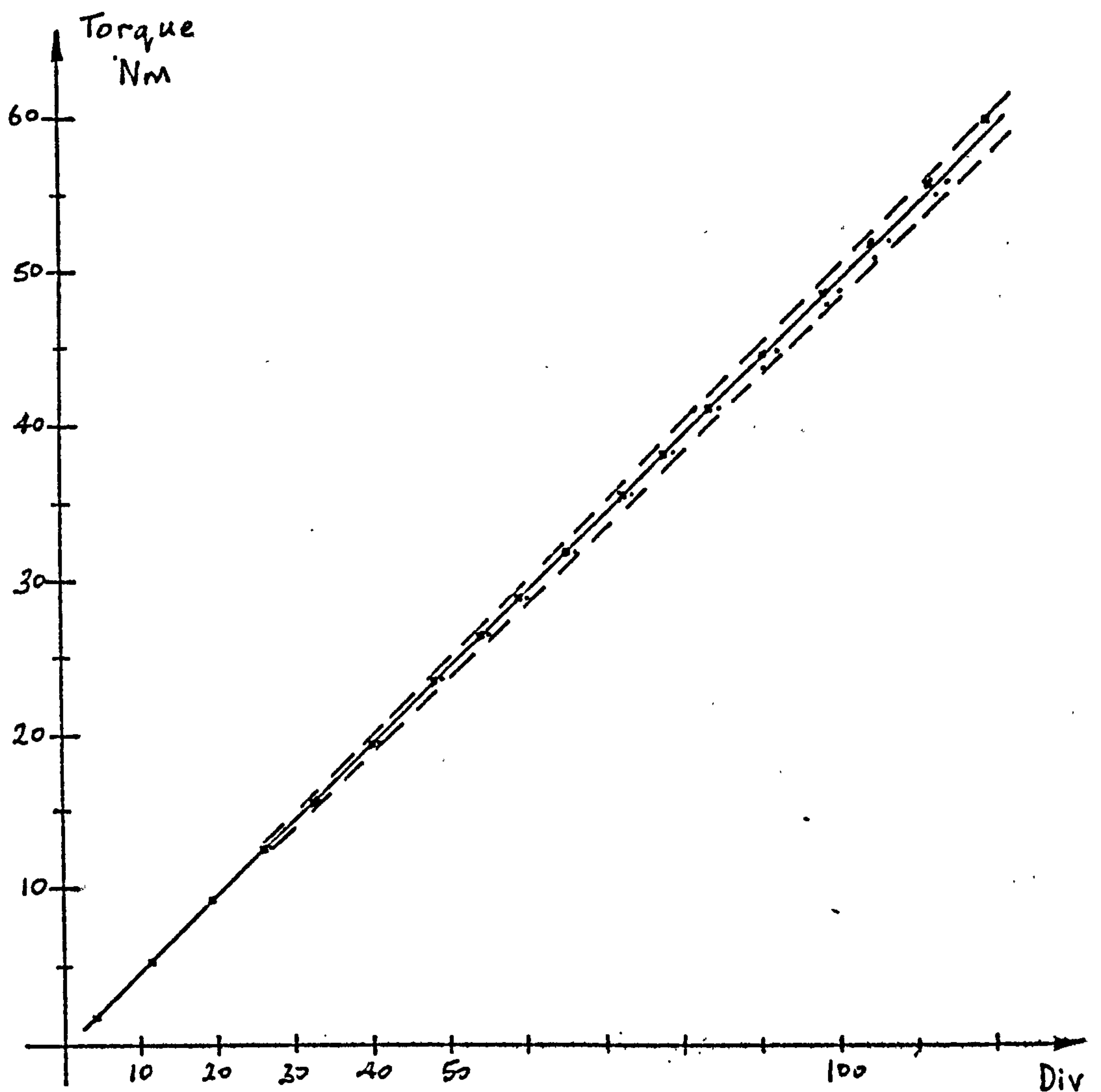


Figure 4.3

Calibration of Torductor

Output factor = $0.5 \text{ Nm per division}$

for clockwise and anticlockwise loading

The limit lines (dashed) represent $\pm 2\%$ variation from the linear output

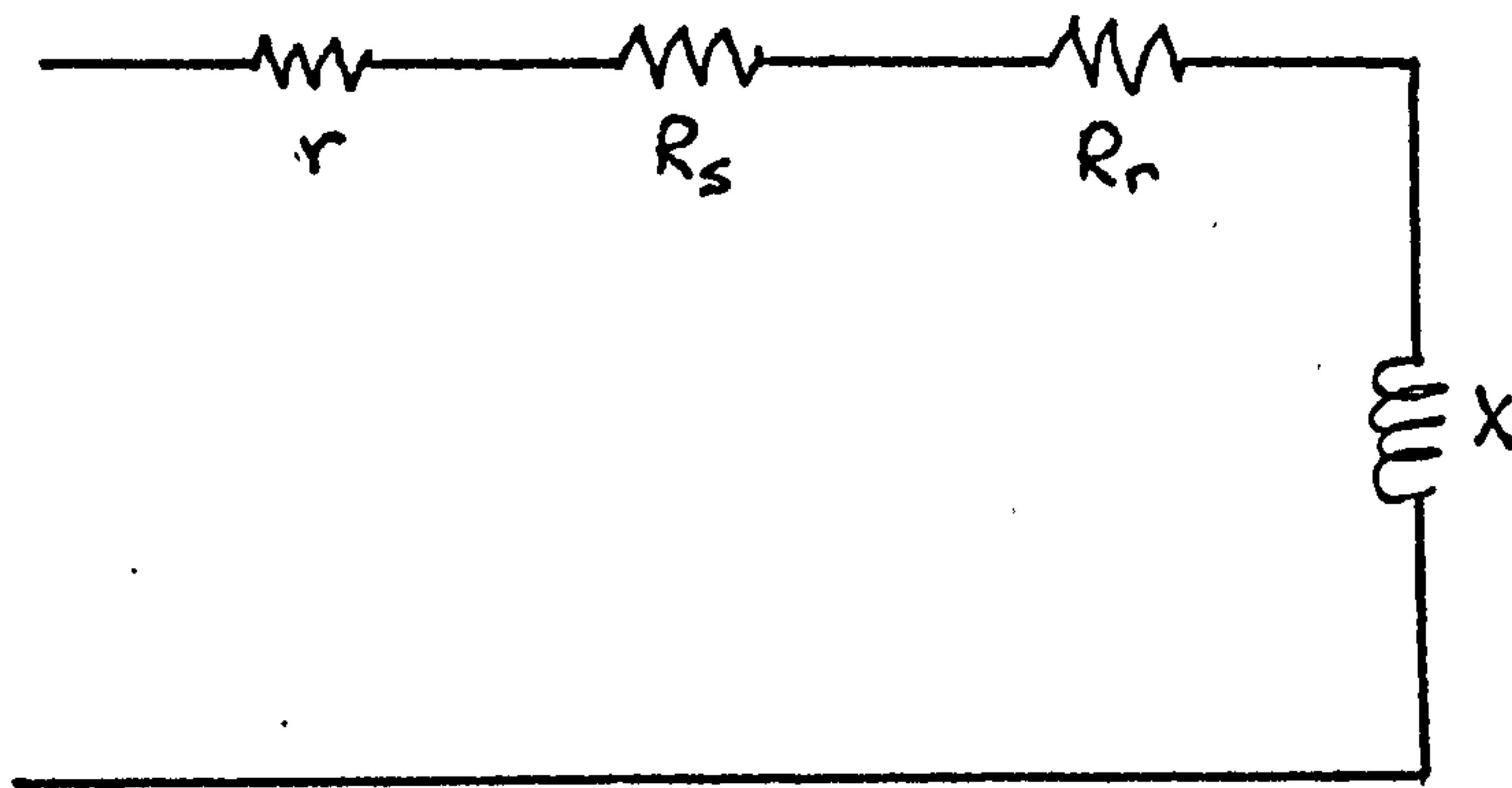
4.2.7 Temperature rise

The temperature was measured using thermo-markers and a maximum rise of 65°C was measured on the stator and rotor in a region close to the shaft when the machine was being run as an induction motor. For the reluctance motor the maximum temperature on the rotor was slightly lower at 60°C . These were only measurements of surface temperatures.

4.3 Performance of the induction motor

4.3.1 Iron losses as a function of speed

With the squirrel cage removed the equivalent circuit, on a per phase basis, of the induction motor becomes a simple resistance-reactance series connected circuit as shown below,



where, r = resistance of the winding

R_s = equivalent resistance representing the stator iron loss

R_r = " " " " rotor " "

X = reactance of the machine.

Attention is drawn to the fact that generally in the equivalent circuit the iron loss component is shown in parallel with the magnetising reactance. There is some justification for this but basically it is a matter of convention. However from the manner in which the iron losses are measured, the series circuit is to be preferred.

The experimental machine was coupled to the d.c machine, the latter being energised and run as a motor from standstill up to and including synchronous speed. The power input to the d.c motor as a function of speed was measured. With the axial machine connected to its supply the test was repeated. From the results it was noted that the speed/power input curve of the d.c motor did alter slightly, though for any speed the decrease in power to this machine was never more than 5% for the latter test. This indicated that there was still a tendency for the axial machine to produce torque even without the copper squirrel cage. This is caused by eddy currents in the rotor but it was not possible to determine whether the eddy currents were in the laminations or in the eight retaining bolts, retaining ring and rotor shaft which would behave as a squirrel cage. This change in power was ignored, consequently the total losses in the axial machine represent purely the copper losses of the stator winding and the total stator plus rotor iron loss, this latter component being given by the difference in input power and copper loss. The total iron losses are shown as a function of speed in figure 4.4.

Since the input current did not vary in the axial machine over the speed range, the flux is considered constant. As indicated by the dotted line in figure 4.4 the deviation from a linear relationship is marginal. This confirms that the cause of the iron loss in the rotor is due mainly to hysteresis effects. The losses at $N=1500$ rpm are losses in the stator alone and these compare very favourably with those obtained from the tests on the stator-stator configuration.

4.3.2 Friction and windage of the d.c machine

With the experimental machine on no load a curve of power input against speed was obtained by varying the supply voltage. The axial machine was then coupled to the d.c machine and the test repeated, the difference between

Rotor of experimental machine driven
mechanically by d.c machine

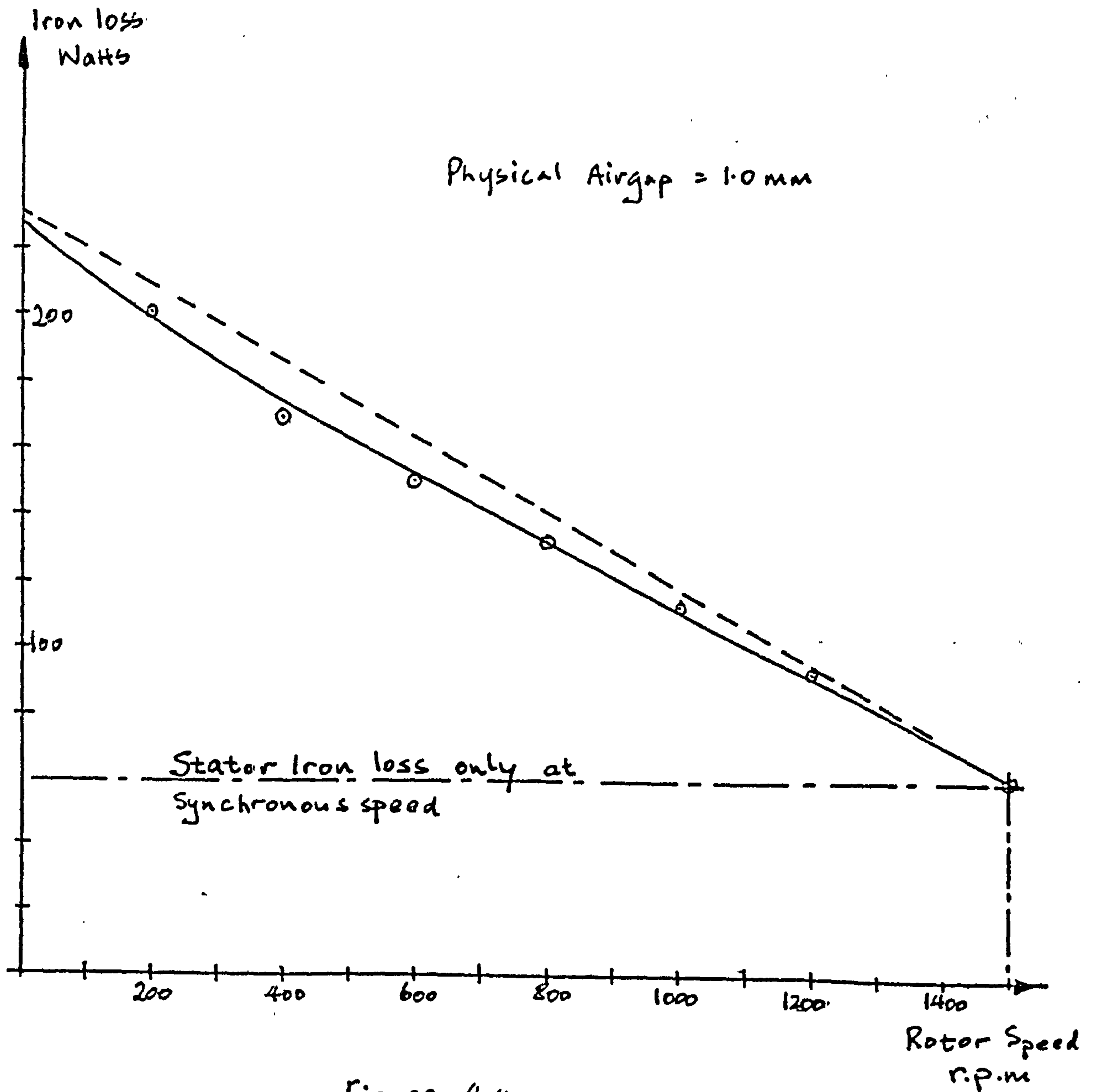


Figure 4.4

Total iron loss as a function of rotor speed
Actual relationship shown in full
Linear relationship shown dashed

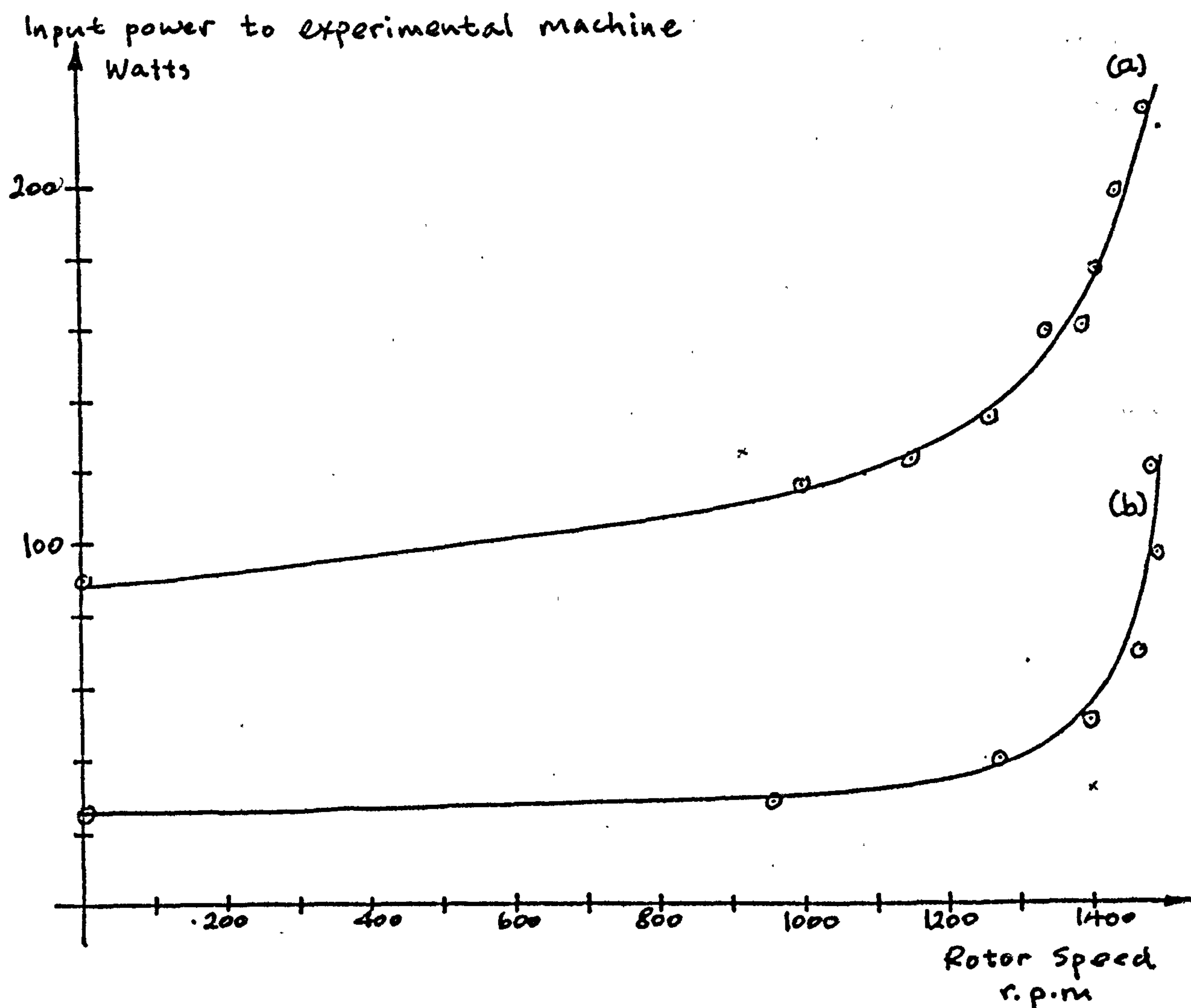


Figure 4.5

No Load test on experimental machine

(a) mechanically coupled to d.c motor rotor

(b) uncoupled

Over speed range 1000 - 1490 r.p.m difference in input figures is approximately constant at 100 watts.

the two input power readings giving the effective friction and windage losses of the d.c. motor as a function of speed. The curves of figure 4.5 show that over the complete speed range the mechanical losses of the d.c. machine were approximately constant at 100 watts. The torductor reading at 1500 rpm gave a torque of 0.68 Nm corresponding to a power of 107 watts.

4.3.3 Equivalent circuit parameters

Of all the parameters in the equivalent circuit the iron loss component, the stator leakage reactance and the rotor leakage reactance are the most difficult to compute. The iron losses have been determined experimentally and since these are in general much smaller than the copper losses the error introduced in ignoring them is considered negligible. Figures 4.6 and 4.7 show how the stator and rotor leakage reactance effect the torque/speed curve. The value used for the comparison with the measured results were taken as,

$$X_1 = 4.82 \text{ ohm}$$

$$X_2 = 0.286 \text{ ohm}$$

The value of R_2 and X_2 in the equivalent circuit is given by, (p.34)

$$R_2 = 4pNK_1 \sqrt{\frac{q}{n_b}} \cdot r_c$$

$$X_2 = 4pNK_1 \sqrt{\frac{q}{n_b}} \cdot x_c$$

where, $4pNK_1 \sqrt{\frac{q}{n_b}}$ = turns ratio of the machine

The terms r_c and x_c are defined in Appendix II as the components of the bar load impedance and these are computed in Appendices III and IV. In terms of the bar and endring impedance

$$r_c \cong r_b + \frac{1}{2}r_e$$

$$x_c \cong x_b + \frac{1}{2}x_e$$

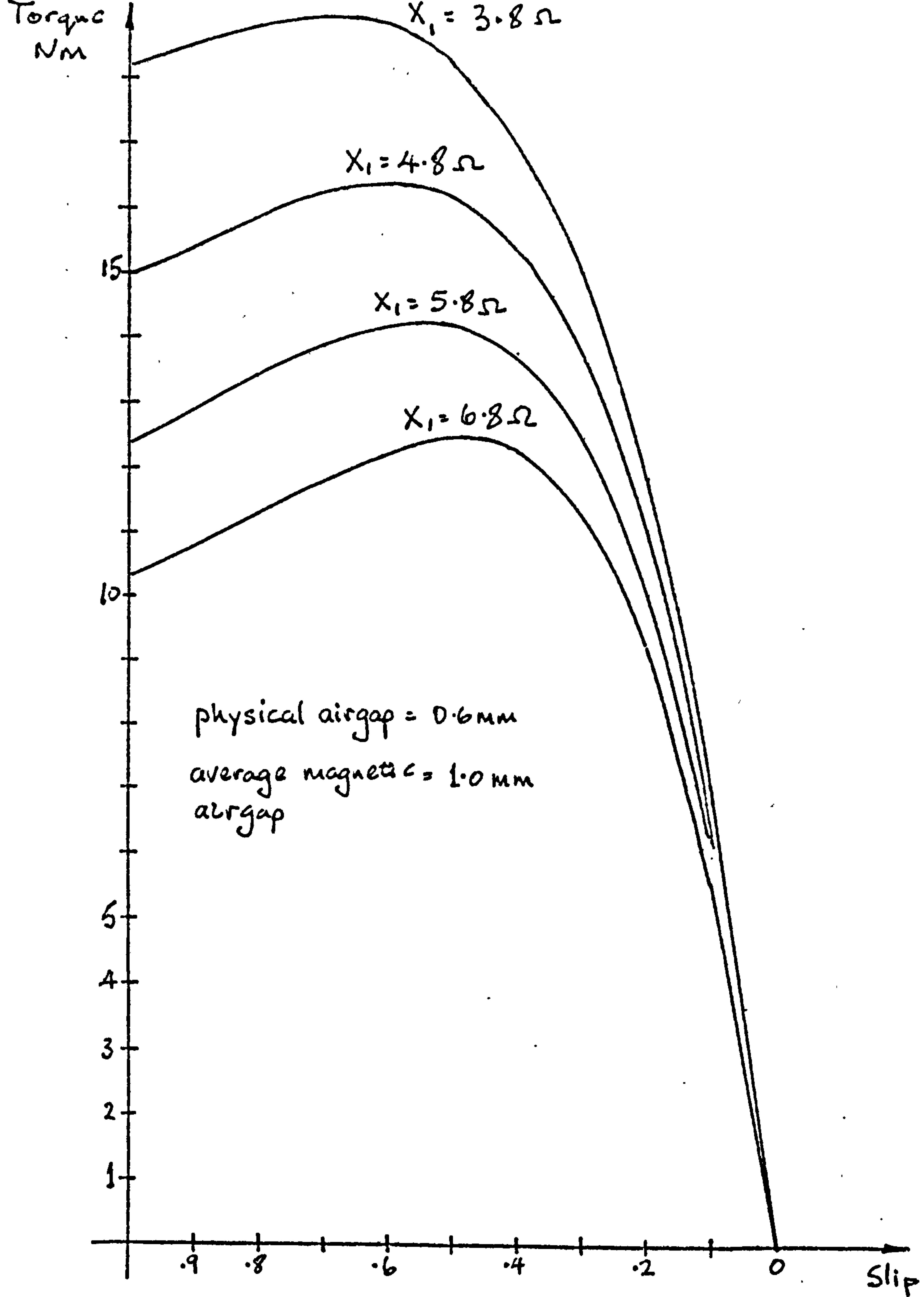


Figure 4.6

Torque/speed curve of induction motor for varying stator leakage reactance.

X_1 = leakage reactance per phase of stator

X_2 = " " " " " rotor referred to primary side of equivalent circuit } = 0.286Ω

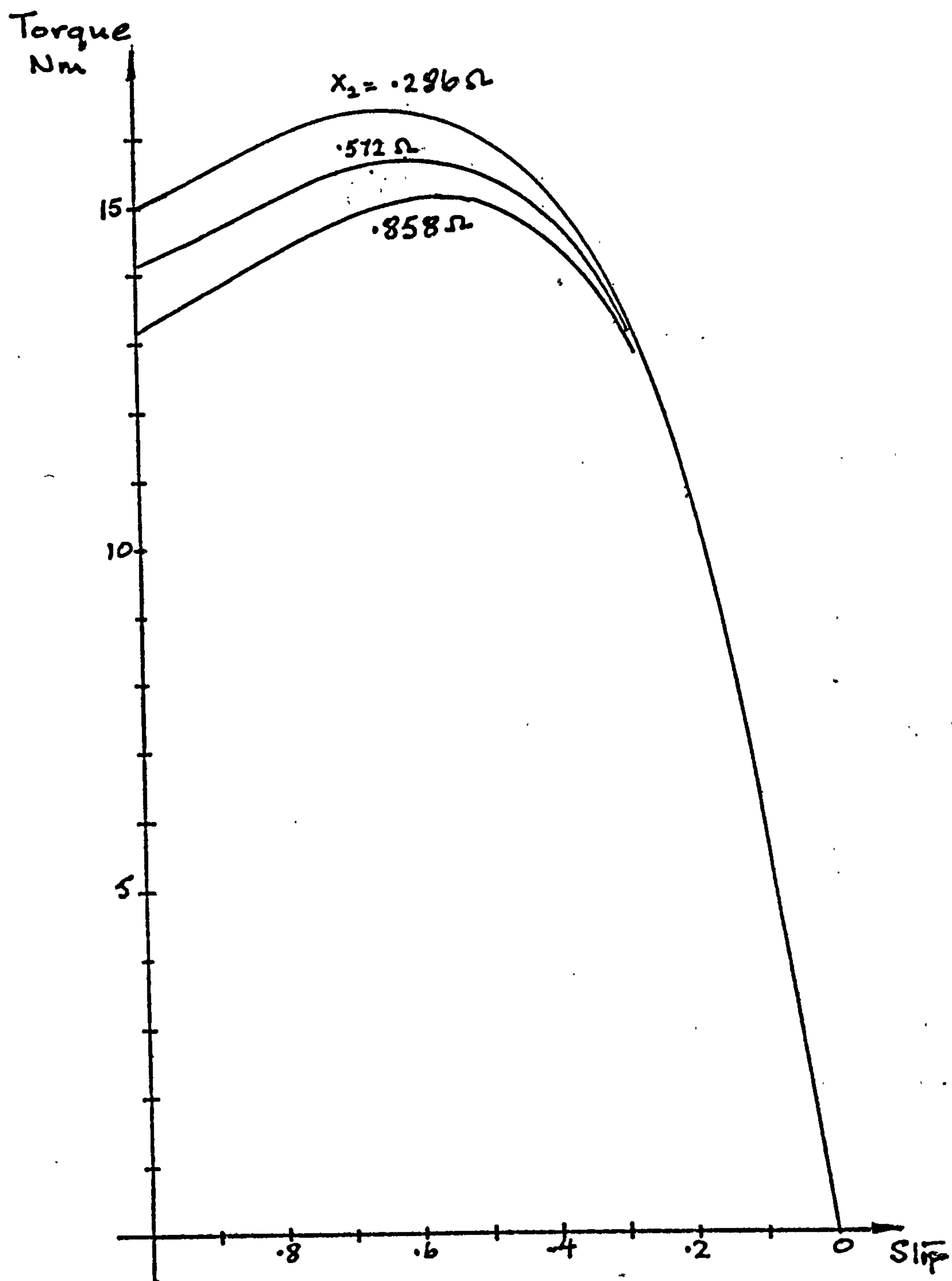
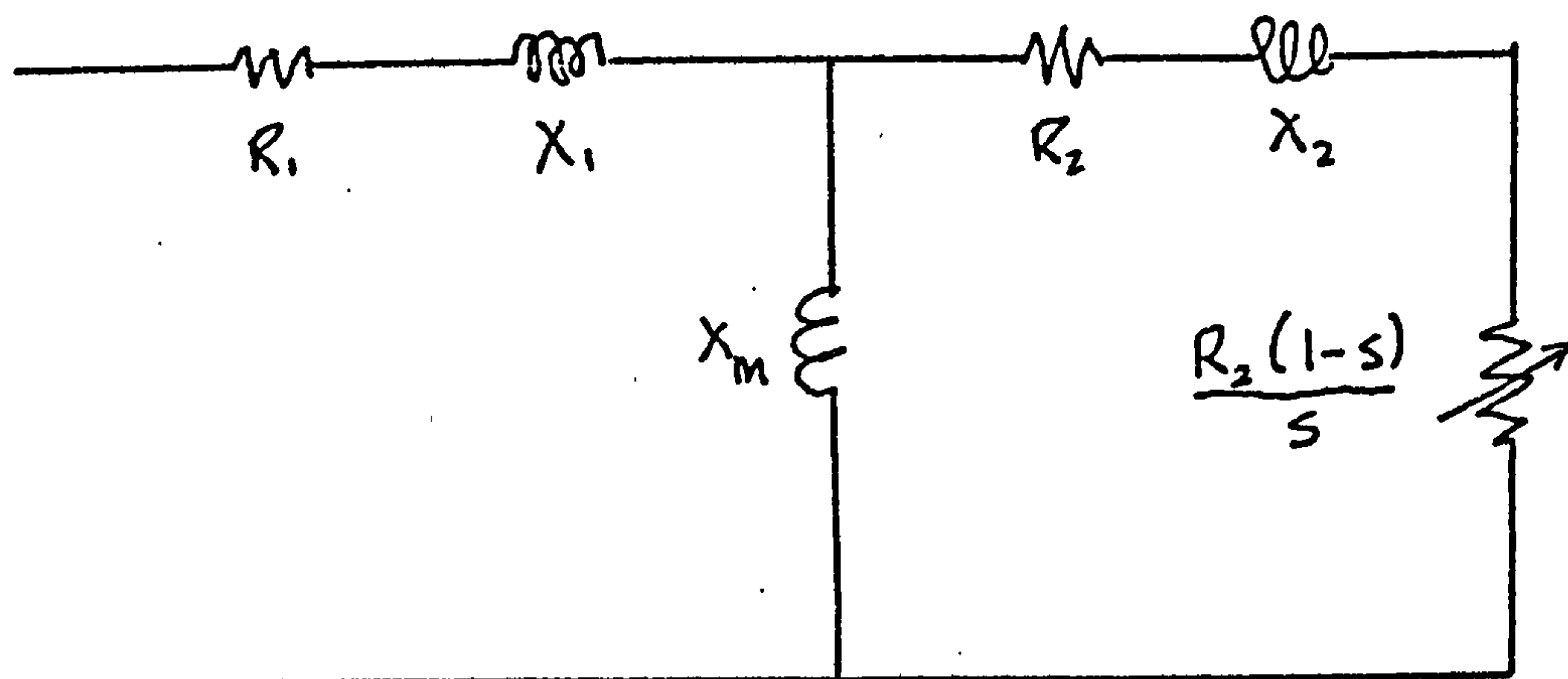


Figure 4.7

Torque/Speed curve of induction motor
for varying rotor leakage reactance

X_1 = stator leakage reactance = 4.82Ω

X_2 = rotor " " referred to stator



Equivalent circuit of the induction motor

where, r_b and x_b are the impedance components of the bar and r_e and x_e are the resistance and reactance components per pole pitch of the inner and outer endrings. In Appendices III and IV the a.c resistance of the squirrel copper is within 1% of the d.c. value for the frequency range encountered in the machine.

4.3.4 Torque/Speed curve

The d.c machine, which was connected to operate as a self excited shunt generator, was coupled to the experimental machine and the torque/speed curves for values of torque approaching maximum torque was measured. The theoretical torque/speed curve was computed in the usual manner using the equivalent circuit of section 4.3.3, the parameters for which are shown below in tabular form.

	$g' = 0.855\text{mm}$		$g' = 1.0\text{mm}$		$g' = 1.123\text{mm}$	
	$g = 0.5\text{mm}$		$g = 0.6\text{mm}$		$g = 0.7\text{mm}$	
R_1	2.4	2.4	2.4	2.4	2.4	2.4
X_1	4.8	4.8	4.8	4.8	4.8	4.8
X_m	28.3	28.3	24.2	24.2	21.6	21.6
R_2	2.86	4.75	2.86	4.75	2.86	4.75
X_2	.286	.286	.286	.286	.286	.286

Two cages were tested and the experimental and computed results for physical airgaps of 0.5mm, 0.6mm and 0.7mm are shown in figures 4.8, 4.9, and 4.10 respectively. The curves are typical of the induction motor with the torque peaking at higher values of slip as the cage resistance is increased. The same endrings were used for both squirrel cages, the varying resistance being due to the different diameter cage bars.

4.3.5 Efficiency, Power factor, and Input current

Figure 4.11 shows the computed and measured results for the low cage resistance and an airgap of $g=0.6\text{mm}$ ($g'=1.0\text{mm}$). The results for other cage resistances and airgaps are very similar to those shown in figure 4.11 with the same order of discrepancies. For this reason only the one set of results have been reproduced.

4.3.6 Starting torque

The theoretical starting torque as a function of supply voltage varies as the square of the voltage. A comparison between computed and measured results is given in figure 4.12 for an airgap of $g=0.5\text{mm}$ ($g'=0.855\text{mm}$). Three cages of different resistances were tested ($r_c=0.00025$, 0.000166 and 0.0001 ohm)

4.3.7 Discussion of results

Six torque/speed curves are shown in figures 4.8, 4.9 and 4.10 and apart from the disparity in figure 4.8a the results are seen to be quite favourable. The complete torque/speed curve was not measured but the starting torque curves of figure 4.12 help to complete the picture and show that, in general, the experimental results agree favourably with the computed values. Wherever possible the motor was allowed to run for several minutes before readings were taken to achieve steady state conditions.

The phase current, power factor and efficiency shown in figure 4.11 are typical of the results obtained for the different cage resistances and

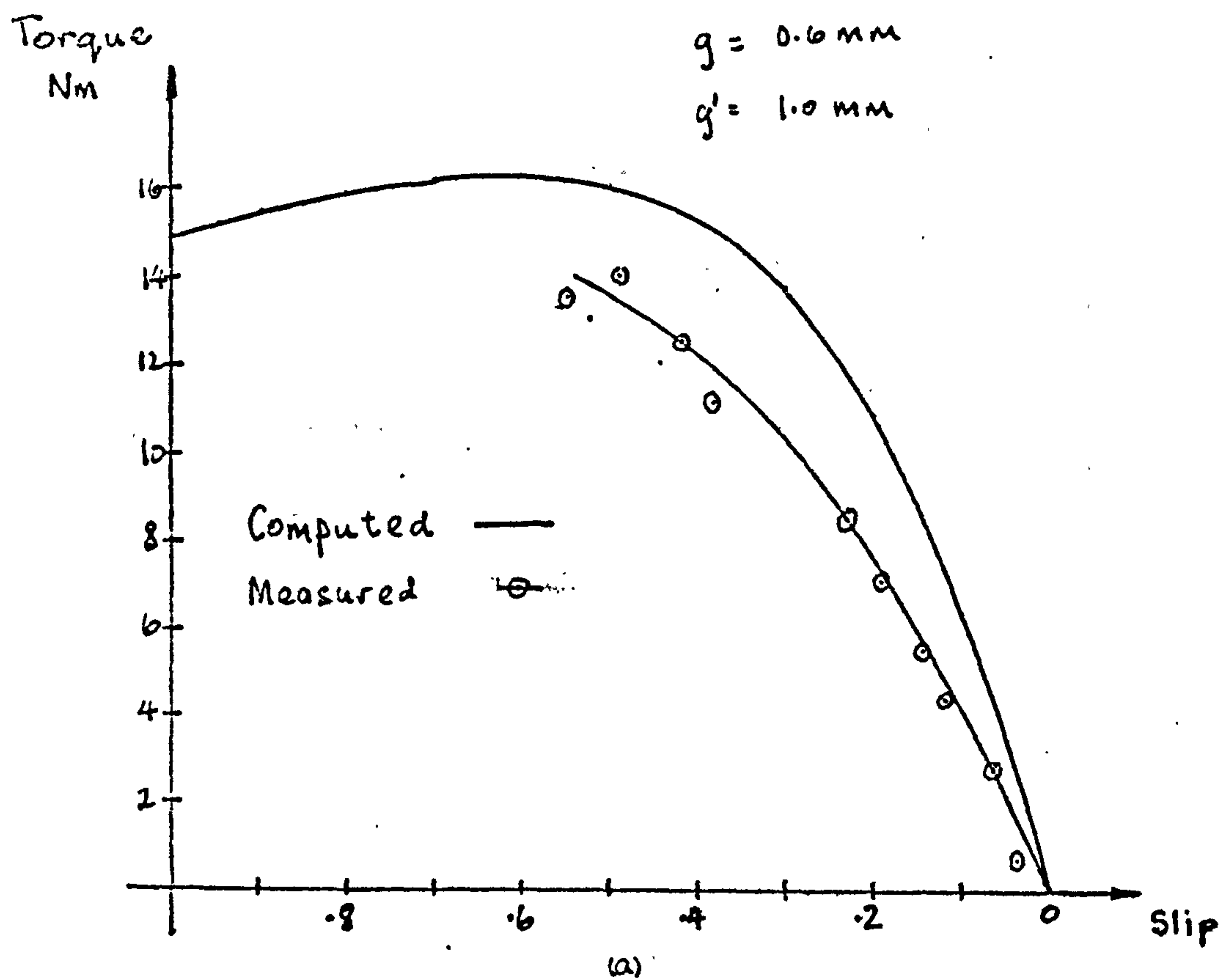
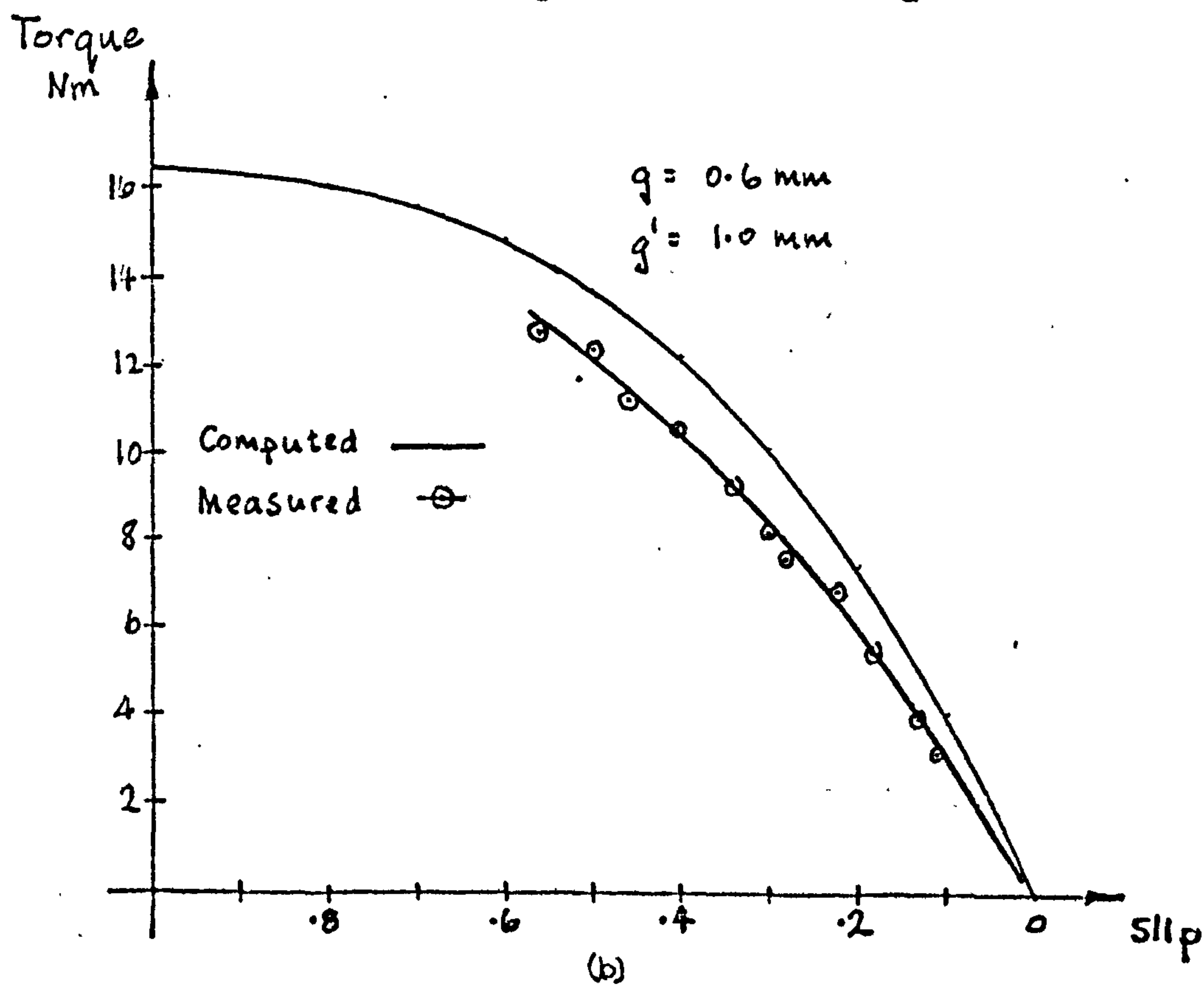


Figure 4.8
Theoretical and Experimental results of induction motor (a) low resistance cage
(b) high resistance cage



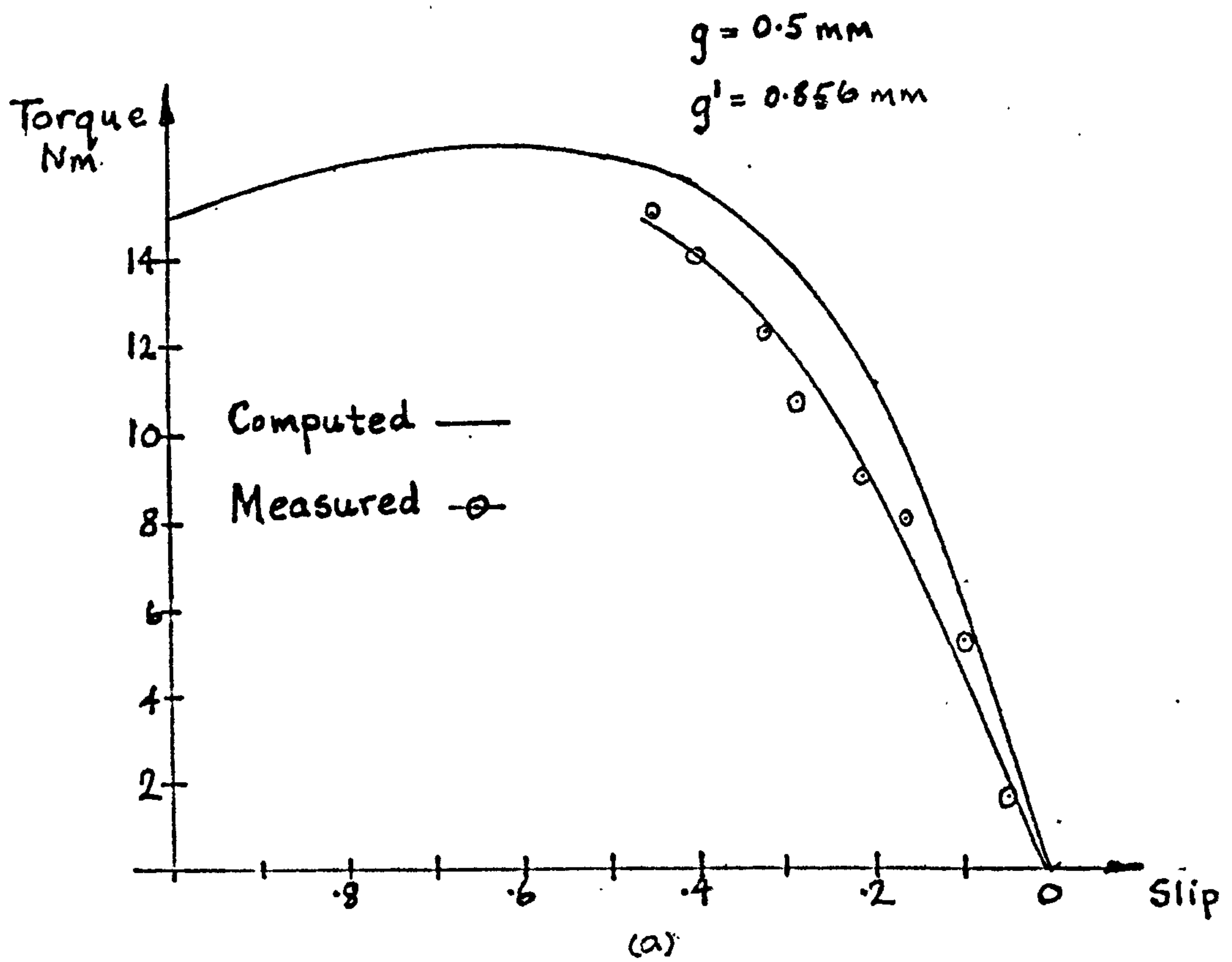
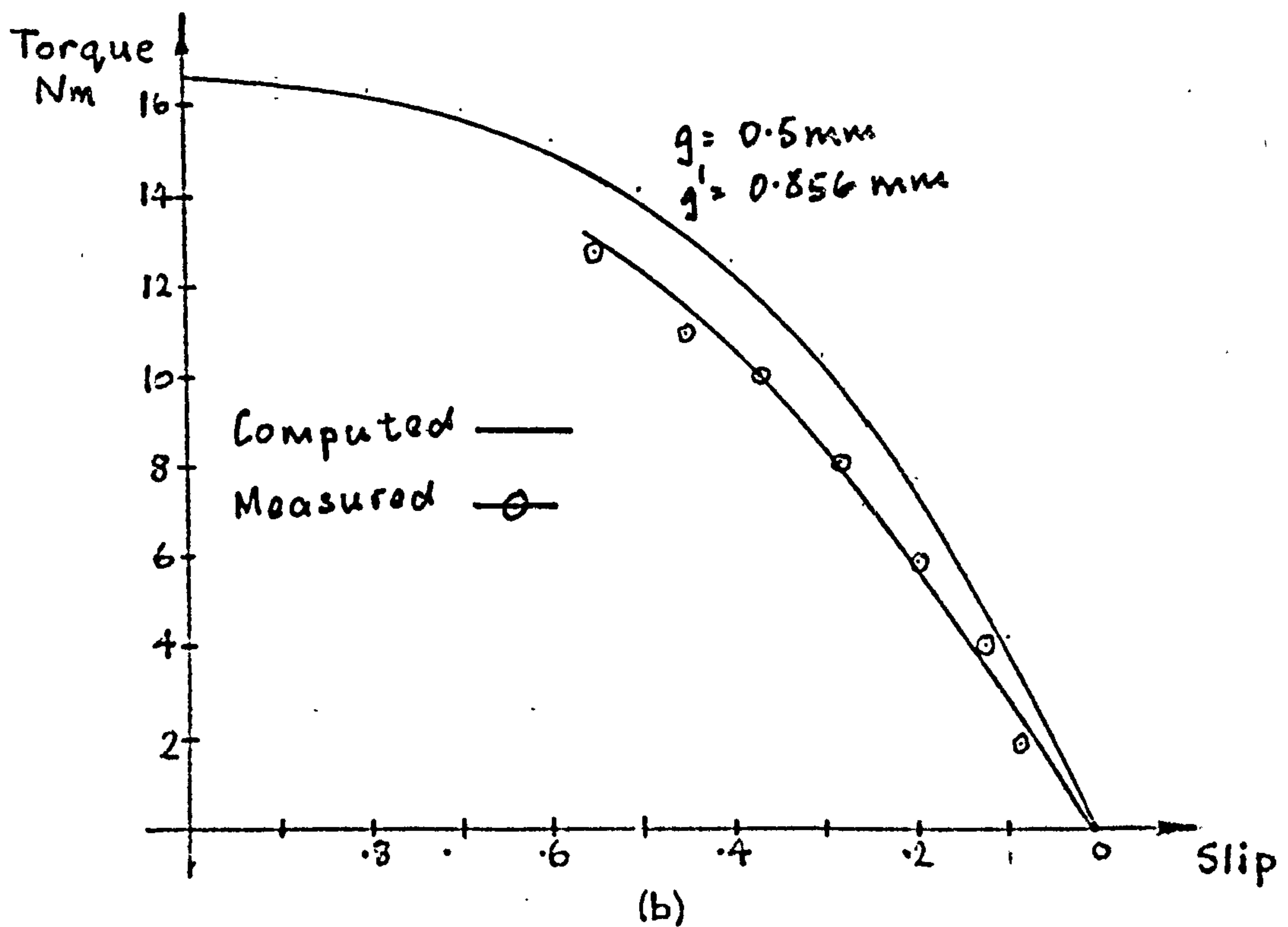


Figure 4.9

Theoretical and Experimental results for induction motor (a) Low resistance cage
(b) High resistance cage



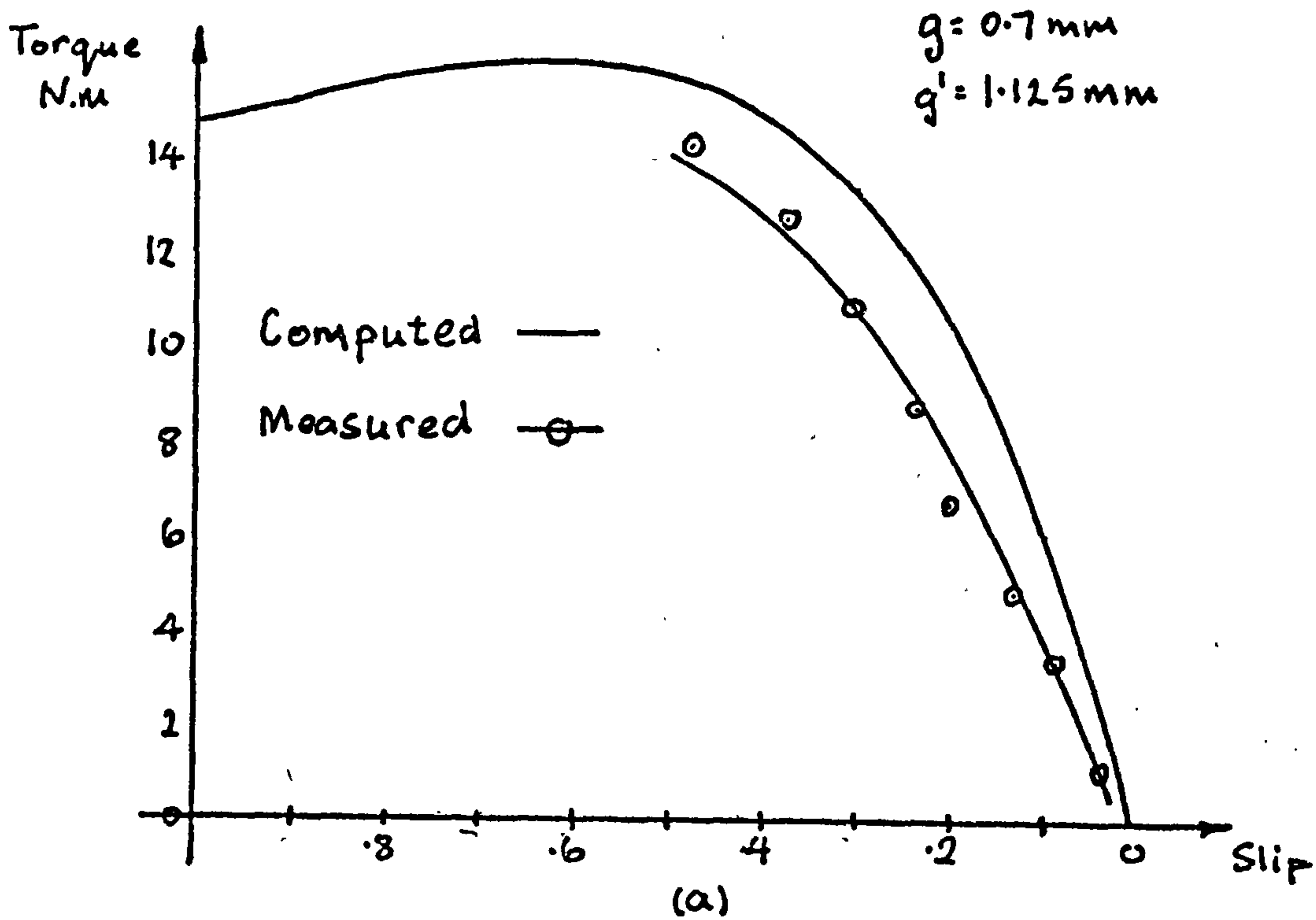
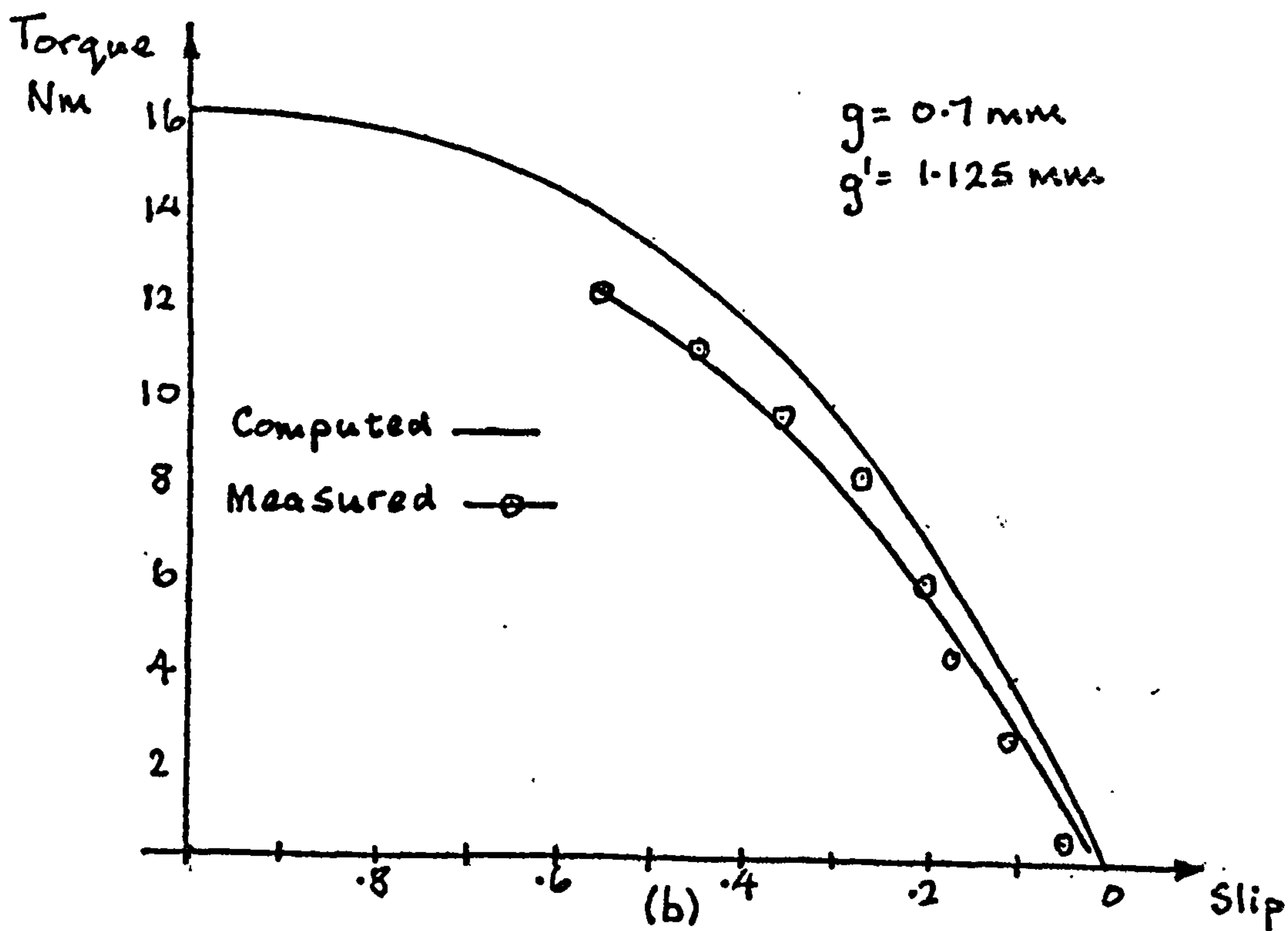


Figure 4.10
 Theoretical and Experimental results for induction motor (a) Low resistance cage
 (b) High resistance cage



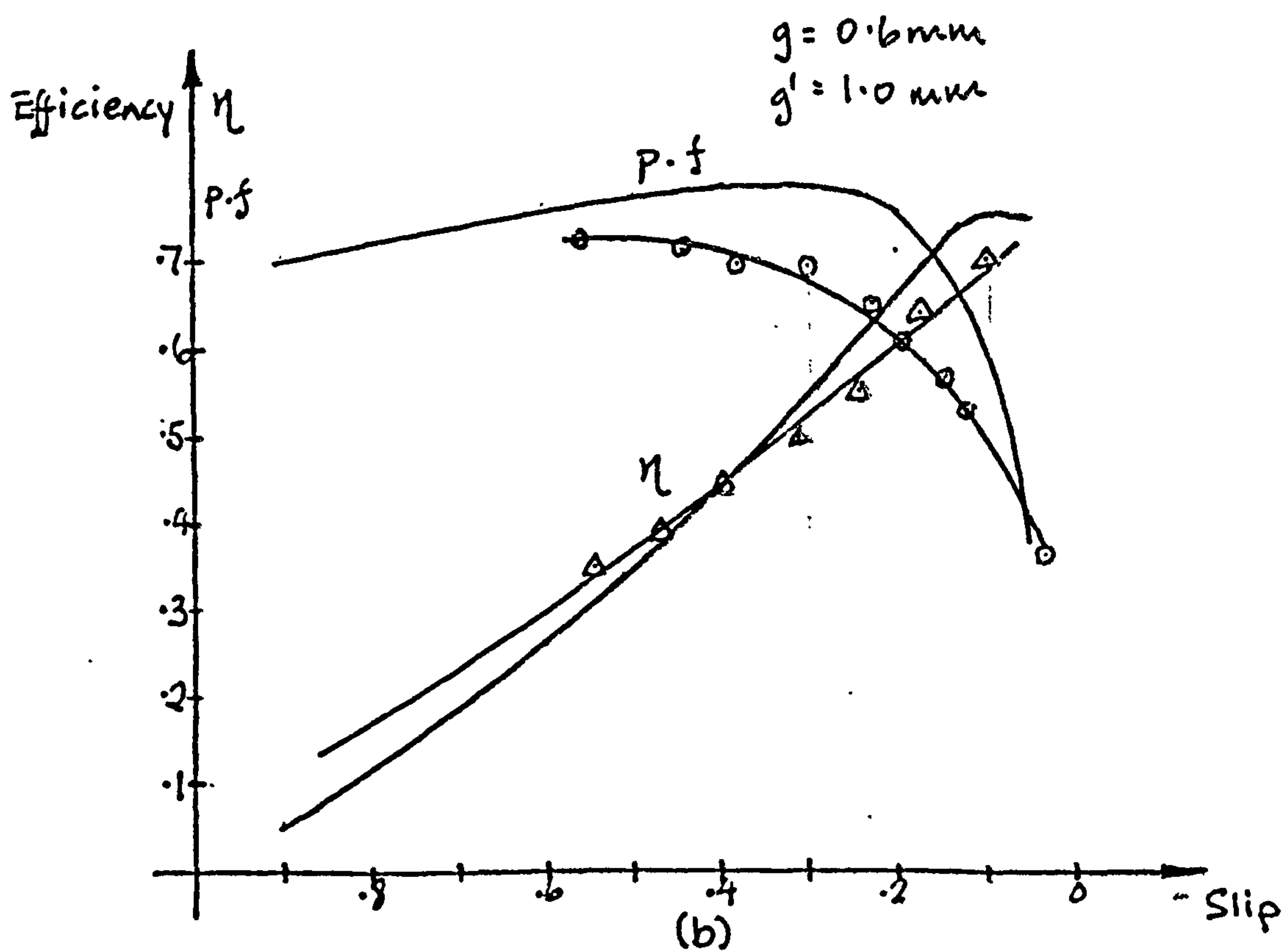
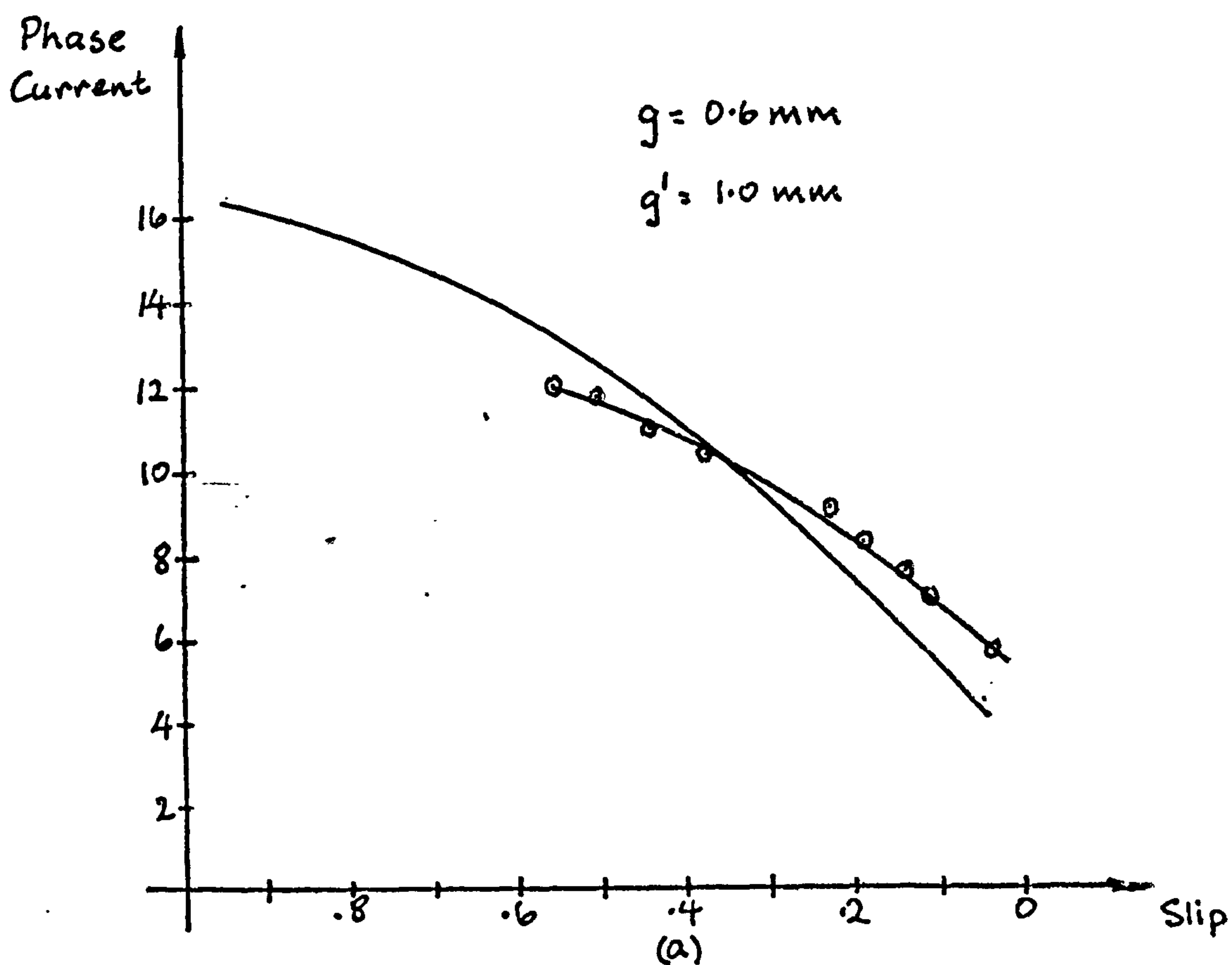


Figure 4.11

Performance curves for low cage resistance induction motor

(a) Phase current

(b) Efficiency η ;

Phase Angle; p.f

-94-

Computed —

Measured —○—

Computed —

Measured —△—

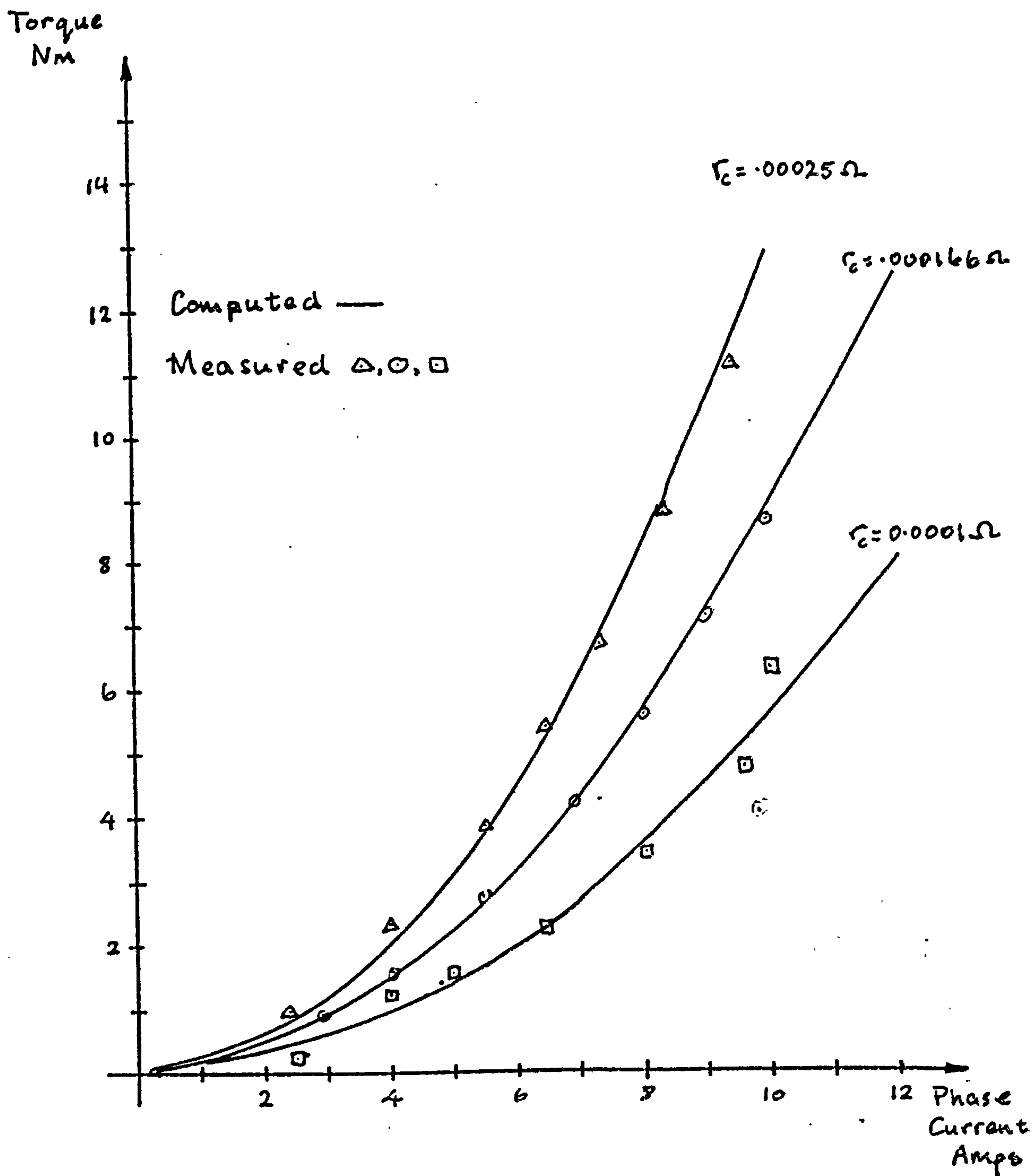


Figure 4.12

Starting torque against phase current

$g = 0.6 \text{ mm}$; $g' = 1.0 \text{ mm}$

r_c is the resistive component of the bar load impedance

airgaps used in the experimental machine. The iron losses were ignored for the computed values. The inclusion of a resistive component in the equivalent circuit to represent this will not greatly effect these parameters. In general the discrepancies between results were acceptable, the greatest differences occurring in the power factor readings. The maximum error was seen to be 24% with the measured results always being smaller than the computed ones. Reference to the torque/speed curves show that the cages appeared to be of higher resistance values than those used for the computations.

The maximum error in the efficiency curve is 13%. This relatively good correlation over the measured speed range is obtained even though the iron losses have been ignored, because the major loss component is the copper loss. For example, at $s=0.4$ the phase current is 11 Amps and for a phase resistance of 2.4 ohms the stator copper loss alone is of the order of 870 watts. The maximum efficiency was measured at $s=0.1$ as 0.69 (0.7 computed). This can be much improved by reducing the stator copper loss and is discussed more fully in chapter VI. The maximum current density for the curves shown in figure 4.11 was 12.6 A/mm^2 (8000 A/in^2). The maximum powers occurred for the low resistance cages at approximately $s=0.3$ and was measured at 1260 watts. The efficiency, power factor and current density at this output were 51%, 0.68 and 10.4 A/mm^2 respectively.

Finally it is apparent that the squirrel cage resistance could be reduced with great benefit to the power output. In fact the cage bars in the experimental machine could be increased from 2.75mm (maximum used) to 3.2mm giving a reduction in bar resistance of 34%. The endrings contribute extensively to the cage resistance but by increasing the cross-section of these the cage resistance could effectively be reduced by 50%.

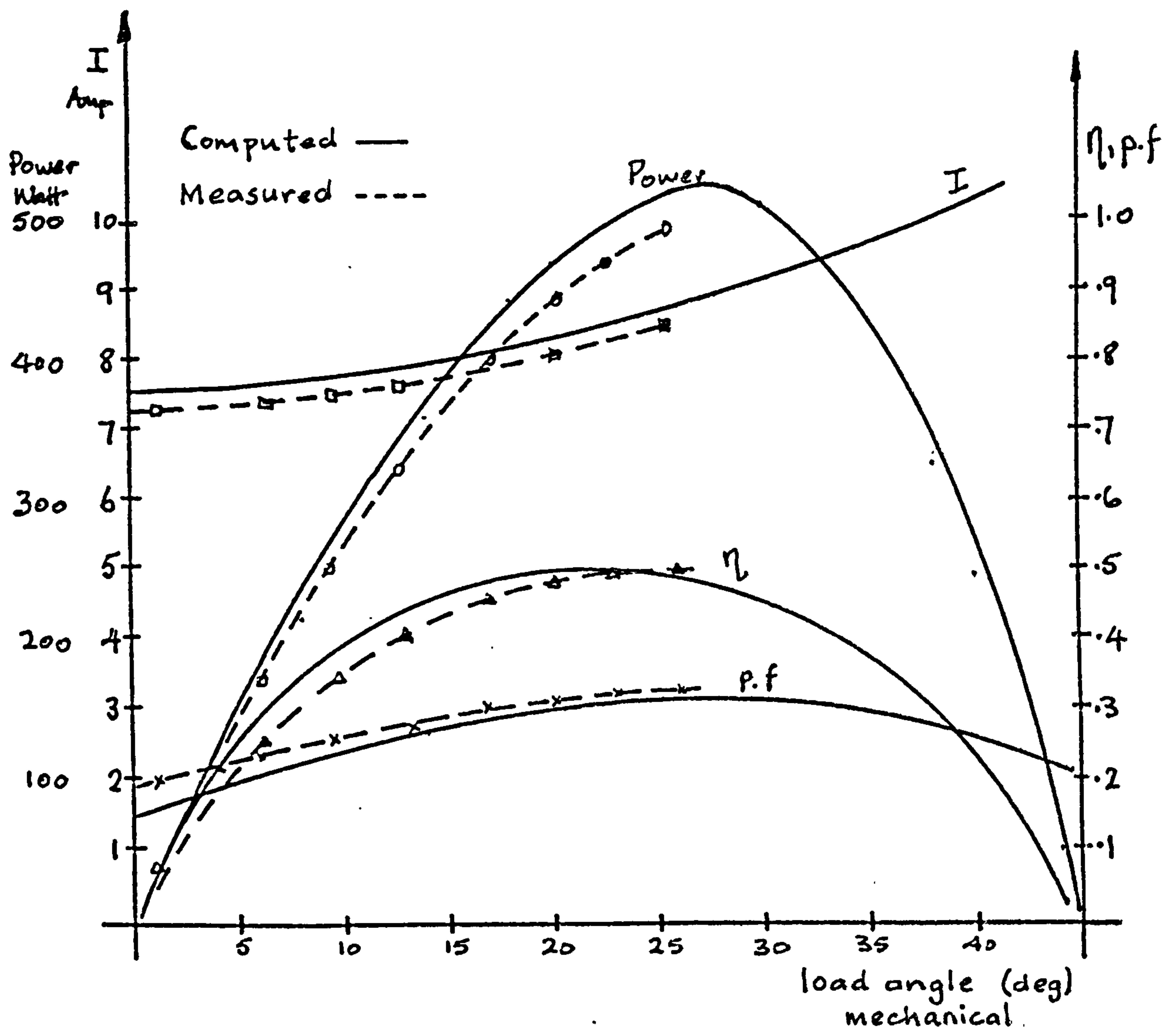
This would give a predicted output of 1530 watts at a slip of 0.15. This would also assist the pull-in of the reluctance motor as the lower cage resistance would increase the subsynchronous speed of the reluctance rotor.

4.4 Performance of the Reluctance Motor

The experimental machine was tested with the lowest cage resistance and a physical airgap of 0.6mm (giving $g' = 1.0\text{mm}$). The range of pole arc/pole pitch ratios was limited to $0.778 \leq \beta \leq 0.445$. For values of β greater than 0.778 the inertia of the d.c motor was too big to be synchronised by the operation of the reluctance motor alone and although it was possible to synchronise the rotor of the d.c motor the friction and windage losses of these two machines was so near to the pull-out power of the reluctance motor for these higher values of β that the slightest additional load caused the motor to run sub-synchronously. For $\beta = 0.778$ (pole arc = 70°) the d.c. motor rotor could still not be pulled into step by the reluctance motor. To overcome this the d.c machine was operated as a motor and run up to synchronous speed. The supply was then connected to the experimental machine and as its voltage was increased the power to the load machine was reduced until the latter machine could be disconnected from its supply leaving the reluctance motor operating synchronously. The d.c machine was then reconnected as a self excited shunt generator for the loading of the reluctance motor.

Figures 4.13, 4.14, 4.15 and 4.16 show the variation of power, current, power factor and efficiency for both the computed and measured results. The theoretical curve of figure 4.17 shows how the pull-out power and load angle vary with the pole arc to pole pitch ratio. The maximum load angles and powers that were measured are also included on these curves.

Satisfactory agreement exists between the results of figures 4.13

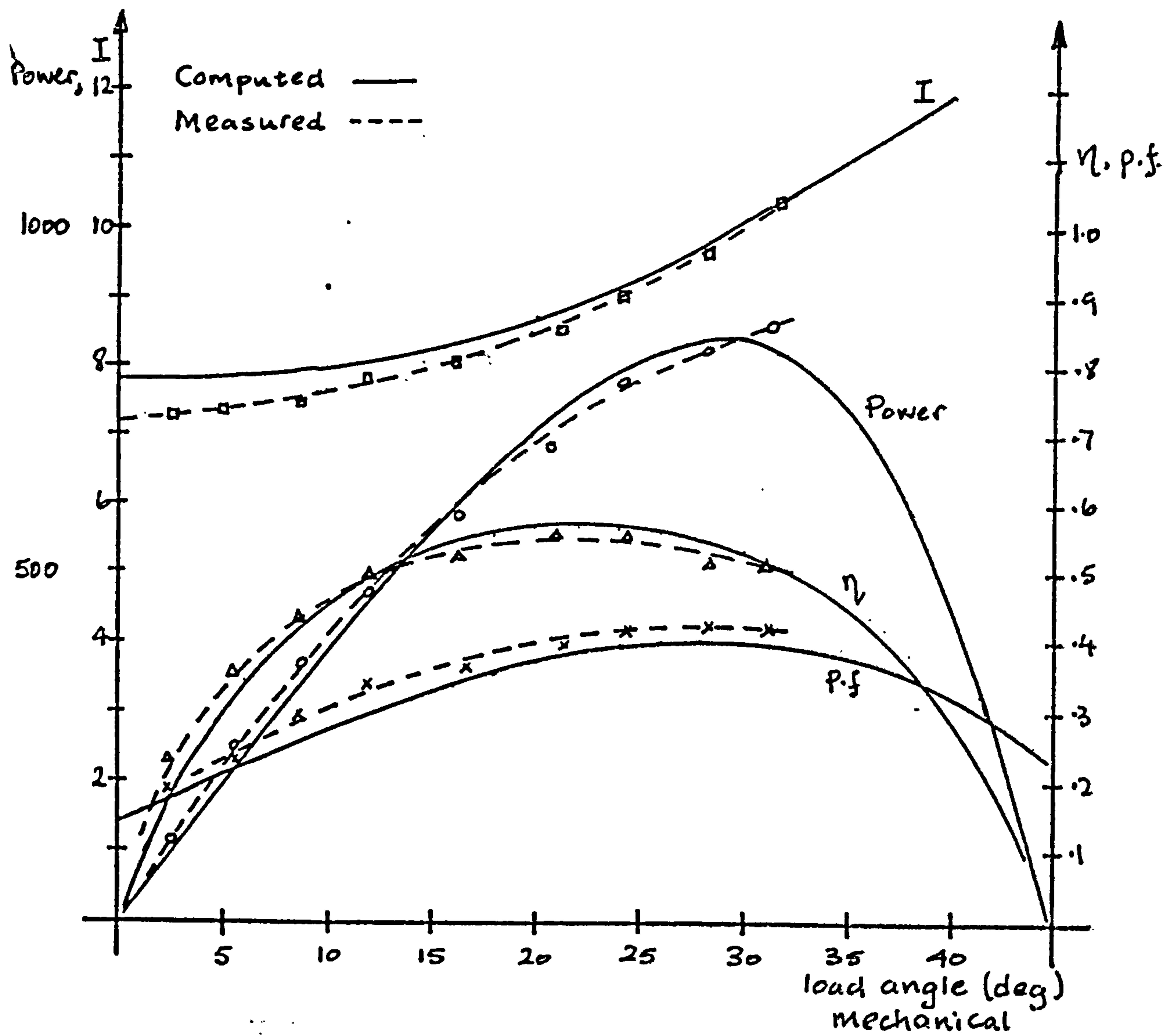


Synchronous performance curves for reluctance motor

$$\beta = 0.778, g = 0.6 \text{ mm}, g' = 1.0 \text{ mm}$$

- Current (I)
- output power
- △ efficiency (η)
- x power factor (p.f)

Figure 4.13



Synchronous performance curves for reluctance motor

$\beta = 0.666$, $g = 0.6 \text{ mm}$, $g' = 1.0 \text{ mm}$,

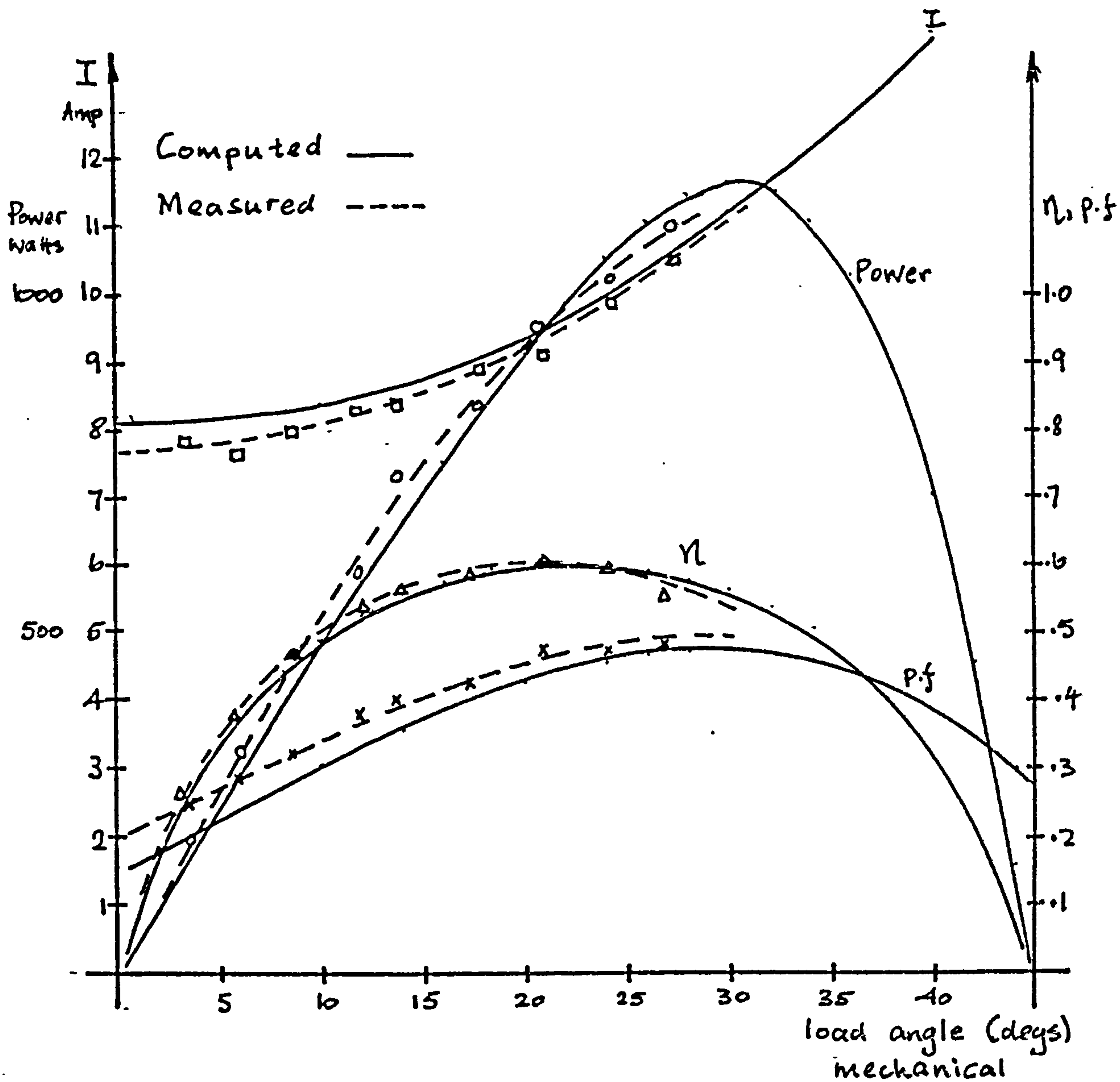
□ Current (I) (Amps)

○ output power (Watts)

△ efficiency (η)

x power factor (p.f.)

Figure 4.14



Synchronous performance curves for reluctance motor

$$\beta = 0.566, g = 0.6 \text{ mm}, g' = 1.0 \text{ mm}$$

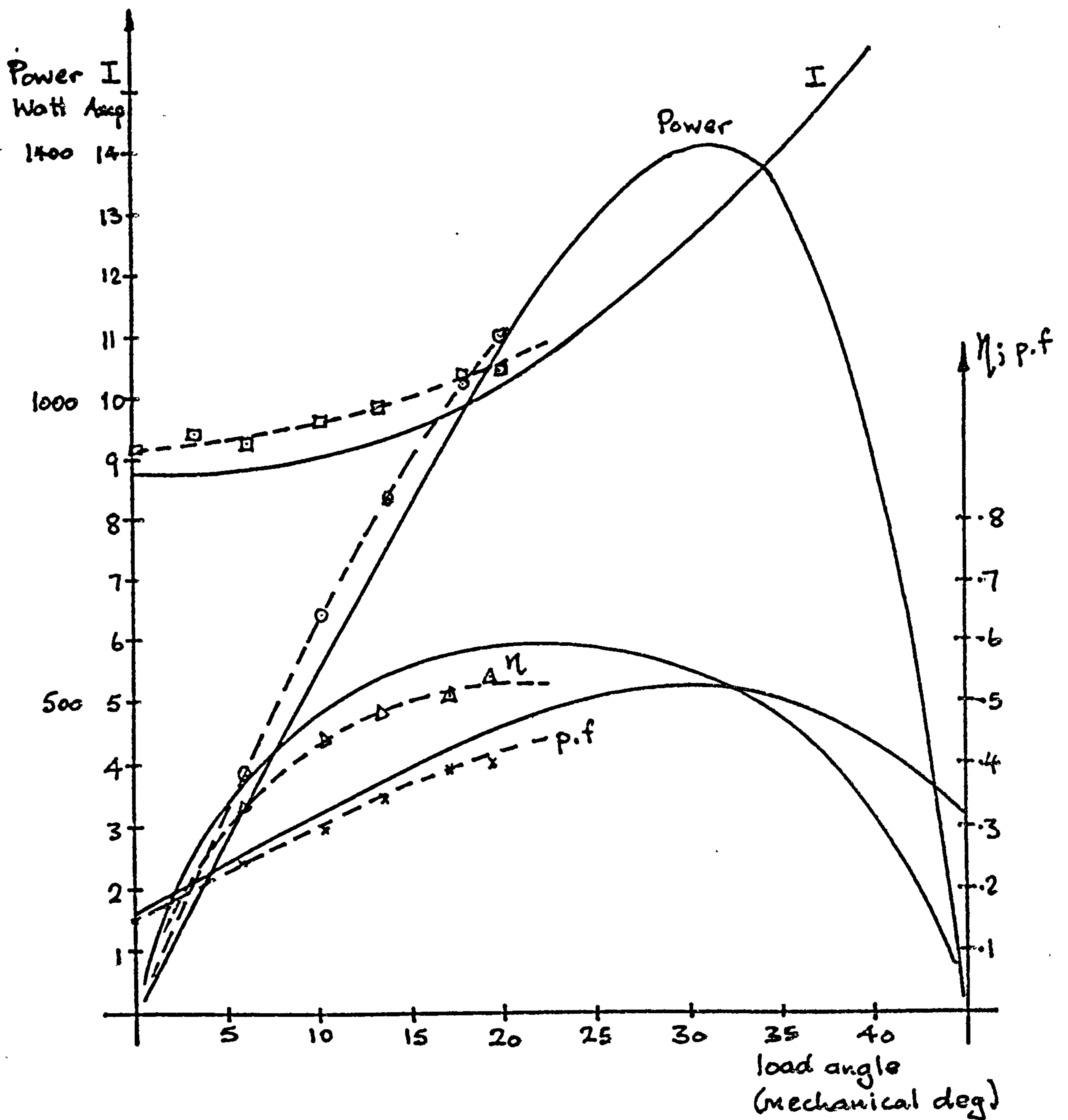
□ Current (I)

o output power

Δ efficiency (η)

x power factor (p.f.)

Figure 4.15



Synchronous performance curves for reluctance motor

$$\beta = 0.445, \quad g = 0.6 \text{ mm}, \quad g' = 1.0 \text{ mm}$$

□ Current (I)

○ output power

△ efficiency (η)

x power factor (p.f)

Figure 4.16

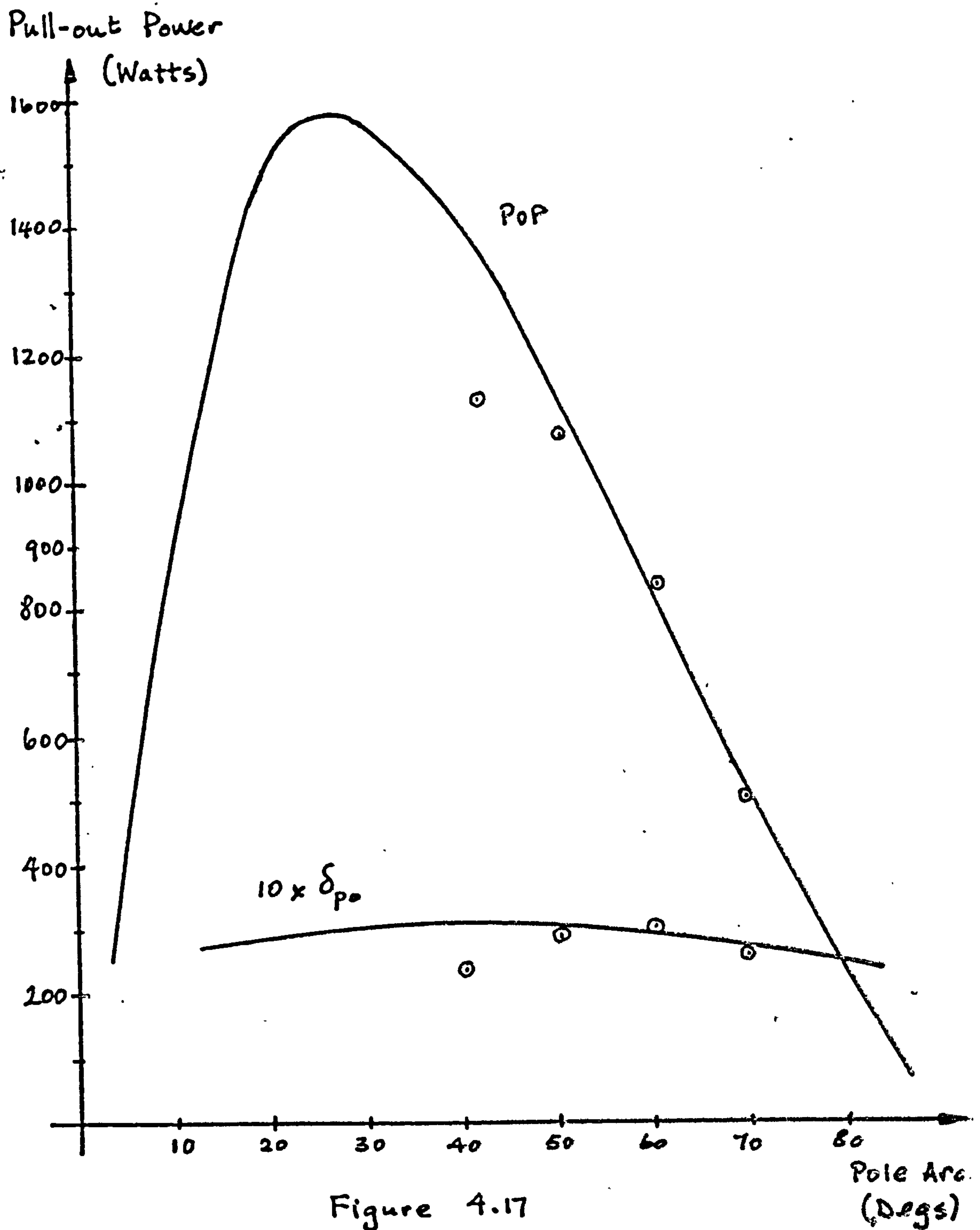


Figure 4.17
 Pull-out Power (POP) and pull-out load angle (δ_{po})
 as a function of β ($\beta = \text{pole arc} / 90$)

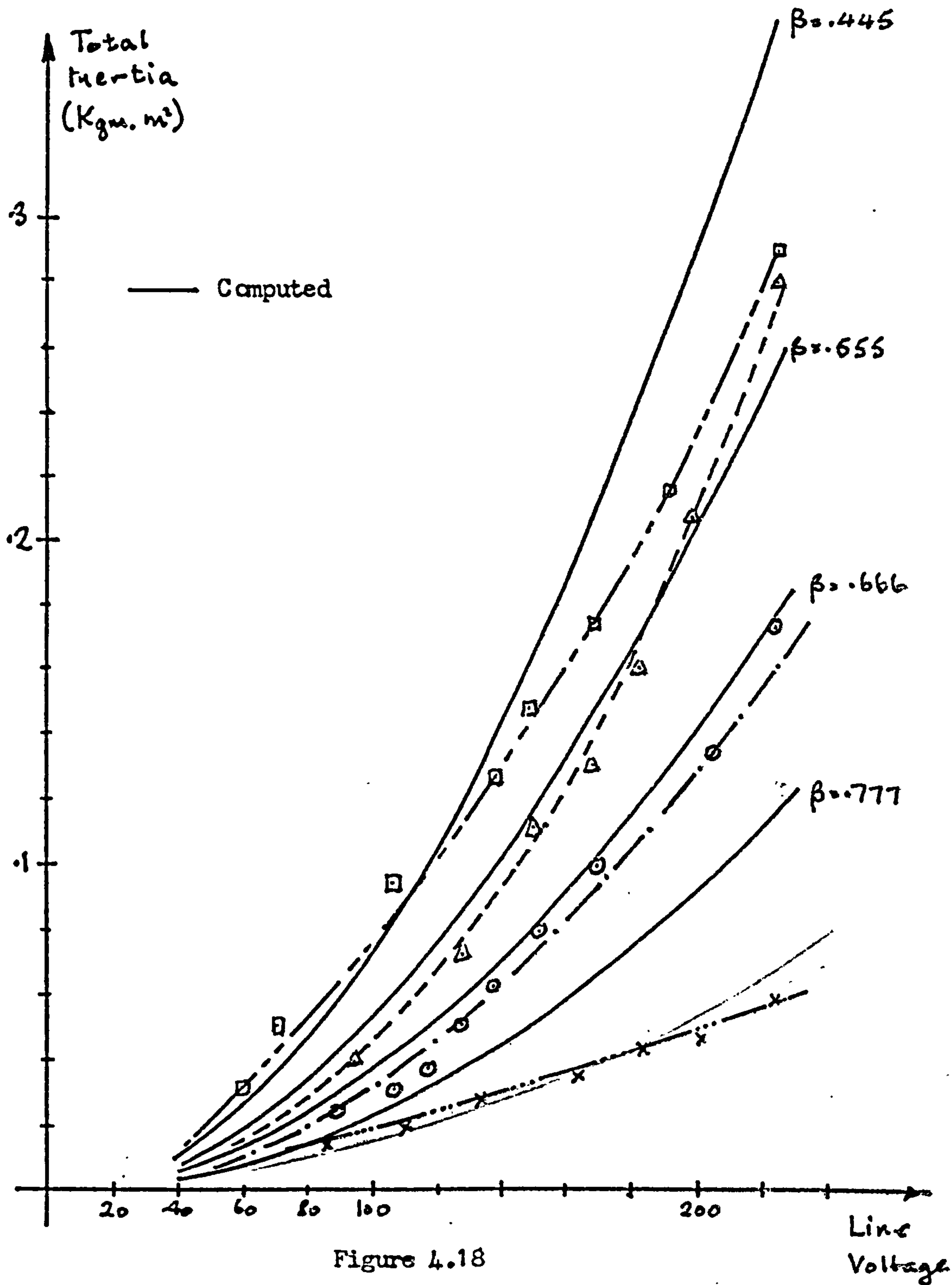
to 4.16. This is to be expected since the only missing parameter from the equivalent circuit of this machine is a resistive component representing the iron loss. There are of course no iron losses in the rotor of this machine; the stator copper losses can again be considered to be much greater than the stator iron losses. The inclusion of an iron loss component would improve the already good correlation between the efficiency and power factor. These are typically low for this type of reluctance motor (modified induction machine) and although the power factor of this design cannot be improved the efficiency could be increased by reducing the resistance of the stator winding.

The maximum power out of 1100 watts was obtained for $\beta = 0.445$ (pole arc of 40°). This figure is slightly smaller than the maximum power obtained from the induction motor. This is not because the reluctance motor is a good design but rather because the induction motor was a bad design from the point of view of the relatively high cage resistance. It can be misleading therefore to draw comparisons between the performance of these two machines.

4.4.2 Maximum inertia

In keeping with the squirrel cage requirements only the low resistance version was used. This ensured that when operating as an induction motor the experimental machine tended to reach the minimum slip possible. In chapter II the maximum inertia that could be synchronised for any given voltage was seen to be proportional to S_m^2 . S_m is the slip corresponding to the minimum speed attained by the rotor during the last half cycle of reluctance variation.

The method of testing the machine was to find the minimum voltage required to synchronise the rotor and load inertia. This latter component



Variation of the total inertia as a function of voltage

- $\beta = 0.445$
- △—△—△ $\beta = 0.555$
- $\beta = 0.666$
- ×—×—× $\beta = 0.778$

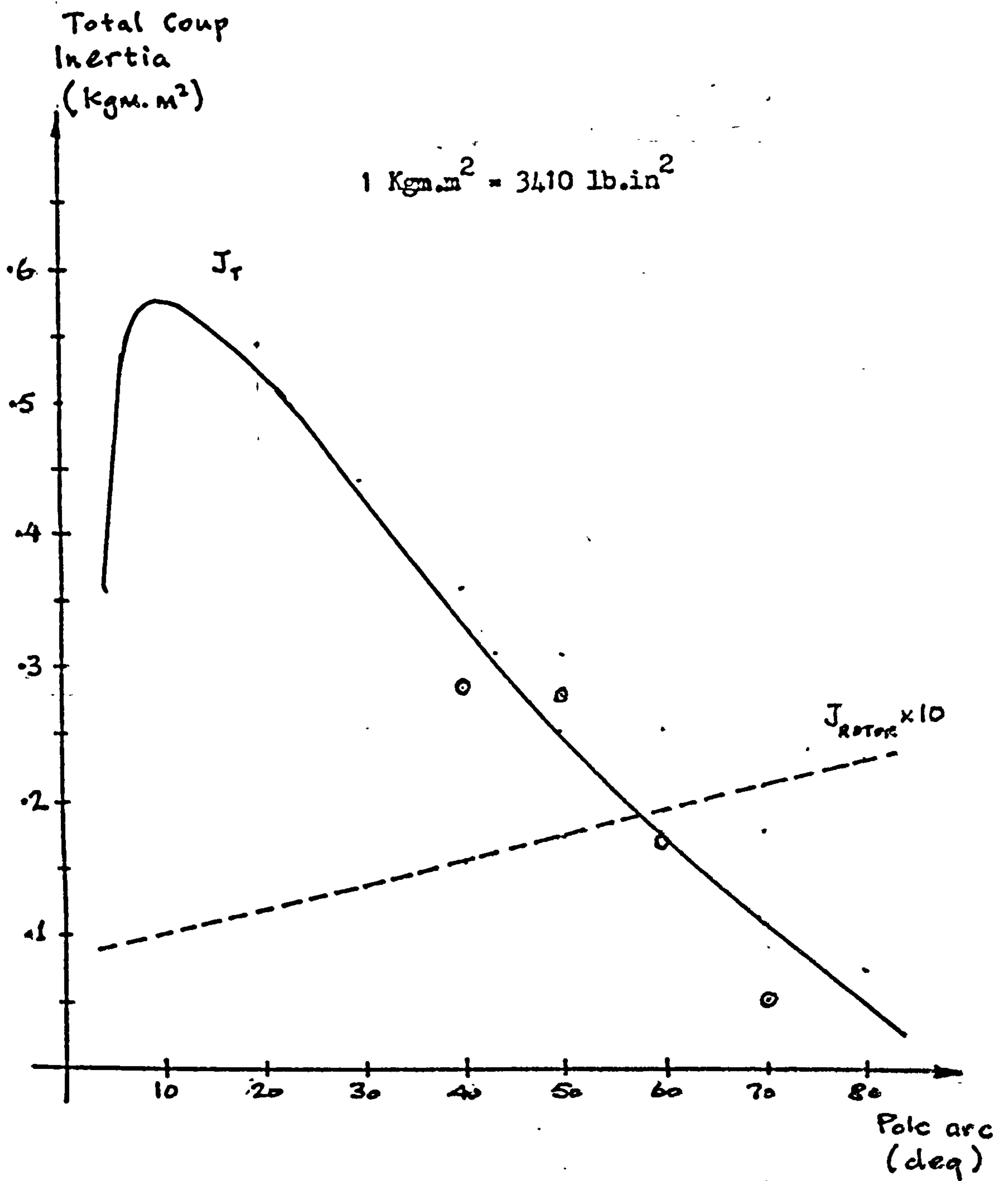


Figure 4.19

Variation of the total inertia as a function of pole arc
 (β = pole arc/90)

----- Variation of the rotor inertia

was simulated by a graded flywheel mechanically coupled to the rotor shaft. For a given inertia the supply voltage was increased until pull-in occurred. The machine was then stopped and the voltage again increased until just below the known pull-in value at which point the machine was just unable to synchronise its load and the familiar hunting characteristic was evident. This was to enable the minimum speed, corresponding to S_m , to be measured. For all values of pole arc to pole pitch ratios and for all coupled inertias this speed was seen to vary from between 1440 rpm and 1450 rpm representing a variation in slip of 0.04 down to 0.033. For the purpose of the computed results the maximum slip was taken as 0.04. The higher slip values correspond to the larger coupled inertias and pole arc to pole pitch ratios. By testing the motor this way it was possible to ensure that S_m remained relatively constant for the variation in coupled inertia and β .

Test results for four values of β are given in figure 4.18. It is to be expected, and is confirmed experimentally, that the inertia will vary as the square of the applied voltage. The medium range of β shows good correlation between the computed and the test results. For $\beta = 0.778$ the measured results differ radically from the computed values. The same is also true for the higher voltage results at $\beta = 0.445$. However both these values of β still approximate to the square law and in general the computed results are greater than the test figures.

Figure 4.19 shows how the total inertia (J_t) varies as a function of β when equation (2.39) is used and this curve is seen to reach a maximum when the pole arc is approximately 10° . The four experimental results, though fairly inconclusive in themselves, tend to indicate that in practice the maximum value of inertia will coincide with a value of β that is greater than the theoretical value.

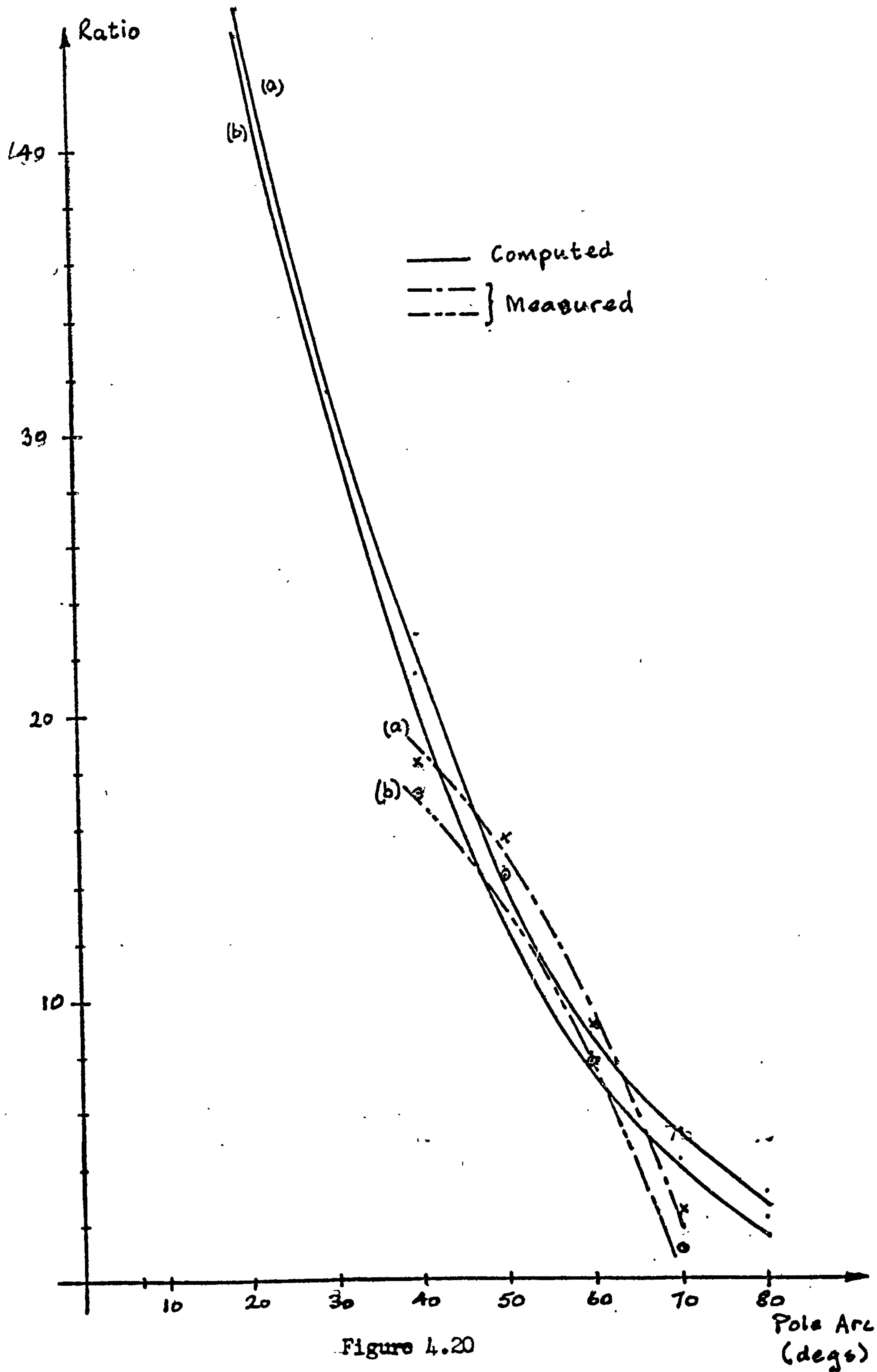


Figure 4.20

(a) Total inertia/rotor inertia

(b) Coupled inertia/rotor inertia

In figure 4.20 the ratio of the total inertia/rotor inertia and coupled inertia/rotor inertia are shown as functions of $\frac{\text{pole}}{\text{arc}}$. The measured curves again indicate that the theoretically high ratios at low values of $\frac{\text{pole}}{\text{arc}}$ would not be encountered though it must be stressed that, as with figure 4.19, there are not sufficient test results to verify this.

4.5 Conclusion

For the induction motor the maximum output that could be considered as a continuous rating was 1260 watts at an efficiency of 51%. This is a poor value for efficiency for this type of machine but this is due mainly to the excessive copper losses in the stator winding. The total weight of the induction motor was 22.5 Kg (50.4 lbs) giving a power to weight ratio of 56 watts/Kg (25watts/lb). This figure is compared with the machines tested by Gupta in chapter VI.

The reluctance motor gave a peak - tested output of 1100 watts at an efficiency of 50% and a power factor of 0.45. The minimum value of pole arc to pole pitch ratio was limited by the high current densities that were encountered. This is only true for this particular machine and is a fault in the design that could not be rectified at such a late stage. In practice, therefore, the optimum pull-in and pull-out characteristics could not be obtained because both occur at low values of β .

In explaining why the machine did not follow the predicted curve of equation (2.39) for the synchronisation of maximum inertia, reference is made to the curves of figure 4.16 in the section on the synchronous performance (p.101). The maximum output was in fact approaching the pull-out power of the machine at a load angle of approximately 21° . The computed values for this pole arc were 1400 watts and 32° . Further more these results show that for the first time the power factor is always lower than the predicted results. It is therefore suggested that the reactance of the

machine is altering in favour of the leakage component. The input impedance of the machine is given by,

$$Z = (R+R_e) + j(X+X_e)$$

If the maximum power transfer theorem were applied to the power dissipated in R_e then for maximum power transfer the magnitude of R_e is related to the other machine parameters by the equation,

$$R_e = (X + X_e)^2 + R^2$$

For the computed results the leakage reactance was kept constant at 4.8 ohm while it is apparent that this value must increase as the pole arc is reduced. Since R_e is proportional to $\sin(\beta\pi)$ then β will tend to increase to meet this demand for maximum power. Alternatively, the resistive component also increases but it is seen (Chapter IV) that variation of the in-phase component of impedance has an adverse effect on the predicted results. It is assumed that the increase in R could be due to the necessity to include a component to represent the iron losses.

Chapter V

Optimisation

5.1 Introduction

For a given frame size, the performance of the induction machine is affected primarily by the ratio D_2/D_1 while the reluctance motor depends on this together with the pole arc/pole pitch ratio. In this chapter emphasis is placed solely on the relationship between the machine performance and these two ratios and in this sense the analysis is termed optimisation. In chapter I the conditions under which an optimised design would be produced were briefly mentioned. In practice there exists a wide spectrum of specifications that effect the design procedure and at either ends of this spectrum could be placed the machine performance and the manufacturing processes. The former is concerned with such parameters as output, efficiency, power factor etc. while the latter is controlled by cost, production techniques, availability of material etc.

The theoretical equations for the induction and reluctance machines differ only by a term equal to the pole arc/pole pitch ratio. Consequently reference will be made to the latter machine only. The methods could equally be applied to the induction machine but, in view of the fact that the reluctance motor equations represent a more generalised approach, such an exercise would tend to be purely academic. Because of the two variables superposition will be used. The equations, which will all be expressed on a per phase basis, can be differentiated to give the condition from which maximum and minimum conditions can be deduced. However, the manipulation of the differential to extract the desired parameter is sometimes difficult and cumbersome. In such instances the resulting equation is stated and the maximum and minimum values (if these exist) are obtained by computation.

The stator winding will be identical to that used in the experimental machine and is a 3phase, double layer, 4pole winding with a coil pitch of 5/6. Hence the number of slots in the stator will always be 24. For such a winding the number of stator slots must be divisible by 12. It is apparent that the slot size must vary as D_1 varies hence either the size of conductor and/or the number of conductors must be allowed to vary. If the number of conductors is kept constant then it is theoretically possible for the resistance of the winding to approach infinity as D_1 is decreased. since the diameter of the wire must approach zero. To allow for a finite resistance the diameter of the wire will be maintained constant. This puts a theoretical limit on the minimum ^{wire} diameter since the smallest slot area must be equal to twice the cross-sectional area of the wire. The practical limitation is determined by the necessity of providing the motor with a rotor shaft and overhang space.

5.2 Assumptions

- (1) The slot/tooth ratio at D_1 is constant and equal to the value used in the experimental machine, hence

$$s_w/t_w = 3.27$$

- (2) The slot depth/slot width is constant and equal to the value used in the experimental machine, hence,

$$s_d/s_w = 1.65$$

- (3) The slot fill factor is constant at 0.26.
- (4) The conductor diameter is constant at 1mm (slightly less than in the experimental machine).
- (5) D_2 will be kept constant for all D_1 .
- (6) The stator slot/rotor slot ratio is constant at 1.2.
- (7) The m.m.f harmonics are ignored.

5.3 Performance Equations

5.3.1 Synchronous Operation

The equivalent circuit for the reluctance motor, is shown in figure 5.1 and based upon this circuit the following performance equations are deducible.

$$I_s = \frac{V}{(R+R_e) + j(X+X_e)} \quad (5.1)$$

$$\cos \phi = \frac{R+R_e}{((R+R_e)^2 + (X+X_e)^2)^{\frac{1}{2}}} \quad (5.2)$$

$$OP = I_s^2 R_e = \frac{V^2 R_e}{(R+R_e)^2 + (X+X_e)^2} \quad (5.3)$$

$$\eta = \frac{I_s^2 R_e}{VI_s \cos \phi} \quad (5.4)$$

$$Cu \text{ loss} = I_s^2 R \quad (5.5)$$

In order to develop equations (5.1) to (5.5) the equivalent circuit components need expressing in terms of D_1 and β .

(1) Stator winding resistance (R)

Let N = turns/phase per pole

and M.L.T = mean length per turn.

then,

$$R = \frac{8p \rho N.(M.L.T)}{\text{wire area}}$$

The conductors/slot = $\frac{\text{slot area}}{\text{wire area}}$ slot fill factor

Now the slot area = $s_w \cdot s_d$

$$= 1.65(s_w)^2 \quad (\text{assumption 2})$$

and $s_w/t_w = 3.27$

where t_w = slot pitch - s_w

$$= s_p - s_w$$

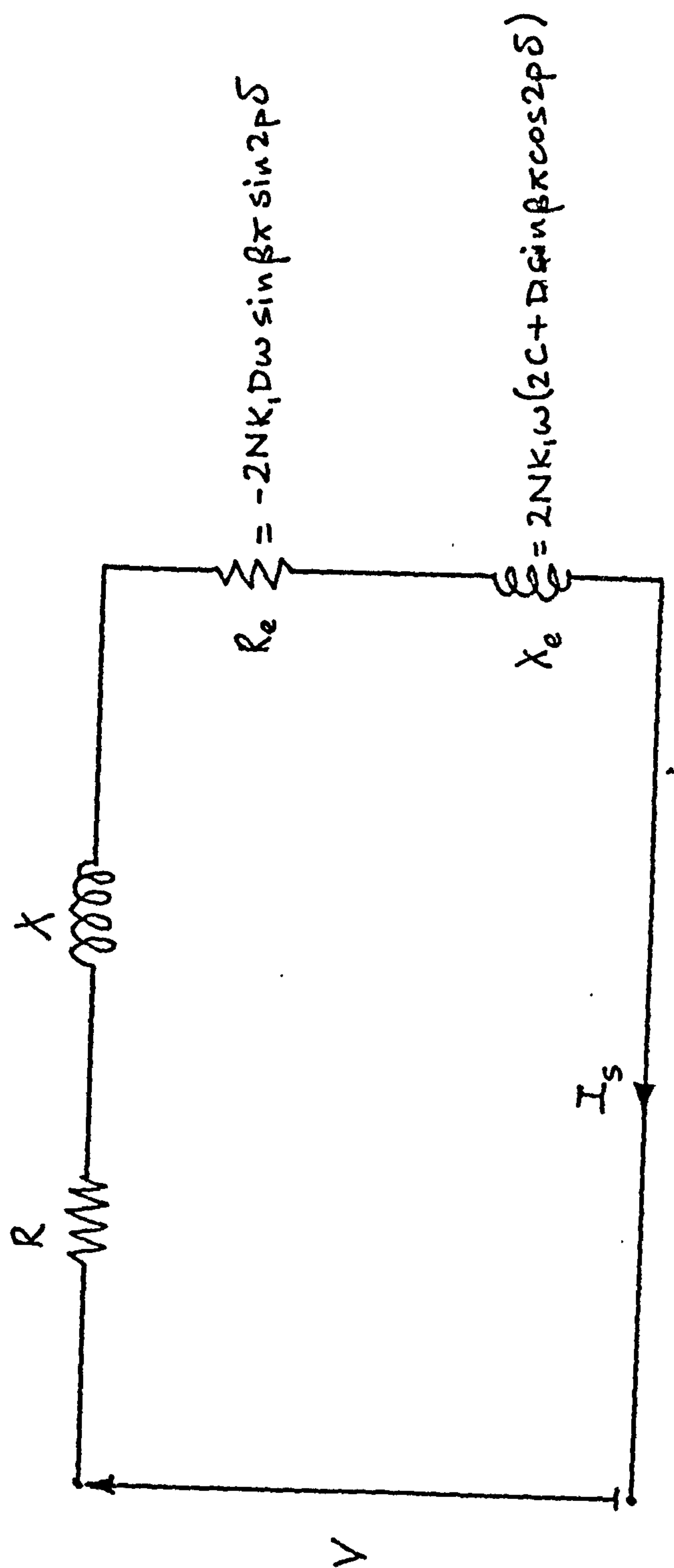


Figure 5.1

therefore, $s_w = 3.27(s_p - s_w)$

giving, $s_w = 3.27.s_p/4.27$

but $s_p = \pi D_1/24$

hence, $s_w = \frac{3.27 \pi D_1}{24 \times 4.27}$

giving conductors/slot = $\frac{D_1^2}{180}$

The number of turns/phase per pole per stator for this type of winding is equal to the conductors per slot giving N as,

$$N = D_1^2/90 \quad (5.6)$$

The mean length per turn is equal to the sum of the active lengths $(D_2 - D_1)$ and the overhang lengths at D_2 and D_1 , hence, for a 5/6 coil pitch

$$M.L.T = (D_2 - D_1) + 0.655(D_2 + D_1)$$

$$\text{and } R = \frac{\rho D_1^2}{17.7} ((D_2 - D_1) + 0.655(D_2 + D_1))$$

$$R = A'(D_2 - D_1)D_1^2 + B'(D_2 + D_1)D_1^2 \quad (5.7)$$

(2) Stator leakage reactance (X)

The leakage reactance is assumed to be independant of β and is therefore a function only of the $(\text{turns})^2$ and the pole area. For the experimental machine,

$$X = 4.82 \text{ ohms}$$

$$N = 80 \text{ turns}$$

$$D_1 = 85 \text{ mm}$$

and expressed as a proportion of the leakage in the experimental machine,

$$X = 4.82 (N/80)^2 \frac{D_2^2 - D_1^2}{D_2^2 - 85^2}$$

Substitution for N(5.6) gives,

$$X = A'' D_1^4 (D_2^2 - D_1^2) \quad (5.8)$$

(3) Effective resistance and reactance (Re and Xe)

From chapter II the relationships for Re and Xe are

$$Re = -2NK_1 Dw \sin \beta \pi \sin 2p \delta \quad (5.9)$$

$$Xe = 2NK_1 w (2C + D \sin \beta \pi \cos 2p \delta) \quad (5.10)$$

where,

$$C = \frac{3\mu_0 (D_2^2 - D_1^2) N (\beta h + g') K_1}{8\pi g' (h + g')}$$

$$D = \frac{3\mu_0 (D_2^2 - D_1^2) N h K_1}{4\pi^2 g' (h + g')}$$

Substituting for N, D and C in (5.10) and (5.9) gives,

$$Re = -D'' h D_1^4 (D_2^2 - D_1^2) \sin \beta \pi \sin 2p \delta \quad (5.11)$$

$$Xe = D'' (\pi (\beta h + g') + h \sin \beta \pi \cos 2p \delta) D_1^4 (D_2^2 - D_1^2) \quad (5.12)$$

where,

$$D'' = \frac{3\mu_0 w (K_1 / 87\pi)^2}{2g' (h + g')}$$

It is now possible to reconsider equations (5.1) to (5.5) and express them in terms of D_1 and β .

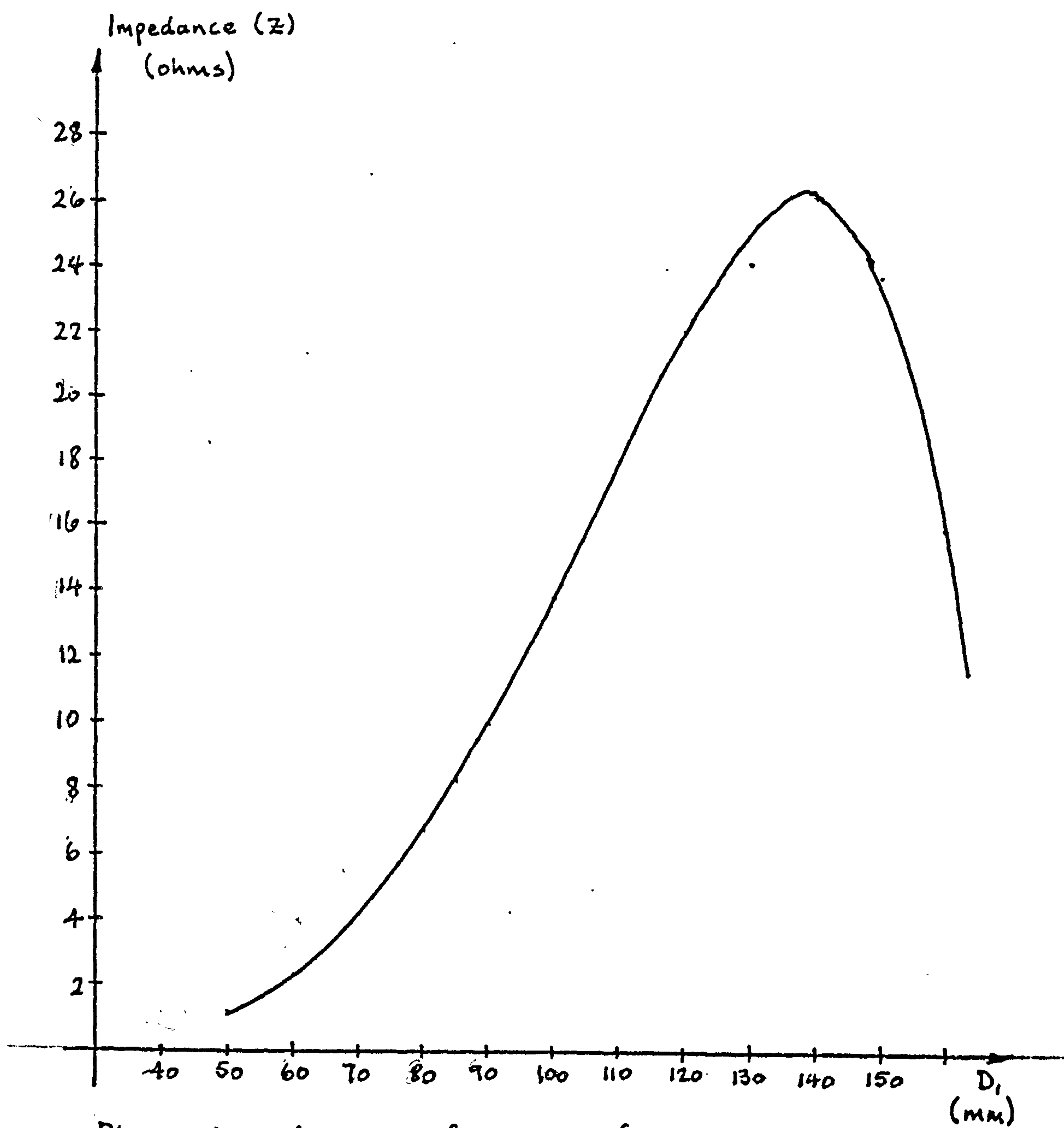
5.3.1.1 Phase current

To obtain the conditions for minimum and maximum current it is necessary to consider the maximum and minimum values respectively of the impedance, hence,

$$\begin{aligned} Z &= ((R + Re)^2 + (X + Xe)^2)^{1/2} \\ &= \left[\left[A' D_1^2 (D_2^2 - D_1^2) + B' D_1^2 (D_2 + D_1) + D'' h D_1^4 (D_2^2 - D_1^2) \sin \beta \pi \sin 2p \delta \right]^2 + \right. \\ &\quad \left. \left[A'' D_1^4 (D_2^2 - D_1^2) + D'' (\pi (\beta h + g') + h \sin \beta \pi \cos 2p \delta) D_1^4 (D_2^2 - D_1^2) \right]^2 \right]^{1/2} \end{aligned}$$

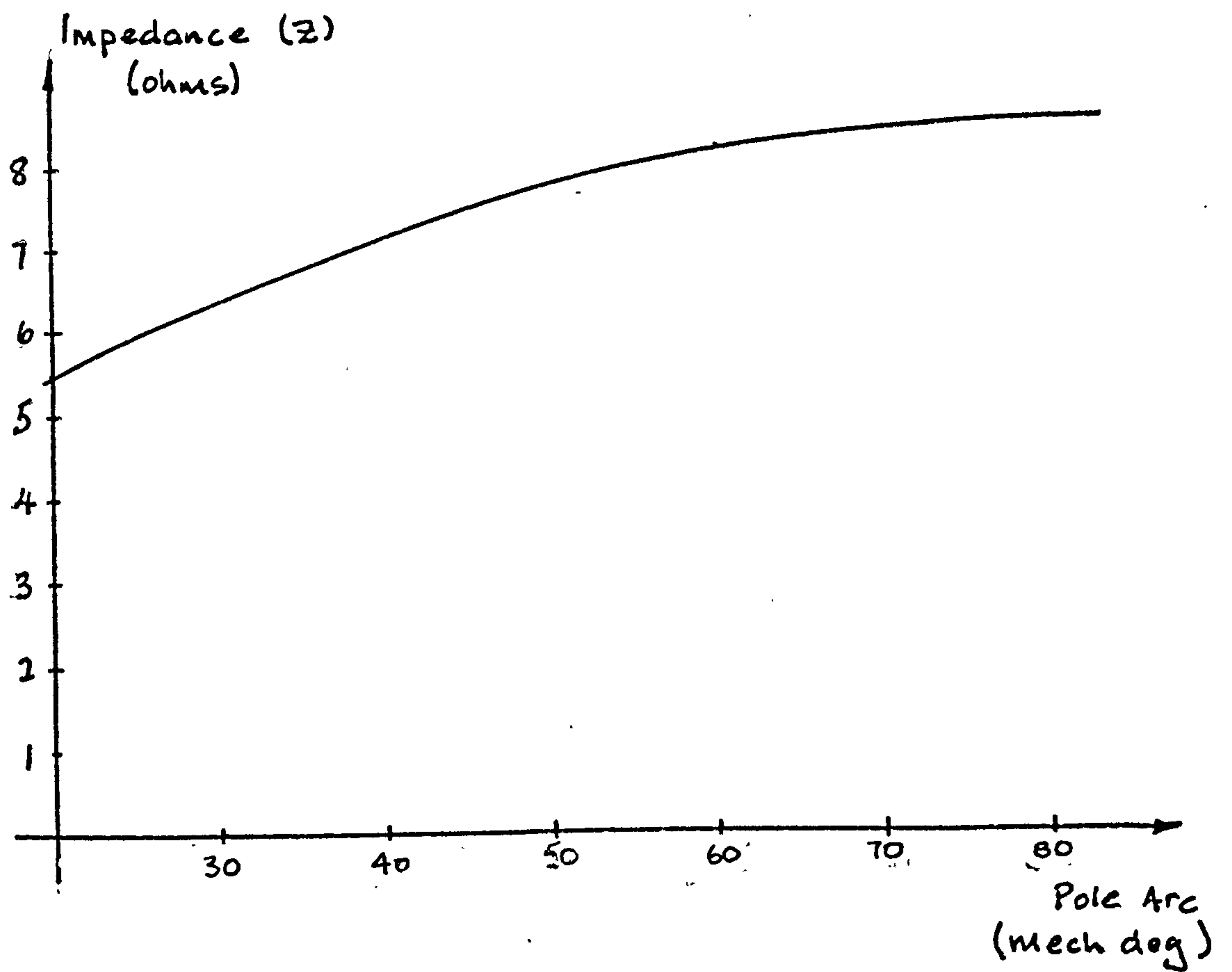
Note that the sign of Re can be changed if β is considered positive for motoring. Furthermore if the resistance is ignored, then,

$$Z = D_1^4 (D_2^2 - D_1^2) \left[(h D'' \sin \beta \pi \sin 2p \delta)^2 + (A'' + D'' (\pi (\beta h + g') + h \sin \beta \pi \cos 2p \delta))^2 \right]^{1/2} \quad (5.13)$$



Phase impedance as function of D_1
 $\beta = 0.666$; $\delta = 0^\circ$ (load angle)

Figure 5.2



Phase impedance as a function of pole arc
 $(\beta = \text{pole arc} / 90^\circ)$
 $D_i = 85 \text{ mm}$; $\delta = 0$ (load angle)

Figure 5.3

Taking $d(Z)/dD_1$ and equating to zero gives a maximum impedance when,

$$D_1 = D_2/\sqrt{1.5}$$

The variation of Z with D_1 is shown in figure 5.2. Consideration of (5.13) indicates that the maximum and minimum values of Z as a function of β can be obtained directly by substitution for $\beta = 1$ and $\beta = 0$ respectively,

$$Z_{\max} = R + j(X + D_1^4(D_2^2 - D_1^2) \frac{3\mu_w(K_1/87)^2}{2\pi g'})$$

$$Z_{\min} = R + j(X + D_1^4(D_2^2 - D_1^2) \frac{3\mu_w(K_1/87)^2}{2\pi(h+g')})$$

Figure 5.3 shows Z as a function of β

5.3.1.2 Power factor

From equation (5.2)

$$\cos \phi = \frac{R + Re}{((R + Re)^2 + (X + Xe)^2)^{\frac{1}{2}}}$$

For most operational conditions R and X can be ignored, hence,

$$\cos \phi = \frac{1}{(1 + (Xe/Re)^2)^{\frac{1}{2}}} \quad (5.14)$$

Both Re and Xe are functions of $D_1^4(D_2^2 - D_1^2)$ consequently variation of D_1 will not have a first order effect on the power factor. It is apparent that the power factor depends primarily on β (R and X are independent of β).

From (5.14) maximum power factor is obtained when,

$$(Xe/Re)^2 = \text{minimum}$$

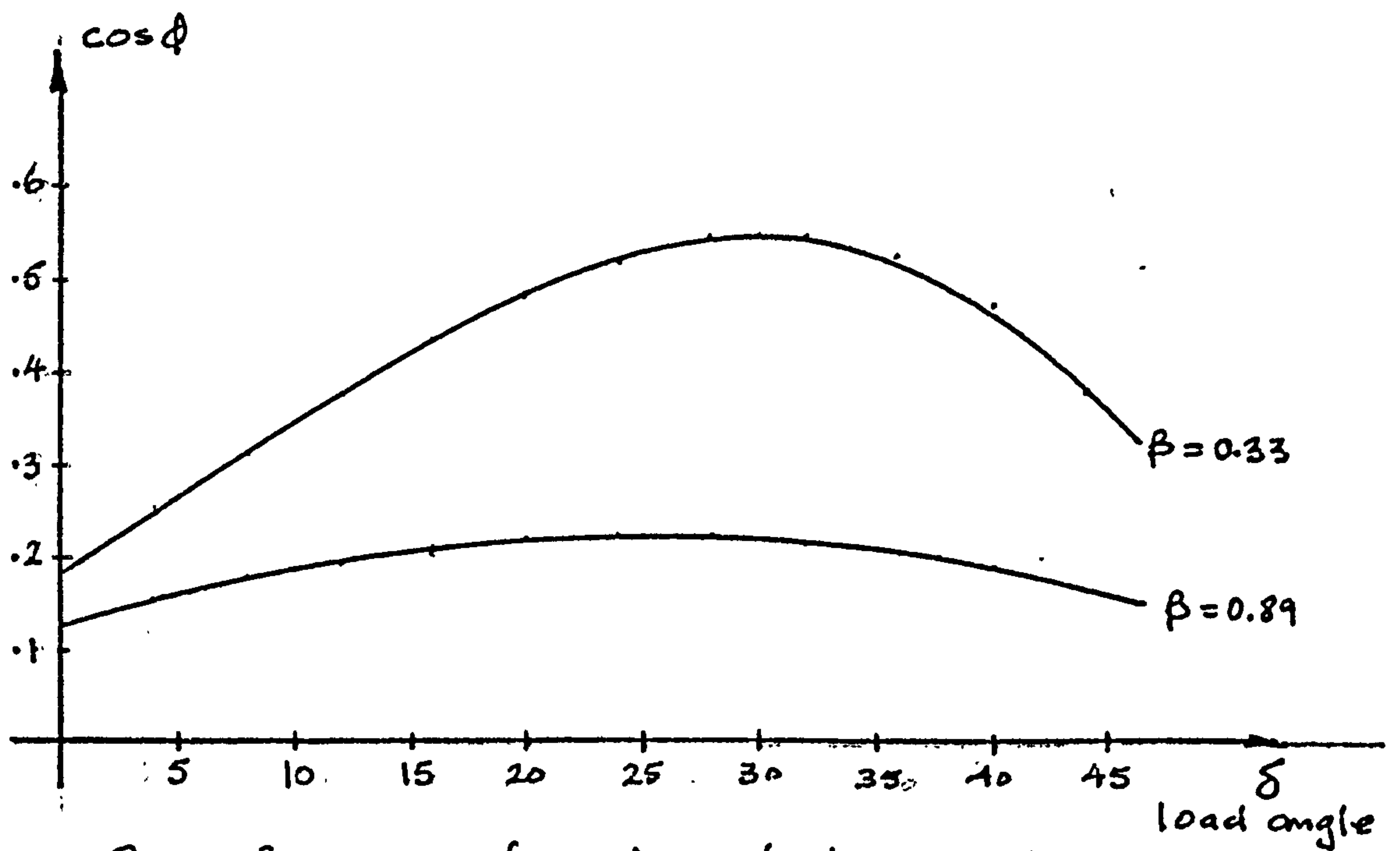
Differentiating with respect to β and equating to zero gives,

$$\tan \beta\pi - \beta\pi = (\pi g'/h)$$

For the experimental machine $h = 14\text{mm}$ and $g' = 1.0\text{mm}$, hence,

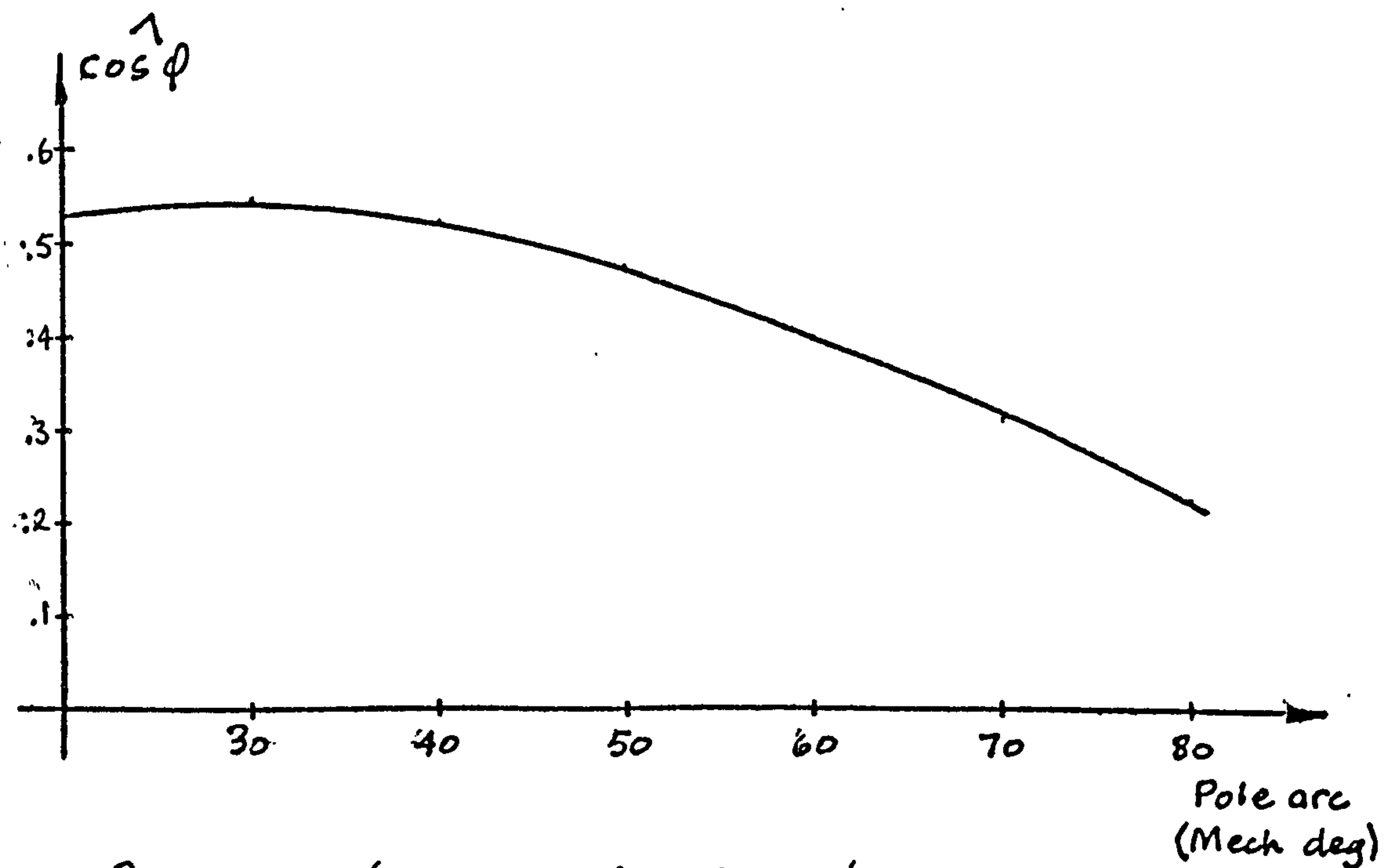
$$\tan \beta\pi - \beta\pi = 0.224$$

The value of β which gives maximum power factor and satisfies the above condition is $\beta \approx 0.24$. Figure 5.4 shows how the power factor varies with the load and the effect that β has on the maximum power factor.



Power factor as function of load angle

$D_1 = 85\text{mm}$



Peak power factor as function of pole arc
 $(\beta = \text{pole arc}/90)$

$D_1 = 85\text{mm}$

Figure 5.4

5.3.1.3 Output power

The output power is given by,

$$OP = I_s^2 R_e = \frac{V^2 R_e}{(R+R_e)^2 + (X+X_e)^2}$$

The maximum power for any set of machine parameters is given by the pull-out power. The pull-out angle can be obtained by differentiating OP with respect to δ . Hence,

$$OP = \frac{V^2 K \sin 2p\delta}{(R+K \sin 2p\delta)^2 + (x+K \cos 2p\delta)^2} \quad (5.14)$$

where $K = 2NK_1 D_w \sin 2p$

and $x = X + 4NK_1 wC$

since $\frac{d(OP)}{d\delta} = 0$ for maximum and minimum it can be shown that,

$$\cos 2p\delta = \frac{-2xK}{R^2 + x^2 + K^2}$$

satisfies the differential and gives maximum output. Substituting for $\cos 2p\delta$ into (5.14) gives the pull-out power as

$$POP = \frac{V^2 K}{\sqrt{(R^2 + x^2 + K^2)^2 - (2xK)^2} + 2RK}$$

If the stator resistance is ignored, then,

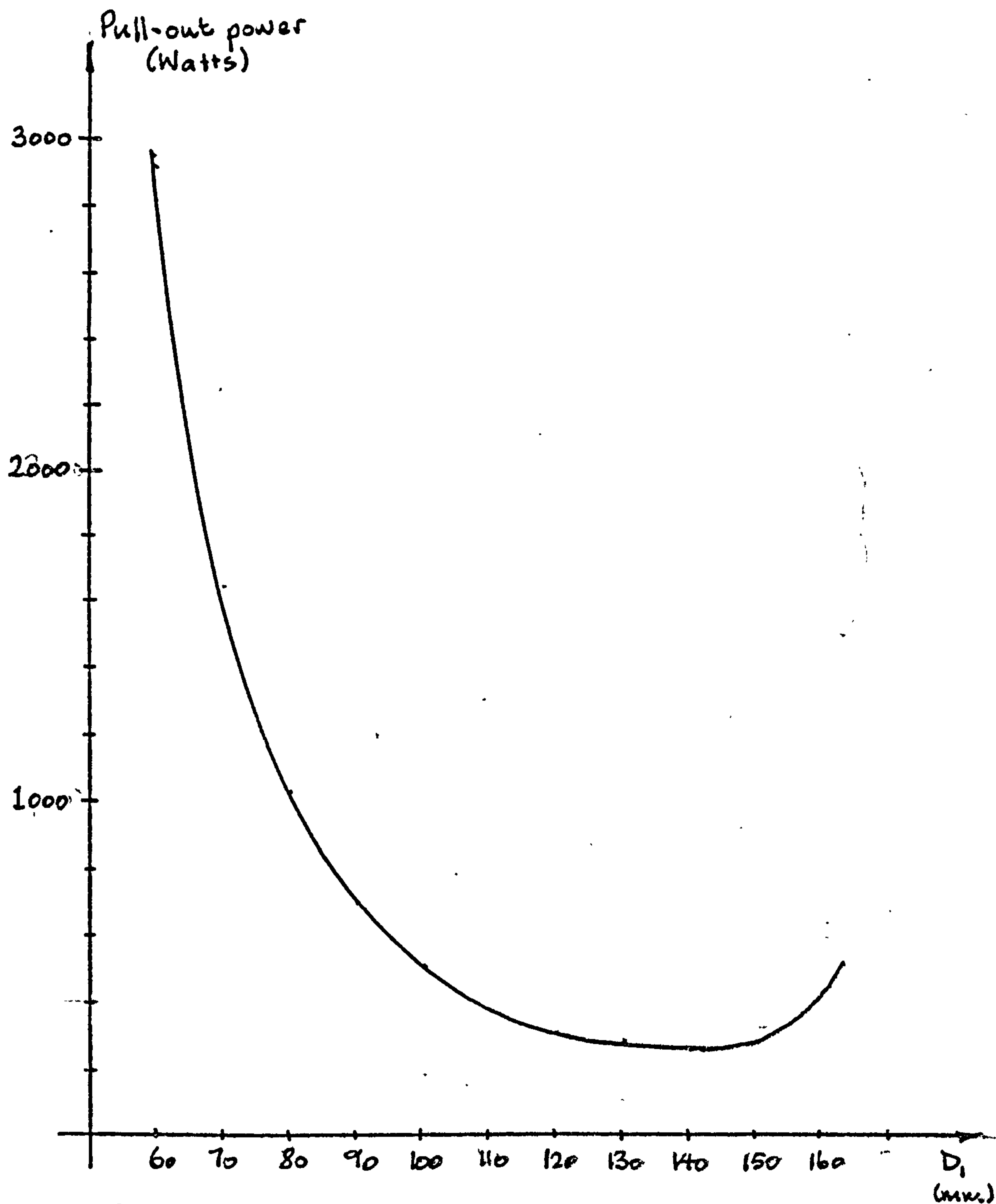
$$POP = \frac{V^2 K}{x^2 - K^2}$$

Both K and x are functions of $D_1^4(D_2^2 - D_1^2)$ and for a given pole arc/pole pitch ratio,

$$POP \propto \frac{1}{D_1^4(D_2^2 - D_1^2)}$$

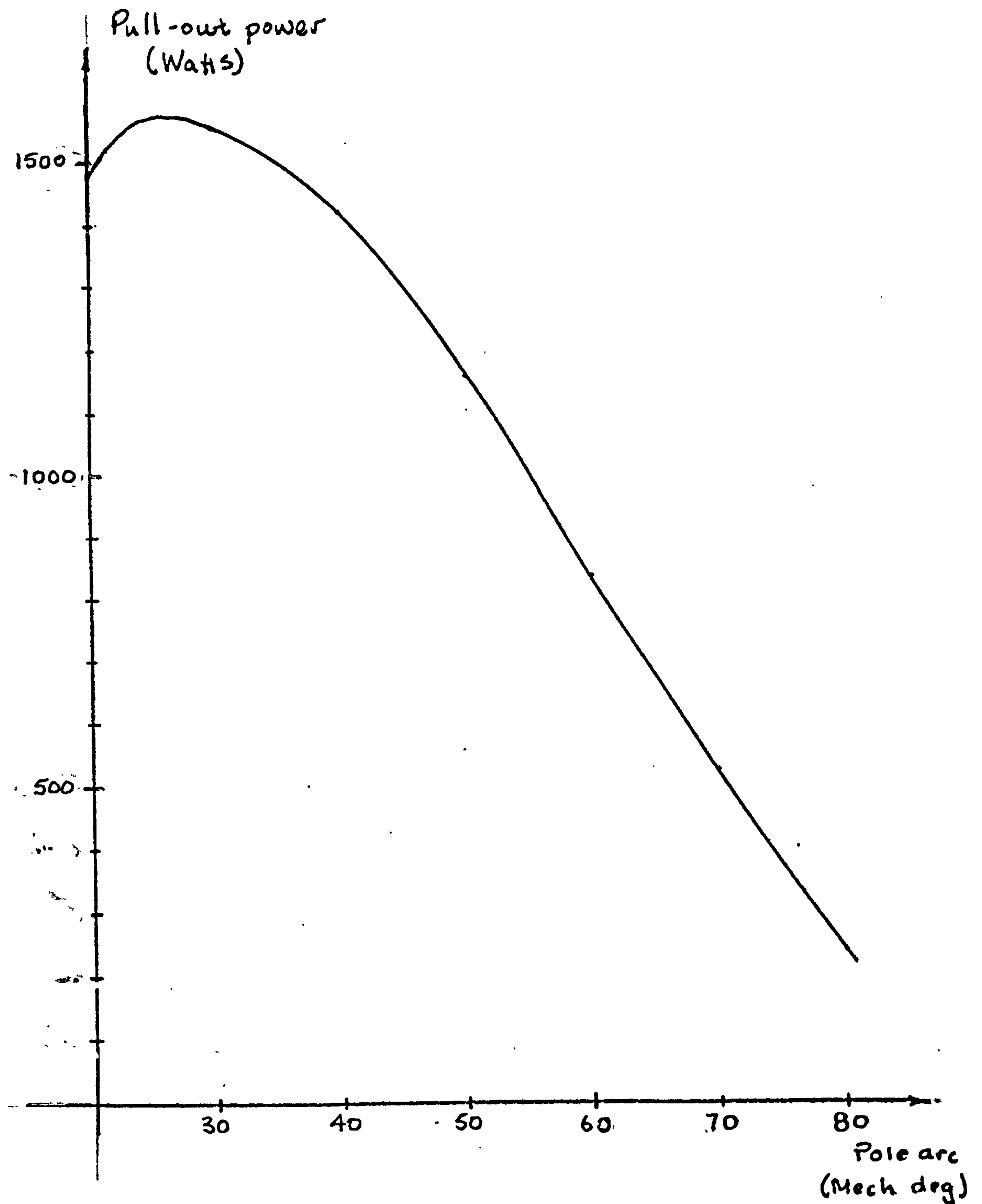
from which, minimum pull-out power (and this coincides with minimum phase current) is obtained when,

$$D_1 = \frac{D_2}{\sqrt{1.5}}$$



Pull-out power as a function of D_1
 $\beta = 0.666$

Figure 5.5a



Pull-out power as a function of pole arc
($\beta = \text{pole arc} / 90$)
 $D_1 = 85 \text{ mm}$

Figure 5.5b

The maximum power dissipated in R_e can be obtained by applying the maximum power transfer theorem to the circuit of figure 5.1. Then OP is a maximum when,

$$R_e^2 = R^2 + (X + X_e)^2$$

and by ignoring R and X gives,

$$R_e = X_e$$

Using (5.11) and (5.12) gives,

$$\begin{aligned} h \sin \beta \pi \sin 2p\delta &= \pi(\beta h + g') + h \sin \beta \pi \cos 2p\delta \\ \sin \beta \pi (\sin 2p\delta - \cos 2p\delta) &= \frac{\pi(\beta h + g')}{h} \end{aligned}$$

From the results in chapter IV it was seen that the pull-out angle is generally about 30° (mechanical) for all β . Substituting for $2p\delta = 120$ gives,

$$1.366 \sin \beta \pi = \frac{\pi(\beta h + g')}{h}$$

Using the values for h and g' encountered in the machine reveals that

$\beta = 0.225$ gives maximum power. The variation of pull-out power as a function of D_1 and β is shown in figure 5.5.

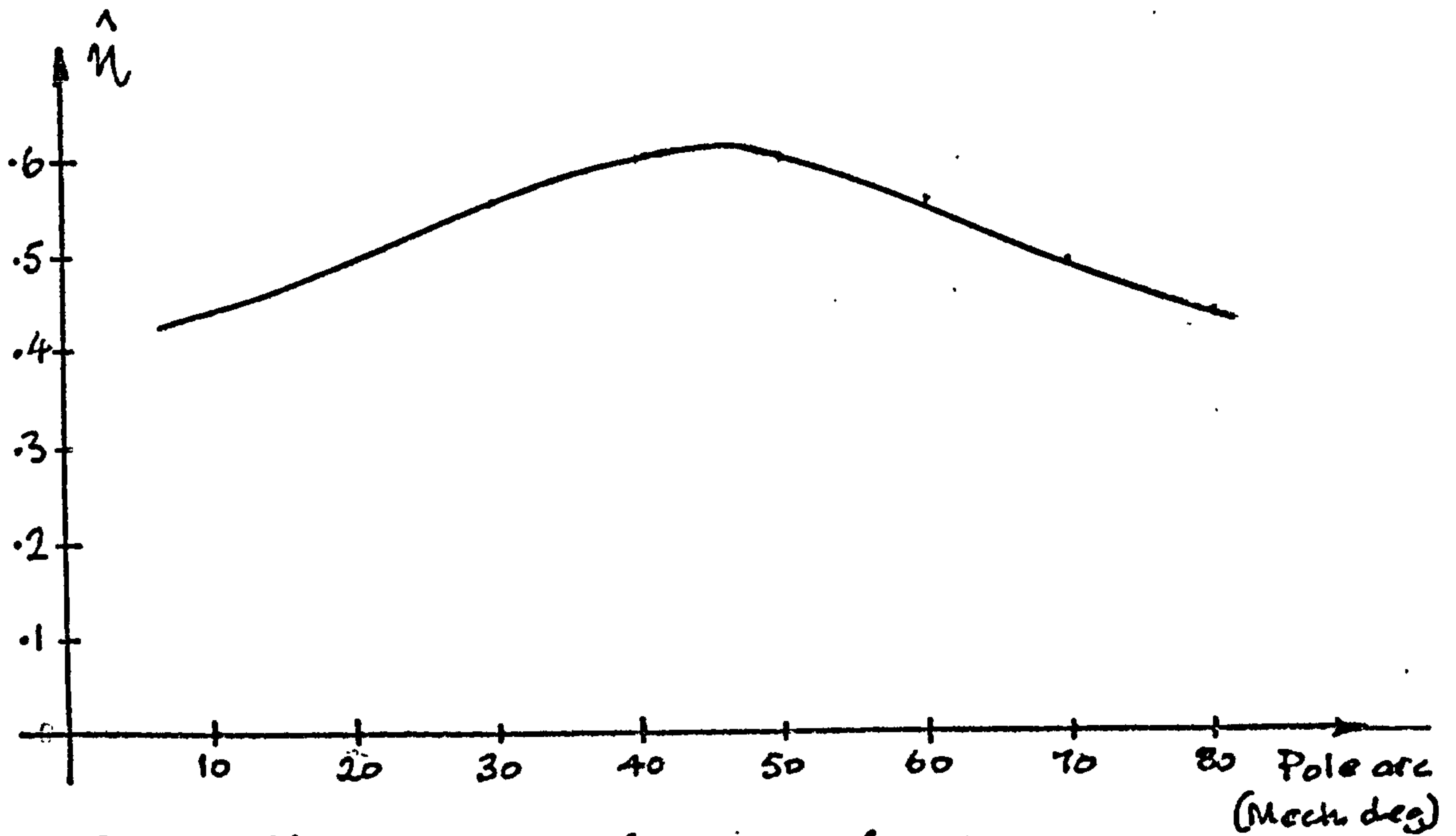
5.3.1.4 Efficiency

The efficiency is given as,

$$\eta = \frac{1}{1 + (R/R_e)}$$

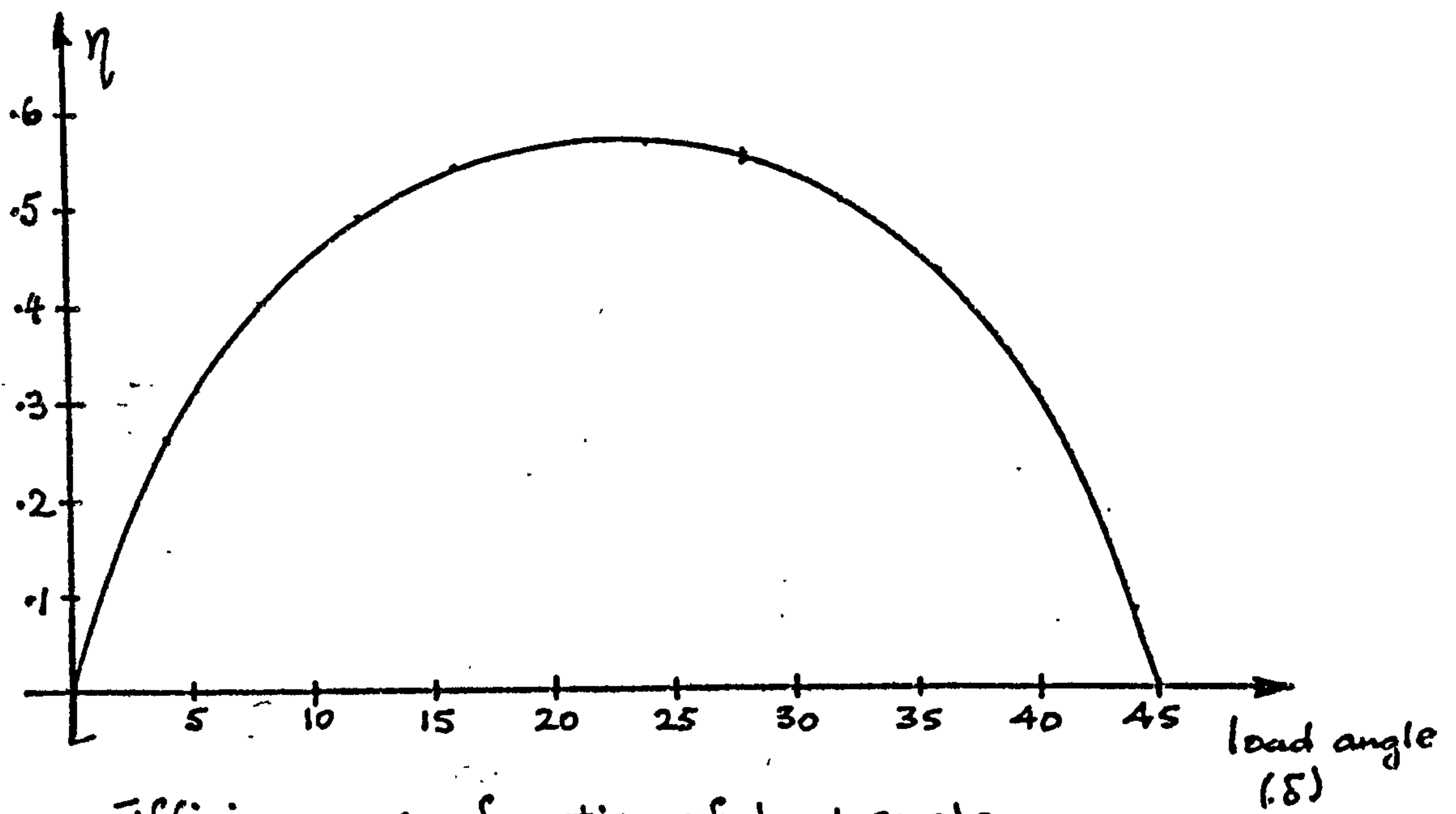
and maximum efficiency is obtained when R/R_e is a minimum. It is apparent from equation (5.11) that R_e is a maximum when $\beta = 0.5$. giving in turn maximum efficiency. Using this value of β and putting $\sin 2p\delta = 1$ gives,

$$\begin{aligned} R/R_e &= \frac{D_1^2 (A' (D_2 - D_1) + B' (D_2 + D_1))}{h D'' D_1^4 (D_2^2 - D_1^2)} \\ &= \frac{(A' (D_2 - D_1) + B' (D_2 + D_1))}{h D'' D_1^2 (D_2^2 - D_1^2)} \end{aligned}$$



Peak efficiency as a function of pole arc
 $(\beta = \text{pole arc} / 90)$

$D_1 = 85 \text{ mm}$



Efficiency as a function of load angle

$\beta = 0.666$; $D_1 = 85 \text{ mm}$

Figure 5r6

For practical values of D_1 , i.e. $0.3D_2 < D_1 < 0.8D_2$, the numerator varies by about 11%, decreasing as D_1 increases. Considering, therefore,

$$R/Re \propto \frac{1}{D_1^2(D_2^2 - D_1^2)}$$

This a minimum, giving maximum efficiency when $D_1 = D_2/\sqrt{2}$. The relationship between D_1 , β and efficiency is shown in figure 5.6.

5.3.1.5 Copper loss

From equation (5.5)

$$\text{Cu loss} = \frac{V^2 R}{(R+Re)^2 + (X+Xe)^2}$$

The d.c. resistance is relatively independent of β , any variation being caused by temperature rises as the current increases with decreasing β . Therefore it is necessary to consider only the variation of the loss with D_1 . Furthermore β can be chosen at any convenient value, hence putting $\beta = 1$ in the expression for Re and Xe reduces the input resistance and reactance to R and

$$\frac{A'' + 3\mu_w(K_1/87)^2 D_1^4(D_2^2 - D_1^2)}{2\pi g'} = A''' D_1^4(D_2^2 - D_1^2)$$

Substituting for R and the reactance into the copper loss gives,

$$\text{Cu loss} = \frac{V^2(A'(D_2 - D_1) + B'(D_2 + D_1))}{D_1^2(A''(D_2 - D_1) + B'(D_2 + D_1))^2 + A'''^2 D_1^6(D_2^2 - D_1^2)^2}$$

As with the efficiency, the term in the numerator and denominator which represents the winding resistance can be considered constant over the practical range of D_1 . It follows that only the variation of the reactance needs consideration, hence minimum Cu losses are given when $D_1^6(D_2^2 - D_1^2)$ is a maximum. This state exists when,

$$D_1 = D_2/\sqrt{5/3}$$

5.3.1.6 Summary

The main effects that D_1 and β have on the synchronous performance parameters of the reluctance motor are shown below in Table 5.1

Parameter	Variable	
	β	D_1
Impedance (Z)	Decreasing β gives decreasing Z.	Maximum at $D_1 = D_2/\sqrt{1.5}$
Current (I_s)	Decreasing β gives increasing I_s .	Minimum at $D_1 = D_2/\sqrt{1.5}$
Output (OP)	Maximum at $\beta = 0.225$	Minimum at $D_1 = D_2/\sqrt{1.5}$
Efficiency (η)	Maximum at $\beta = 0.5$	Maximum at $D_1 = D_2/\sqrt{2}$
Power factor ($\cos \phi$)	Maximum at $\beta = 0.225$	Virtually no variation
Cu loss (Cu)	Decreasing gives increasing Cu.	Minimum at $D_1 = D_2/\sqrt{5/3}$

Table 5.1

5.3.2 Maximum inertia

The maximum inertia that can be synchronised is given by,

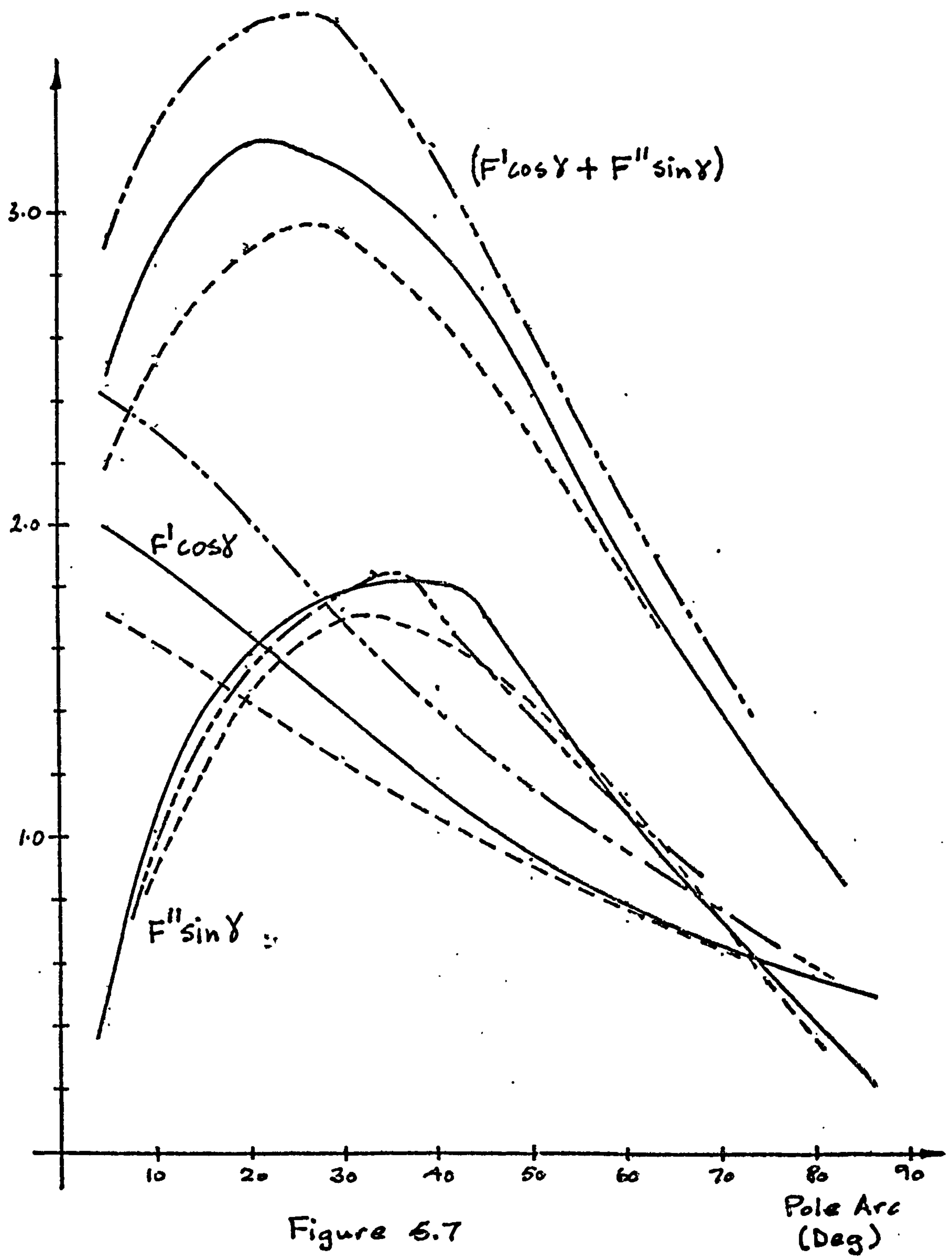
$$\hat{J} = \frac{6I_{\text{st}}}{S_m^2 \omega_s^3} \quad (5.15)$$

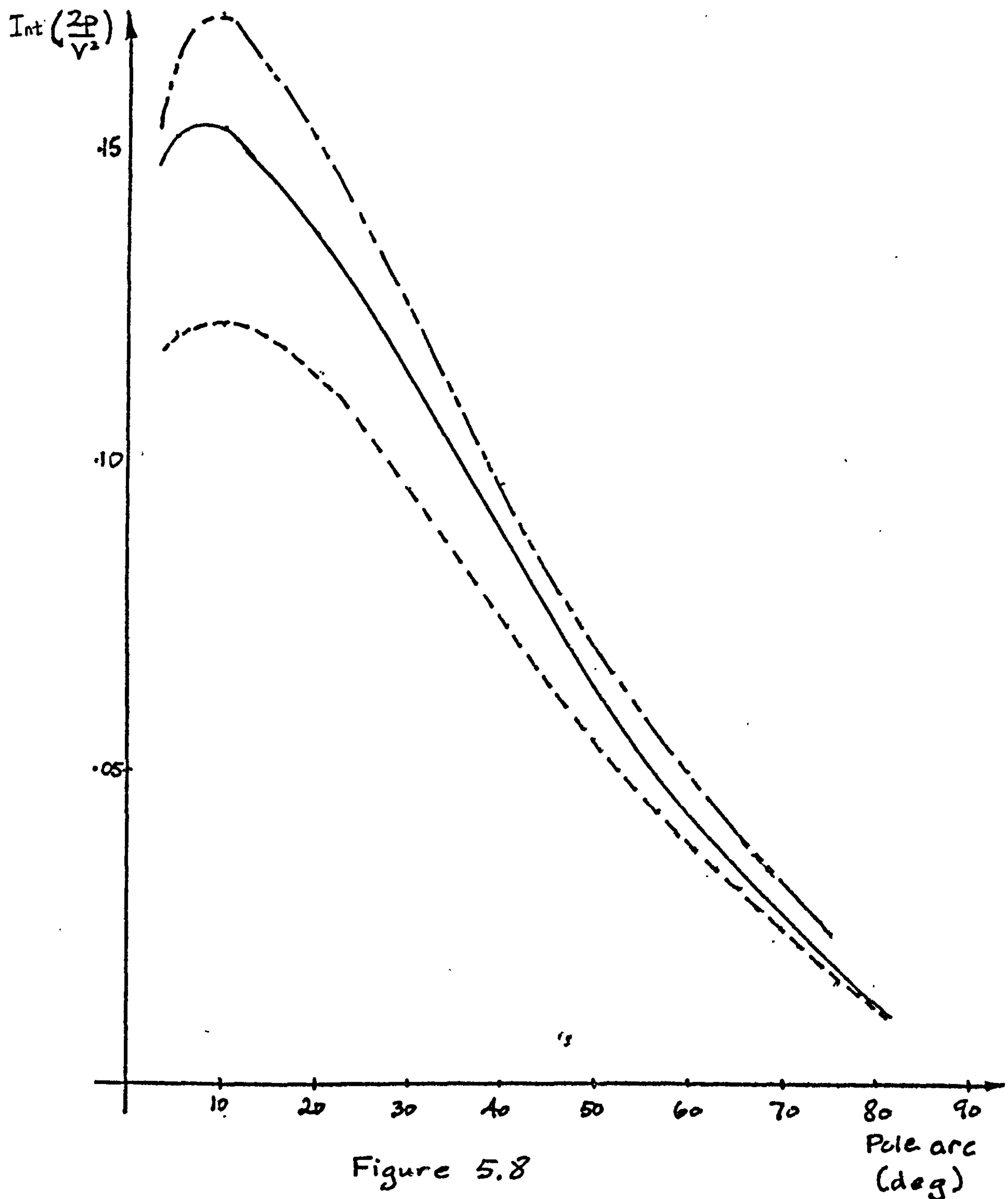
where I_{st} is the complete integral given by,

$$I_{\text{st}} = \frac{V^2 E}{2pb} \left[\cos \gamma \left(\pi - \frac{2F}{\sqrt{F^2 - b^2}} \left(\tan^{-1} \left(\frac{F \tan \frac{1}{2}(\pi + \gamma) + b}{\sqrt{F^2 - b^2}} \right) - \tan^{-1} \left(\frac{F \tan \frac{1}{2}\gamma + b}{\sqrt{F^2 - b^2}} \right) \right) + \sin \gamma \log \left(\frac{F + b \sin \gamma}{F - b \sin \gamma} \right) \right] \quad (5.16)$$

$$= \frac{V^2 E}{2p} (F' \cos \gamma + F'' \sin \gamma)$$

and where E , F , b and γ are constants of the machine and are defined in chapter II.





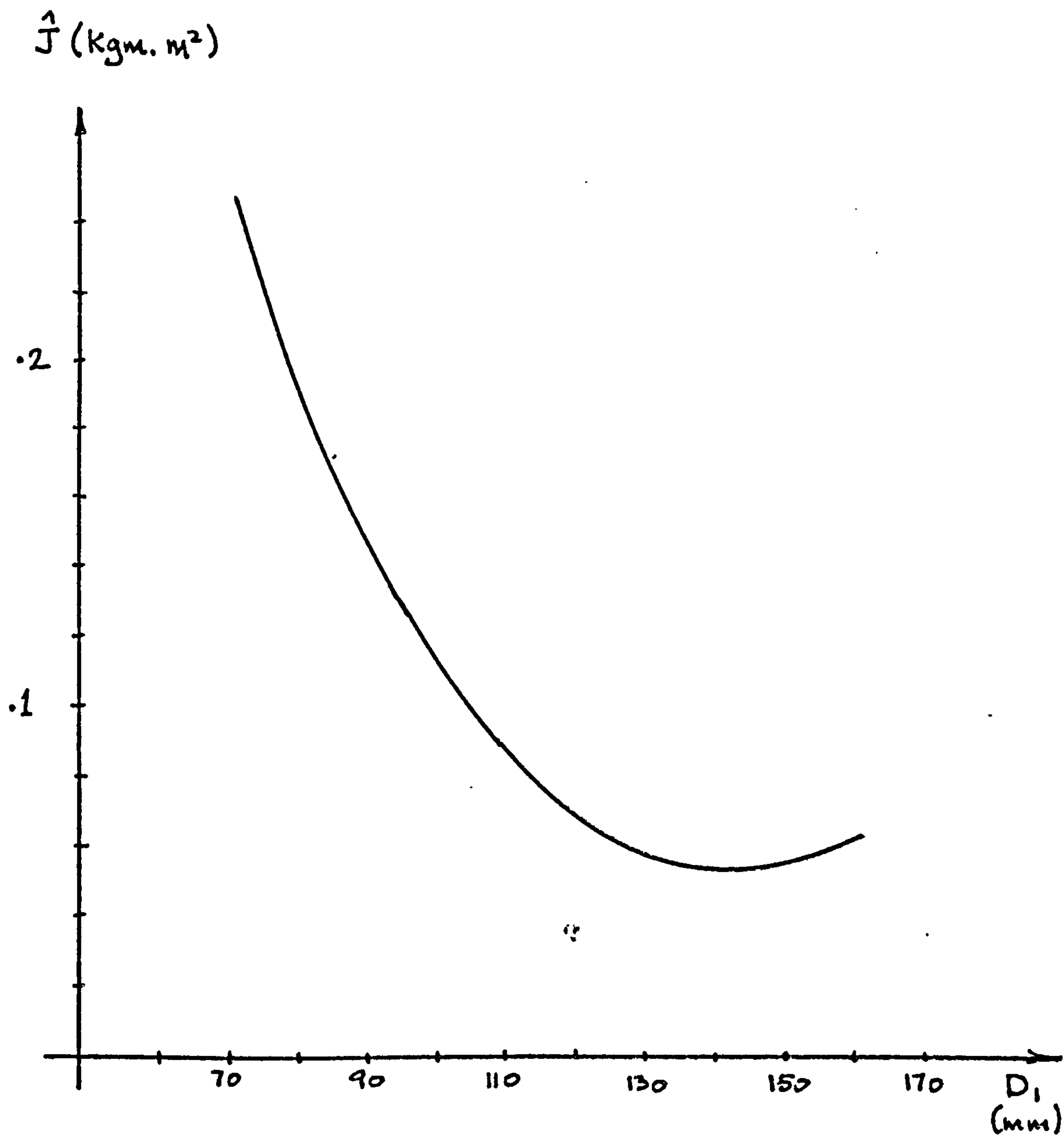


Figure 5.9

Maximum Inertia as a function of D_1

$$\beta = 0.666$$

This integral represents the area under the power/load angle curve for $0 \leq \delta \leq \pi/2p$ and \hat{J} is a maximum when this area is a maximum. This condition has been shown to coincide with $\beta \approx 0.1$. However, the validity of this result is questionable particularly in view of the results of Chapter IV. This theoretical value was reached on the assumption that the iron losses were negligible and that the leakage reactance remained constant for all values of β . It is nevertheless, worthwhile considering how the various factors in 'Int' depend on β and how they are affected by variations in the resistance and reactance of the machine. Figure 5.7 shows how the terms $F' \cos \gamma$ and $F'' \sin \gamma$ depend on the pole arc. The effect of increasing the resistance and reactance are also included on this curve. Both these components have been increased by 25% (resistance from 2.4 to 3.0 ohms and reactance from 4.8 to 6.0 ohms separately) and while $F'' \sin \gamma$ is seen to alter only slightly these variations have a marked effect on $F' \cos \gamma$. Figure 5.8 shows the variation of $\text{Int}(2p/V^2)$ with β and again the effect of varying R and X is shown. From these results it is apparent that an increase in leakage reactance, as β decreases, helps to explain the discrepancy the measured and computed values of the maximum inertia.

The variation of the expression for \hat{J} with D_1 is shown in figure 5.9. The similarity of this curve with figure 5.5a (pull-out power against D_1) is to be expected because, for any given β , the area of the curve depends to a large extent on the pull-out power.

5.5 Conclusion

In general it is desirable to design the reluctance motor for maximum efficiency, power factor, pull-out power, and pull-in power but on the basis of the theoretical results shown in table 5.1 it is not possible to optimise all these parameters.

The minimum value of D_1 would be limited by the overhang space and

the diameter of the rotor shaft. An upper limit also exists because of the minimum pull-out power at $D_1/(\sqrt{1.5})$. The variation of pull-out power with D_1 shows that the power increases more rapidly for D_1 less than this value, hence the benefit of limiting the maximum value. Corbett⁽⁸⁾ has shown that, for an iron free rotor in a d.c machine, maximum power was obtained when $D_1 = D_2/(\sqrt{3})$ and this value lies between the condition for minimum copper loss and that used in the experimental machine. With more careful regard to the stator winding resistance, this loss would have a less effect on the machine performance. It follows that D_1 should be set to give the maximum pull-out power in relation to the minimum practical limit. The value used in the experimental machine was $D_1 = D_2/2$.

The range $0.5 \geq \beta \geq 0.255$ covers the optimum synchronous performance requirements. The results for both the synchronous and asynchronous performance suggests that the theoretically low values of β (0.225 and 0.1 respectively) would in practice be too low for either maximum pull-out or maximum inertia. though the value for the former will still be greater than the value of β for the latter. The conflicting requirements for these two aspects of the machine performance is a well known feature of the reluctance motor.

Chapter VI

General Discussion

6.1 Introduction

This Chapter deals with improvements to the machine with suggestions for further work. A strong emphasis is placed on simplifying the construction of the machine, particularly the rotor, and forms the basis of the suggestions for further work. A comparison is also made of the power to weight ratio with a radial flux machine. Two features not mentioned in the previous Chapters are also discussed briefly, and finally the type of market in which the axial machine might find initial outlets is considered.

6.2 Aspects of the Experimental Machine Performance

For an ideal motor with identical stators, airgaps and symmetrical rotor (mechanically, electrically and magnetically) there will be no unbalanced magnetic pull. Because of the double stator it was possible to observe this feature in the experimental machine. In this machine the airgaps were maintained by using shims between the shoulders of the inner race of the bearings and the shoulder on the rotor shaft. Initially the motor was set up with a total physical airgap of 1.0 mm and a total end play of 0.8 mm thus allowing the possibility of the motor operating with airgaps of 0.1 mm and 0.9 mm. It was virtually impossible to get the motor to run with even airgaps in this state and, as would be expected, once energised the rotor pulled hard over to one stator. The direction of axial movement depended solely on the position of the rotor at rest and in general an initially smaller airgap was always reduced. For an apparently symmetrical airgap arrangement, the rotor always preferred a particular direction, thus suggesting a dissimilarity between the separate identifiable motors. The effect of

this unbalanced magnetic pull manifested itself in two ways. Firstly, the line current increased and secondly, the one bearing was subjected to a strong axial force. Although no measurements were taken of either current or force, the noise emitted from this bearing was plainly audible.

As the end play was reduced (symmetrically at both bearings) the axial movement still persisted but the increase in line current and the noise were both decreased. At a point where the total endplay was approximately 20-25% of the total airgap, the rotor began to exhibit axial oscillations at low voltages. This oscillation persisted up to approximately 60% of full voltage after which the rotor would pull over to one of the stators. The rotor appeared to have no particular preference for either direction of axial movement under these conditions.

The two operational modes of the double stator machine have already been discussed and although the rotor was not axially thick enough to operate under the alternative mode, it was possible to misalign the stators with respect to each other. For misalignments of up to 30° (mechanical) the line current remained virtually constant after which the increase was extremely sharp. This was due mainly to the fact that the iron in the rotor was saturating causing a reduction in the magnetising reactance of the machine. Total misalignment was possible only at reduced voltage and at 50% full voltage the line current for 90° (mechanical) misalignment (thus giving the condition where the stator m.m.f.'s were mutually opposing) was greater by a factor of approximately 3. The power factor also decreased. This variation of the angular position of the two stators was performed on the induction motor and the reluctance motor on no load and for the latter machine the rotor, when synchronised at 50% line voltage, showed the 90° displacement between the preferred

axes of the machine mentioned in Chapter I.

6.3 Improvements to the Experimental Machine

The maximum output of the induction motor was 1,260 watts with an efficiency of 51% at a slip of .3. The stator copper losses were 665 watts. Considering the stator copper losses, it is possible to nearly double the ~~cross~~ sectional area of the wire used in the stator winding by increasing the slot size from 13.5 mm x 8.0 mm to 18.0 x 10.5 giving a reduction in stator copper loss of nearly 330 watts. This would increase the efficiency to 58%. Furthermore, the slip is very high and the copper losses in the cage (computed) for this slip were 630 watts. There is a twofold benefit in increasing the copper section of the ~~cage~~ . Firstly, the slip is reduced and secondly, these losses are reduced. Using the round bars it is possible to decrease the resistance of the squirrel cage again by a factor of 2. The slip is reduced down to .15 (still rather high). This increases the power output to 1,530 watts and the efficiency to approximately 85%.

Finally, the rotor is approximately twice as thick as is necessary (the reasons were given in Chapter III). In this machine the rotor accounts for $\frac{1}{3}$ of the total weight of the induction motor which is 22.5 Kgm. By reducing the length of the rotor, the weight is reduced to 18.7 Kgm and the length from 110 mm to 95 mm.

For the reluctance motor, proper consideration of the stator winding resistance will also increase the efficiency while the reduction of the rotor mass gives an apparent improvement in the maximum value of coupled inertia/rotor inertia of a factor of 2. In fact, this serves to demonstrate how misleading it is to judge the pull-in capabilities of the reluctance motor on this basis. For example at $\beta = 0.666$ the total inertia that would be synchronised was 0.173 Kgm. m^2 giving a figure of

9.8 for this ratio. By reducing the axial length by 2 this ratio increases to 19, yet the total inertia will still only be 0.173 Kgm. m².

6.4 Comparison of Machine Performance

The following table compares all the relevant figures on the experimental machine performance with the results obtained by Gupta.

	Gupta's Machine		Axial Machine	
	Induction	Reluctance	Induction	Reluctance
Diameter	194 mm	194 mm	220 mm	220 mm
Length	216 mm	216 mm	110 mm	110 mm
Rotor Inertia	-	.0049 Kgm m ²	.025 Kgm. m ²	.015 Kgm. m ² @ $\beta = 0.445$
Power out	1000 watts @ s = 0.075	† 1235 watts	1260 watts @ s = 0.3	1100 watts @ $\beta = 0.445$
Efficiency	82%	† 82%	51%	51%
Power factor	0.39	† .725	.78	0.4
Weight	45 Kgm	45 kgm	22.5 Kgm	18.5 Kgm @ $\beta = 0.445$
Power/weight	22.2 watts/ Kgm	27.4 watts/ Kgm	55 watts/ Kgm	59 watts/ Kgm

† Segment arc/pole pitch ratio approximately 0.85.

It would be hoped to improve the efficiency of both axial machines by increasing the copper content on the stator and rotor to 85% and 61% for the induction and reluctance motors respectively. The power factor of the induction motor would be reduced to approximately 0.65 (theoretically).

It is apparent from these figures that, apart from the efficiency and power factor of the reluctance motor, the axial machine compares extremely favourably with radial machines. The main benefits are in the reduction in size and the increase in the power/weight ratios.

6.5 Suggestions for further work

6.5.1 Unbalanced Magnetic Pull

The effect of U.M.P. on machine performance has been widely studied⁽²⁶⁾. The need for such a study is related not only to the need to understand how the machine characteristics alter, but also on the types and size of materials to use, particularly in the rotor. The double stator axial machine is ideal for such a study for two reasons.

- (1) The method usually employed in measuring the force on the rotor in radial machines requires strain gauges. In the axial machine, direct readings would be possible. Because the force is transmitted axially, it is not necessary for the main bearings to counteract this force - the use of suitable stops external to the machine but attached to the rotor would relieve the main bearings of this duty and offer scope for the adaptation of force measurements.
- (2) The airgap could be varied while the motor is running. It is often the case that to alter the mechanical proportion of machines, dis-assembly is necessary, resulting, even though great care is taken, in the introduction of unwanted constraints. Again, by the use of external mechanical supports, it is possible to alter the air-gap while the motor is operating.

Such a study would necessarily complement previous work on this feature of electrical machines.

6.5.2 Variation in Rotor configuration

6.5.2.1 Induction Motor (Ironless rotor)

The axial machine lends itself very well to the use of a copper disc without iron in the rotor. This will naturally lead to a large airgap, but one of the variables in the machine was this parameter with a maximum total value of 1.4 mm. Magnetically this appears as an airgap of 2.2 mm. The removal of the iron will reduce the U.M.P to zero. Under such circumstances, the distance between the rotor and stator surface is restricted solely by mechanical and manufacturing limitations. In the present experimental machine it is possible, within the stator separation of 1.4 mm, to incorporate a copper disc 1 mm thick with a stator-rotor separation of 0.2 mm (.008"). In effect the disc behaves approximately like a cage with an infinite number of bars. One of the difficulties of analysing such a machine is that the airgap flux is not necessarily predominantly axial because of the skin effect in the disc.

Nasar⁽²⁷⁾ has considered such a machine. His work does not appear to have been an exhaustive one and indeed his main emphasis is on the ability to obtain speed control by misalignment of the two stators. It is apparent from the nameplate rating of his motor (1/4 h.p., 1800 r.p.m., 3 phase, 60 Hz, 50 volt supply) that the superior power/weight ratio of the axial machine was not relevant to his work. It would seem then, that such a motor is worthy of further consideration, together with the rotor discussed in the next section, because of the two benefits of low inertia and simplified production.

6.5.2.2 Induction Motor (Iron rotor)

In the production of the rotor of the experimental machine the method of producing the slots for the cage and the fixing of the rotor

iron to the shaft is not particularly easy. The intermediate stage between the experimental rotor and the copper disc rotor mentioned above offers some easing in the production of the rotor and some of the benefits of the low inertia copper disc. In this instance, as with the iron-less rotor, the copper disc is keyed on to the shaft. Rectangular holes (Figure 6.1) are punched or machined in the surface of the copper disc and iron inserts are fixed into the holes. It is tentatively suggested that the inserts are solid and it is appreciated that the method of attaching the iron inserts to the copper disc would require careful consideration.

6.5.2.3 Reluctance Motor

A similar rotor to that suggested in Section 6.5.2.2. is a natural step for the reluctance motor rotor. The iron inserts would naturally be confined to a particular pole arc. In this instance, there is a strong case in favour of using solid inserts as there are no iron losses in the rotor once synchronisation has been achieved. In keeping with the requirement of minimum rotor inertia, the condition in which the stator m.m.f.'s are mutually additive would appear to offer the most preferable design. One other feature of the low inertia is its ability to be accelerated and decelerated more rapidly.

6.6 Type of Market

It is obvious that a synchronous motor is not a competitor, in the widest sense, to the induction motor since, in general, either is chosen to perform a specific function. The first for its ability to run at constant speed, the second for its greater reliability and smaller cost. In the same sense, it is unrealistic to think that the axial machine would or should be a competitor in all areas of the market held by radial machines. Nevertheless, there are applications where radial machines

/// Iron Inserts

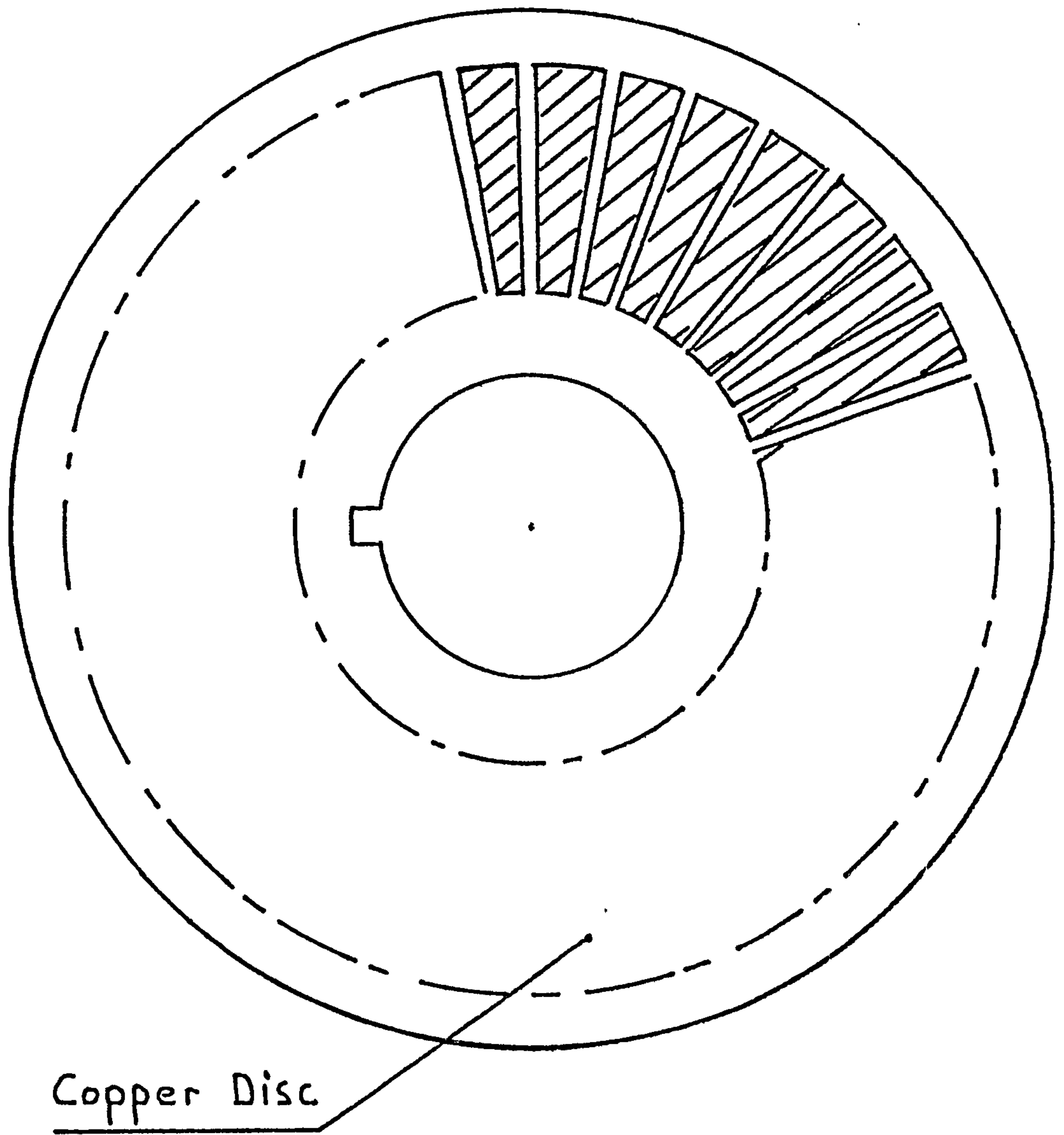


Figure 6.1

are used mainly because there are no alternatives. It is in these areas that the axial machine has the best possible outlet, at least initially. Consequently, use should be made of the superior power to weight ratio, the shape of the axial machine, and the possible low inertia of the rotor. In the first instance, the limitation is the total weight of the unit or equipment in which the motor forms an integral part. For example, portable measuring equipment, tape recorders, etc., the aerospace industry where the cost of developing equipment is outweighed by other considerations (notably the cost of keeping the equipment off the ground). In the second instance, the limitation is not only available volume (which could apply to any of the above examples) but also the "stream line" shape of the motor. For example, domestic extractor fans can be particularly bulky. Finally, the inertia often limits the time taken to accelerate the rotor from standstill. One well known sewing machine manufacturer uses a printed circuit motor because of its low inertia for determining the sewing speed. The a.c. supply is used on conjunction with a 'chopper' circuit to give speed control, continuously variable, of the motor.

All the above examples have tended to be quite small and often require a single phase supply. This does not exclude the possibility of developing larger machines for industrial use but the above examples do have the special requirements that suit the axial machine.

6.7 Conclusion

The experimental machine has given results which indicate the potential of the axial machine in a fairly comprehensive manner. It is worthwhile noting that the modern designs of reluctance motors show a great improvement over the simple modified induction motor.⁽³⁾ These designs have permanent magnet rotors, segmental rotors and axial laminated rotors

and some have the basic reluctance rotor with flux guides or flux barriers. The experimental machine could easily be modified to incorporate permanent magnets and it has already been shown that the double stator machine could behave in a manner similar to the segmental machine. However, although these are possible methods of improving the experimental machine performance, they do not ease the problems associated with the manufacture of the rotor.

Appendix I

Airgap Permeance

The developed diagram of the double stator machine is shown in Figure I.1. The variation of the total airgap length, assuming the iron has infinite permeability is shown in Figure I.2 as a function of α , while the variation of $1/g(\alpha)$ is shown in Figure I.3. The following nomenclature is used,

θ = angular displacement between the rotor pole
and the axis of phase.1.

β = the pole arc to pole pitch ratio.

$2h$ = axial length of the rotor.

g = airgap between the rotor and a stator.

The function $g(\alpha)$ represents the length of the airgap at any position, hence the permeance of an elemental length dR in the radial direction at radius R and of angular width $d\alpha$ is given by,

$$P_r = \frac{R dR d\alpha}{g(\alpha)}$$

where $RdRd\alpha$ is the cross-sectional area of the element and $g(\alpha)$ is its length. Using figure I.3 the function $1/g(\alpha)$ can be expressed in terms of a Fourier series as,

$$\frac{1}{g(\alpha)} = \frac{1}{2}(a_0) + \sum a_n \cos\left(\frac{n\pi\alpha}{T}\right) + \sum b_n \sin\left(\frac{n\pi\alpha}{T}\right)$$

where,

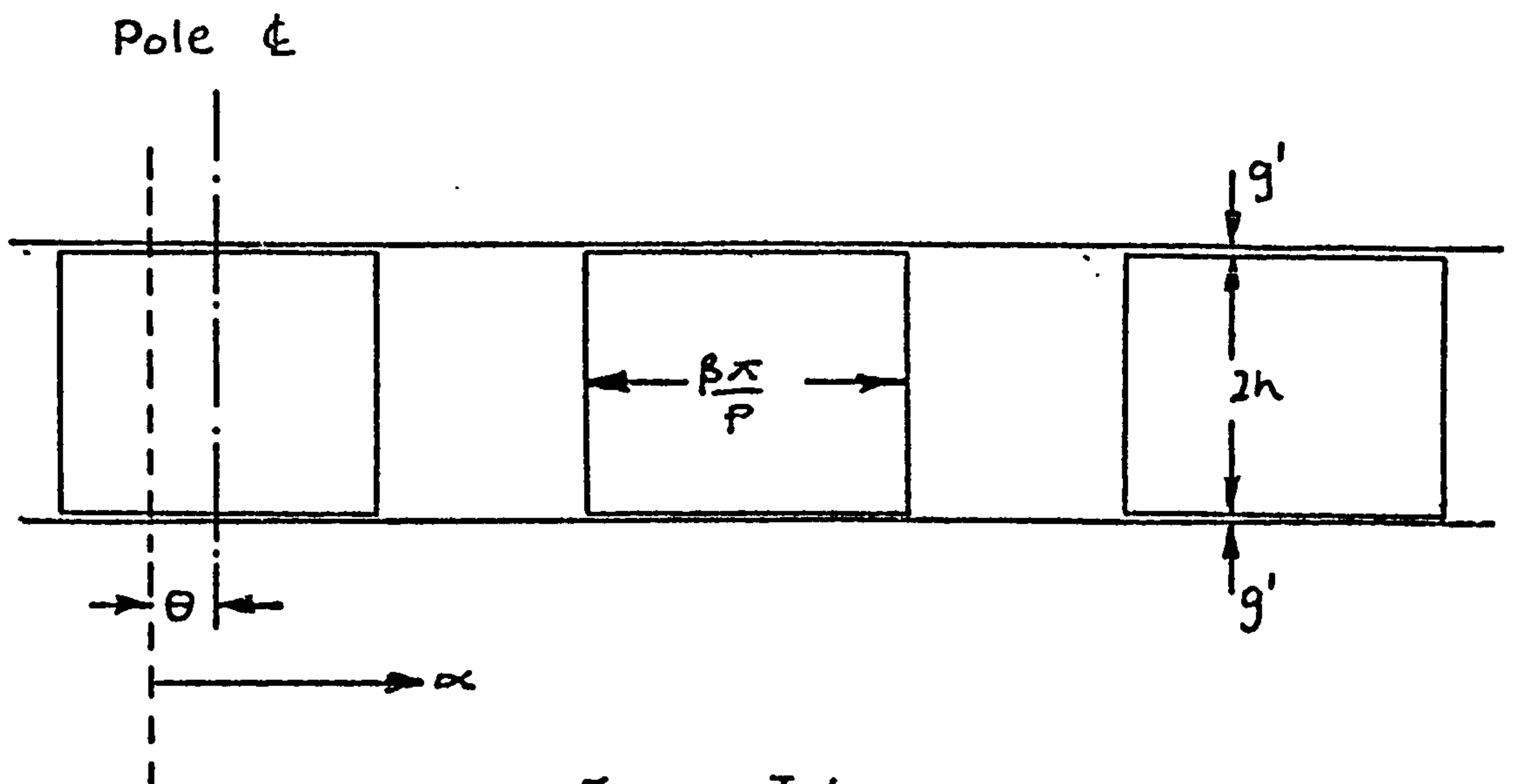
$$a_0 = \frac{1}{T} \int_0^{2T} \frac{d\alpha}{g(\alpha)}$$

$$a_n = \frac{1}{T} \int_0^{2T} \frac{1}{g(\alpha)} \cos\left(\frac{n\pi\alpha}{T}\right) d\alpha$$

$$b_n = \frac{1}{T} \int_0^{2T} \frac{1}{g(\alpha)} \sin\left(\frac{n\pi\alpha}{T}\right) d\alpha$$

Consequently,

$$P_r = \frac{\mu_0 R dR}{g(h+g)} \left[\frac{\beta h+g}{2} + \frac{h}{\pi} \sum_{n=1}^{\infty} \frac{\sin(n\beta\pi)}{n} \cos(2n\pi(\alpha - \theta)) \right]$$



Axis of
Phase I

Figure I.1

Developed diagram of experimental machine .

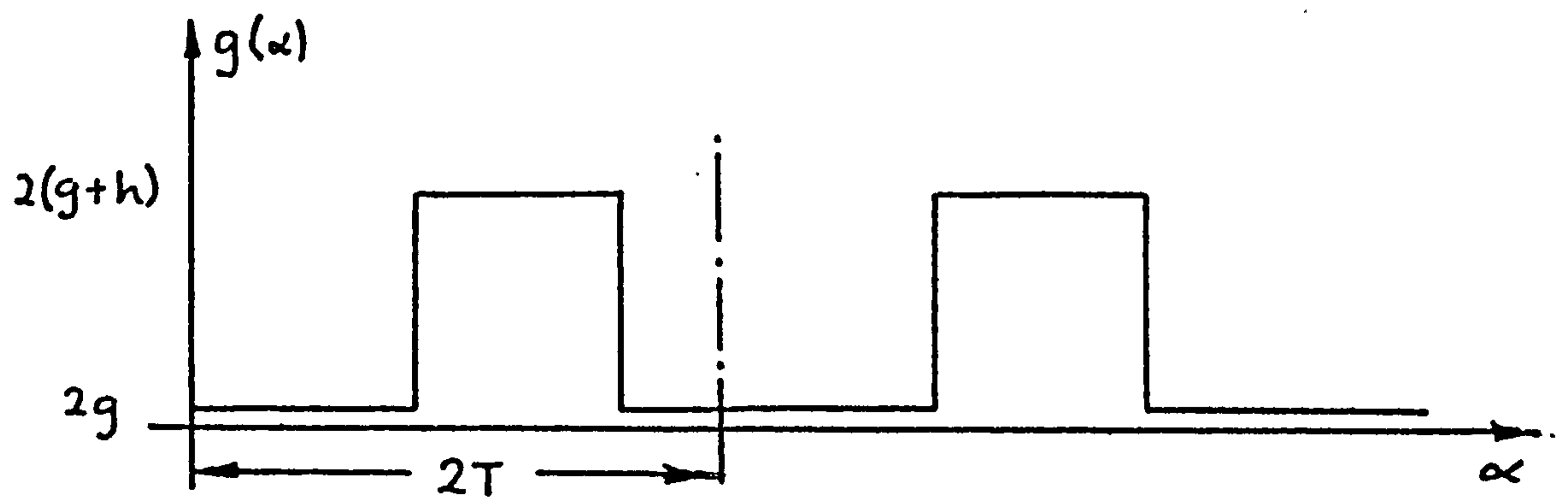


Figure I.2

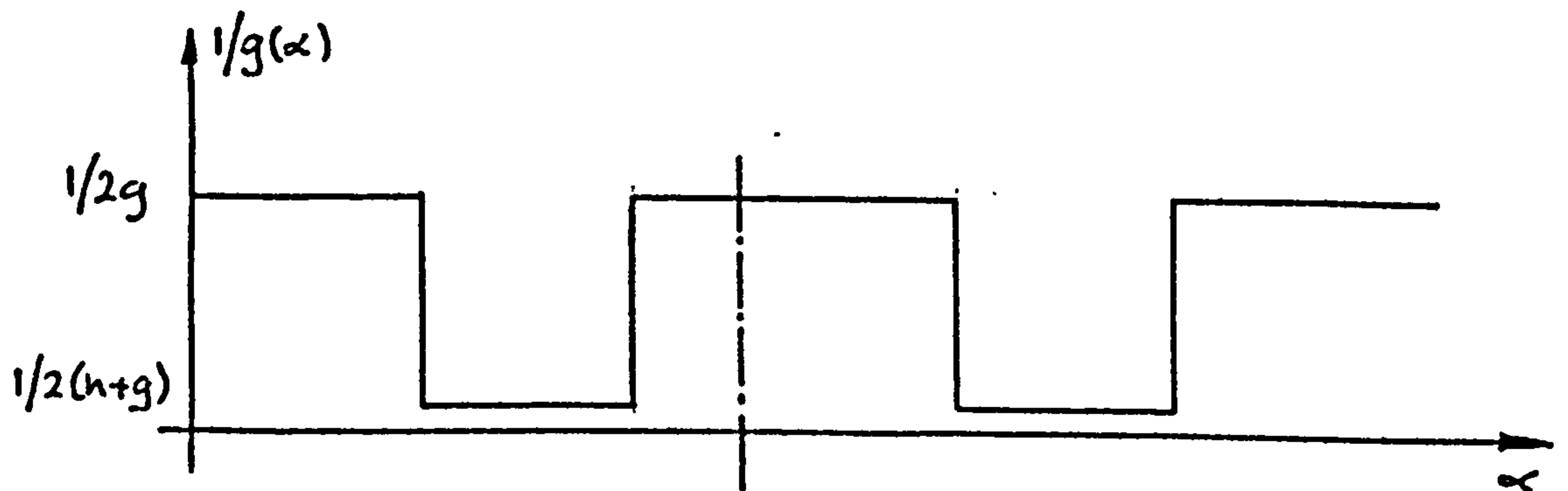


Figure I.3

Appendix II

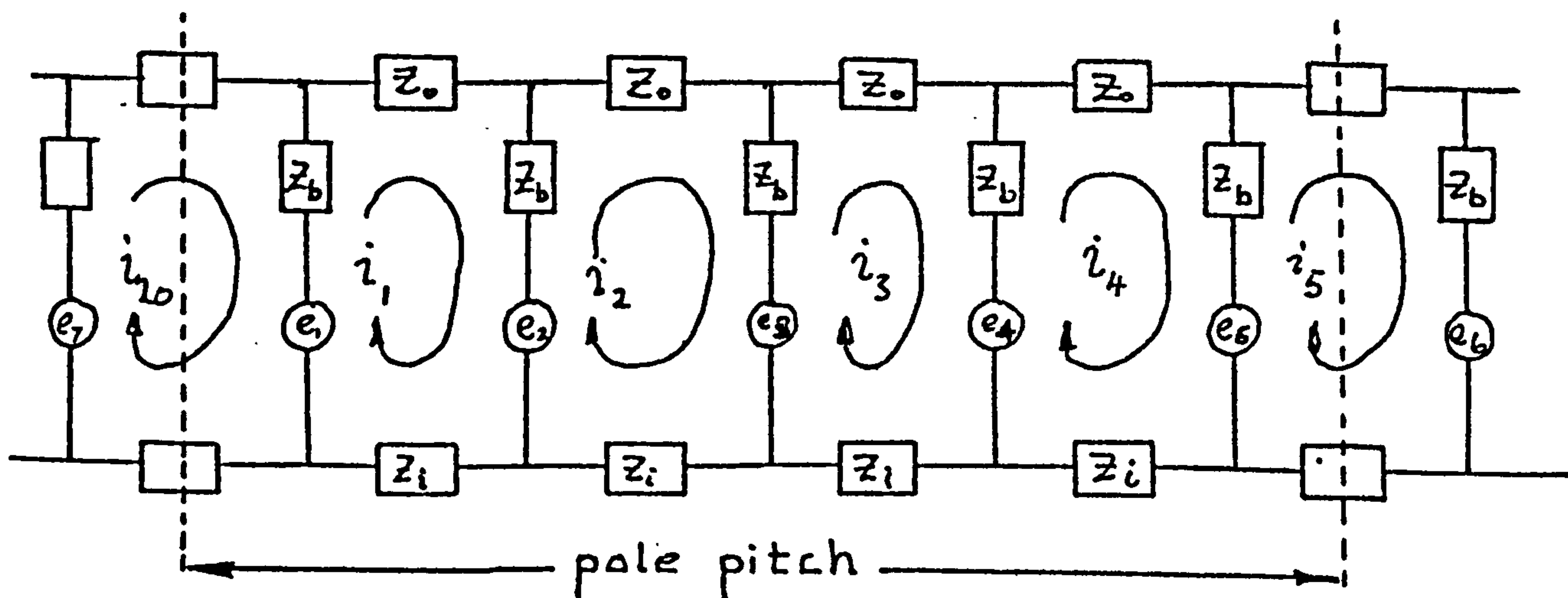
Bar load impedance

II.1 Introduction

When the bars of the squirrel cage interact with the rotating magnetic field an e.m.f is induced along the length of the bar. Provided the ends are connected, as they are in the complete cage, by the endrings currents will flow. The current in any bar is a function of the e.m.f induced across all the bars and the impedances of the bars and endrings. In the axial machine the e.m.f induced in an elemental length dR will be a function of the radius so that for an increasing radius each element will have a greater e.m.f than its predecessor. (This is not the case in radial machines). It is assumed that all the elemental e.m.f's can be added together and furthermore that a "lumped" parameter technique can be used.

II.2 Circuit Diagram

It is apparent that due to the symmetry of the cage only the e.m.f's and currents in the bars and endring portions which span a pole pitch need be considered. Each bar is assumed to have the same impedance and the impedance per unit length of the outer ring is also assumed to equal the impedance per unit length of the inner end ring. The following circuit represents one pole pitch of the squirrel cage.



The squirrel cage has twenty bars and the mesh equations for the five bars gives,

$$E_1 = i_1 Z - i_2 Z_b - i_{20} Z_b$$

$$E_2 = i_2 Z - i_3 Z_b - i_1 Z_b$$

$$E_3 = i_3 Z - i_4 Z_b - i_2 Z_b$$

$$E_4 = i_4 Z - i_5 Z_b - i_3 Z_b$$

$$E_5 = i_5 Z - i_6 Z_b - i_4 Z_b$$

where $E_1 = e_1 - e_2$, $E_2 = e_2 - e_3$, etc.

e_1 = voltage induced in bar 1 (e_2 , e_3 , etc.)

i_1 = loop current associated with bar 1 and bar 2 (i_2 , i_3 , etc.)

Z_b = impedance of bar.

$$Z = 2Z_b + Z_o + Z_i$$

Z_o (Z_i) = impedance of the outer (inner) endring segment between two bars.

In matrix form the simultaneous equations become,

$$\begin{bmatrix} E_1 \\ E_2 \\ E_3 \\ E_4 \\ E_5 \end{bmatrix} = \begin{bmatrix} Z & -Z_b & 0 & 0 & Z_b \\ -Z_b & Z & -Z_b & 0 & 0 \\ 0 & -Z_b & Z & -Z_b & 0 \\ 0 & 0 & -Z_b & Z & -Z_b \\ Z_b & 0 & 0 & -Z_b & Z \end{bmatrix} \begin{bmatrix} i_1 \\ i_2 \\ i_3 \\ i_4 \\ i_5 \end{bmatrix}$$

$$\text{i.e. } [E] = [Z'] [I]$$

and therefore,

$$[I] = [Z']^{-1} [E]$$

The transposition of the $[Z']$ matrix involves finding both the determinant of Z and the adjoint matrix. Both require lengthy procedures. The final matrix is shown overleaf and the value of the determinant is given below.

$$\Delta = Z^5 - 5Z^3 Z_b^2 + 5Z Z_b^4 + 2Z_b^5$$

The current in bar 1 is given by,

$$\begin{aligned}
 i_{b1} &= i_1 - i_{20} \\
 &= i_1 + i_5 \\
 &= \frac{1}{\Delta} \left[E_1(z^4 - z^3 z_b - 3z^2 z_b^2 + 2z z_b^3 + 2z_b^4) + \right. \\
 &\quad E_2(z^3 z_b - z^2 z_b^2 - z z_b^3) + E_3(z^2 - z z_b - z_b^2) 2z_b^2 + E_4(z^3 z_b - z^2 z_b^2 - z z_b^3) + \\
 &\quad \left. E_5(z^4 - z^3 z_b - 3z^2 z_b^2 + 2z z_b^3 + 2z_b^4) \right]
 \end{aligned}$$

and similar expressions are obtained for the other bar currents, hence,

$$i_{b1} = \frac{E_1(z^2 - 2z_b^2) + E_2 z z_b + E_3 2z_b^2 + E_4 z z_b + E_5(z^2 - 2z_b^2)}{(z^2 - z z_b - z_b^2)(z + 2z_b)}$$

Substituting for $E_1 = e_1 - e_2$; $E_2 = e_2 - e_3$, etc.

gives,

$$i_{b1} = \frac{2e_1(z^2 - 2z_b^2) - e_2(z^2 - z z_b - 2z_b^2) - e_3(z - 2z_b)z_b + e_4(z^2 - z z_b - 2z_b^2) + e_5(z^2 - z z_b - 2z_b^2)}{(z + 2z_b)(z^2 - z z_b - z_b^2)}$$

From chapter II section 2.4.2 the voltage induced across any bar is given by,

$$\begin{aligned}
 e_b &= \frac{IC'sw \cos(p\alpha)}{p} \\
 &= \hat{E} \cos(p\alpha)
 \end{aligned}$$

and when $e_1 = \hat{E} \cos(p\alpha)$

then $e_2 = \hat{E} \cos(p\alpha + \gamma)$

$e_3 = \hat{E} \cos(p\alpha + 2\gamma)$ etc

where γ = the rotor slot pitch in degrees. For twenty rotor bars,

$e_1 = \hat{E} \cos(p\alpha)$

$e_2 = \hat{E} \cos(p\alpha + 18)$

$e_3 = \hat{E} \cos(p\alpha + 36)$ etc

Substituting for the bar e.m.f's and rearranging gives the bar current in terms of the peak e.m.f.

$$i_{b1} = \frac{\hat{E}}{(Z+2Z_b)(Z^2-ZZ_b-Z_b^2)} \cdot$$

$$\left[\begin{aligned} &Z^2(2\cos p\alpha - \cos p(\alpha + 18) + \cos p(\alpha + 72)) + \\ &ZZ_b(\cos p(\alpha + 18) - \cos p(\alpha + 36) + \cos p(\alpha + 54) - \cos p(\alpha + 72)) - \\ &2Z_b^2(2\cos p\alpha - \cos p(\alpha + 18) - \cos p(\alpha + 36) + \cos p(\alpha + 54) + \cos p(\alpha + 72)) \end{aligned} \right]$$

Putting $p=2$ and considering the coefficient of Z^2 ,

$$\begin{aligned} &(2\cos 2\alpha - \cos 2(\alpha + 18) + \cos 2(\alpha + 72)) \\ &= (2\cos 2\alpha - \cos 2\alpha \cos 36 + \sin \alpha \sin 36 + \cos 2\alpha \cos 144 - \sin 2\alpha \sin 144) \end{aligned}$$

But $\sin 144 = \sin 36$; $\cos 144 = -\cos 36$;

consequently, the coefficient reduces to $2(\cos 2\alpha - \cos 2\alpha \cos 36)$

By a similar process on the coefficients of ZZ_b and $2Z_b^2$ the bar current becomes,

$$i_{b1} = \frac{\hat{E} \cos p\alpha \left[Z^2(1 - \cos 36) + ZZ_b(\cos 36 - \cos 72) - 2Z_b^2(1 - \cos 36 - \cos 72) \right]}{(Z+2Z_b)(Z^2-ZZ_b-Z_b^2)}$$

But $\cos 36 = (0.5 + \cos 72)$, hence,

$$i_{b1} = \frac{\hat{E} \cos 2\alpha \left[(Z-Z_b) - 2\cos 72(Z-2Z_b) \right]}{Z^2 - 2Z_b Z - Z_b^2}$$

therefore,

$$i_{b1} = \frac{\hat{E} \cos 2\alpha}{z}$$

$$\text{where, } z = \frac{Z^2 - 2Z_b Z - Z_b^2}{(Z-Z_b) - 2\cos 72(Z-2Z_b)}$$

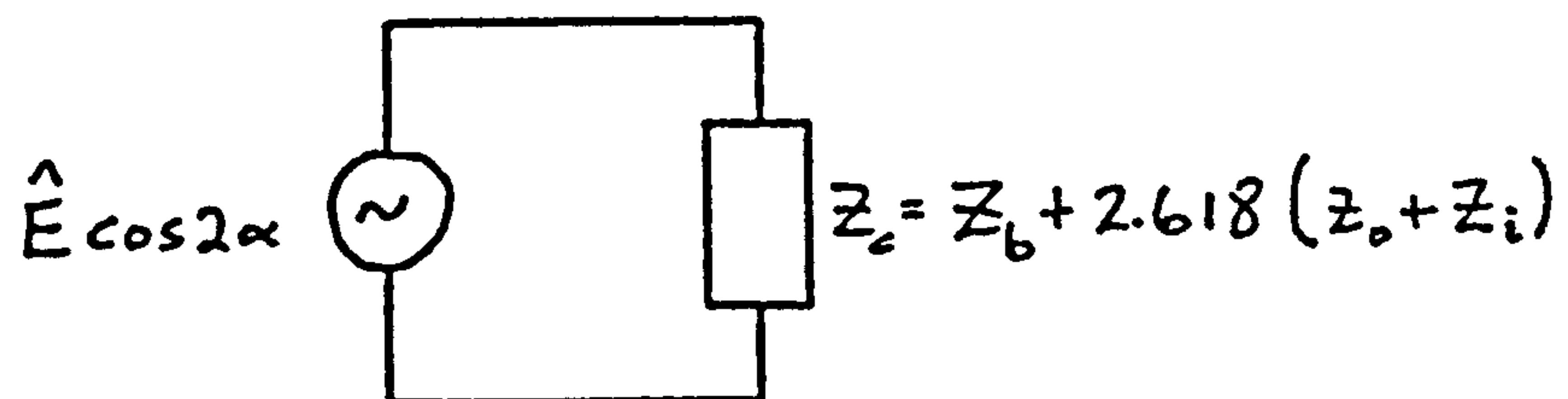
since $Z = 2Z_b + (Z_o + Z_i)$ it can be shown that,

$$z = Z_b + 2.618(Z_o + Z_i)$$

$$\text{and } i_{b1} = \frac{\hat{E} \cos 2\alpha}{Z_b + 2.618(Z_o + Z_i)}$$

The currents in all the other bars are given by identical equations. The "lumped parameter" equivalent circuit for each bar is represented by

a series connected e.m.f source and an impedance as shown below.



Appendix III

Calculation of the squirrel cage bar impedance

For the induction motor all the bars are surrounded by iron while in the reluctance motor some of the cage bars have no iron boundaries. The number of bars in the latter case depend on the pole arc/pole pitch ratio. The solutions to the resistance and reactance of the bars in either instance is obtained in the form of Bessel functions and it is seen that both cases are limiting conditions for the semi-open slot. The round bar in the semi-open slot has been investigated by Swann and Salmon⁽²⁸⁾ and it is necessary to consider only what happens to the factor k_n in their final equations for R_b and X_b to reach the solutions for the two states being considered.

Figure III.1 shows the configuration used by Swann and Salmon. In their analysis they assume that

- (1) The iron has infinite permeability.
- (2) The bar completely fills the slot.
- (3) Proximity effects can be ignored.

The relationships obtained for R_b and X_b by Swann et al are given in equations III.1 and III.2

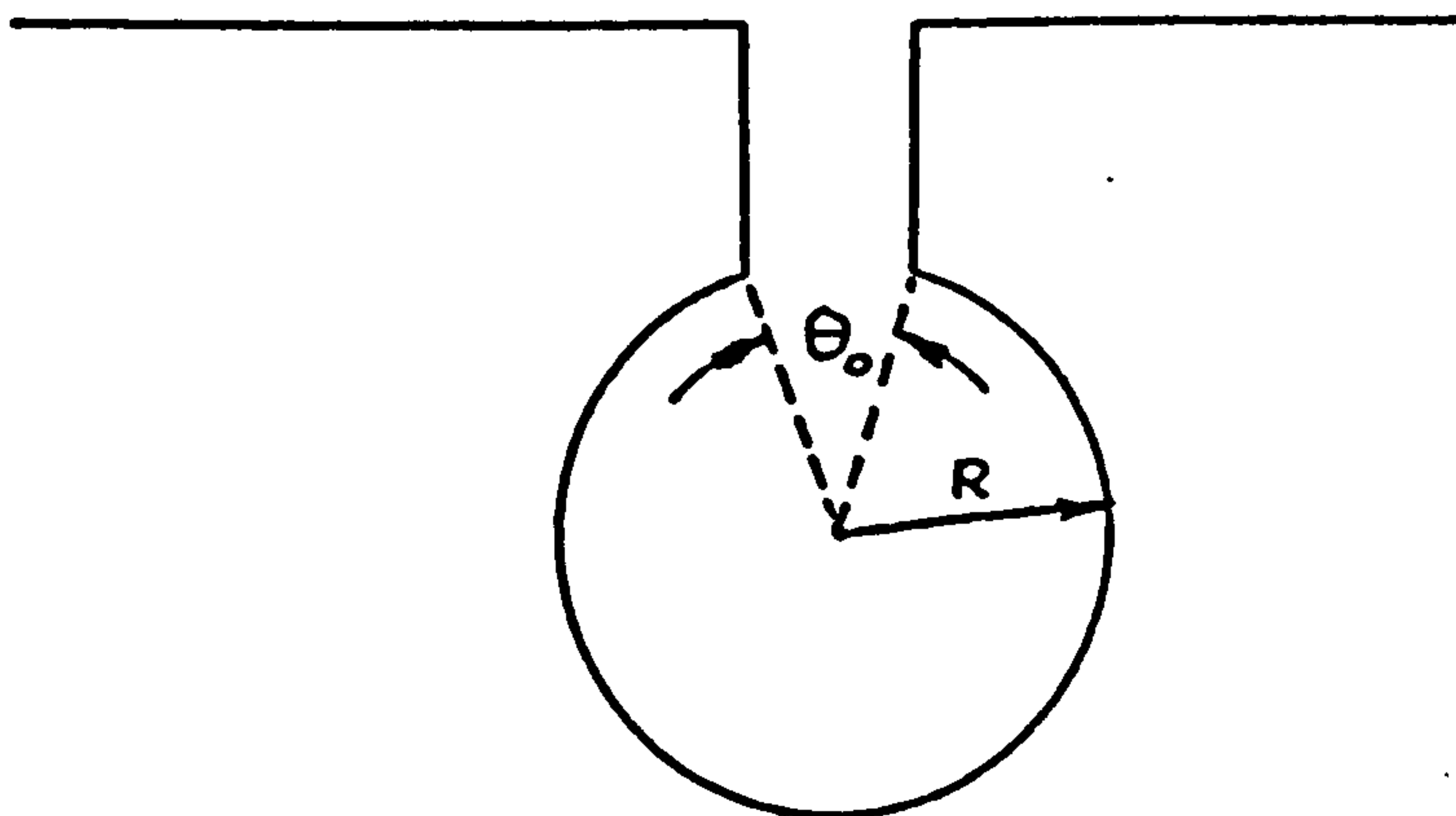


Figure III.1

$$\frac{R_b}{R_d} = \frac{\alpha R}{2} \left[\frac{\text{ber} \alpha R \text{bei}' \alpha R - \text{bei} \alpha R \text{ber}' \alpha R}{(\text{ber}' \alpha R)^2 + (\text{bei}' \alpha R)^2} + 2 \sum k_n \frac{(\text{ber}_n \alpha R \text{bei}'_n \alpha R - \text{bei}_n \alpha R \text{ber}'_n \alpha R)}{(\text{ber}'_n \alpha R)^2 + (\text{bei}'_n \alpha R)^2} \right] \quad (\text{III.1})$$

$$\frac{X_b}{R_d} = \frac{\alpha R}{2} \left[\frac{\text{ber} \alpha R \text{ber}' \alpha R + \text{bei} \alpha R \text{bei}' \alpha R}{(\text{ber}' \alpha R)^2 + (\text{bei}' \alpha R)^2} + 2 \sum k_n \frac{(\text{ber}_n \alpha R \text{ber}'_n \alpha R + \text{bei}_n \alpha R \text{bei}'_n \alpha R)}{(\text{ber}'_n \alpha R)^2 + (\text{bei}'_n \alpha R)^2} \right] \quad (\text{III.2})$$

In these equations,

R = radius of bar.

R_d = d.c resistance of the bar/unit length

R_b = a.c " " " " " "

X_b = reactance " " " " "

$\alpha = \sqrt{\mu_0 \sigma w}$

μ_0 = permeability of free space

σ = conductivity of copper

w = frequency

$$k_n = \frac{\sin \frac{1}{2} n \theta_0}{\frac{1}{2} n \theta_0}$$

θ_0 = angle subtended by the slot opening with respect to the axis of the bar.

For the induction machine, $\theta_0 = 0$

while for the interpolar bars of the reluctance motor, $\theta_0 = 2\pi$

and consideration of the limiting conditions for k_n show that,

(1) For the induction motor:-

$$\text{Lim } k_n = 1$$

$$\theta_0 \rightarrow 0$$

(2) For the interpolar bars:-

$$\text{Lim } k_n = 0$$

$$\theta_0 \rightarrow 2\pi$$

Consequently for bars with iron boundaries,

$$\frac{R_{ib}}{R_d} = \frac{\alpha R}{2} \left[\frac{\text{ber} \alpha R \text{bei}' \alpha R - \text{bei} \alpha R \text{ber}' \alpha R}{(\text{ber}' \alpha R)^2 + (\text{bei}' \alpha R)^2} + 2 \sum \frac{\text{ber}_n \alpha R \text{bei}'_n \alpha R - \text{bei}_n \alpha R \text{ber}'_n \alpha R}{(\text{ber}'_n \alpha R)^2 + (\text{bei}'_n \alpha R)^2} \right] \quad (\text{III.3})$$

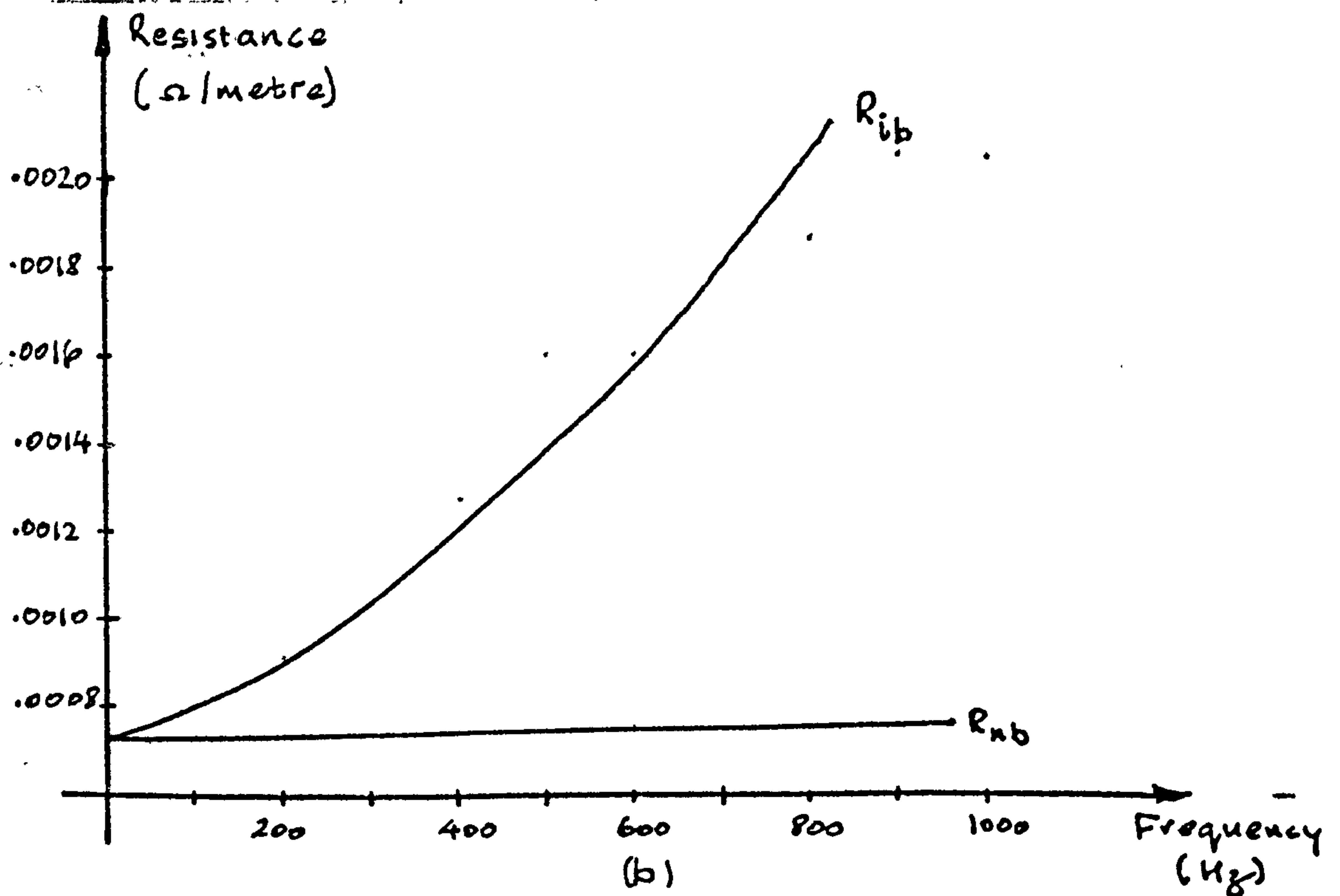
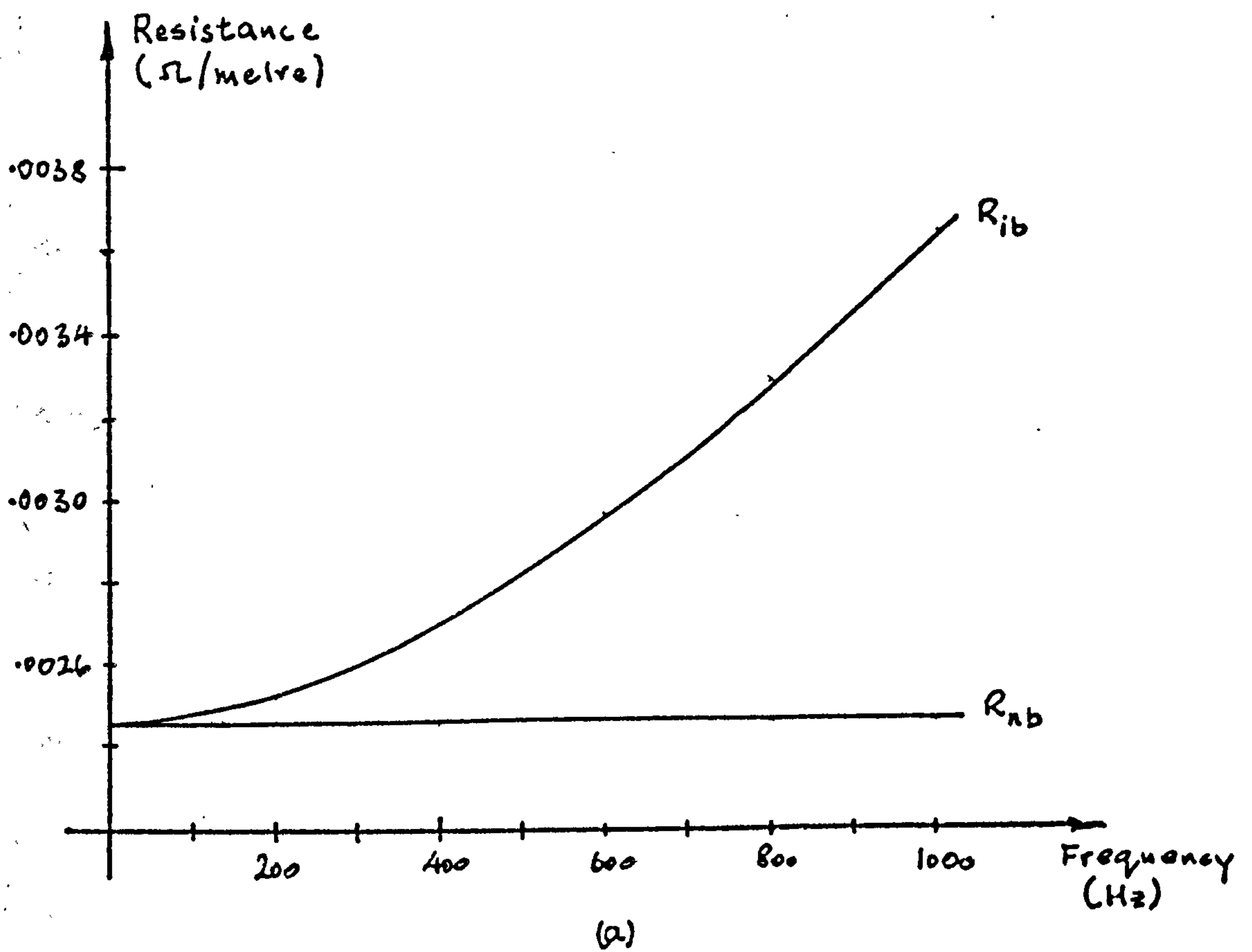
$$\frac{X_{ib}}{R_d} = \frac{\alpha R}{2} \left[\frac{\text{ber} \alpha R \text{ber}' \alpha R + \text{bei} \alpha R \text{bei}' \alpha R}{(\text{ber}' \alpha R)^2 + (\text{bei}' \alpha R)^2} + 2 \sum \frac{\text{ber}_n \alpha R \text{ber}'_n \alpha R + \text{bei}_n \alpha R \text{bei}'_n \alpha R}{(\text{ber}'_n \alpha R)^2 + (\text{bei}'_n \alpha R)^2} \right] \quad (\text{III.4})$$

and for bars remote from iron,

$$\frac{R_{nb}}{R_d} = \frac{\alpha R}{2} \left[\frac{\text{ber} \alpha R \text{bei}' \alpha R - \text{bei} \alpha R \text{ber}' \alpha R}{(\text{ber}' \alpha R)^2 + (\text{bei}' \alpha R)^2} \right] \quad (\text{III.5})$$

$$\frac{X_{nb}}{R_d} = \frac{\alpha R}{2} \left[\frac{\text{ber} \alpha R \text{ber}' \alpha R + \text{bei} \alpha R \text{bei}' \alpha R}{(\text{ber}' \alpha R)^2 + (\text{bei}' \alpha R)^2} \right] \quad (\text{III.6})$$

Figure III.2 compares R_{ib} and R_{nb} while a comparison of the reactance is given in figure III.3. The effect of the presence of the iron on both the resistance and reactance is clear. However at 25Hz (the maximum fundamental) the difference between the resistance is very small being less than 1%. The reactance values at this frequency differ by a factor of 10.

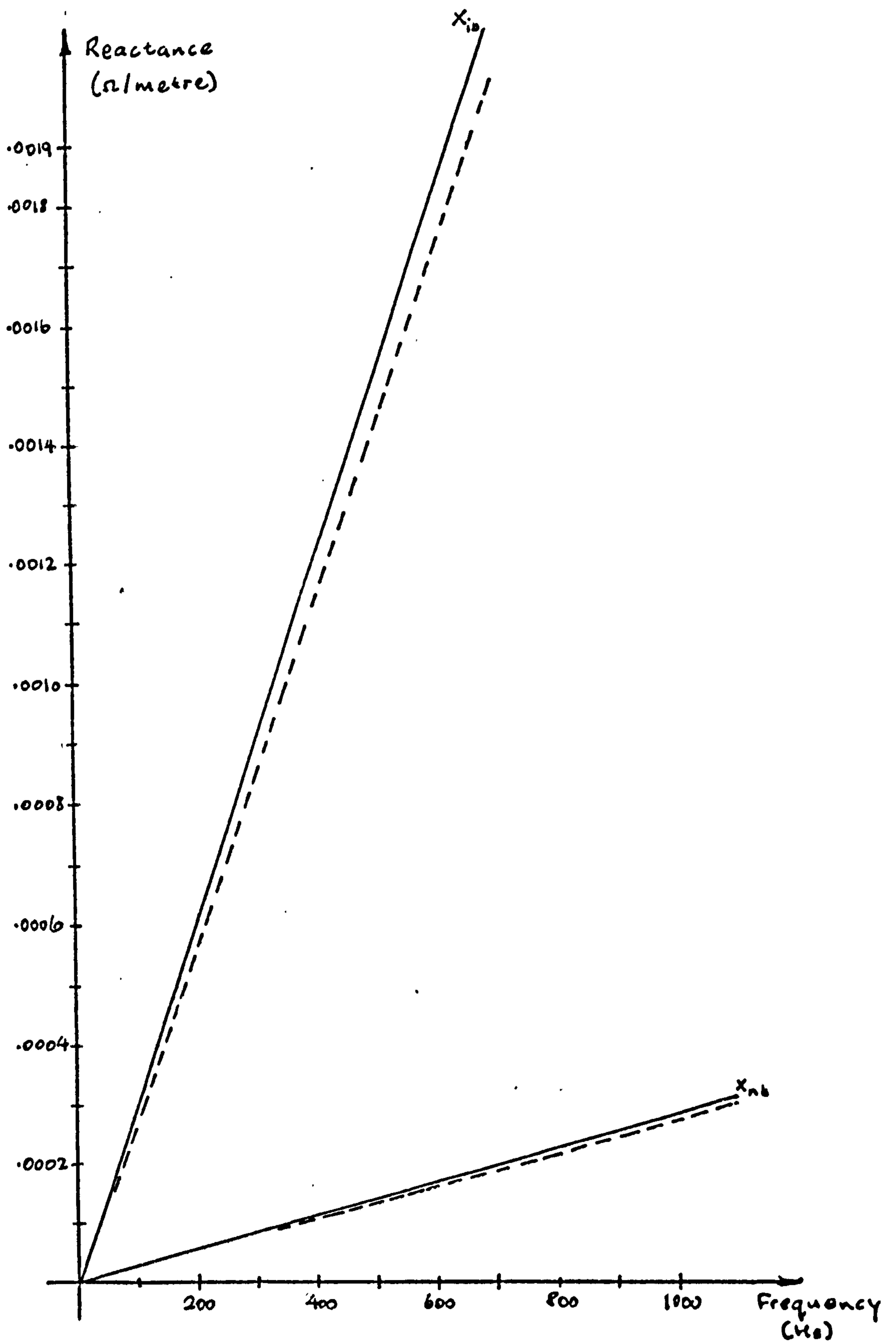


A.C. resistance of squirrel cage bars v_s frequency

(a) bar diameter = 3.0mm

(b) bar diameter = 5.5mm

Figure III.2



Reactance of squirrel cage bars Vs frequency

----- bar diameter = 3.5mm.

———— " " " 3.0mm

Figure III.3

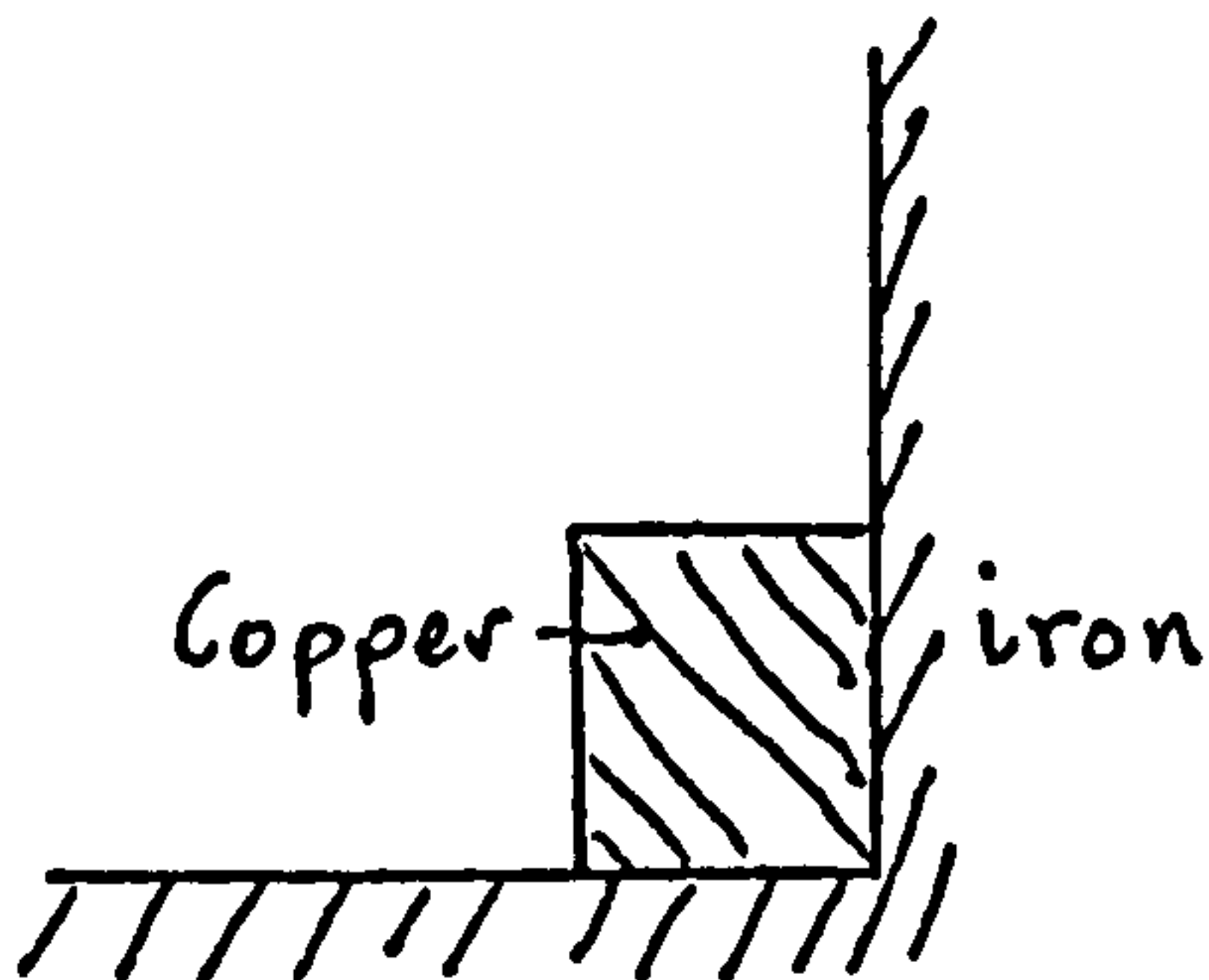
Appendix IV

Impedance of the squirrel cage endring

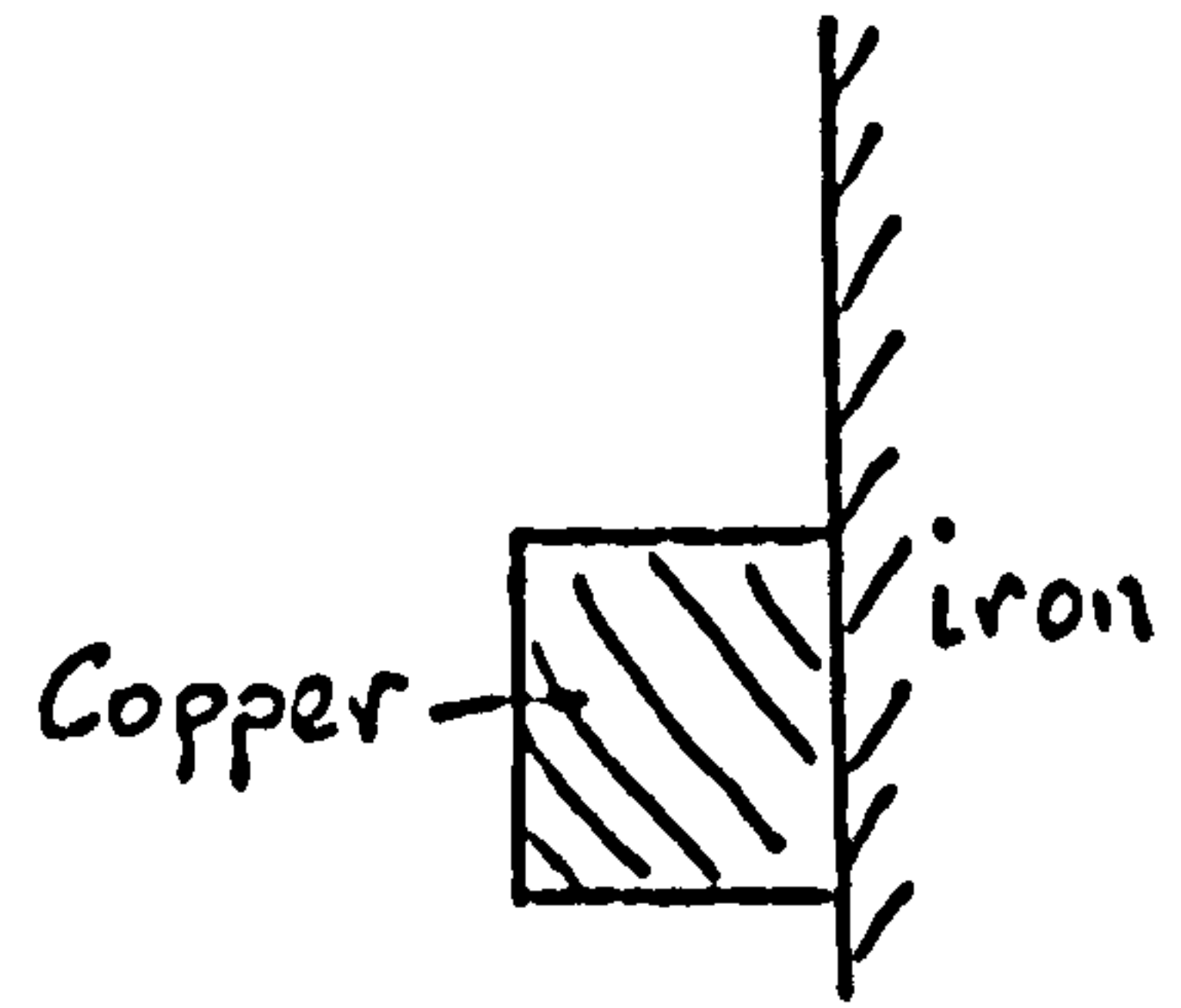
As with the cage bars there are two conditions to be analysed:-

- (1) Where the copper has two iron boundaries (intrapolar)
- (2) Where the copper has one iron boundary (interpolar)

These two states are demonstrated in figures IV.1 and IV.2. For the purpose of the analysis it is assumed that all the iron boundaries extend to infinity and are in contact with the copper section. Consequently figures IV.1 and IV.2 are modified as shown below in diagrams 'i' and 'ii'.



Assumed condition for copper
over pole span (i)



Assumed condition for copper
in interpolar span (ii)

It is apparent that, because of the iron boundaries, diagram 'ii' represents the more general condition and that the solution to 'i' can be extracted from solution 'ii'.

Consider then the flow of current in conductor 'ii'. The current density J in this conductor satisfies the second order differential equation

$$\frac{\partial^2 J}{\partial x^2} + \frac{\partial^2 J}{\partial y^2} = ja^2 J \quad (\text{IV.1})$$

$$\text{and} \quad \nabla \times J = -ja^2 H \quad (\text{IV.2})$$

where $a = \sqrt{w\sigma\mu_0}$

$\nabla \times J$ can be expanded to give

$$\frac{\partial J}{\partial y} = -ja^2 H_x \quad (\text{IV.3})$$

$$\frac{\partial J}{\partial x} = ja^2 H_y \quad (\text{IV.4})$$

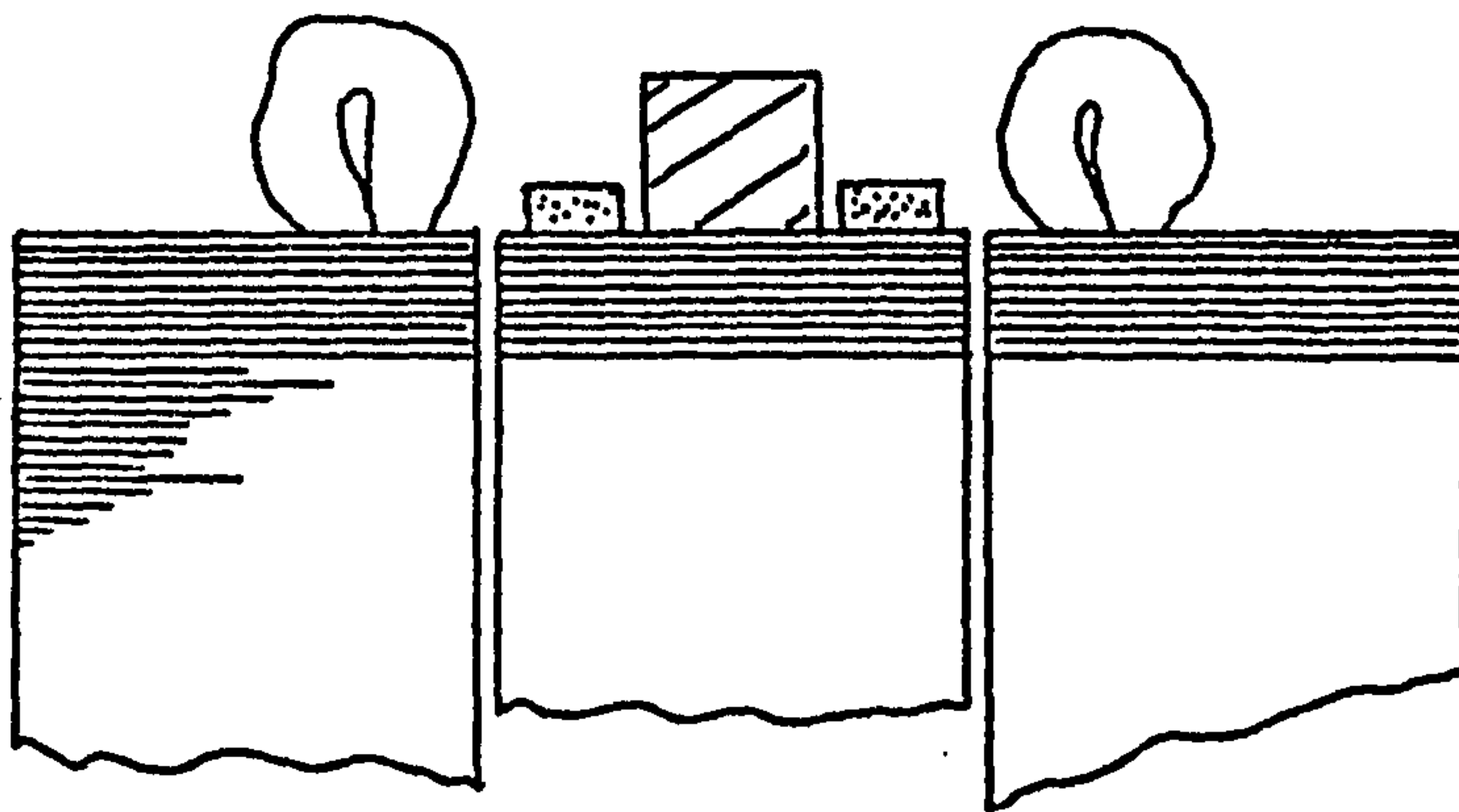


Figure IV.1

Axis of
Machine

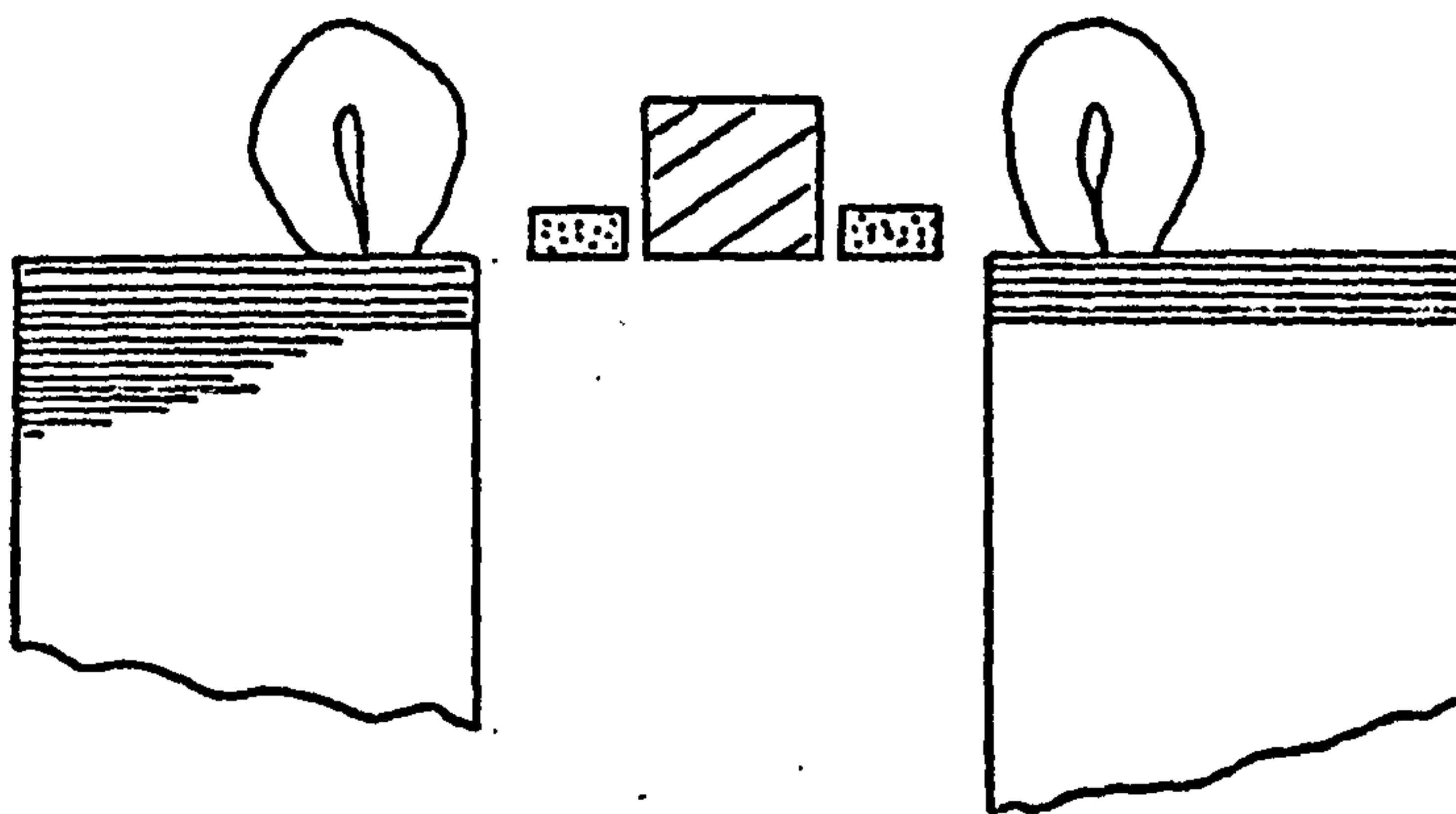
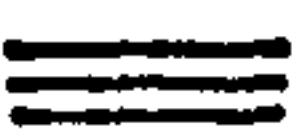




Figure IV.2

Axis of
machine

Key  Laminated stator and rotor
  Copper end ring
  mild steel retaining ring

The endring has the dimensions shown in figure IV.3 on which the boundary conditions are given in terms of H_x and H_y .

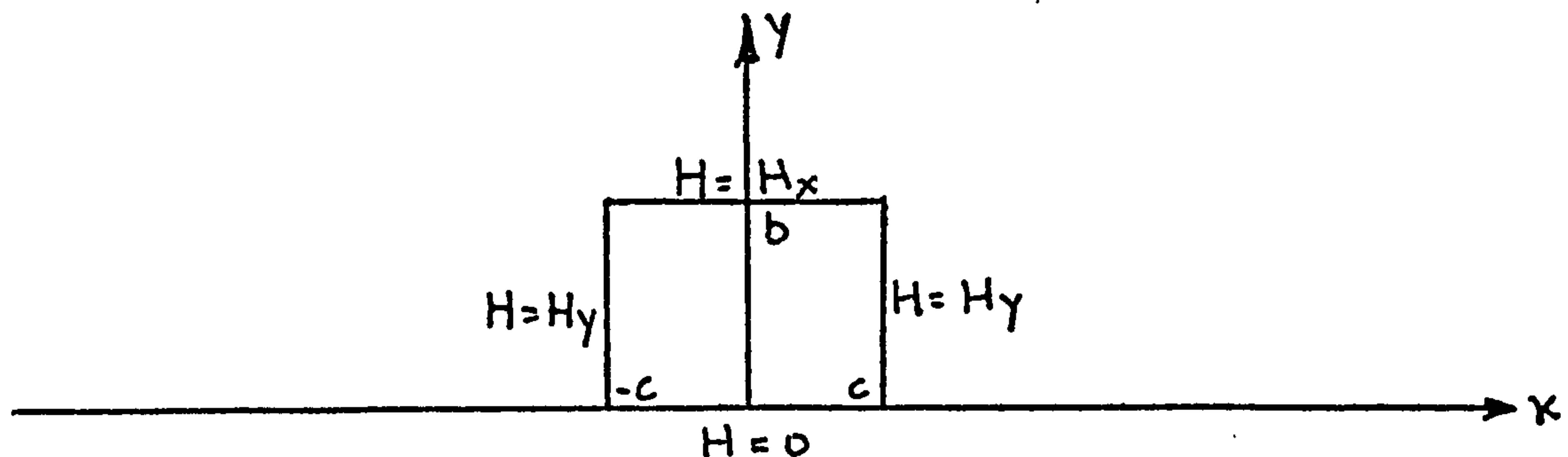


Figure IV.3

The problem which has three non-zero boundary conditions is simplified by treating it as three separate problems each having only one non-zero boundary. Diagrammatically this becomes,

$$\begin{array}{c} H_y \\ \square \\ H_y \end{array} J_z = \begin{array}{c} H_x \\ \square \\ 0 \end{array} J_a + \begin{array}{c} 0 \\ \square \\ 0 \end{array} J_b + \begin{array}{c} 0 \\ \square \\ 0 \end{array} J_c$$

Each individual problem is still satisfied by equations (IV.1) and (IV.2) and,

$$J_z = J_a + J_b + J_c \quad (IV.5)$$

Consider the solution for J_a

Let $J_a = f(x) \cdot f(y)$ be a solution to the differential equation,

$$\frac{\partial^2 J}{\partial x^2} + \frac{\partial^2 J}{\partial y^2} = ja^2 J_a$$

where $f(x)$ and $f(y)$ are functions of x and y respectively. Because $H_y = 0$ on $x = \pm c$, $f(x)$ is oscillatory and in general will contain sine and cosine terms only. However, because $H_x = 0$ only on $y = 0$ then $f(y)$ will be non-oscillatory and contain hyperbolic functions⁽²⁹⁾.

Therefore, let

$$J_a = (A \cos kx + B \sin kx)(C \cosh ly + D \sinh ly) \quad (IV.6)$$

be the general form of the solution.

Boundary conditions

$$(1) H_x = 0, \text{ on } y=0$$

$$(2) H_y = 0, \text{ on } x=0$$

$$(3) H_y = 0, \text{ on } x=\frac{t}{c}$$

$$(4) H_x = \frac{I}{t}, \text{ on } y=b \quad \text{where } t = b+c \text{ for the intrapolar copper} \\ = 2b+2c \text{ for the interpolar copper}$$

Using the first three boundary conditions and equations (IV.3), (IV.4) and (IV.6) the solution to the current density distribution can be shown to have the form,

$$J_a = A' \cos \frac{n\pi x}{c} \cosh ly$$

where $f(x) = \cos(n x/c)$ and $f(y) = \cosh ly$

Returning to equation (IV.1) and substituting for $f(x)$ and $f(y)$ reveals that,

$$1 = \sqrt{ja^2 + (n\pi/c)^2}$$

hence,

$$J_a = A' \cos(n\pi x/c) \cosh y \sqrt{ja^2 + (n\pi/c)^2} \\ = A' \cos(n\pi x/c) \cosh y (u_n + jv_n) \quad (IV.7)$$

$$\text{where } (u_n + jv_n)^2 = ja^2 + (n\pi/c)^2$$

Completing the square and equating real and imaginary parts gives,

$$u_n^2 - v_n^2 = (n\pi/c)^2$$

$$\text{and } 2u_n v_n = a^2$$

the solution of these two simultaneous equations gives,

$$u_0 = (a/\sqrt{2}); \quad u_n = \frac{n\pi}{c\sqrt{2}} \sqrt{1 \pm \sqrt{1 + (ca/n)^4}} \\ v_0 = (a/\sqrt{2}); \quad v_n = \frac{n\pi}{c\sqrt{2}} \sqrt{-1 \pm \sqrt{1 + (ca/n)^4}}$$

Boundary condition (4)

The solution for J_a (IV.7) is in the form of an infinite series and using (IV.7) and (IV.3) gives,

$$-ja^2 \frac{I}{t} = \frac{d}{dy} \sum_{n=0}^{\infty} A'_n \cos(n\pi x/c) \cosh(u_n + v_n)y \quad (\text{IV.8})$$

when $n=0$,

$$-ja^2 \frac{I}{t} = A'_0 (u_0 + jv_0) \sinh(u_0 + jv_0)b$$

hence,

$$A'_0 = -\frac{ja^2 I}{t} ((u_0 + jv_0) \sinh(u_0 + jv_0)b)^{-1}$$

The solution for A'_n ($n=1,2,3$ etc) is obtained by Fourier analysing equation (IV.8). The left hand side of (IV.8) is represented by a square wave of width $2c$ and since

$$-ja^2 \frac{I}{t} \int_{-c}^c \cos(n\pi x/c) dx = 0$$

$$\text{then } A'_n = 0$$

and the complete solution for J_a is given by,

$$J_a = -ja^2 \frac{I}{t} \left[\frac{\cosh(u_0 + jv_0)y}{(u_0 + jv_0) \sinh(u_0 + jv_0)b} \right]$$

Similarly,

$$J_b = -ja^2 \frac{I}{t} \left[\frac{\cosh(u_0 + jv_0)(c-x)}{(u_0 + jv_0) \sinh(u_0 + jv_0)2c} \right]$$

$$J_c = -ja^2 \frac{I}{t} \left[\frac{\cosh(u_0 + jv_0)(c+x)}{(u_0 + jv_0) \sinh(u_0 + jv_0)2c} \right]$$

Therefore, $J_{z1} = J_a + J_b$ (or $J_a + J_c$)

for all parts of the endrings of the induction motor and for those sections of the reluctance motor which span a pole,

For the parts of the reluctance motor endring in the interpolar region,

$$J_{z2} = J_a + J_b + J_c$$

Consider J_{z1}

$$J_{z1} = \frac{ja^2}{t_1} \left[\frac{\cosh(u_o + jv_o)y}{(u_o + jv_o)\sinh(u_o + jv_o)b} + \frac{\cosh(u_o + jv_o)(c-x)}{(u_o + jv_o)\sinh(u_o + jv_o)2c} \right]$$

But, $J = \sigma E$

$$\text{and } I(R_{e1} + jX_{e1}) = \frac{J_{o,b}}{\sigma}$$

where R_{e1} and X_{e1} are the resistance per unit length of the endring.

Therefore, substituting for $u_o, v_o, x=0$ and $y=b$ gives,

$$R_{e1} + jX_{e1} = \frac{a}{\sigma t_1 \sqrt{2}} \left[\frac{j(1-j)}{2\sinh(1+j)B} + j(1-j)\text{ctnh}(1+j)C \right]$$

$$\text{where } B = \frac{ba}{\sqrt{2}}; C = \frac{ca}{\sqrt{2}} \text{ and } t_1 = (b+2c)$$

Expanding the sinh and ctnh terms and equating the real and imaginary terms gives,

$$R_{e1} = \frac{a}{\sigma t_1 \sqrt{2}} \left[\frac{\sinh C \cos C + \cosh C \sin C}{\cosh 2C - \cos 2C} + \frac{\sinh 2B + \sin 2B}{\cosh 2B - \sin 2B} \right]$$

$$X_{e1} = \frac{a}{\sigma t_1 \sqrt{2}} \left[\frac{\sinh C \cos C - \cosh C \sin C}{\cosh 2C - \cos 2C} + \frac{\sinh 2B - \sin 2B}{\cosh 2B - \sin 2B} \right]$$

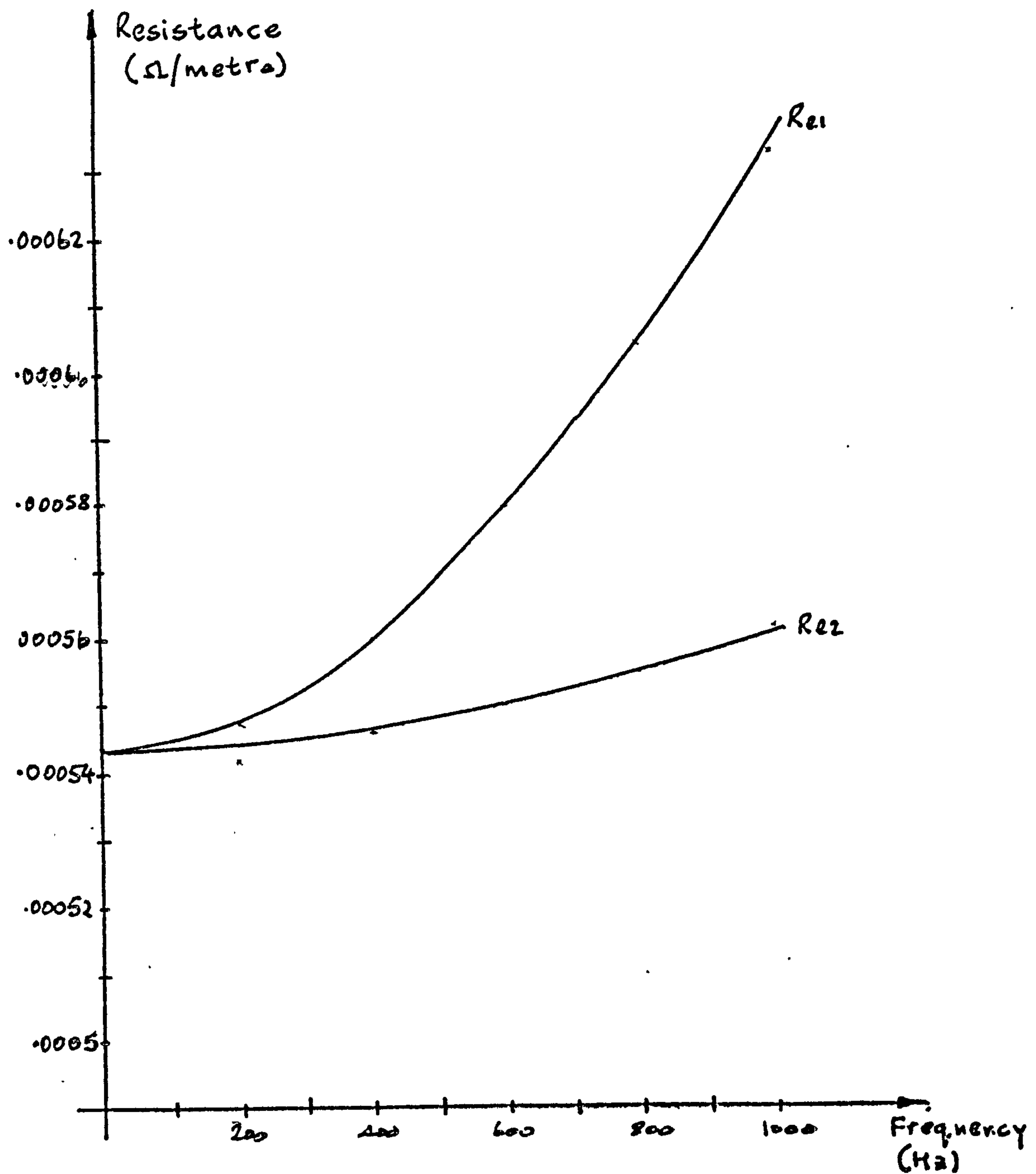
Similarly from J_{z2}

$$R_{e2} = \frac{a}{\sigma t_2 \sqrt{2}} \left[2 \left[\frac{\sinh C \cos C + \cosh C \sin C}{\cosh 2C - \cos 2C} \right] + \frac{\sinh 2B + \sin 2B}{\cosh 2B - \cos 2B} \right]$$

$$X_{e2} = \frac{a}{t_2} \left[2 \left[\frac{\sinh C \cos C - \cosh C \sin C}{\cosh 2C - \cos 2C} \right] + \frac{\sinh 2B + \sin 2B}{\cosh 2B - \cos 2B} \right]$$

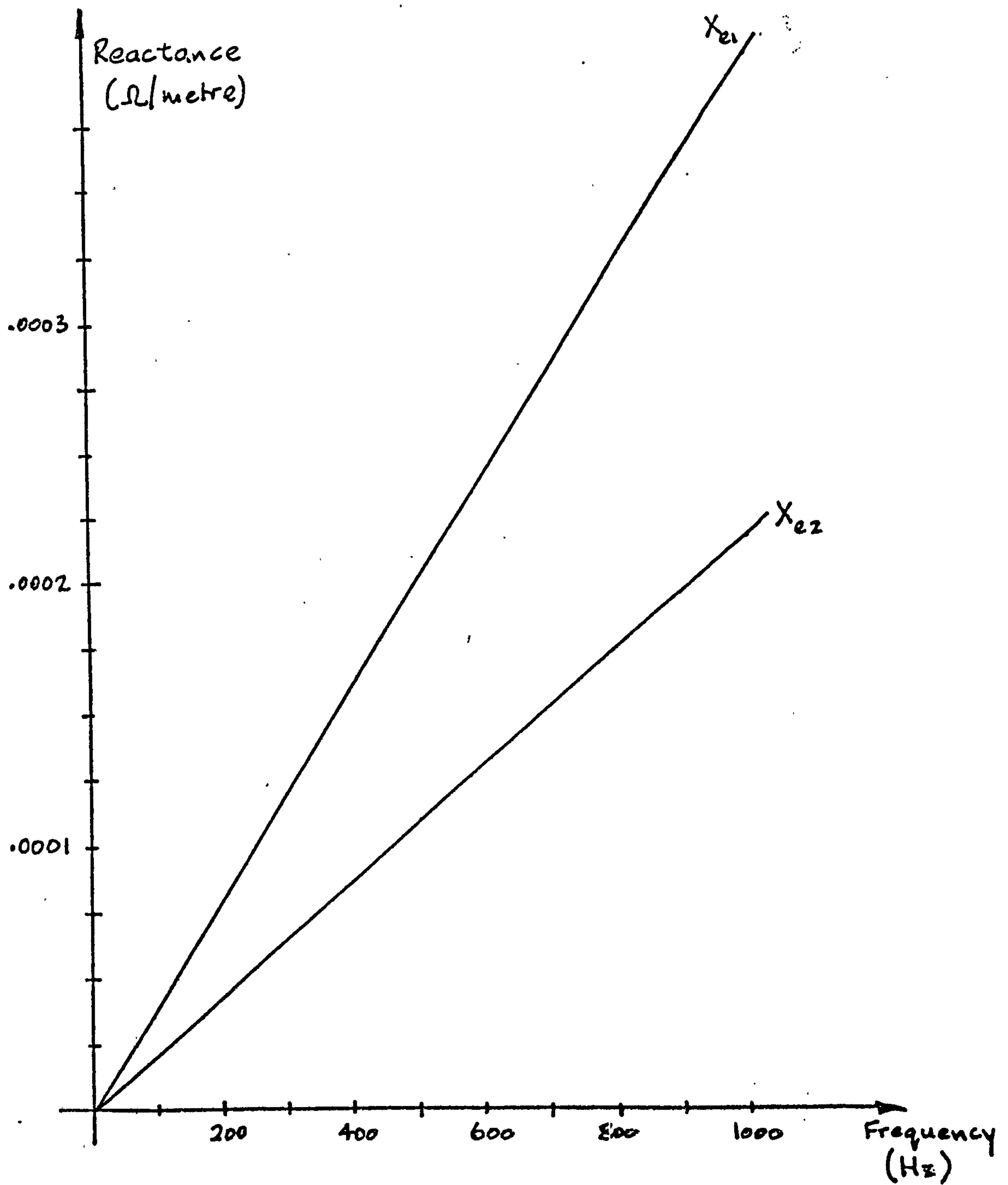
where $t_2 = 2(b+c)$.

A comparison of R_{e1} and R_{e2} is given in figure IV.4 and of X_{e1} and X_{e2} in figure IV.5



AC resistance of squirrel cage and ring V_s frequency
 End ring cross-section 4mm x 8mm

Figure IV.4



Reactance of squirrel cage endring $\frac{1}{2}$ frequency

Endring cross-section 4mm x 8mm

Figure IV.5

Appendix V

Rotor Inertia

On the basis of the rotor lamination material having a density of ρ it was found by measurement that the solid iron portions and the copper had densities of 0.94ρ and 1.14ρ respectively. The calculation of the moment of inertia of various shaped bodies is covered in most texts on Mechanical Engineering and consequently only the final results are quoted below.

For the rotor iron alone:-

$$J_r = \pi \rho 10^8 (6.87 + 2.17)$$

For the copper endrings:-

$$J_c = \pi \rho 10^8 1.21$$

For the squirrel cage bars:-

$$J_b = \pi \rho 10^8 0.125$$

Therefore,

$$J_t = \pi \rho 10^8 (\beta 6.87 + 3.505) \text{ gm mm}^2$$

where $\rho = 7.8 \times 10^{-3} \text{ gm/mm}^3$

References

The references are divided into three main categories which are defined below.

- (a) Prime Source:- This covers the necessary theoretical background. These references are identified with an asterisk (*) and have been used extensively in developing the theory.
- (b) Secondary Source:- The reference numbers have been underlined and are used, in conjunction with (a), for necessary background information. Although the majority of these references have a mathematical basis, they have been used for non-theoretical information.
- (c) Additional Source:- The remaining references have not been used in the development of the thesis but have been included as a further bibliographical source.

-
- (1) Henry-Baudot, J. and Burr, R. P. "Unique operating characteristics offered by printed circuit motors". Electrical Manufacturing (U.S.A.) May, 1959, p116 - 121.

Scott, A. "Printed Armature lightens d.c. motor". Engineering, August, 1969, vol 208, p196-197.

Printed Motors Ltd. "Printed Armature d.c. Servomotor". Publication No. 01 (Aldershot, Hants.)

- (2) Laithwaite, E. R. and Barwell, F. T. "Application of Linear Induction Motors to high speed transport system". Proc.I.E.E., 1969, 116, (5), p713-722.

- * (3) Lawrenson, P. J. and Agu, L. A. "Theory and Performance of polyphase reluctance machines". Proc.I.E.E., 1964, 111, (8), p1435 -1445.

- (4) Mackecnie-Jarvis. "The History of Elec. Eng." J.I.E.E., vol. 1, Sept., 1955, p566-574.

- (5) Dunsheath, P.A. "The history of Elec. Eng". Faber, London, 1962. (Book)

- (6) Jehl, F. "Dynamo-Electric Machine". U.S. Patent 376307, Jan 1888.

Nelson, L.W. "Dynamo-Electric Machine". U.S. Patent 1038494, Sept 1912.

Societe D'Electronique et D'automatisme. "A flat airgap Electrical Rotating Machine". British Patent 874394, August 1961.

Carter, A.H. and Corbett, A.E. "Electrical Motor". British Patent 1231782, May 1971.

- (7) Appleton,D.A. "Status of Superconducting Machines". I.R.D.C. Ltd
Newcastle-U-Tyne, 1972.
- (8) Corbett,A.E. "A disc armature motor". EM70 Conference, University of
Dundee, July 1970.
- (9) Campbell,P. "A new wheel motor for electric commutor cars".
Electrical Review, vol 190, March 1972, p332-333.
- (10) Capaldi,B. and Corbett,A.E. "Feasibility study on the disc armature
motor". Engineering Dept., university of Warwick, 1971.
- (11) Frazier,R.H. "Analysis of the a.c. drag-cup Tachometer". Trans AIEE,
1951, pt II, vol 70, pl894-1901.
- (12) Cruickshank,AJ. et al, "Theory and performance of reluctance motor
with axially laminated anisotropic rotors". Proc I.E.E. 118, (7),
July 1971, p887-894.
- *(13) Gupta,S.K. "Theory and Performance of segmental rotor reluctance
machines (including a new numerical conformal transformation method)".
Ph.D Thesis, University of Leeds, 1966-67.
- (14) Carter,F.W. "Note on the Airgap and Interpolar Induction". J.I.E.E.
1900. 29, p925-933.
- (15) Coe,R.T. and Taylor,H.W. "Some problems in electrical machine design
involving elliptic functions". Phil. Mag. 1928, (6), pl00-145.
- (16) Binns,K.J. "Calculation of some basic flux quantities in induction
and other doubly slotted machines". Proc I.E.E. 1964, 111, (2),
pl847-1858.
- *(17) Binns,K.J. and Lawrenson,P.J. "Analysis and computation of Electric
and Magnetic Field Problems". Pergamon Press (1963), (Book).
- (18) Alger,P.L. "The nature of polyphase induction machines". Wiley,
New York, (1951). (Book).
- (19) Tallet,M.E. "Stability state and transient synthesis of reluctance motors"
Trans AIEE, 1951, 70 III, pl963-1970.
- *(20) Douglas,J.F.H. "Pull-in criterion for reluctance motors". Trans AIEE,
1960, 79 III, pl39-142.
- (21) Lipo,J.A. and Krause,P.C. "Stability analysis of a reluctance motor".
IEEE Trans, 1967, PAS-86, p825-834.
- (22) Krause,P.C. "Methods of stabilising a reluctance synchronous
machine". IEEE Trans, 1968, PAS-87, p641-649.
- (23) Khanijo,M.K. and Mohanty,J.K. "Stability of reluctance motors". ibid,
p2009-2015.
- *(24) Gibbs,W.J. "Conformal Transformation in Electrical Engineering".
Chapman and Hall, London, 1958, (Book).
- *(25) Dwight,H.B. "Tables of integrals and other mathematical functions".
MacMillan, New York, 1964, (Book).
- (26) von-Kaehne,P. "Unbalanced magnetic pull in Electrical Machines".
Electrical Research Association, Z/T142, 1963.

- (27) Nasar,S.A. "An axial airgap, variable speed, eddy current motor".
IEEE Trans 1968, PAS-87, p1599-1603.
- *(28) Swann,S.A. and Salmon,J.W. "Effective resistance and reactance of
a solid cylindrical conductor placed in a semi-closed slot".
Proc I.E.E. 109C, 1962, p611-619,
- *(29) Wylie ,C.R. "Advanced Engineering Mathematics". McGraw-Hill,
New York, 1966, (Book).